AD NUMBER
AD617170
CLASSIFICATION CHANGES
TO: **UNCLASSIFIED**
FROM: **CONFIDENTIAL**
LIMITATION CHANGES
TO: **Approved for public release; distribution is unlimited. Document partially illegible.**
FROM: **Distribution authorized to U.S. Gov't. agencies only; Test and Evaluation; JUL 1959. Other requests shall be referred to Defense Atomic Support Agency, Albuquerque, NM. Document partially illegible.**
AUTHORITY
DASA notice 49 dtd 18 Nov 1960, per document marking; DASA per document marking

UNCLASSIFIED
~~CONFIDENTIAL~~

WT-1155

This document consists of 216 pages

No. 178 of 195 copies, Series A

AD617170

Operation TEAPOT

NEVADA TEST SITE

February – May 1955

Official Classification of this report
UNCLASSIFIED
although the original classification may not have been removed from all pages.
Classification changed by authority of TIS Change Notice No.

Project 1.14b

MEASUREMENTS OF AIR-BLAST PHENOMENA WITH SELF-RECORDING GAGES (U)

Issuance Date: July 16, 1959

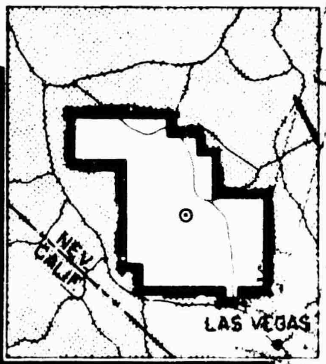

UNCLASSIFIED

~~FORMERLY RESTRICTED~~ DATA
~~Handle as~~ Restricted Data in foreign dissemination. Section 144b, Atomic Energy Act of 1954.

This material contains information affecting the national defense of the United States within the meaning of the espionage laws, Title 18, U.S.C., Secs. 793 and 794, the transmission or revelation of which in any manner to an unauthorized person is prohibited by law.

HEADQUARTERS FIELD COMMAND, DEFENSE ATOMIC SUPPORT AGENCY
SANDIA BASE, ALBUQUERQUE, NEW MEXICO

PROCESSING COPY

ARCHIVE COPY

EVALUATION COPY

UNCLASSIFIED
~~CONFIDENTIAL~~

DISCLAIMER NOTICE

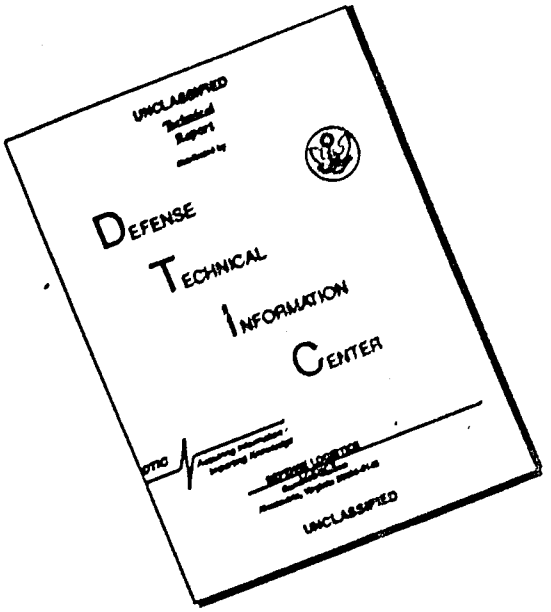

THIS DOCUMENT IS BEST QUALITY AVAILABLE. THE COPY FURNISHED TO DTIC CONTAINED A SIGNIFICANT NUMBER OF PAGES WHICH DO NOT REPRODUCE LEGIBLY.

Inquiries relative to this report may be made to

Chief, Defense Atomic Support Agency
Washington 25, D. C.

When no longer required, this document may be destroyed in accordance with applicable security regulations.

DO NOT RETURN THIS DOCUMENT

AEC Technical Information Service Extension
Oak Ridge, Tennessee

WT - 1155

OPERATION TEAPOT - PROJECT 1.14b

Report to the Test Director

MEASUREMENTS OF AIR-BLAST PHENOMENA WITH SELF-RECORDING GAGES (U)

E. J. Bryant
N. H. Ethridge
J. H. Keefer

Explosion Kinetics Branch
Terminal Ballistics Laboratory
Ballistic Research Laboratories
Aberdeen Proving Ground, Maryland

SUMMARY OF SHOT DATA, OPERATION TEAPOT

Shot	Code Name	Date	Time*	Area	Type	Latitude and Longitude of Zero Point
1	Wasp	18 February	1200	T-7-4†	762-ft Air	37° 05' 11.6956" 116° 01' 18.7366"
2	Moth	21 February	0545	T-3	300-ft Tower	37° 02' 52.2654" 116° 01' 15.6967"
3	Tesla	1 March	0530	T-9b	300-ft Tower	37° 07' 31.5737" 116° 02' 51.0077"
4	Turk	7 March	0520	T-2	500-ft Tower	37° 05' 15.4944" 116° 07' 03.1679"
5	Hornet	12 March	0520	T-3a	300-ft Tower	37° 02' 25.4943" 116° 01' 31.3674"
6	Bee	22 March	0505	T-7-1a	500-ft Tower	37° 05' 41.3880" 116° 01' 25.5474"
7	ESS	23 March	1230	T-10a	67-ft Underground	37° 10' 06.1263" 116° 02' 37.7010"
8	Apple	29 March	0455	T-4	500-ft Tower	37° 05' 43.0200" 116° 06' 09.0040"
9	Wasp'	29 March	1000	T-7-4‡	740-ft Air	37° 05' 11.6856" 116° 01' 18.7366"
10	HA	6 April	1000	T-5§	36,620-ft MSL Air	37° 01' 43.2642" 116° 03' 28.2824"
11	Post	9 April	0430	T-9c	300-ft Tower	37° 07' 19.6965" 116° 02' 03.8860"
12	MET	15 April	1115	FF	400-ft Tower	37° 47' 52.6887" 115° 55' 44.1096"
13	Apple 2	5 May	0510	T-1	500-ft Tower	36° 03' 11.1095" 116° 06' 09.4937"
14	Zucchini	15 May	0500	T-7-1a	500-ft Tower	37° 05' 41.3880" 116° 01' 25.5474"

* Approximate local time, PST prior to 24 April, PDT after 24 April.
† Actual zero point 36 feet north, 426 feet west of T-7-4.
‡ Actual zero point 94 feet north, 62 feet west of T-7-4.
§ Actual zero point 36 feet south, 397 feet west of T-5

ABSTRACT

The self-recording mechanical gages developed for recording overpressure versus time and dynamic pressure versus time were installed on 12 shots. For several shots more than one blast line was instrumented. In addition to these blast lines, gage stations were prepared in locations to meet specific data requirements, such as in the vicinity of structures, and in particular on a circle of gages at a radius of 2,500 feet on Shots 12 and 14. Furthermore, a very-low-pressure gage was employed to record the wave shapes and magnitudes at large distances from the explosions. Particular application of this gage was made on Shot 10.

The gages performed well, and the results were a wealth of data on a wide range of yields for a variety of surface conditions. Tabulations are presented of peak overpressure, positive-phase duration and arrival times at ground surface, and peak dynamic pressure, peak total overpressure, and peak static overpressure at the 3-foot level. The curves for peak overpressure versus distance and peak dynamic pressure versus distance are shown plotted as observed and reduced to 1 KT at sea level in comparison with appropriate curves from TM 23-200 and ideal pressure-distance curves.

Comparisons are shown between gage results under a smoke layer and on clear desert for Shot 5, between gage results on asphalt and desert surfaces of Shot 6, and between gage results on asphalt, desert, and water surfaces of Shot 12. Comparisons are also made of gage results of various shots with similar conditions.

The data indicated that precursors formed on all shots instrumented except the first: gage failure to record pressure-time histories provided no data for determining precursor formation on this shot.

Precursor formation over asphalt was more pronounced than over the desert or water surface. The rate of propagation and the positive phase duration were increased and overpressures decreased on the asphalt more than on the desert or the water surface.

The good-surface-condition curve and the poor-surface-condition curve of TM 23-200 bracketed the measured overpressure curves within the precursor zone. The more pronounced the precursor, the greater is the depression of the measured overpressure-distance curve. The smoke layer during Shot 5 reduced the thermal effects.

The presence of a precursor affecting shock-wave parameters will depend on surface conditions and the height of burst and yield of the weapon or device.

The enhancement of dynamic pressure will depend on surface conditions and is related to the depression of the overpressure-distance curve. An analytical method was used which describes the differences between the measured dynamic pressure and ideal dynamic pressures. This method can be used to predict fairly well the dynamic pressures over an asphalt surface but will underestimate the dynamic pressure over a desert surface.

FOREWORD

This is one of the reports presenting the results of the 47 projects participating in the Military Effects Tests Program of Operation TEAPOT, which included 14 test detonations. For readers interested in other pertinent test information, reference is made to ITR-1153, Summary Report of the Technical Director, Military Effects Program. This summary report includes the following information of possible general interest.

a. An over-all description of each detonation, including yield, height of burst, ground zero location, time of detonation, ambient atmospheric conditions at detonation, etc., for the 14 shots.

b. Discussion of all project results.

c. A summary of each project, including objectives and results.

d. A complete listing of all reports covering the Military Effects Tests Program.

PREFACE

This report presents the results of air shock overpressure measurements and dynamic pressure measurements during Operation TEAPOT by the Ballistic Research Laboratories in connection with Projects 1.14, 3.1, and 3.10. The scope of the measurements was such that a separate report describing them was necessary.

This report is based on the work of many men , since it is derived from efforts made in connection with three projects of the Ballistic Research Laboratories. In particular, grateful acknowledgement is given to the members of the BRL projects organization. These men performed the work of gage development, preparation, installation, recovery, and reduction of data.

Grateful acknowledgement is extended to Dr. E. E. Minor for providing technical and administrative guidance to the BRL organization. Special appreciation is due CDR W. M. McLellon of Directorate, Weapons Effects Tests and his staff for their generous assistance and cooperation. To Dr. C. W. Lampson, grateful appreciation is expressed for the technical guidance and suggestions given in the analysis of the data.

The excellent work of W. J. Taylor, who organized, directed, and expedited the efforts of the BRL projects organization in the field work which was essential for the collection of the pressure data, is greatly appreciated.

Particular recognition is given to the outstanding work of: R. E. Anderson, for his work in development of timing techniques and initiation methods for the pressure-time gages: R. C. Wagner, who continued development of the dynamic pressure gage: and J. E. Gurgel, for his work with the very low pressure gage.

Appreciation is expressed to C. N. Kingery for providing the pressure-time curves for the shock tube model of the Project 3.6 structure.

The efforts of Marion Hause and Shirley Ishbaugh in typing and assembling the text and the work of J. E. Gurgel and J. D. Day in preparation of the figures in final form is greatly appreciated.

The preparation of the record photographs and the reduction and preparation of the field data in final tabular form was done by J. H. Keefer and R. C. Wise with the aid of members of the BRL projects organization.

The work of R. C. Wise in the reduction of the pressure data into pressure-time form and the plotting of these curves in final form is greatly appreciated.

The work of the Shock Tube personnel in calibrating the "q" gage and the assistance of R. J. Drexler in reducing and analyzing the data is gratefully appreciated.

Contributing authors for particular sections of the report are as follows: Appendix A, Instrument Design, by R. E. Anderson, J. E. Gurgel, C. H. Hoover, M. R. Johnson and R. C. Wagner; Appendix B, Asymmetrical Study, by J. J. Meszaros and W. J. Taylor: Appendix C, Structures Instrumentation by P. H. Lorrain and J. H. Keefer; Appendix D, Very Low Pressure Gage, by C. H. Hoover and J. H. Keefer and Appendix E, Record Presentation by J. H. Keefer.

CONTENTS

FIGURES

TABLES

Chapter 1
INTRODUCTION

1.1 OBJECTIVES

The primary objective of the measurements described in this report was to provide medium blast data required for the proper interpretation of the results obtained by Project 3.1 and to supplement the pressure data required by Project 1.14.

For Project 3.1 the required data were overpressure versus time and dynamic pressure versus time at each project installation. In addition, similar data in front and behind the project installation were required to indicate the development of the blast wave.

In meeting these requirements the resultant primary objective was to obtain overpressure versus distance and dynamic pressure versus distance for each shot of interest to either project.

Secondary objectives included: (1) An investigation of the symmetry of the blast wave from Shot 12; (2) a comparison of overpressure for a given shot measured in the open and under a smoke layer; (3) an investigation of pressures on or in the vicinity of structures for Project 3.10, Structures Instrumentation; (4) an evaluation of a very-low pressure-time gage; and (5) continued evaluaton of modifications in gage construction, components, and techniques.

1.2 BACKGROUND

Previous operations indicated uncertainty in the blast parameters most significant in producing damage effects of military interest. The occurrence of precursor phenomena and distorted wave forms made uncertain in particular the relations between overpressure, dynamic pressure, and drag force.

To provide data for better understanding of the conditions prevailing in the blast waves, Project 3.1 was concerned with measurements of the response of typical military drag type targets, such as vehicles, and the resulting damage.

In conjunction with the measurements of the project, records of overpressure versus distance and dynamic pressure versus distance were required for proper interpretation of data obtained. The scope of the

project indicated a large number of measurements were needed, the majority located where no blast shelters were available.

The development of the self-recording pressure-time gage began during UPSHOT-KNOTHOLE. A modified form of the gage was employed on a large scale during Operation CASTLE (Reference 1). Self-recording dynamic-pressure gages were first designed for use on CASTLE, and the results indicated that a satisfactory gage and mounting system had been developed.

To meet the requirements of Project 3.1 in TEAPOT, therefore, a large number of pressure-time and dynamic-pressure gages and mounts were prepared for use on blast lines for each shot of interest

Chapter 2
DESIGN AND OPERATIONS

The possible participation in any or all shots by Project 3.1 required that blast lines be prepared for all shots. These blast lines were prepared well in advance of the shots to the point that only actual installation of the gages was required for completion of the lines.

The possibility of delayed recovery caused by heavy contamination, plus the very short time schedule between shots, made independence of gage installation on a shot from those shots immediately preceding it very necessary. The simultaneous ready dates for several Group A and Group B shots made it necessary that two blast lines, complete with instruments, be ready for operation at the same time.

Surveys for the blast lines were made by the civilian contractor, by members of the Engineers Corps from Camp Desert Rock, and in some cases, by project personnel. Gage and gage mount installation was done by project personnel at all stations.

For all shots in which Project 3.1 participated, a total of 163 stations were employed, with a total of 247 gage installations distributed among the stations. This does not include gage installations used for investigations discussed in Appendixes B, C, and D. Table 2.1 indicates the number of stations and the number of types of gages used for each shot.

2.1 FIELD LAYOUT

The gage stations for each shot were located to provide pressure-time and dynamic pressure data for Project 3.1. In general, a gage station was placed at each vehicle station, and additional gage stations were located to complete the blast line.

The pressures expected at each station were predicted by scaling from the height-of-burst curves in TM 23-200 (Reference 2) to the expected yield and atmospheric conditions. Where the range of yield expected was wide, the gage ranges were based on the maximum yield predicted to minimize the possibility of overstressing the gage sensing elements.

For several shots gage stations were prepared off the main blast lines. The description of the installation of a circle of gages for Project 1.14 on Shot 12 and Shot 14 is contained in Appendix B, a description of installations near structures for Project 3.10 is given

in Appendix C, and stations employed for the very-low-pressure gage are discussed in Appendix D.

A map of Yucca Flat showing the relation of the shot areas to each other is given in Fig. 2.1. The station locations for each shot, the distance from ground zero, and the number and type of instrumentation at each station are given in Figs. 2.2 through 2.13. The locations of stations off the main blast lines are given in the appendices.

Except for the type of ground surface, the stations differed only in the number and type of gages installed and in the mounts required for the gages. The pressure-time gage station consisted of the gage

TABLE 2.1 Station and Gage Summary

Shot	No. of Stations	No. of Pressure-Time Gages	No. of Dynamic Pressure Gages
1	11	15	5
2	11	14	4
3	5	5	4
4	10	10	4
5	14	14	4
6	18	18	9
8	14	14	5
9	11	11	5
11	11	11	4
12	17	17	20
13	9	9	4
14	32	32	9

case and its attached bearing plate buried in the ground until the gage plane was level with the ground surface. Stations at which dynamic pressure gages were located required the installation of a special mount. The mount designed to place the gage at the 3 foot level consisted of two 3-inch vertical pipes separated by welded cross braces and set in Cal seal. The mount designed to place the gage at the 10 ft level consisted of two 3-inch vertical pipes separated by welded cross braces and set in Cal seal with the addition of three guy wires fastened on the mount just below the gage and set in concrete in the ground. All mounts were accurately leveled and sighted on ground zero to provide proper orientation for the gage. Fig. 2.14 shows a typical gage station.

A small drill rig was used to dig the necessary holes and greatly facilitated the rapid preparation of the blast lines.

2.2 INSTRUMENTATION

The two types of gages used at the blast-line stations were the pressure-time gage, for measuring the shock overpressure versus time,

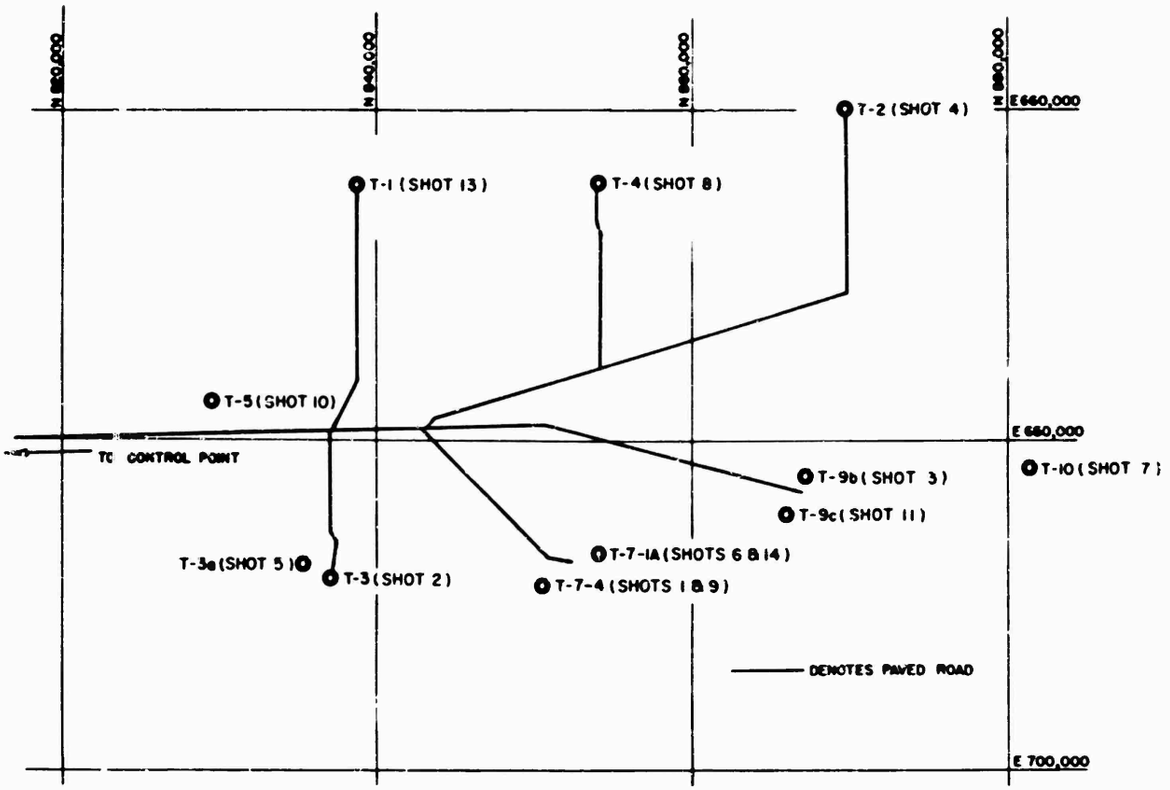

Fig. 2.1 Area and Shot Location in Yucca Flat

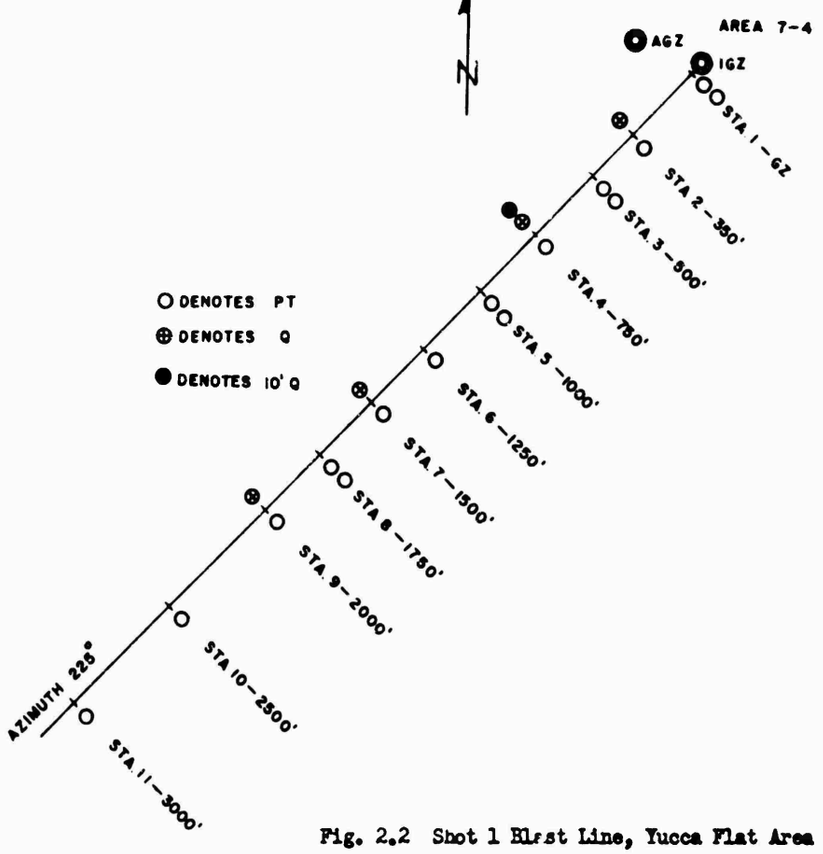

Fig. 2.2 Shot 1 Elrst Line, Yucca Flat Area 7-4

Fig. 2.3 Blast Line Layout for Shot 2 in Yucca Flat Area T-3

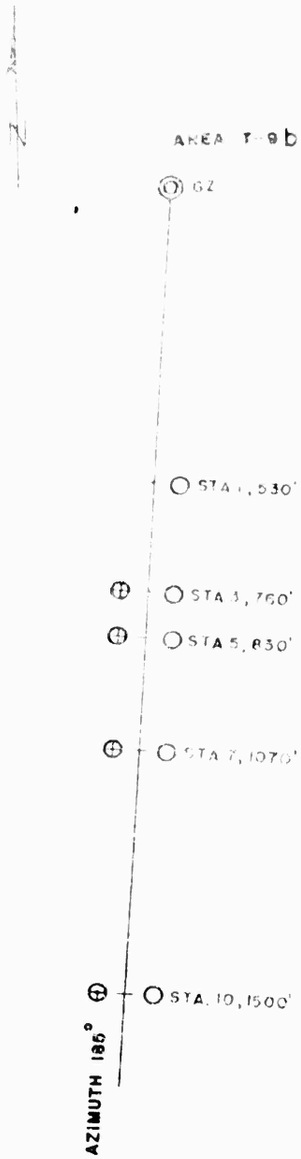

Fig. 2.4 Shot 3 Blast Line Yucca Flat Area T-9b

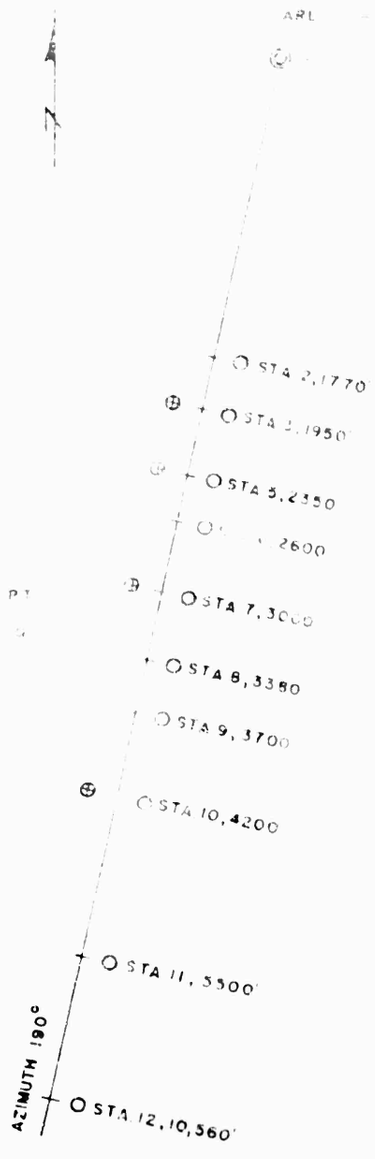

Fig. 2.5 Shot 4 Blast Line Yucca Flat Area T-2

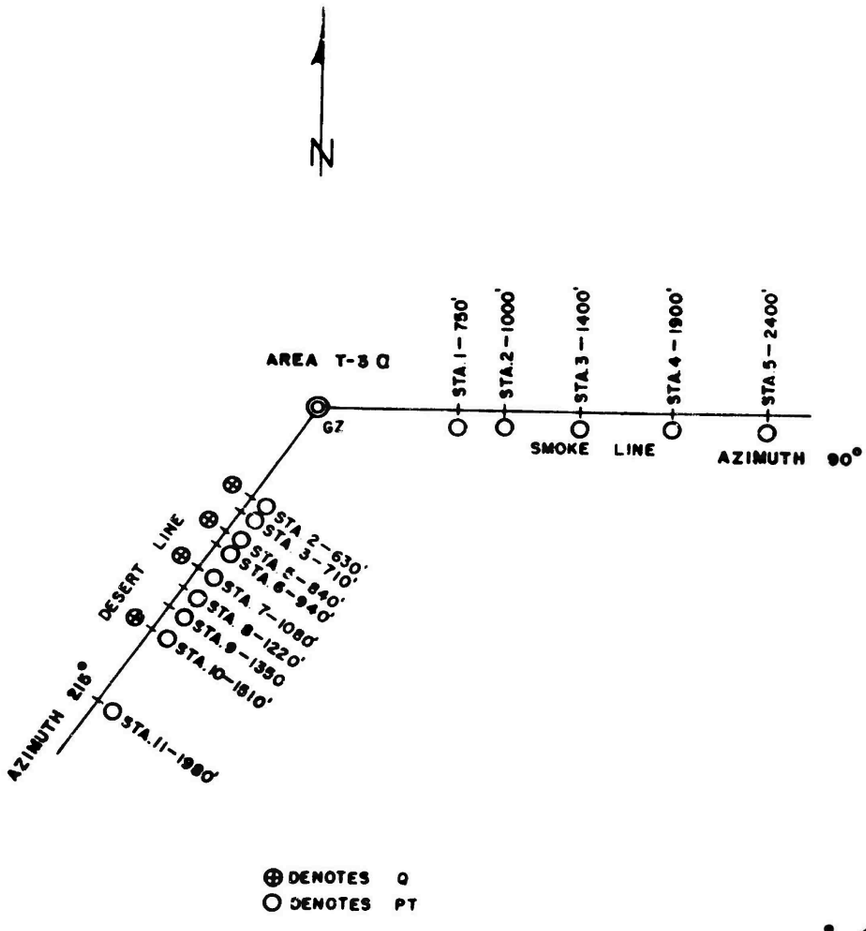

Fig. 2.6 Shot 5 Blast Line, Yucca Flat Area T-3a

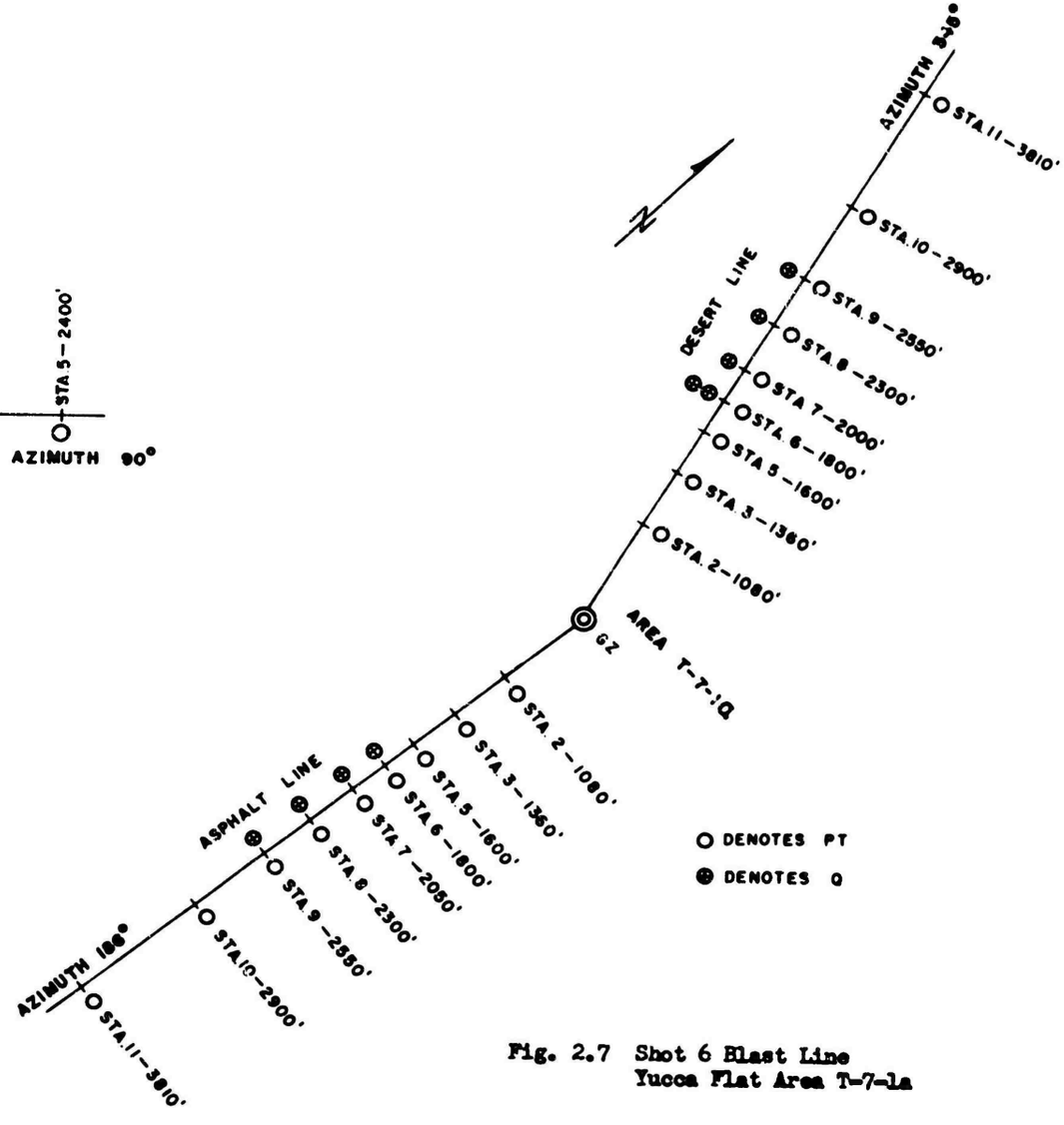

Fig. 2.7 Shot 6 Blast Line
Yucca Flat Area T-7-1a

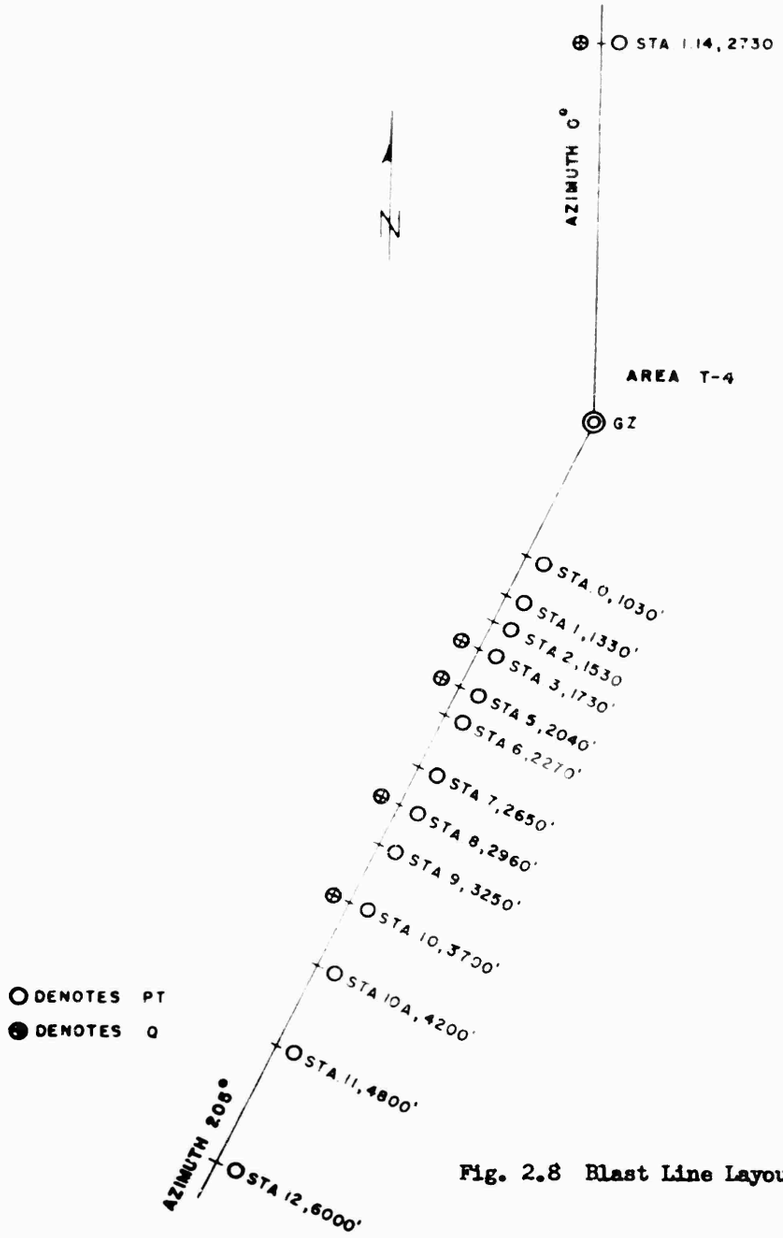

Fig. 2.8 Blast Line Layout for Shot 8 in Yucca Flat Area T-4

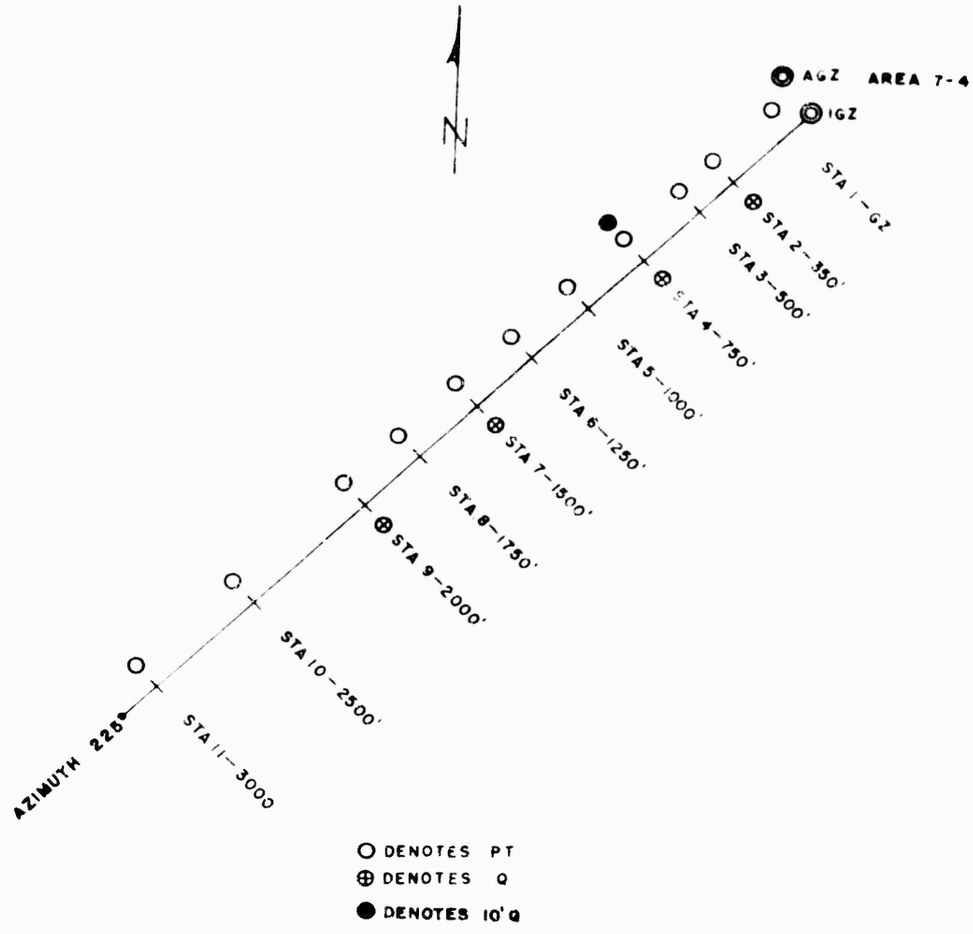

Fig. 2.9 Blast Line Layout for Shot 1 in Yucca Flat Area 7-4

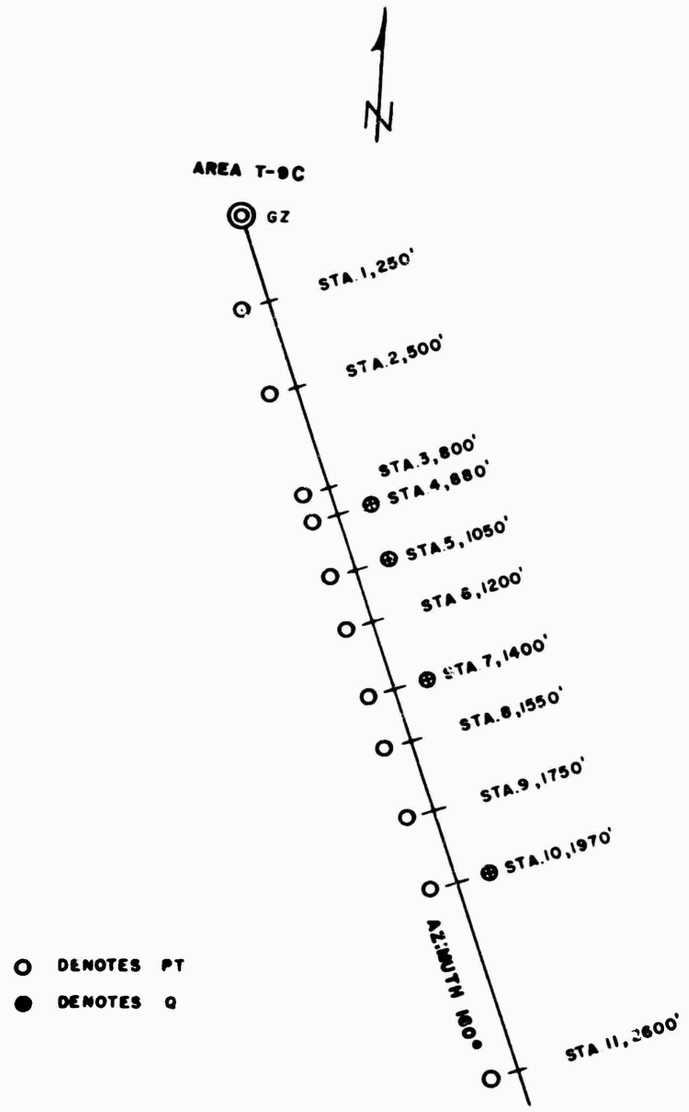

Fig. 2.10 Shot 11 Blast Line, Yucca Flat Area T-9c

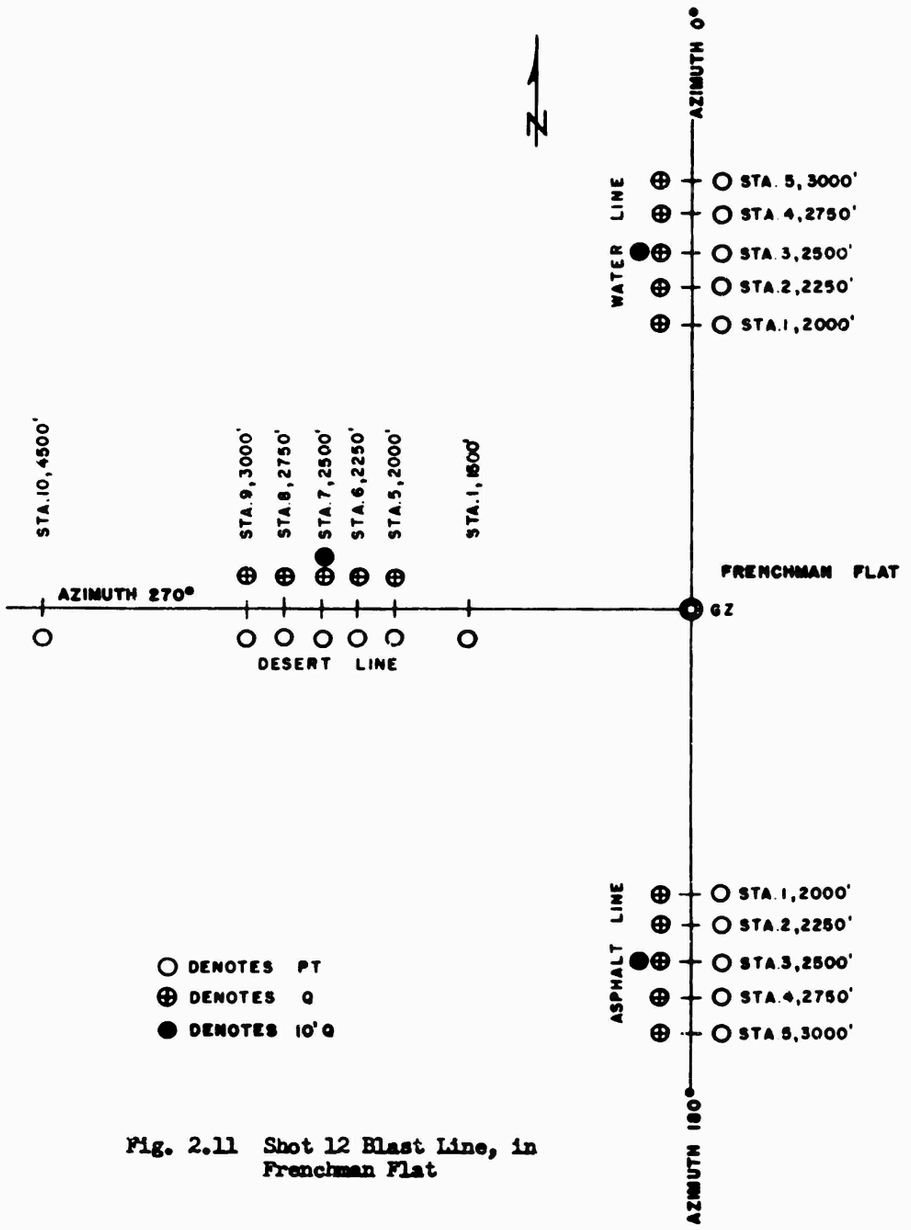

Fig. 2.11 Shot 12 Blast Line, in Frenchman Flat

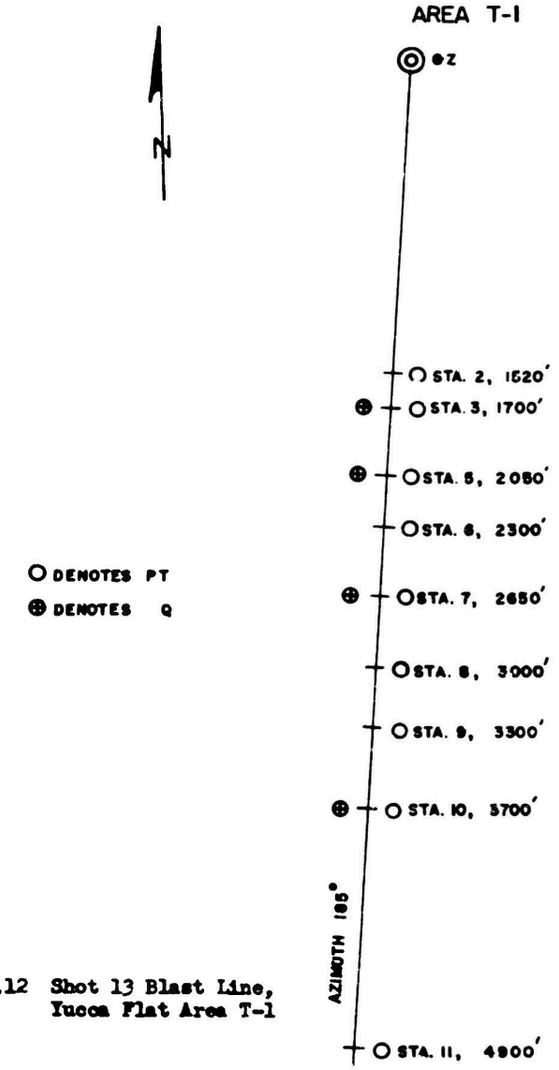

Fig. 2.12 Shot 13 Blast Line, Yucca Flat Area T-1

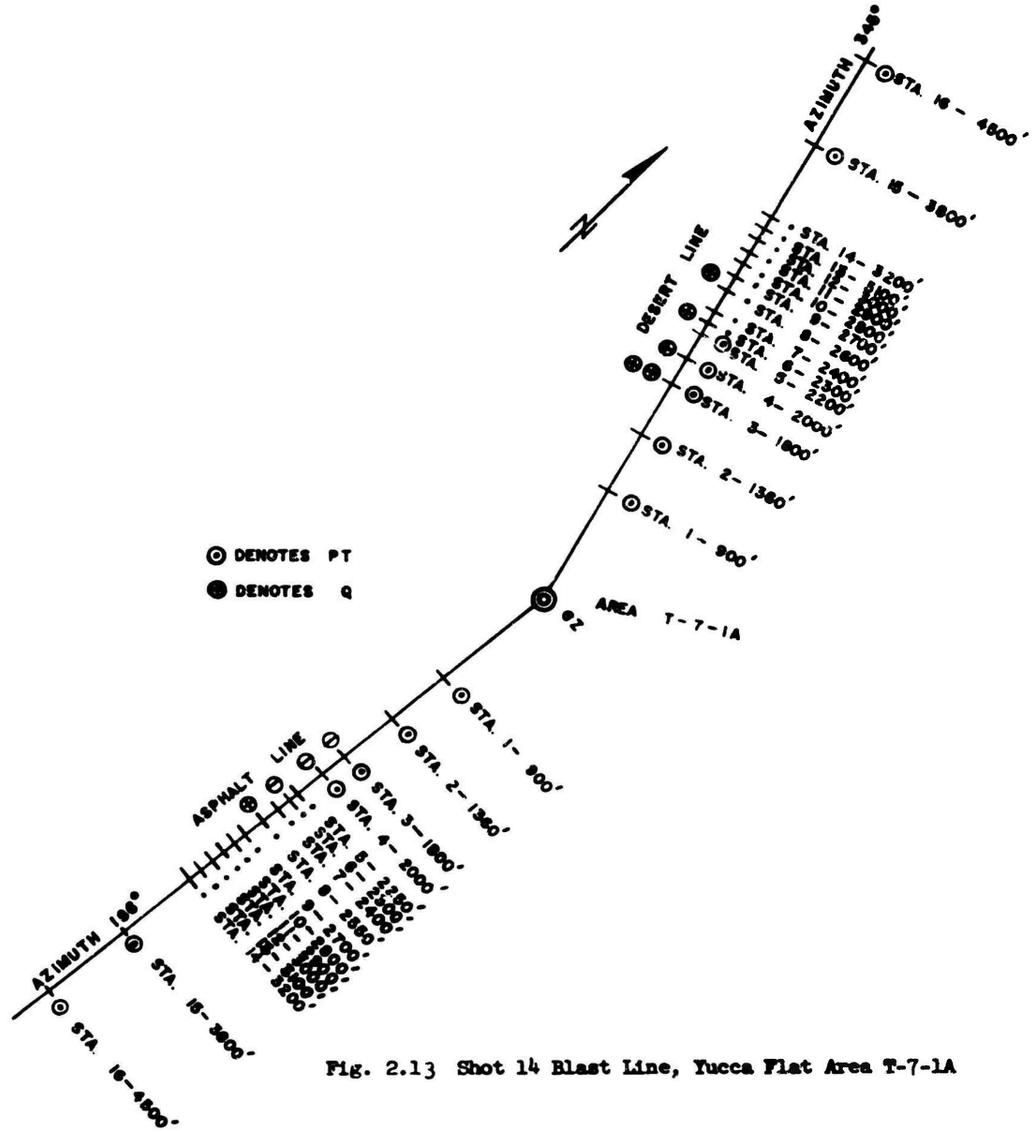

Fig. 2.13 Shot 14 Blast Line, Yucca Flat Area T-7-1A

and the dynamic pressure gage, designed to record the total shock overpressure versus time and the static shock overpressure versus time. All the gages were self-recording and flash initiated with no external power requirements or cabling, except for gages placed in the smoke region in Shot 5. Because of a presumed large amount of attenuation of light and thermal radiation by the smoke, the gages within the smoke region were initiated by photoflash bulbs fired at -5 seconds. A

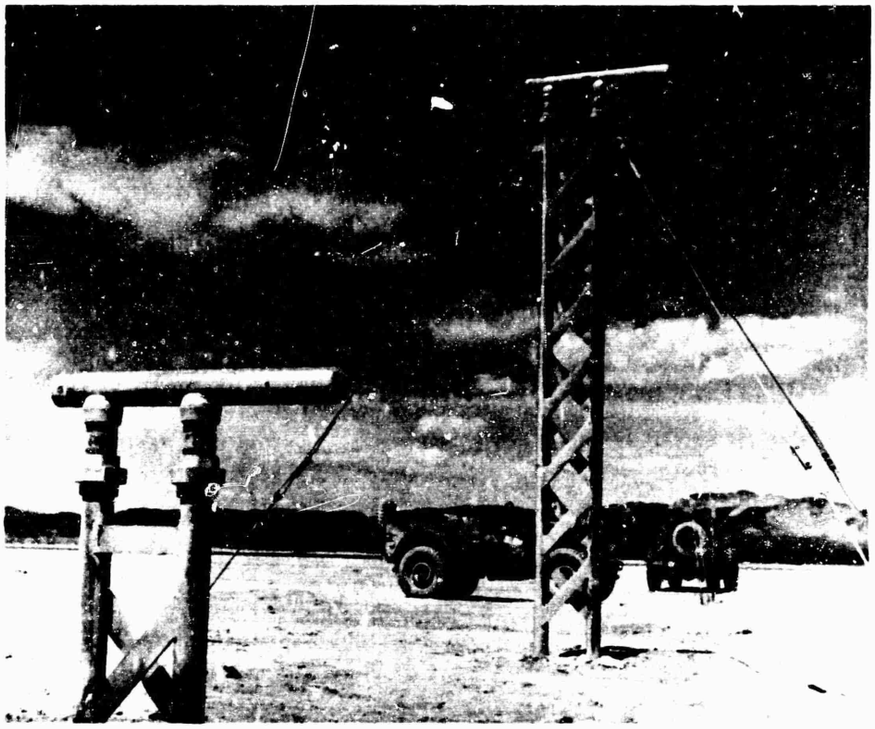

Fig. 2.14 Photograph of Typical Dynamic-Pressure Gage Installation

number of the pressure-time gages incorporated an oscillator designed to place timing marks directly on the record blanks.

The pressure-sensing element of both types of gages was a nested diaphragm capsule . The elements were interchangeable and available in pressure ranges from 0-to-1 psi to 0-to-400 psi. All such elements were individually calibrated.

A very-low-pressure gage (VLP) was used for recording the blast wave at distances up to 35 miles from the shot ground zero. The sensing element for this gage was a simple convoluted diaphragm.

A discussion of the construction and characteristics of the various gages is contained in Appendix A.

2.3 GAGE PERFORMANCE AND RECOVERY

During the 12 shots, 247 self-recording gages were used to obtain pressure-time versus distance data and information concerning various

flow phenomena. Table 2.2 shows the number of gages used on each shot and the type of record obtained. In Appendix A the overpressure-time and dynamic pressure-time gages are described and instrumentation procedure outlined.

The loss of pressure-time records, in most cases, was due to the gage being initiated prior to zero time. Where no record of any kind was obtained, the gage opening was filled with sand and dirt.

The recovery of the gages was greatly facilitated by the use of a 3/4 ton bomb service truck with an extendable boom and a set of tongs especially designed for clamping around the flange of the pressure-time

TABLE 2.2 Gage Performance

Shot	Pressure-time Gages	Pressure-time Gages			Dynamic Pressure Gages	Dynamic Pressure Gages		
		Pressure-time Record	Peak Pressure Only	No Record	"q" Pressure Gages	Pressure-time Record	Peak Pressure Only	No Record
1	15	0	15	0	5	1	4	0
2	14	10	2	2	4	3	1	0
3	5	3	2	0	4	3	1	0
4	10	7	3	0	4	4	0	0
5	14	14	0	0	4	2	1	1
6	8	18	0	0	9	9	0	0
8	14	12	1	1	5	5	0	0
9	11	9	2	0	5	5	0	0
11	11	9	1	1	4	4	0	0
12	17	15	2	0	20	20	0	0
13	9	8	1	0	4	3	1	0
14	32	26	3	3	9	8	1	0
Total	170	131	32	7	77	67	9	1

gage. The time of recovery of a pressure-time gage from the ground by using this equipment was very short; therefore, project personnel were able to recover a complete blast line with a minimum of dosage. A blast line of 10 gages could be recovered in 20 minutes or less.

The dynamic pressure gages were designed for rapid removal from their mounts, and no difficulties were experienced in recovery.

On some shots the heavy contamination caused several days of delay in the recovery of stations close to ground zero. This did not impair

the quality of the records in any way and, since additional gages were available, did not impede the instrumentation of succeeding shots.

2.4 RECORD READING AND DATA REDUCTION

Test data obtained from the dynamic-pressure gage were recorded on 2 1/4-inch-diameter glass discs, whereas the P_t gages recorded information on 3 1/2-inch-diameter glass discs. The q-gage records have two deflection curves, one indicating the total pressure and the other indicating static overpressure. The total pressure waveform is located on the outer circle. The P_t-gage records have only the one waveform traced, static overpressure, which is also in polar coordinates. All the records were examined with aid of a Gaertner toolmaker's microscope for peak deflection, positive duration, general appearance and readability. There appeared, on most records, many oscillations of short time duration, both regular and irregular in shape, which caused some difficulty in reading the peak deflection. In addition, there was some difficulty with some records in determining the true zero time, as well as the true crossover time-ending the positive duration.

With the disc centered on the platform of the microscope, the curve was read and tabulated in the rectangular coordinate form. A magnification of 50 times was used on the microscope to increase the reading accuracy. The angle of rotation (read to the nearest 0.1^{o}) was converted to msec units by using the rotational speed of the disc of the gage. The deflections (read to the nearest 0.001 mm) were converted to psi units by use of the calibration curves previously calculated for the gage capsule used. The approximate error in record reading was $\pm$ 3 percent. The total error of the overall system was approximately $\pm$ 10 percent.

An attempt was made to smooth the curves while reading the record, espeically through an interval of small regular oscillations or irregular oscillations of very short duration. The q records for Shot 2 through Shot 12 were made in this manner. The data for Shots 13 and 14 were read differently in the sense that very little smoothing was attempted.

The pressure and time coordinate values for each point on each curve were punched on IBM cards for the purpose of using a Mosely Autograph Machine to plot each curve.

Dynamic pressure data were obtained by plotting the two curves together so that the static pressure could be subtracted from the total pressure at similar times. During the subtraction process the values of dynamic pressure were tabulated and placed on IBM cards for later plotting.

The total pressure and static pressure waveforms were recorded originally on the same glass disk with separate base lines. Therefore, it was difficult to establish corresponding units of time for each record. The possible errors (error in selection of corresponding time

units, errors in deflection readings, errors in capsule calibrations, and errors in plotting) which may occur could combine and significantly effect the shape and peak value of the resulting dynamic pressure curves.

All readable pressure-time records from the main blast lines of all shots were reduced in the manner described above. These records are shown in Appendix E. For those pressure-time records not on the main blast lines photographs were taken with a Polaroid Land Camera adapted to be used on the Gaertner Toolmaker Microscope. These photographs are shown in the various Appendices.

Chapter 3
RESULTS

3.1 SHOT 1

All of the pressure-time gages ran preshot and only peak overpressures were obtained. A pressure-versus-distance curve is presented in Fig. 3.1 . The tabulated values of corrected distance and peak overpressure are given in Table 3.1. Two gages at Station 3 differ by 6.2 psi. This difference in pressure is apparently due to the fact that the gage with lower values was covered with sand. At the rest of the stations, good agreement for measured values of pressure was obtained from each of the two gages.

A dynamic pressure-time record was obtained at Station 4 (see Table 3.2). The other gages ran preshot. The value of dynamic pressure obtained at Station 2 and Station 4 are in question because of the angle of incidence of the shock front with gage orientation. The actual ground zero was 433 foot from the intended ground zero. A dynamic-pressure versus distance curve was not plotted since a correction factor for the large angle of incidence cannot be determined.

3.2 SHOT 2

The blast line layout for this shot is given in Fig. 2.3. The nine gages on the main blast line give good pressure-time records. The station numbers, distances, arrival time, duration of positive phase, and peak overpressure are listed in Table 3.3. The overpressure versus distance curve is presented in Fig. 3.2. The remainder of the gages near the Shot 5 tower are also listed in Table 3.3. In most cases only peak pressures were obtained from these gages. Two of the gages failed to yield any information since carbon paper placed over the opening of the gage to prevent dust infiltration failed to burn off at that distance and the pressure level was so low that the carbon did not break properly.

A precursor was recorded at the first station at 670 foot. The wave did not seem to completely clean up until about 1,350 feet.

The dynamic pressure data are given in Table 3.4. The gage mount at Station 3 failed, as a result, the total pressure value is questionable. A discussion on failure of mounts on various shots is given in Appendix A. The dynamic pressure versus distance curve is given in Fig. 3.3.

3.3 SHOT 3

Participation in Shot 3 was limited to an investigation of experimental gage systems, particularly new circuitry for initiation of gages

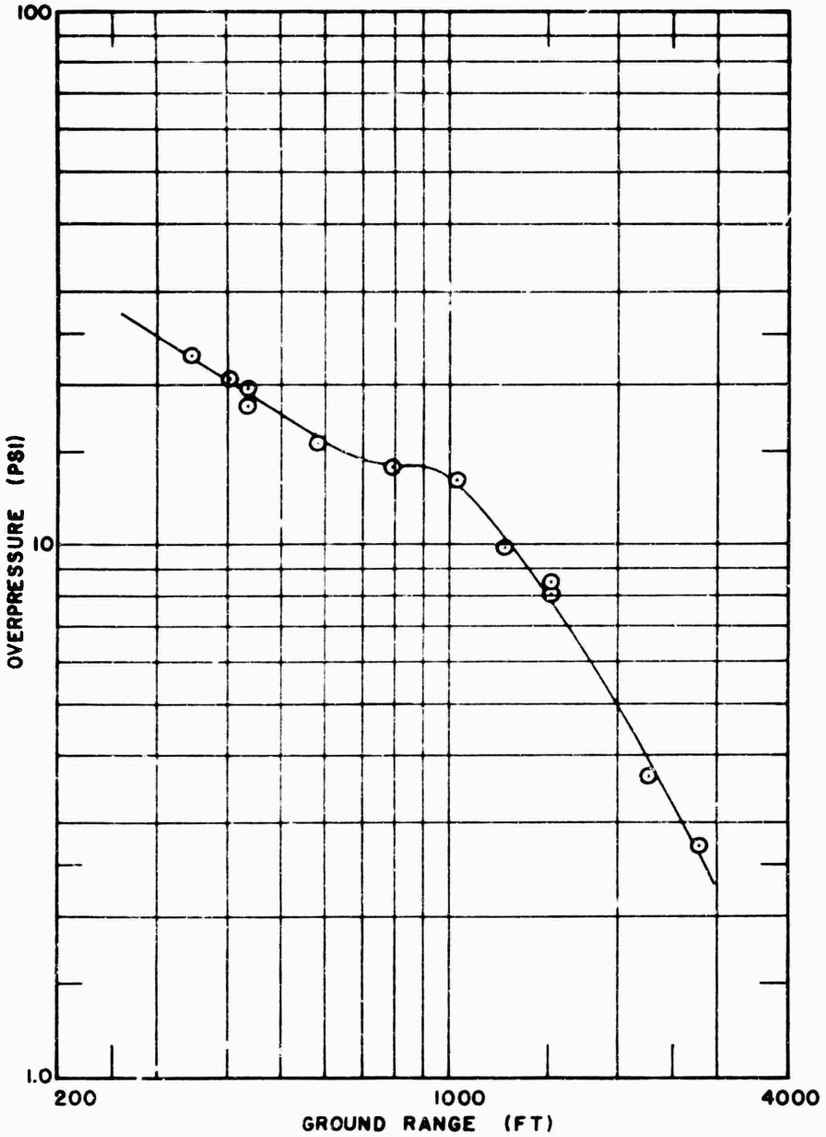

Fig. 3.1 Peak overpressure versus Ground Range for Shot 1 (AS Observed)

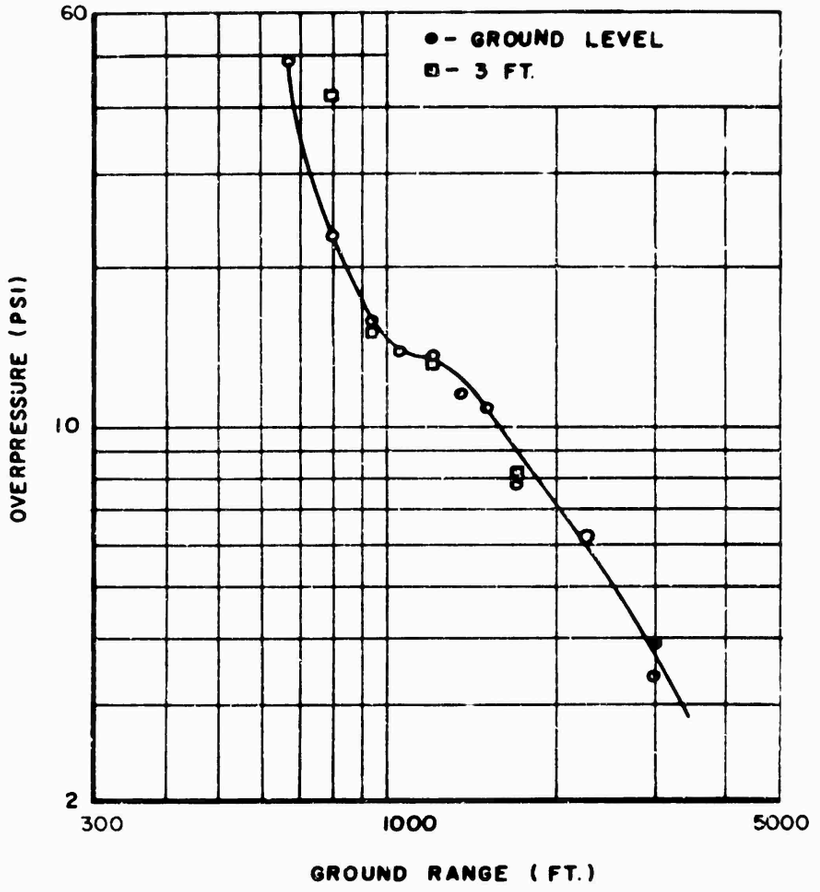

Fig. 3.2 Peak Overpressure versus Ground Range For Shot 2 (As Observed)

TABLE 3.1 Pressure-Time Gage Results for Shot 1

Station	Intended Ground Range (ft)	Corrected Ground Range (ft)	Peak Overpressure* (psi)
1	0	433	19.7
1	0	433	18.5
2	350	343	22.9
3	500	402	20.7
3	500	402	14.5
4	750	580	15.6
5	1000	795	14.1
5	1000	795	14.0
6	1250	1030	13.3
7	1500	1250	9.9
8	1750	1510	8.45
8	1750	1510	8.10
9	2000	1760	3.80
10	2500	2250	3.65
11	3000	2750	2.70

* Peak Pressure only; gages were initiated preshot.

TABLE 3.2 Dynamic Pressure Gage Results for Shot 1

Station	Intended Ground Range (ft)	Corrected Ground Range (ft)	Static Overpressure (psi)	Total Overpressure (psi)	Dynamic Pressure (psi)
2	350	343	18.9*	22.0*	3.1*
4	750	580	20.8	21.8	1.0
4**	750	580	15.0*	16.4*	1.4*
7	1500	1250	10.6*	15.0*	4.4*
9	2000	1760	8.2*	9.1*	0.9*

* Peak Pressure only; gages were initiated preshot

** 10 foot mount

NOTE: Dynamic pressure values are uncorrected for change in angle of incidence of blast wave resulting from miss distance.

TABLE 3.3 Pressure-Time Gage Results for Shot 2

Station	Ground Range (ft)	Peak Overpressure (psi)	Arrival Time (sec)	Positive Duration (sec)
2	670	48.4	0.147	0.19
3	795	23.0	0.163	0.22
5	940	15.8	0.174	0.22
6	1050	13.9	0.285	0.18
7	1200	13.5	0.291	0.29
8	1350	11.5	-	0.28
9	1500	10.9	0.458	0.28
10	1700	7.8	0.744	0.34
11	2240	6.2	1.188	0.38
12A	2980	3.9	2.337	0.47
12B	2980	3.35*	-	-
13**	2980	-***	-***	-***
14**	2980	2.10*	-*	-*
15	4500	-***	-***	-***

* Peak Pressure only; gage did not run

** Tower Station

*** No Record

TABLE 3.4 Dynamic Pressure Gage Results for Shot 2

Station	Ground Range (ft)	Peak Static Overpressure (psi)	Peak Total Overpressure (psi)	Peak Dynamic Pressure (psi)
3*	795	42.0	128.0	86.0
5	940	15.0	38.5	24.0
7	1200	13.1	16.9	4.7
10	1700	8.2	11.1	2.9

* Peak Pressure only; gage did not run.

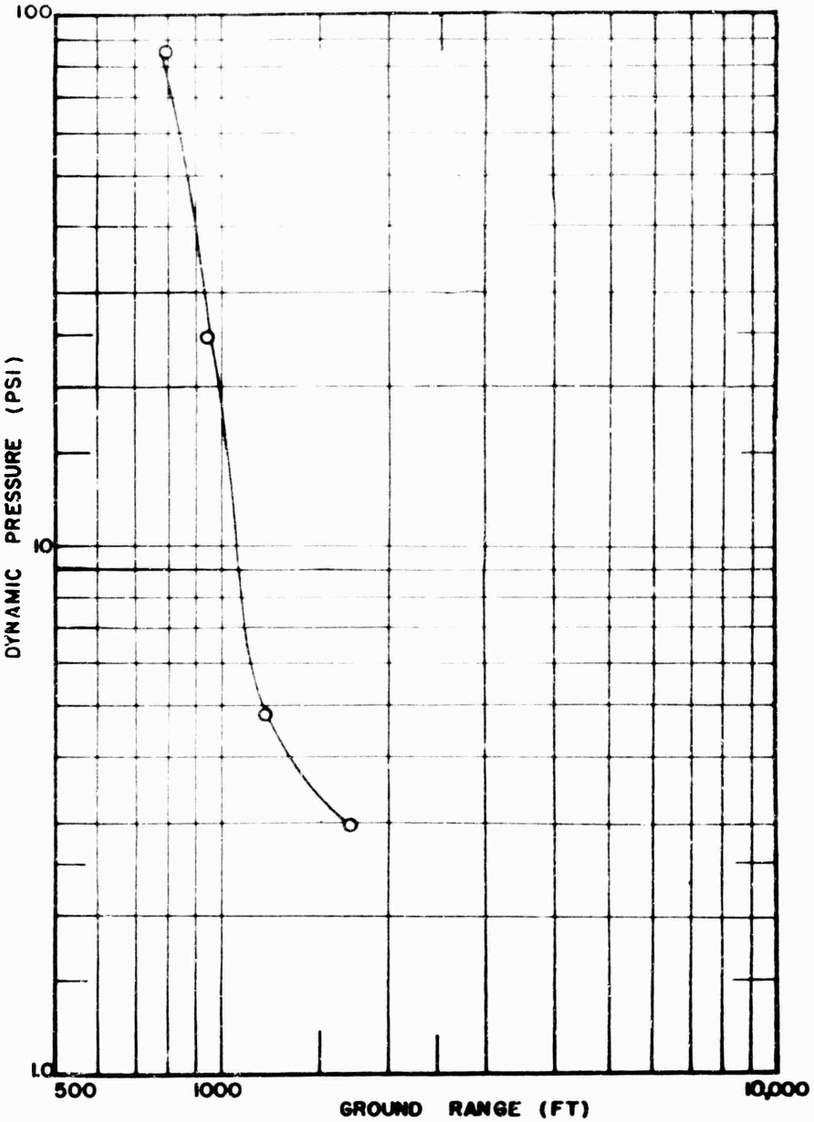

Fig. 3.3 Peak Dynamic Pressure versus Ground Range For Shot 2 (As Observed)

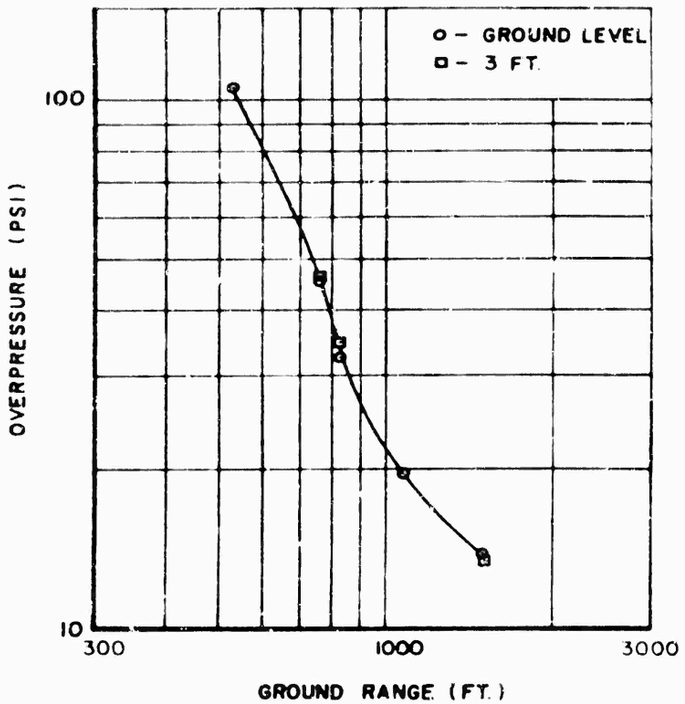

Fig. 3.4 Peak Overpressure versus Ground Range For Shot 3 (As Observed)

and capsule design for the q-gages. A detailed description of changes made on both the pressure-time and q-gages are described in Appendix A. Of the five pressure-time gages, three gave pressure-time records and two gave peak pressure only. The pressure-distance curve is given in Fig. 3.4. Since Shot 1 failed to furnish any information concerning the most desirable recording speed, two of the five pressure-time gages on this shot were recorded at 10 rpm. Both of the 10 rpm gages operated and gave pressure-time records. The recording speed of 10 rpm is considered to be satisfactory. The results are given in Table 3.5.

The differential pressure element used in the dynamic pressure gages gave reasonable results. On the basis of these results this type of element was used on some of the later shots. The results are contained in Table 3.6 and the dynamic pressure versus distance curve is plotted in Fig. 3.5.

Since the yield was over twice the predicted value, three of the pressure capsules were badly overstressed. This caused a permanent displacement in the diaphragm and the stylus did not return to the baseline. The capsules were recalibrated and also a good capsule was overstressed to obtain the same deflection as was read on the shot record, to determine what pressure would be required to produce that deflection. A note has been made on the tables as to the readings that were obtained from overstressed capsules. The error may be as much as $\pm$ 15 percent for values obtained from overstressed capsules.

3.4 SHOT 4

The station numbers, distance, arrival times, duration of positive phase, and peak overpressure are listed in Table 3.7. At Station 8 the gage started with the shock wave and thus the arrival time and positive phase durations were lost. The additional arrival time snd positive phase durations were lost because of insufficient stylus pressure on the recording disk and non-uniformity in the recording disk surfaces. The pressures versus distance curve for peak pressures is given in Fig. 3.6.

Pressure-time records were obtained from all q-gages. At Station 3, the q-gage mount failed. This has been noted in Table 3.8 where the peak dynamic pressure values are presented. Questionable values caused by difficulty in reading, due to light traces, have not been included in the tables. High frequency oscillations superimposed on the total pressure-time record tend to decrease the accuracy in reading. This oscillation seems to be caused by a ringing in the tube leading to the total pressure element from tne nose of the gage. The measured values of dynamic pressure versus distance from ground zero are shown in Fig. 3.7.

3.5 SHOT 5

Pressure-time records were obtained at all stations on both the smoke and clear lines. The smoke screen dimensions (Reference 3) along

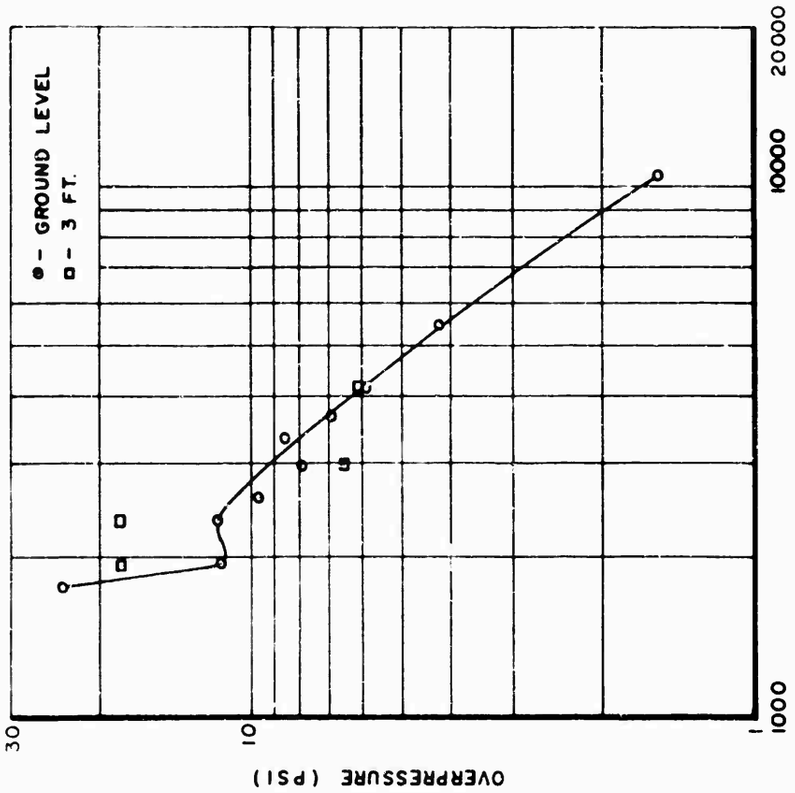

Fig. 3.6 Peak Overpressure versus Ground Range For Shot 4 (As Observed)

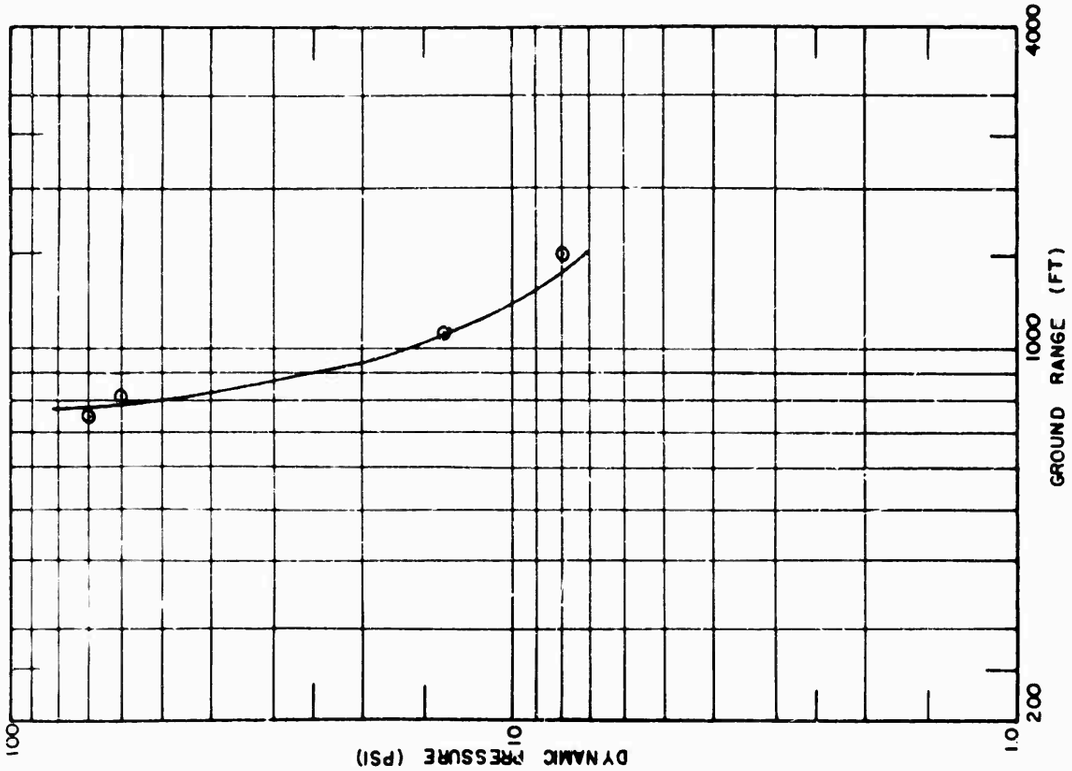

Fig. 3.5 Peak Dynamic Pressure versus Ground Range for Shot 3 (As Observed)

TABLE 3.5 Pressure-Time Gage Results for Shot 3

Station	Ground Range	Peak Overpressure	Arrival Time	Positive Duration
	(ft)	(psi)	(sec)	(sec)
1**	530	105.1	0.087	-
3	760	45.5	0.134	-
5*	830	32.4	-	-
7	1070	19.7	0.221	0.25
10*	1500	13.7	-	-

* Peak Pressure only; gage did not run
** Overstressed Capsule

TABLE 3.6 Dynamic Pressure Gage Results for Shot 3

Station	Ground Range	Peak Static Overpressure	Peak Total Overpressure	Peak Dynamic Overpressure
	(ft)	(psi)	(psi)	(psi)
3**	760	46.1	120.2	70.0
5**	830	35.0	100.0	60.0
7*	1070	-	-	13.8
10	1500	13.6	20.9	7.3

* Differential pressure element
** Overstressed Capsule

TABLE 3.7 Pressure-time Gage Results for Shot 4

Station	Ground Range	Peak Overpressure	Arrival Time	Positive Duration
	(ft)	(psi)	(sec)	(sec)
2	1700	23.6	-	0.64
3	1950	11.5	0.399	0.64
5	2350	11.6	0.571	0.73
6	2600	9.6	-	-
7	3000	7.9	0.604	0.87
8**	3380	8.5	-	-
9	3700	6.9	1.145	0.87
10	4200	5.9	1.771	0.93
11*	5500	4.2	-	-
12*	10,560	1.55	-	-

* Peak Pressure only
** Gage initiated by shock

TABLE 3.8 Dynamic Pressure Gage Results for Shot 4

Station	Ground Range (ft)	Peak Static Overpressure (psi)	Peak Total Overpressure (psi)	Peak Dynamic Pressure (psi)
3*	1950	18.1	75.1	50.0
5	2350	18.2	51.2	28.0
7	3000	6.5	12.9	6.0
10	4200	6.0	7.5	1.5

* Gage mount failed; was found inclined away from GZ

TABLE 3.9 Pressure-time Gage Results for Shot 5

Station	Ground Range (ft)	Peak Overpressure (psi)	Arrival Time (sec)	Positive Duration (sec)
		CLEAR BLAST LINE		
2	630	75.8	0.112	0.15
3	710	43.6	0.121	0.16
5	840	30.2	0.137	0.25
6	940	17.2	0.163	0.28
7	1080	16.1	0.242	0.35
8	1220	13.9	0.303	0.34
9	1350	11.5	0.305	0.32
10	1510	12.9	0.584	0.34
11	1980	7.5	0.859	0.42
		SMOKE BLAST LINE		
1	750	32.8	0.112	0.20
2	1000	19.1	0.222	0.27
3	1400	15.4	-	0.31
4	1900	8.0	0.887	0.35
5	2400	6.0	1.210	0.41

TABLE 3.10 Dynamic Pressure Gage Results for Shot 5

Station	Ground Range (ft)	Peak Static Overpressure (psi)	Peak Total Overpressure (psi)	Peak Dynamic Pressure (psi)
2*	630	-	-	-
5**	840	29.7	115.4	85.0
7	1080	16.7	46.6	27.0
10	1510	12.6	15.8	5.0

* Gage mount failed; bent away from GZ about 60°
** Gage mount failed; bent slightly away from GZ

Line 2 were estimated to be about 80 to 90 feet above the surface and the west edge of the screen was located on Line 2 between 750 feet to 1000 feet and the east edge of the screen extended beyond 2400 feet. Little difference was noted in wave shapes on the two blast lines. A pressure versus distance curve is presented in Fig. 3.8. Other pertinent data pertaining to this shot are listed in Table 3.9. A precursor was recorded on both blast lines. The number of gages on the smoke line unfortunately were limited.

The same degree of success was not obtained on the dynamic pressure measurements records as on the pressure-time records. An overstressing of the total pressure capsules caused most of the trouble. A permanent displacement in the diaphragm caused a zero shift which tended to make the record questionable. The same procedure in reading and reducing the records from an overstressed capsule was used as described for Shot 3. Two gage mounts failed, one of the gages produced a record and the other failed to give any information. Fig. 3.9 shows the dynamic pressure versus distance curve. Table 3.10 gives the stations, ground range, static overpressure and total overpressure for the four stations instrumented on this shot.

3.6 SHOT 6

The pressure values from the two blast lines are tabulated in Table 3.11 and are plotted in Fig. 3.10. Two curves were drawn, one for the desert line and one for the asphalt line.

All dynamic pressure gages functioned and good pressure-time records were obtained. The arrival times on these gages check very well with the arrival times on the pressure-time gages. The dynamic pressure versus ground distance curve is presented in Fig. 3.11. There were no mount failures on this shot. At Station 6 where there were two dynamic pressure gages at the same elevation with similar type recording elements, a good comparison was obtained. The difference between the two values for dynamic pressure was 0.1 psi as shown in Table 3.12. In a few cases there was apparently insufficient stylus pressure causing an intermittent trace.

3.7 SHOT 8

A plot of the pressure-distance curve is given in Fig. 3.12 Pressure-time records were obtained on 13 of the 14 gages used on this shot. The records had very thin traces which increased the reading accuracy.

Stations, ground distance, static overpressure, total overpressure, and dynamic pressure are listed in Tables 3.13 and 3.14. The curve for dynamic pressure versus ground distance was plotted and is presented in Fig. 3.13. All mounts were in good condition after the shot and pressure-time records were obtained for both static and total overpressure at each station.

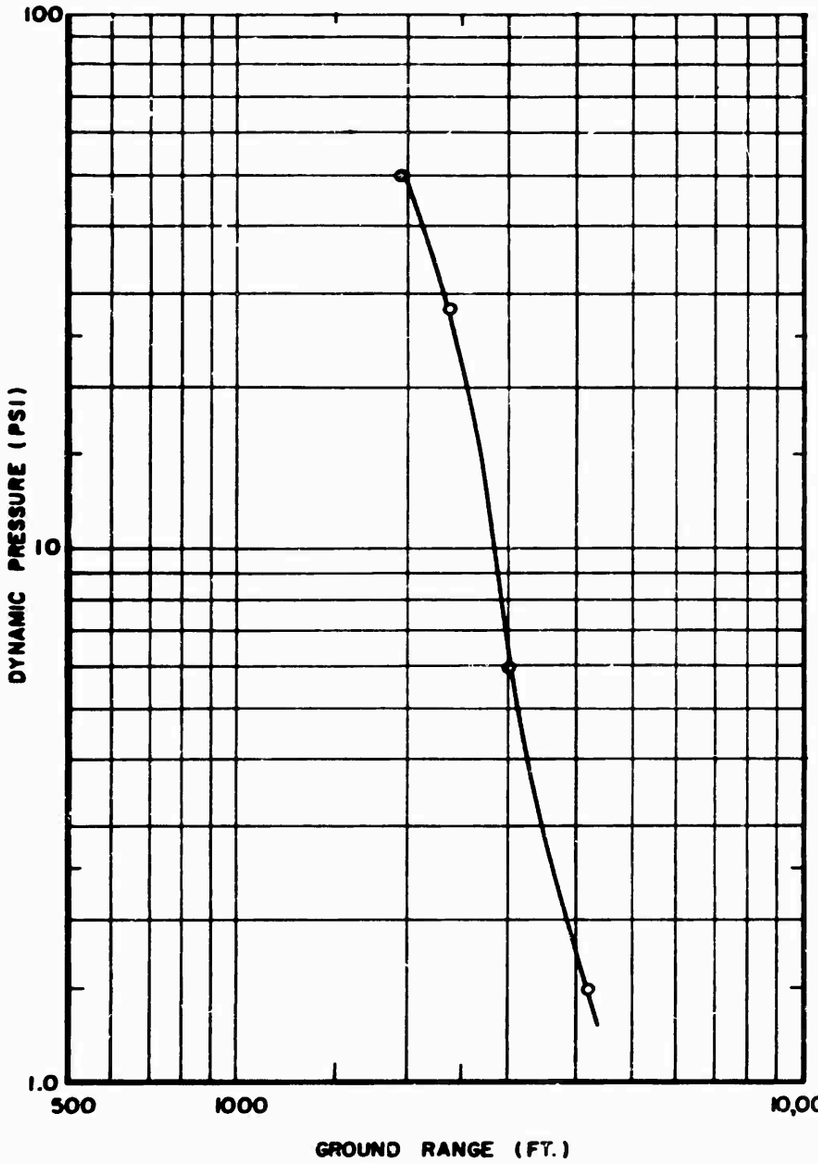

Fig. 3.7 Peak Dynamic Pressure versus Ground Range For Shot 4 (As Observed)

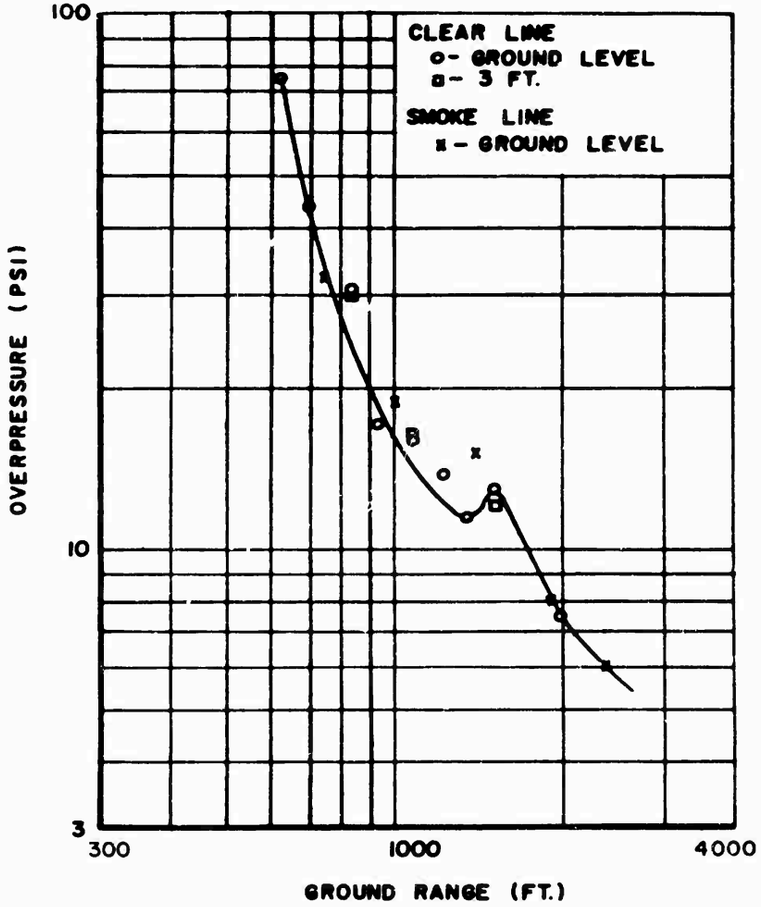

Fig. 3.8 Peak Overpressure versus Ground Range For Shot 5 (As Observed)

TABLE 3.11 Pressure-time Gage Results for Shot 6

Station	Ground Range	Peak Overpressure	Arrival Time	Positive Duration
	(ft)	(psi)	(sec)	(sec)
		DESERT BLAST LINE		
2	1080	19.2	0.265	0.27
3	1360	12.0	0.295	0.38
5	1600	10.4	0.525	0.41
6	1800	12.2	0.515	0.36
7	2000	11.2	0.765	0.44
8	2300	9.4	1.005	0.47
9	2550	7.4	1.145	0.52
10	2900	5.8	1.485	0.58
11	3810	4.5	2.185	0.68
		ASPHALT BLAST LINE		
2	1080	23.7	0.185	0.33
3	1360	12.2	0.245	0.43
5	1600	7.7	0.475	0.51
6	1800	6.2	0.415	0.47
7	2050	6.6	0.735	0.53
8	2300	8.0	0.905	0.51
9	2550	9.3	1.125	0.57
10	2900	5.5	1.485	0.57
11	3810	4.0	2.735	0.68

TABLE 3.12 Dynamic Pressure Gage Results for Shot 6

Station	Ground Range	Peak Static Overpressure	Peak Total Overpressure	Peak Dynamic Pressure
	(ft)	(psi)	(psi)	(psi)
			DESERT BLAST LINE	
6A	1825	11.0	16.6	5.7
6B	1825	11.4	15.6	5.2
7	2000	10.7	16.0	5.5
8	2300	9.6	12.0	2.8
9	2550	7.3	9.5	2.0
			ASPHALT BLAST LINE	
6	1800	6.0	12.2	5.8
7	2050	5.1	6.9	1.9
8	2300	7.7	10.9	2.0
9	2550	7.8	9.8	1.0

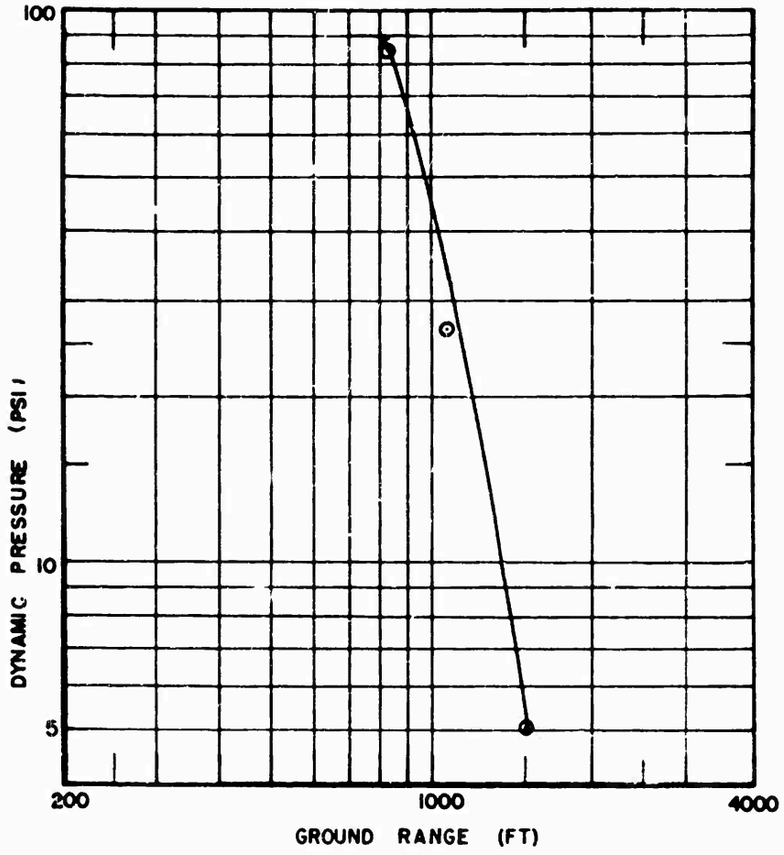

Fig. 3.9 Peak Dynamic Pressure versus Ground Range For Shot 5 (As Observed)

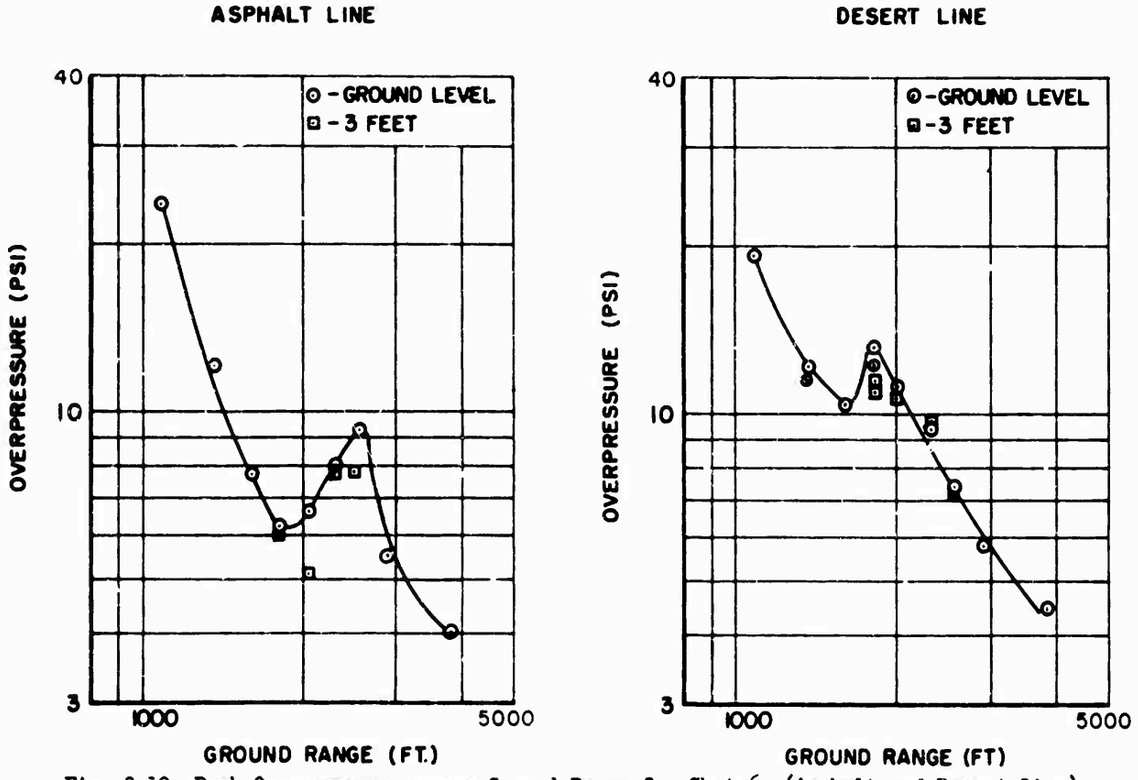

Fig. 3.10 Peak Overpressure versus Ground Range for Shot 6, (Asphalt and Desert Line), (As Observed)

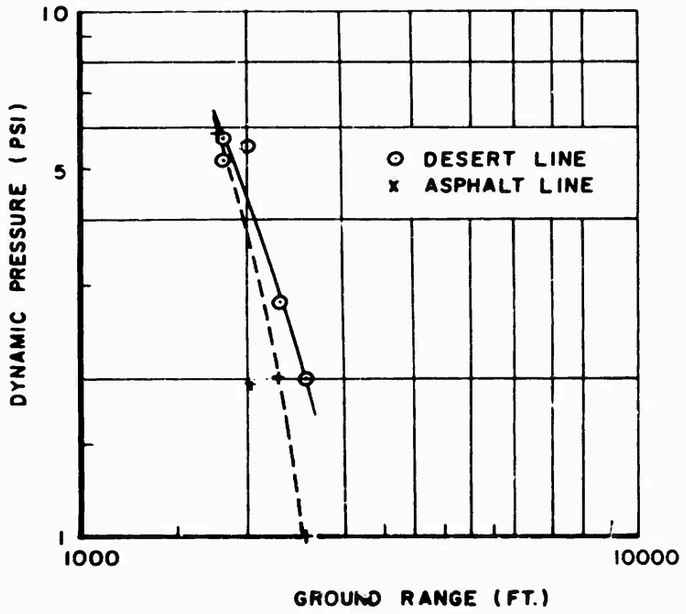

Fig. 3.11 Peak Dynamic Pressure versus Ground Range For Shot 6, Asphalt and Desert Line, (As Observed)

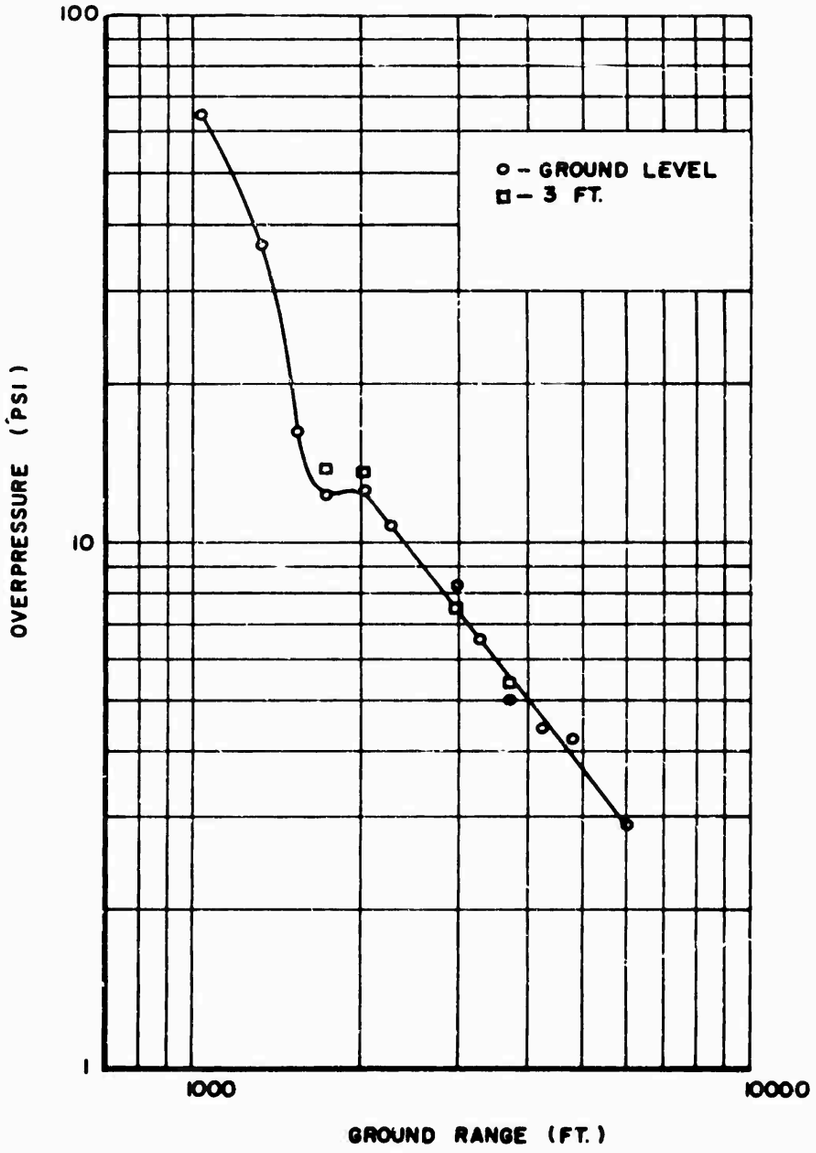

Fig. 3.12 Peak Overpressure versus Ground Range For Shot 8 (As Observed)

TABLE 3.13 Pressure-time Gage Results for Shot 8

Station	Ground Range	Peak Overpressure	Arrival Time	Positive Duration
	(ft)	(psi)	(sec)	(sec)
0	1030	64.3	0.195	0.28
1*	1330	36.8	*	*
2	1530	16.2	0.380	0.35
3	1730	12.3	0.515	0.44
5	2040	12.5	0.735	0.47
6	2270	10.8	0.845	0.45
7**	2650	**	**	**
8	2960	8.3	1.355	0.67
9	3250	6.5	-	0.46
10	3700	5.0	1.895	0.81
10A	4200	4.4	2.005	0.78
11	4800	4.2	2.735	-
12	6000	2.9	3.805	-
1.14***	2730	10.1	1.176	0.63

* Questionable; poor record ** Gage did not run;no record
*** Station off main blast line; see Figure 2.8 for location

TABLE 3.14 Dynamic Pressure Gage Results for Shot 8

Station	Ground Range	Peak Static Overpressure	Peak Total Overpressure	Peak Dynamic Pressure
	(ft)	(psi)	(psi)	(psi)
3	1730	13.8	28.0	16.0
5	2040	13.6	17.5	5.5
8	2960	7.5	9.1	1.5
*	3700	5.4	6.0	.8
1.14**	2730	7.0	15.3	8.3

* Questionable record - overshoot on total pressure
** Station off main blast line - See Figure 2.8 for location

TABLE 3.15 Pressure-time Gage Results for Shot 9

Station	Intended Ground Range	Corrected Ground Range	Peak Overpressure	Arrival Time	Positive Duration
	(ft)	(ft)	(psi)	(sec)	(sec)
1	0	117	77.0	0.181	-
2	350	389	46.1	0.131	0.10
3	500	534	37.2	0.158	0.21
4	750	780	21.4	0.309	-
5*	1000	1029	13.0	0.404	*
6	1250	1277	11.9	0.382	0.20
7	1500	1527	10.1	0.638	0.31
8	1750	1776	8.2	-	0.35
9	2000	2026	7.5	1.125	0.41
10	2500	2525	5.5	0.847	0.32
11	3000	3025	4.8	1.428	0.46

* Gage initiated by shock

3.8 SHOT 9

Peak overpressures were obtained from gages at all stations. Two of the pressure-time records were lost. One gage apparently was initiated by shock blast and the other had a loose stylus pen. Table 3.15 gives the tabulated results and Fig. 3.14 is a plot of the pressure distance curve. The recording speed of 10 rpm used in this shot was satisfactory. For low yield bursts, this speed gives a more reliable pressure-time record than the 3 rpm speed.

Dynamic-pressure time records were recorded with speeds of 40 rpm. The time resolution with these speeds is very good. The measured pressure points plotted in Fig. 3.15 require a correction factor to take into account the angle of incidence of the shock blast with gage orientation, particularly, for the gages closest to the ground zero.

3.9 SHOT 11

The results from Shot 11 are summarized in Table 3.17 and 3.18. At Station 2, the gage range was apparently too large and the value recorded is questionable. On this particular record the base line was approximately 5 mils in thickness and thus could have concealed the small deflection resulting from the shock. A large amount of hash was present on the record at Station 1 and only a peak pressure record was recorded at 2,600 feet. The remaining eight pressure-time gages have good pressure-time records. The pressure versus distance curve is presented in Fig. 3.16.

All the dynamic pressure gages gave pressure-time histories. The peak dynamic pressure versus distance curve is shown in Fig. 3.17. There was excessive hash and high frequency oscillation on the records at 880 and 1,050 feet.

3.10 SHOT 12

Of the 17 gages used on the three blast lines all gave pressure-time records except Station 1 on the asphalt line which was covered with asphalt prior to shot time and the value is questionable. The gage at 1500 feet on the desert line recorded small deflections, but since the trace was thin, the peak pressure could be read with a high degree of accuracy. A definite precursor was present on the desert line at all stations except the most distant station at 4500 feet. On the other two lines a disturbance of the wave was noted at all stations. A lower pressure was recorded on the desert line than on the other two blast lines. In Table 3.19 the overpressure, arrival times, and positive durations for the three lines are summarized. The curves for overpressure versus distance for the three lines are shown in Fig. 3.18.

The dynamic pressure gages gave 100 percent results with some high frequency oscillations present on the total overpressure records.

TABLE 3.16 Dynamic Pressure Gage Results for Shot 9

Station	Intended Ground Range (ft)	Corrected Ground Range (ft)	Peak Static Overpressure (psi)	Peak Total Overpressure (psi)	Peak Dynamic Pressure
2	350	389	43.1	51.7	30.0
4	750	780	21.1	35.2	19.0
4*	750	780	19.5	25.1	8.0
7	1500	1527	10.6	13	3.0
9	2000	2026	6.9	8.6	1.7

* 10 ft mount

TABLE 3.17 Pressure-time Gage Results for Shot 11

Station	Ground Range (ft)	Peak Overpressure (psi)	Arrival Time (sec)	Positive Duration (sec)
1	250	190.8	-	0.07
2	500	59.3	-	0.11
3	800	16.0	0.226	0.23
4	880	15.8	0.189	0.23
5	1050	13.8	0.398	0.27
6	1200	12.1	0.398	0.26
7	1400	9.0	0.577	0.26
8	1550	8.0	0.664	0.27
9	1750	6.8	0.829	0.30
10	1970	5.5	0.954	0.32
11	2600	5.0	-	-

TABLE 3.18 Dynamic Pressure Gage Results for Shot 11

Station	Ground Range (ft)	Peak Static Overpressure (psi)	Peak Total Overpressure (psi)	Peak Dynamic Pressure (psi)
4	880	14.2	30.7	17.3
5	1050	13.3	17.5	6.4
7	1400	8.4	11.3	2.2
10	1970	5.0	6.0	1.0

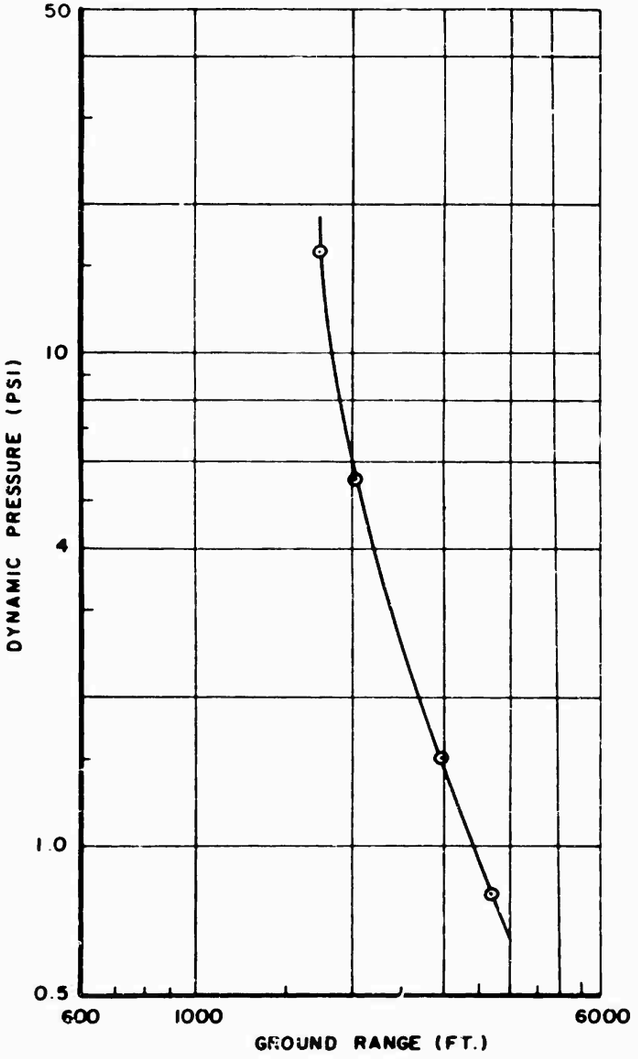

Fig. 3.13 Peak Dynamic Pressure versus Ground Range For Shot 8 (As Observed)

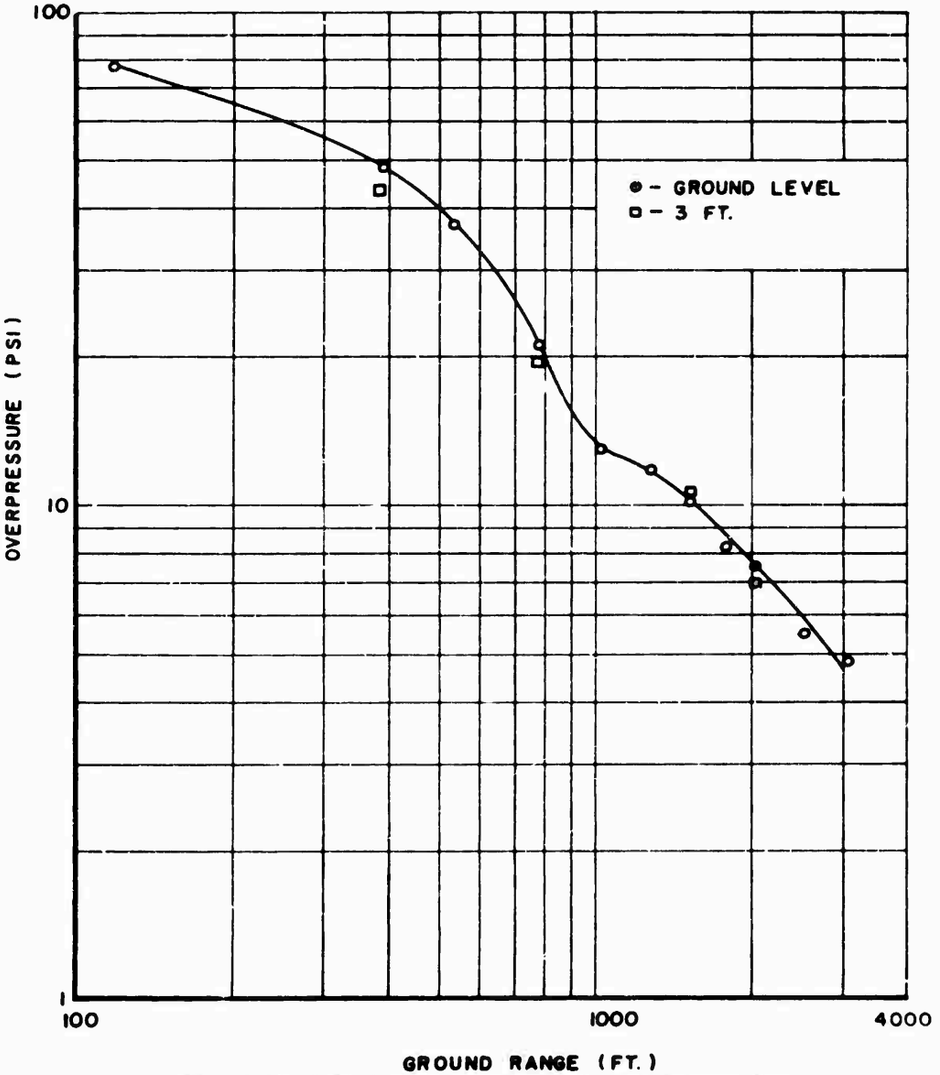

Fig. 3.14 Peak Overpressure versus Ground Range For Shot 9 (As Observed)

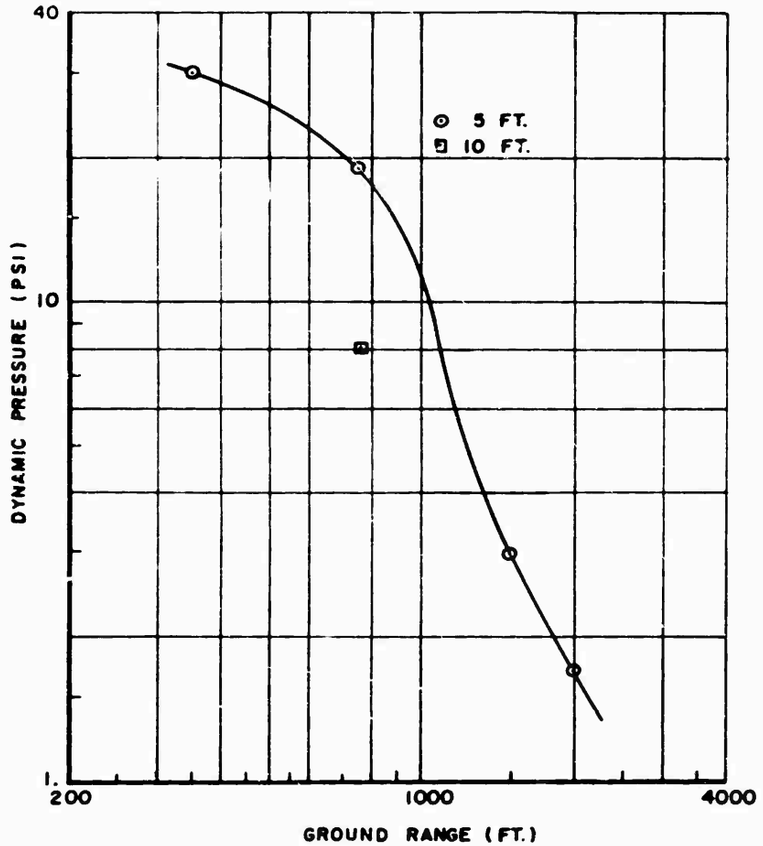

Fig. 3.15 Peak Dynamic Pressure versus Ground Range For Shot 9 (As Observed)

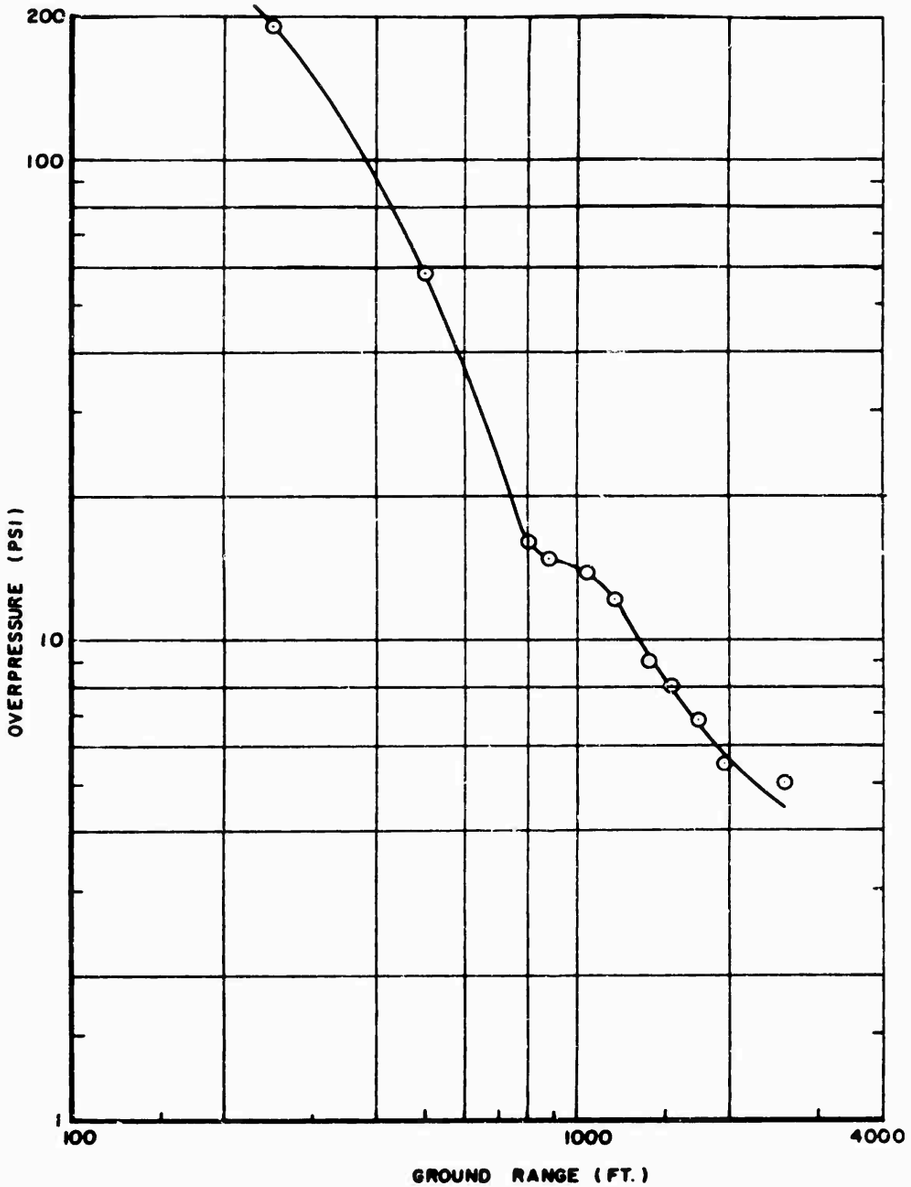

Fig. 3.16 Peak Overpressure versus Ground Range For Shot 11 (As Observed)

TABLE 3.19 Pressure-time Gage Results for Shot 12

Station	Ground Range (ft)	Peak Overpressure (psi)	Arrival Time (sec)	Positive Duration (sec)
		ASPHALT LINE		
1*	2000	21.3	-	-
2	2250	10.5	0.545	0.77
3	2500	8.0	0.615	0.82
4	2750	5.8	0.805	0.98
5	3000	5.8	0.965	1.03
		DESERT LINE		
1	1500	27.7	0.225	0.42
5	2000	9.8	0.395	0.73
6	2250	5.9	0.515	0.79
7	2500	7.0	0.725	0.77
8	2750	7.3	-	0.67
9	3000	7.9	1.065	0.76
10	4500	4.7	2.355	0.89
		WATER LINE		
1	2000	25.7	0.525	0.51
2	2250	12.0	0.695	0.58
3	2500	12.7	0.845	0.61
4	2750	13.0	0.965	0.56
5	3000	10.0	1.205	0.68

* Peak Pressure only; gage did not run

TABLE 3.20 - Dynamic Pressure Gage Results for Shot 12

Station	Ground Range (ft)	Peak Static Overpressure (psi)	Peak Total Overpressure (psi)	Peak Dynamic Pressure (psi)
		ASPHALT BLAST LINE		
1	2000	14.7	31.6	16.1
2	2250	10.6	21.0	10.6
3	2500	8.2	17.4	8.5
3*	2500	7.3	13.2	6.8
4	2750	6.4	12.6	6.4
5	3000	5.6	7.4	1.7
		DESERT BLAST LINE		
5	2000	13.6	59.0	40.0
6	2250	14.3	34.6	20.0
7	2500	9.0	20.0	11.3
7*	2500	8.7	21.0	12.4
8	2750	7.7	15.8	7.7
9	3000	8.0	9.0	1.1
		WATER BLAST LINE		
1	2000	24.1	50.3	35.0
1A**	2000	**	**	15.2
2	2250	14.2	39.0	28.3
3	2500	9.8	20.1	10.0
3*	2500	14.9	18.0	5.4
4	2750	11.6	16.6	4.0
5	3000	10.5	13.2	2.6
5A**	3000	**	**	2.3

* 10 ft Mount ** Differential pressure capsule

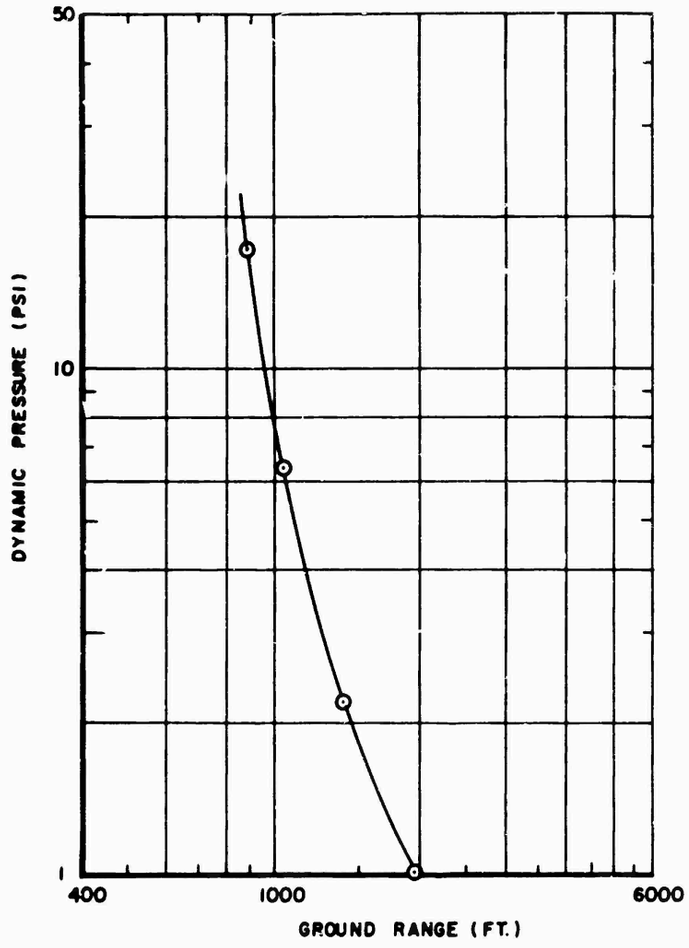

Fig. 3.17 Peak Dynamic Pressure versus Ground Range For Shot 11, (As Observed)

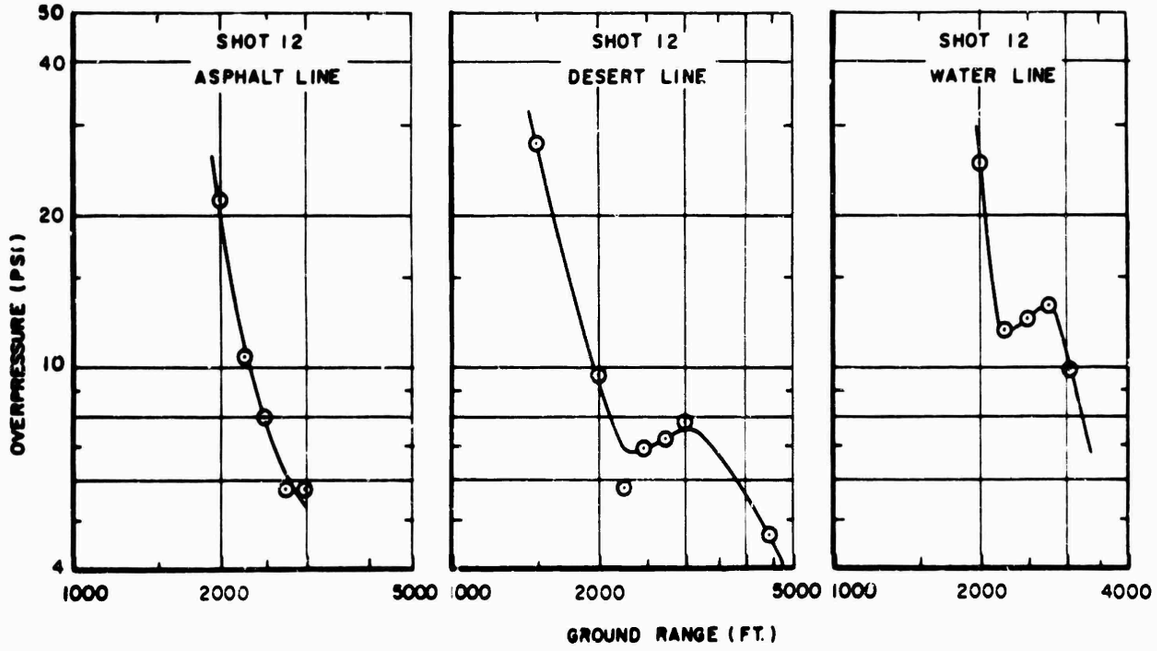

Fig. 3.18 Peak Overpressure versus Ground Range for Shot 12, Asphalt, Desert, and Water Line, (As Observed)

Where two gages were placed at the same station very similar records were obtained. The dynamic pressures were highest on the desert line. Four gage mounts failed but satisfactory records were obtained. The 3 foot mount at 2,250 feet on the water line was rotated backward slightly and as a result the total pressure value is questionable. The 10 foot mount at 2,500 feet on the water line was found rotated to the left rear with the guy wires cut or loose, and therefore, the gage total overpressure is questionable. On the desert line at 2,500 feet, the 3 foot mount was torn out of the ground by flying debris. The displacement record occurred after the major portion of the record was completed, and therefore the record is satisfactory. The guy wires on the 10 foot mount at the same station were cut and the mount was rotated backward slightly. The pressure data obtained on the three surfaces are given in Table 3.20, and the curves of dynamic pressure versus distance are shown in Fig. 3.19.

3.11 SHOT 13

The observed data on peak overpressure, shock arrival time and positive phase duration are given in Table 3.11. The positive durations at Stations 7 and 8 were questionable and have been omitted from the table of gage results. A high range capsule was used in the P_t gage at 1,520 feet and since a lower than expected pressure was experienced the results obtained at this location is questionable due to reading error. Eight of the nine P_t gages used on this shot functioned properly. The overpressure versus distance curve is presented in Fig. 3.20.

All dynamic pressure gages functioned and pressure-time records were obtained. Data from the q-gage records are given in Table 3.22. The dynamic pressure versus ground distance curve is presented in Fig. 3.21. All mounts were in good condition after the shot. A large amount of hash and oscillation was present on the three closest stations to ground zero. The deflection was small on the 1700 foot station and also the recording stylus gave a very wide trace. These difficulties could cause a large reading error, and for this reason, there is some doubt in the pressure value given at the first station.

3.12 SHOT 14

A total number of 32 P_t-gages were used on the two blast lines. The layout of the two blast lines is given in Fig. 2.13. A circle of gages was instrumented on this shot to supplement the results of Shot 12. The results from the circle of gages is presented in Appendix B. The results from the two blast lines are tabulated in Table 3.13 and are plotted in Fig. 3.22. These gages were placed in the ground approximately four weeks before the shot and a large percentage of pressure-time records were obtained. Twenty-two gages on the blast lines gave good pressure-time records. Of the ten remaining gages only three failed to give any information. This complete fail-

TABLE 3.21 Pressure-time Gage Results for Shot 13

Station	Ground Range (ft)	Peak Overpressure (psi)	Arrival Time (sec)	Positive Duration (sec)
2	1520	25.0	0.275	0.43
3	1700	15.0	0.365	0.52
5	2050	11.5	0.515	0.73
6	2300	10.0	0.645	0.83
7	2650	9.6	0.805	-
8*	3000	9.5	-	-
9	3300	8.6	1.325	0.80
10	3700	6.8	1.585	0.90
11	4900	4.8	2.525	1.01

* Peak Pressure only; gage did not run

TABLE 3.22 Dynamic Pressure Gage Results for Shot 13

Station	Ground Range (ft)	Peak Static Overpressure (psi)	Peak Total Overpressure (psi)	Peak Dynamic Pressure (psi)
3*	1700	28.1	56.3	26.0
5	2050	21.0	57.0	30.0
7	2650	13.1	30.7	17.0
10	3700	6.7	9.4	2.2

* Total Pressure Capsule Overstressed

TABLE 3.23 - Pressure-time Gage Results for Shot 14

Station	Ground Range (ft)	Peak Overpressure (psi)	Arrival Time (sec)	Positive Duration (sec)
ASPHALT BLAST LINE				
1	900	197.7	0.141	0.17
2**	1360	40.0	-	-
3	1800	15.2	0.283	0.78
4	2000	10.4	0.324	0.86
5	2250	8.2	0.441	0.95
6	2300	7.7	-	1.01
7	2400	6.3	0.580	0.99
8	2550	7.4	0.628	0.94
9	2700	7.0	0.707	0.95
10	2800	5.8	0.739	0.97
11	2900	5.5	0.943	0.95
12	3000	5.5	0.916	0.92
13**	3100	5.1	0.916	0.92
14*	3200	-	-	-
15**	3800	7.6	-	-
16	4500	6.3	2.102	1.06
DESERT BLAST LINE				
1	900	142	0.124	-
2*	1360	-	-	-
3**	1800	15.6	-	-
4	2000	7.5	0.412	0.88
5	2200	5.4	-	0.50
6	2300	8.6	0.56[illegible]	0.91
7	2400	6.6	0.599	0.98
8*	2600	-	-	-
9	2700	6.0	0.756	0.99
10	2800	6.0	0.792	0.98
11	2900	6.2	-	-
12	3000	6.7	1.019	1.08
13	3100	6.4	1.067	0.99
14**	3200	6.1	-	-
15	3800	5.8	1.686	0.99
16	4500	4.3	2.179	1.06

* No readable record

** Peak value only; gage did not run or started with shock

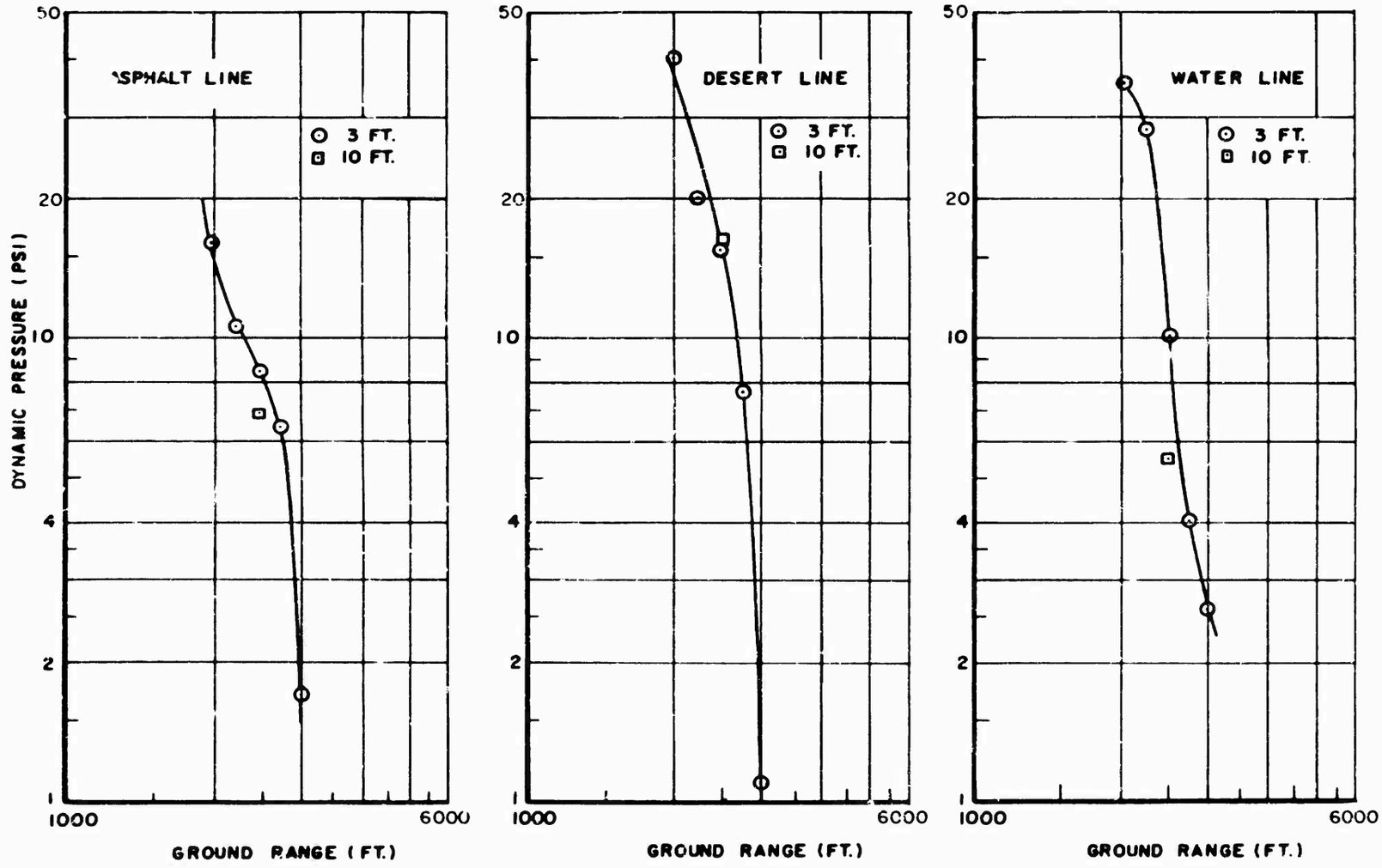

Fig. 3.19 Peak Dynamic Pressure versus Ground Range for Shot 12, Asphalt, Desert, and Water Line, (As Observed)

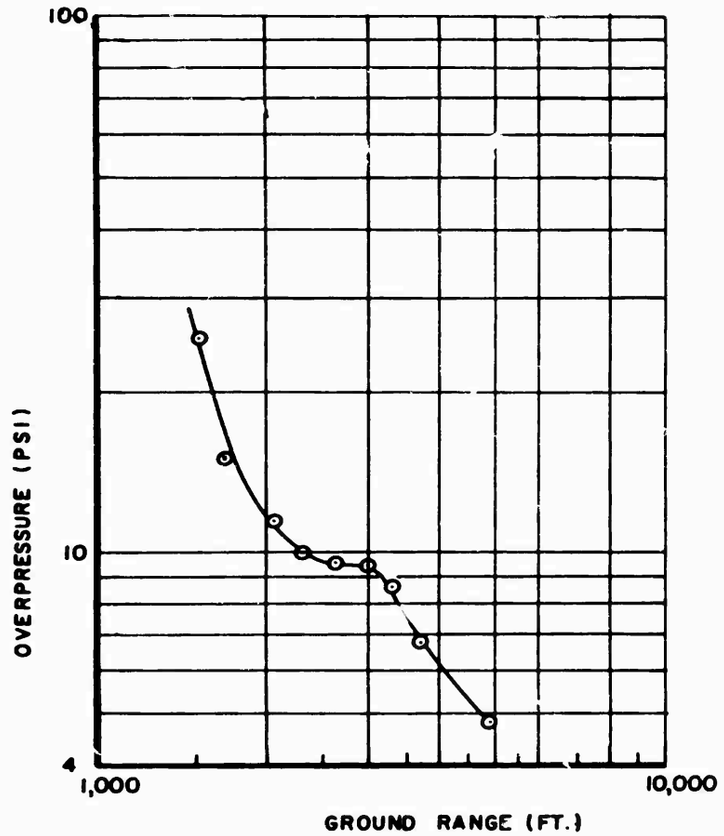

Fig. 3.20 Peak Overpressure versus Ground Range For Shot 13, (As Observed)

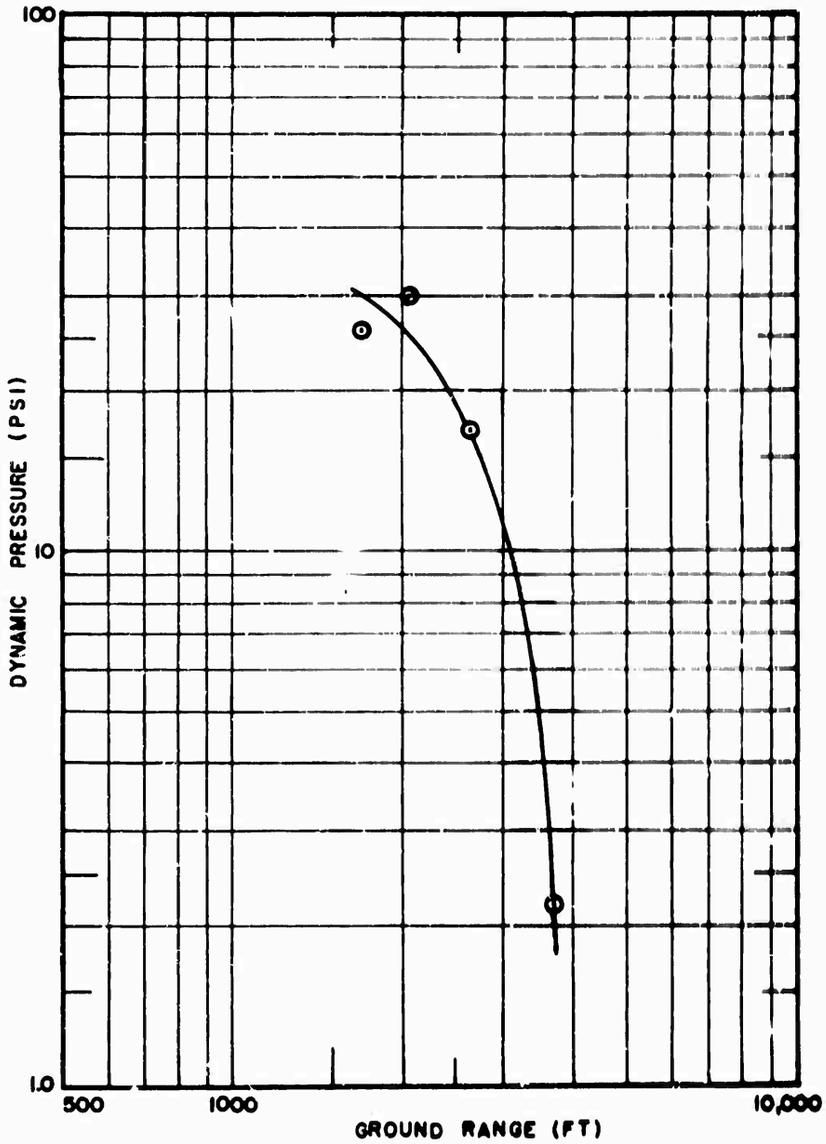

Fig. 3.21 Peak Dynamic Pressure versus Ground Range For Shot 13, (As Observed)

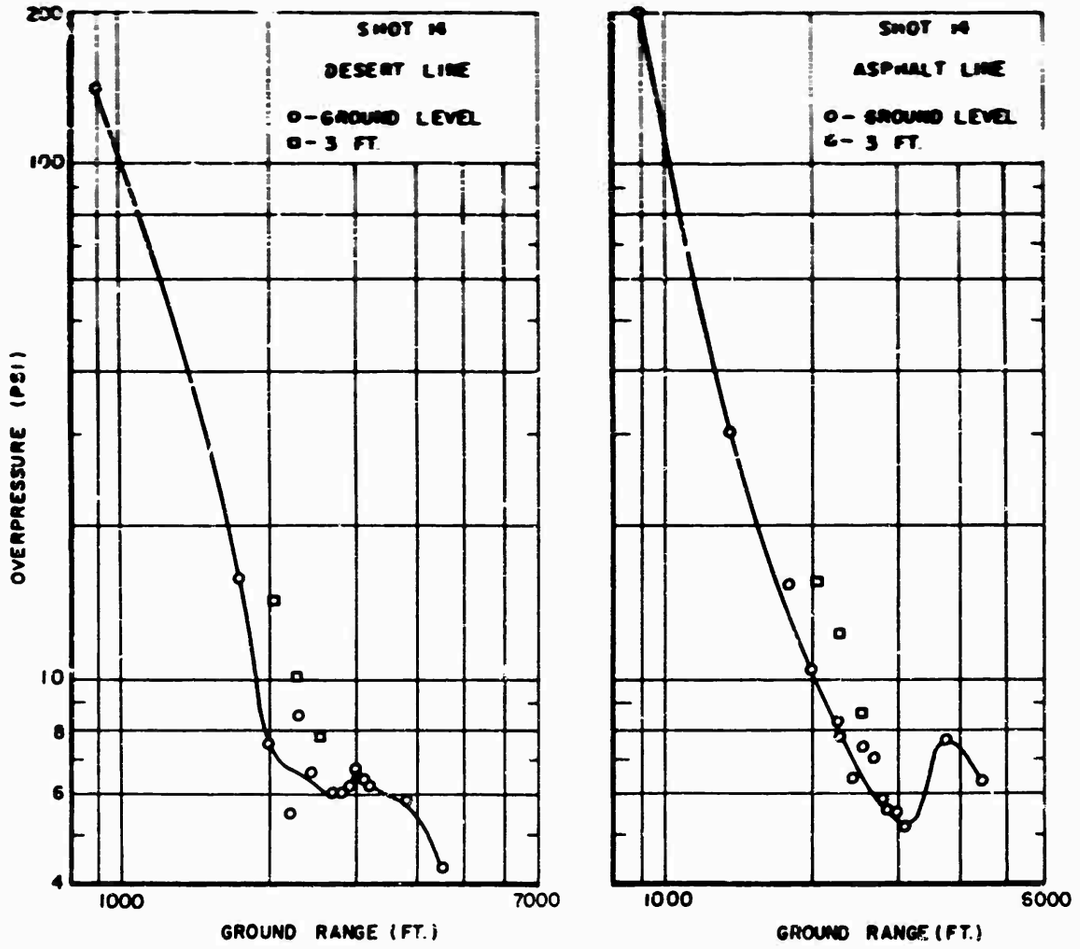

Fig. 3.22 Peak Overpressure versus Ground Range for Shot 14, Desert and Asphalt Line (As Observed)

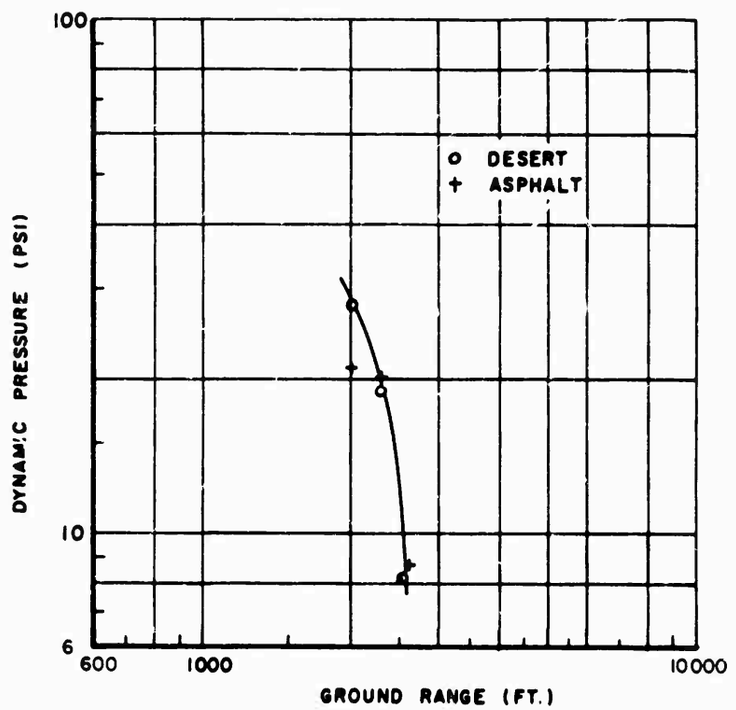

Fig. 3.23, Peak Dynamic Pressure versus Ground Range for Shot 14, (As Observed)

TABLE 3.24 Dynamic Pressure Gage Results for Shot 14

Station	Ground Range (ft)	Peak Static Overpressure (psi)	Peak Total Overpressure (psi)	Peak Dynamic Pressure (psi)
ASPHALT BLAST LINE				
4	2000	15.7	37.4	21.0
6*	2300	12.3	36.1	20.5
8	2550	8.6	19.2	8.7
DESERT BLAST LINE				
4**	2000	12.0	31.5	28.0
6**	2300	10.0	29.3	19.0
8	2600	7.8	17.6	8.2

* Gage Mount Bent Slightly
** Gage Mount Blown Out of Mount Hole

ure was caused by dust and sand completely covering the gage prior to shot time.

The same degree of success was not obtained on the dynamic pressure measurements as on the pressure-time records. The tabulated results are shown in Table 3.24. The gage mounts at five of the nine stations failed, as a result the total pressure values are questionable. Three of the gage mounts were blown out of the ground and the other two were bent back. The bent mounts both occurred on the asphalt line and the three that were blown out were on the Desert blast line. At 1800 feet on the desert the gage and mount was displaced approximately 30 feet. The dynamic pressure versus ground distance curve is presented in Fig. 3.23.

Chapter 4
DISCUSSION

The overpressure-time and dynamic pressure-time gages performed satisfactorily on all shots, and their ease of installation and recovery proved ideal for the instrumentation requirements for Operation Teapot. Overpressure-time and dynamic pressure-time gage exposure provided data on every shot, except Shot 7 (which was not instrumented). Although additional gages would have illuminated uncertain sections in the pressure distance curves, the data permitted the construction of curves for overpressure and dynamic pressure versus distance on nearly all shots instrumented. Because of the difficulties encountered in measuring dynamic pressure, the reliability of the dynamic pressure-distance curves are somewhat uncertain. From the data gathered, it was also possible to construct curves for time of arrival vs distance, as well as positive-phase duration versus distance.

The scaling factors used for reducing the data to 1 KT at sea level or A-Scaling, were the Standard Sachs scaling factors,

Pressure: $S_p = 14.7/P_o$

Distance: $S_d = (P_o/14.7)^{1/3}(1/W)^{1/3}$

Time: $S_t = (T_o + 273/293)^{1/2} (P_o/14.7)^{1/3}(1/W)^{1/3}$

Table 4.1 lists the computed scale factors as well as other pertinent information for shots of interest.

4.1 PEAK OVERPRESSURE VERSUS GROUND RANGE

The A-scaled values of measured peak overpressure versus distance are presented in Figs. 4.1 through 4.10. For shots with more than one blast line, the values of pressure were plotted on the same figure. Included in these same figures for comparison purposes, are values of the ideal pressure (Porzel) (Reference 4) and the value from the height of burst charts in TM 23-200 (Reference 2) for the good and the poor surface conditions. In other figures, plots were made of the shots at essentially the same scaled height of burst. Comparisons are also made of shots with similar surface conditions. Curves from previous operations were plotted to compare with the measured peak values obtained from one of the shots of this operation.

The values of pressure obtained on Shot 12 over the asphalt, desert, and water surfaces are shown in Fig. 4.1. A precursor was definitely

evident on the asphalt and desert line. On the water line, there is a possibility of a precursor existing; however, the distortions in the pressure-time waveform could result from crossover effects or loading of the shock wave due to water and sand. Inspection of the waveforms obtained over the desert surface shows the pressure decays to zero pressure less rapidly than pressures on the asphalt surface (See Figs. E.48 and E.49). This is particularly true at closer stations to ground zero. The peak overpressures, on the other hand, are less at these stations on the desert surface than on the asphalt surface. The pres-

TABLE 4.1 Summary of Shot Data

Shot	Yield	Height of Burst (ft)	A-Scaled Height of Burst	P_o	T_o	S_p	S_d	S_t
1	1.16	761	682.1	846	-6.6	1.197	0.8963	0.8546
2	2.39	300	213.4	871	-4.2	1.163	0.7112	0.6812
3	6.85	300	150.0	868	3.3	1.167	0.5001	0.4857
4	43.0	500	134.8	854	5.83	1.186	0.2696	0.2630
5	3.61	300	186.1	872.8	7.0	1.161	0.6203	0.6064
6	7.76	500	240.2	871	5.0	1.163	0.4803	0.4679
8	14.2	500	195.1	854.1	11.2	1.186	0.3901	0.3842
9	3.16	739	474.8	849	12.6	1.193	0.6425	0.6343
10	3.3	32,607	14,831.1	222	-47.2	4.565	0.4090	0.3586
11	1.45	300	251.2	862.5	10.3	1.174	0.8374	0.8234
12	22	400	137.0	895.1	18.9	1.132	0.3425	0.3418
13	28.5	500	154.7	855.3	15.6	1.184	0.3094	0.3071
14	28.2	500	155.0	851	2.1	1.190	0.3100	0.3004

sures on the desert surface increase above that on the asphalt surface as distance from ground zero becomes greater. The pressure-distance curve for the asphalt line is depressed more than either the desert or water line curves and recovery of the precursor on the asphalt surface occurs at farther distances from ground zero.

In Fig. 4.2 the A-scaled pressure-distance curves are given for Shot 6 over the asphalt and desert surfaces. A precursor was formed over both surfaces. At the closest station to ground zero, pressure on the desert line is less than on the asphalt line, and as the distance increases, pressures on the desert line become greater. The pattern of wave forms on both surfaces are approximately similar.

The patterns of the pressure-distance curves similar to Shots 6 and 12 are also observed on Shot 14 over the asphalt and desert surfaces. As shown in Fig. 4.3, the pressure-distance curve over the asphalt surface for Shot 14 is depressed more than the curve over the desert surface and the precursor over the asphalt extends further from ground zero. In this shot a number of P_t-gages were placed at short intervals within the precursor zone to study more comprehensively the growth of

the pressure-time histories. Within this zone, between the scaled range from 600 feet to 1000 feet, peak overpressure values fluctuate as a function of distance. An examination of the pressure-time histories do not indicate obvious discrepancies in the peak pressure values recorded. These fluctuations may be part of the precursor phenomena. However, the fluctuations may be attributed to inherent errors of approximately ± 10 percent in data recording and reduction. The percent error quoted is about the variation of pressure within this zone.

The waveform patterns over the asphalt and desert surfaces between 2000 feet and 3000 feet (See Figs E.51 and E.52, desert surface and E.53 and E.54, asphalt surface) are approximately the same. Recovery of the precursor waveform to a steep rising blast wave over the asphalt surface results in peak overpressure higher than the values over the desert surface. This is observed for Shots 6 and 14.

The results of Shot 5, the clear line and the smoke line are shown in Fig. 4.4. A precursor was evident on both lines. Along the smoke line, the smoke screen extended from between 750 and 1000 feet out beyond 2400 feet. The smoke screen did not cover the first air blast station, 750 feet, on the smoke line. The remaining air blast stations on the smoke line were covered. The waveform pattern of the first smoke line station is similar to that on the clear line at 710 feet, (See Figs. E.36 and E.38). A more rapid recovery of the precursor is observed on the smoke line. The waveforms become steep-rising waves sooner on the smoke line than on the clear line. The smoke screen affected to some degree the formation of the precursor. Sine the thermal energy was reduced by the smoke screen (Reference 3), it can be stated that thermal energy influences the degree and extent of precursor formation.

The scaled pressure-distance curve of Shots 1 and 9 are given in Figs. 4.5 and 4.6,respectively. Peak values of pressure only were recorded on Shot 1 so it is not certain that a precursor formed. On the other hand, a precursor formed on Shot 9. The small depression of the pressure-distance curve along with a quick recovery of precursor waveforms to steep-rising waves imply that the precursor is not as pronounced as those shots with similar yield but lower height of burst. For the same yields but lower heights of bursts, the pressure-distance curves have greater depressions, and the front of waveforms to steep-rising waves do not recover as rapidly.

Fig. 4.7 presents the results of Shots 2, 5, 8 and 11. A precursor was formed on each of these shots. Of these four shots, Shot 8 was the largest yield detonated and Shot 11 was the lowest yield detonated. From the curve, the greatest lowering of pressure is on Shot 8, while the least lowering of pressure is on Shot 11. This indicates that the yield influences the precursor formation and the extent of lowering of overpressure. Of further interest is the fact that beyond a scaled range of about 900 feet or outside the precursor zone the majority of measured values of pressure are above the ideal overpressure-distance curve.

Curves of Shots 3, 4 and 12 (desert) are given in Figure 4.8. To

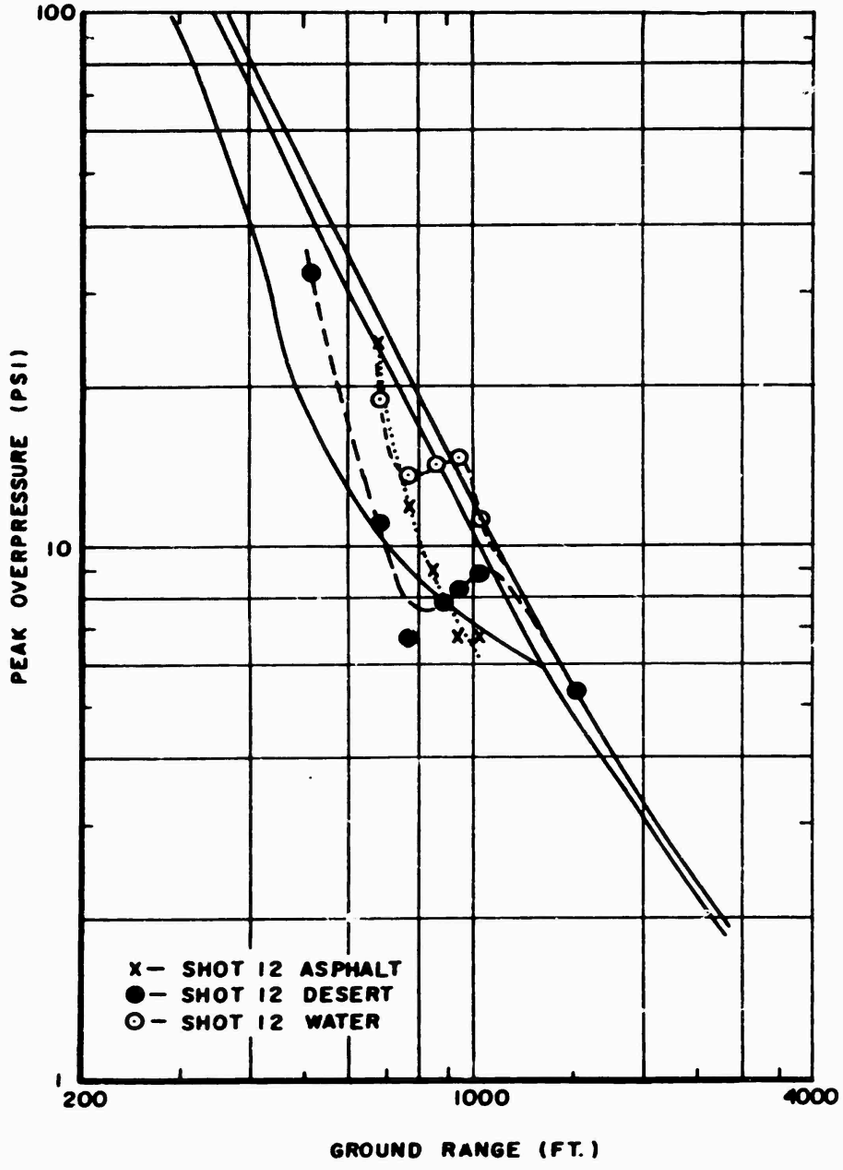

Fig. 4.1 Comparison of Peak Overpressure versus Ground Range for Shot 12, Asphalt, Desert and Water Lines. A-Scaled

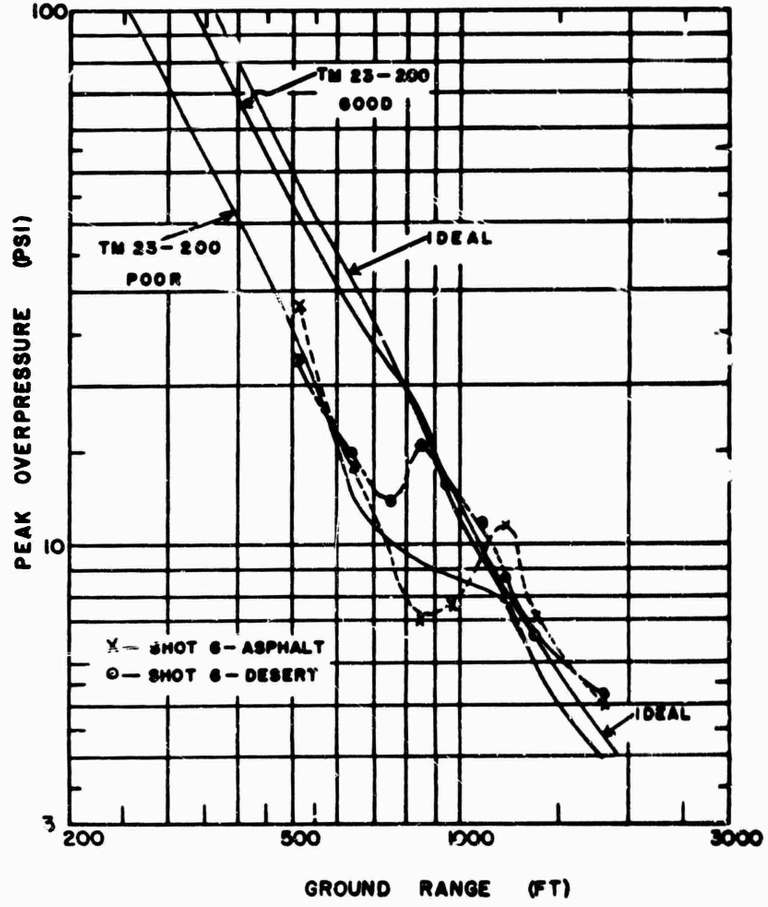

Fig. 4.2 Comparison of Peak Overpressure versus Ground Range for Shot 6, Asphalt and Desert Lines. A-Scaled

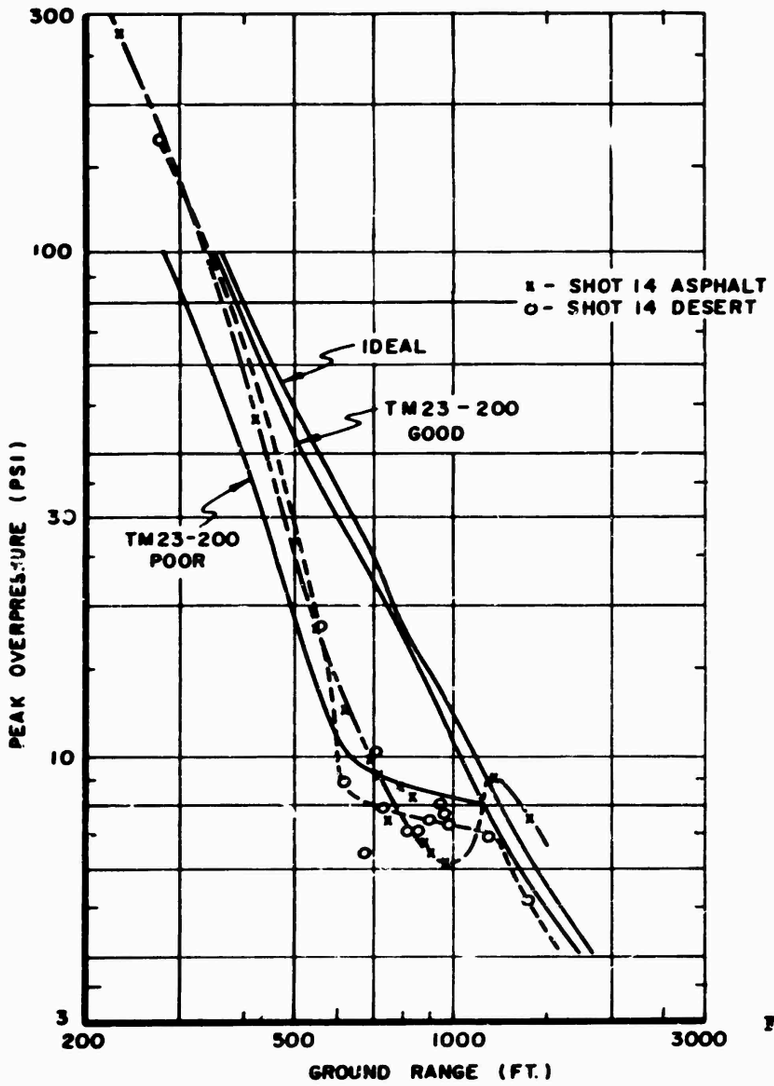

Fig. 4.3 Comparison of Peak Overpressure versus Ground Range for Shot 14, Asphalt and Desert Lines. A-Scaled

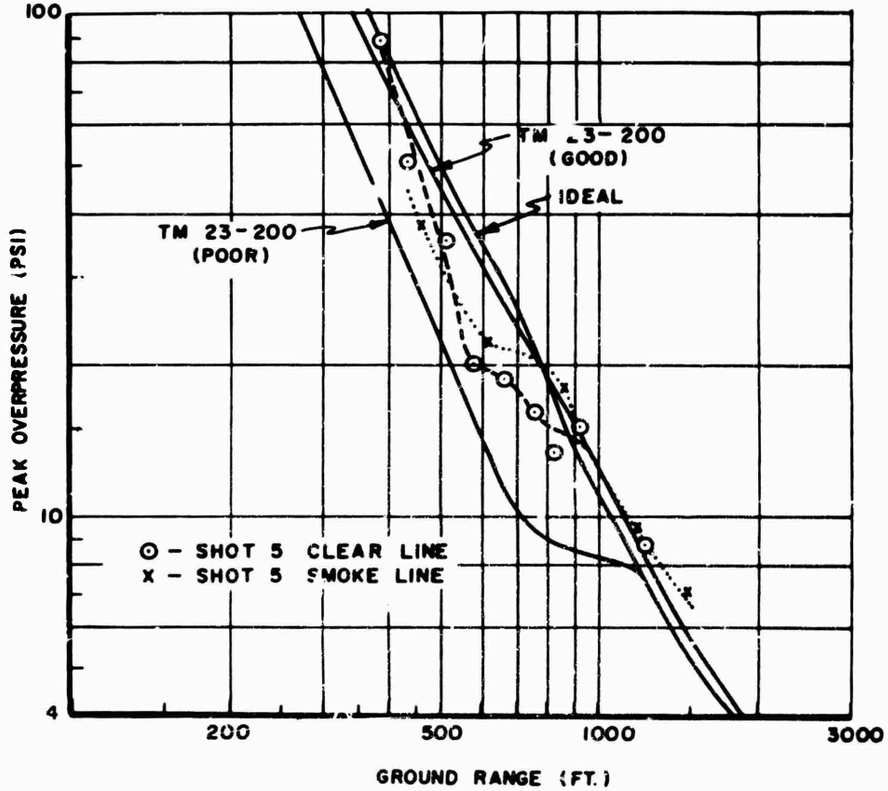

Fig. 4.4 Comparison of Peak Overpressure versus Ground Range for Shot 5, Clear and Smoke Line. A-Scaled

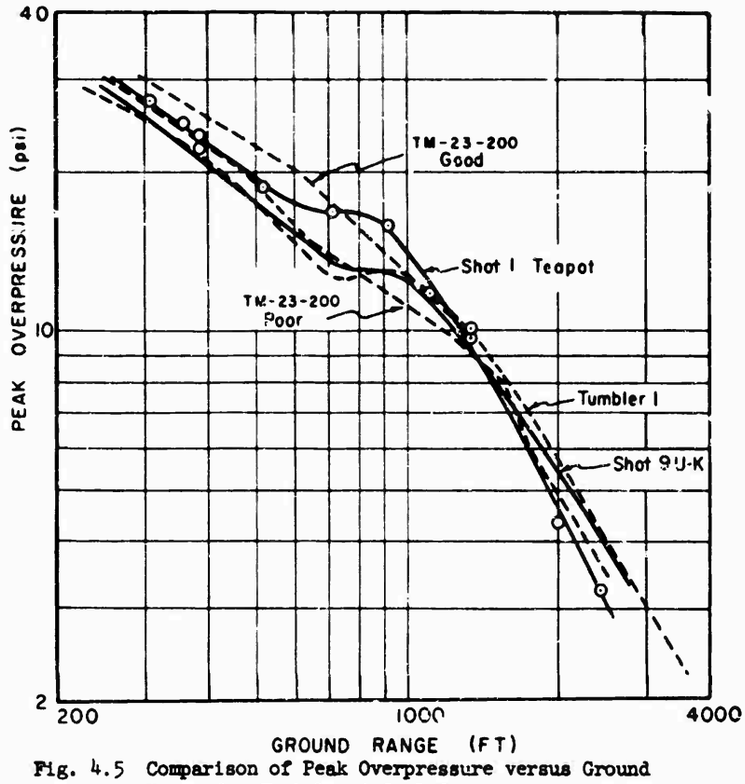

Fig. 4.5 Comparison of Peak Overpressure versus Ground Range for Shot 1. A-Scaled

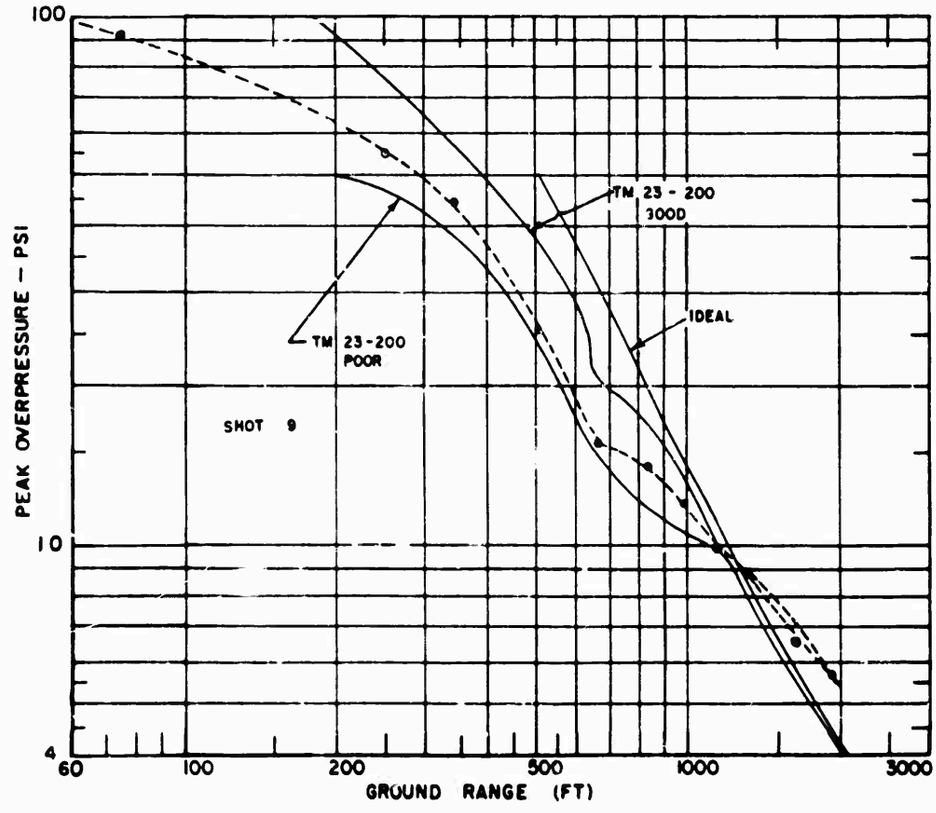

Fig. 4.6 Comparison of Peak Overpressure versus Ground Range for Shot 9. A-Scaled

follow the trend noted in the preceding paragraph the pressure-distance curve of Shot 4 (highest yield) should be below that of Shot 12 but the opposite is true. The curve of Shot 3 follows the trend and it is to be noted that Shot 4 when compared to the shots of the preceding paragraph has the greatest depression, it being the highest yield. The difference between Shot 4 and 12, although not too large, can possibly be attributed to the slight variation of the terrain features. Shot 4, as all of the other above shots, were detonated in the Yucca region, consisting of sand, rocks and vegetation. On the other hand, Shot 12 detonated in the Frenchman Flats region consisted of very fine particles of sand. This comparison may then imply that slight differences in terrain features will influence the precursor formation.

Further influence of yield on precursor formation is shown in the comparison of results of Shots 6, 12 and 14 over the desert and asphalt surfaces. The results are shown in Figs. 4.9 and 4.10 over the desert and asphalt surface, respectively. Shot 13 was the same scaled height of burst as Shot 14 and is included in Fig. 4.9. Except for Shot 13, both on the desert and asphalt surfaces the depression of the pressure-distance curves are greater for the higher yield weapons. No reason can be given for the discrepancy noted on Shot 13. For all practical purposes the conditions of Shot 13 and 14 were the same. The yields of both shots were the same and surface conditions were the same. Underneath the tower of Shot 13 was an asphalt pad like that of Shot 14 in the direction of the desert blast line. Hence, the data of Shot 13 can be suspect.

4.2 PEAK DYNAMIC PRESSURES VERSUS GROUND RANGE

The data on dynamic pressures as reported in this section are the peak values only. Whether this is the most meaningful way of presenting the data can be subject to much discussion, particularly when a considerable number of oscillations were present on the pressure records. The oscillations are believed to be part of the phenomena present and are real; hence, these should not be completely disregarded. However, the magnitudes of oscillations are local, and it would be questionable that at the same position in a lateral direction, similar values would be recorded.

It was stated that errors will result in dynamic pressure, because of the difficulty of superimposing the static pressure-time curves on the total pressure-time curves at corresponding times. When the errors were obvious, they were corrected. There was no problem with records that were free of high-frequency oscillations or where classical-type shock waves were obtained. Other sources of error resulted when the gage mount was knocked over or bent back. Although these values are questionable, they were still plotted. A summary of the gage mount failure is given in Table 4.2.

Furthermore, the values of dynamic pressure given in the curves were not corrected either for Mach compressibility or angle of orientation. All values reported in this section are for the 3-foot gage level.

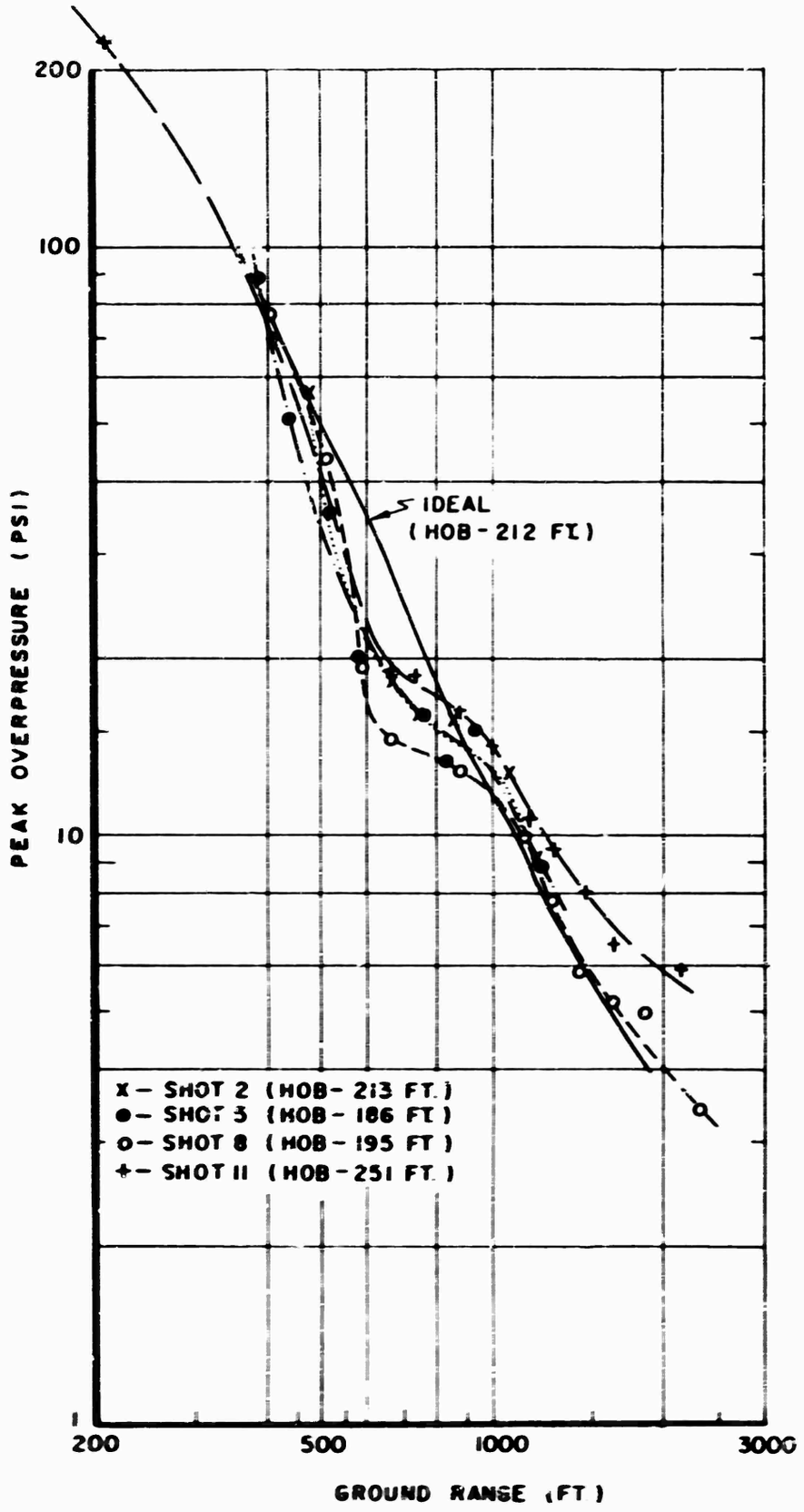

Fig. 4.7 Comparison of Peak Overpressure versus Ground Range for Shots 2, 5, 8 and 11. A-Scaled

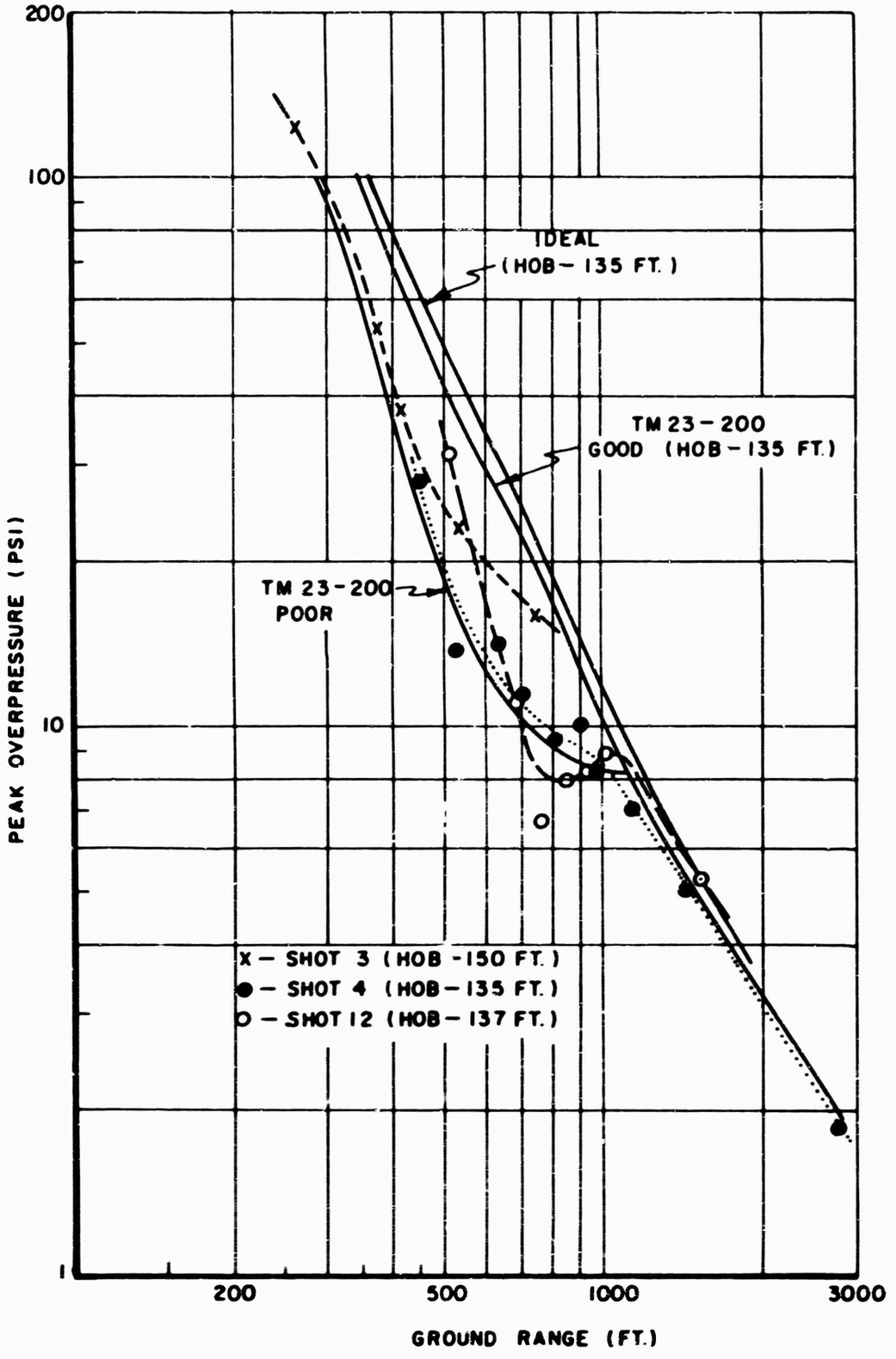

Fig. 4.8 Comparison of Peak Overpressure versus Ground Range for Shots 3, 4, and 12 (Desert) A-Scaled

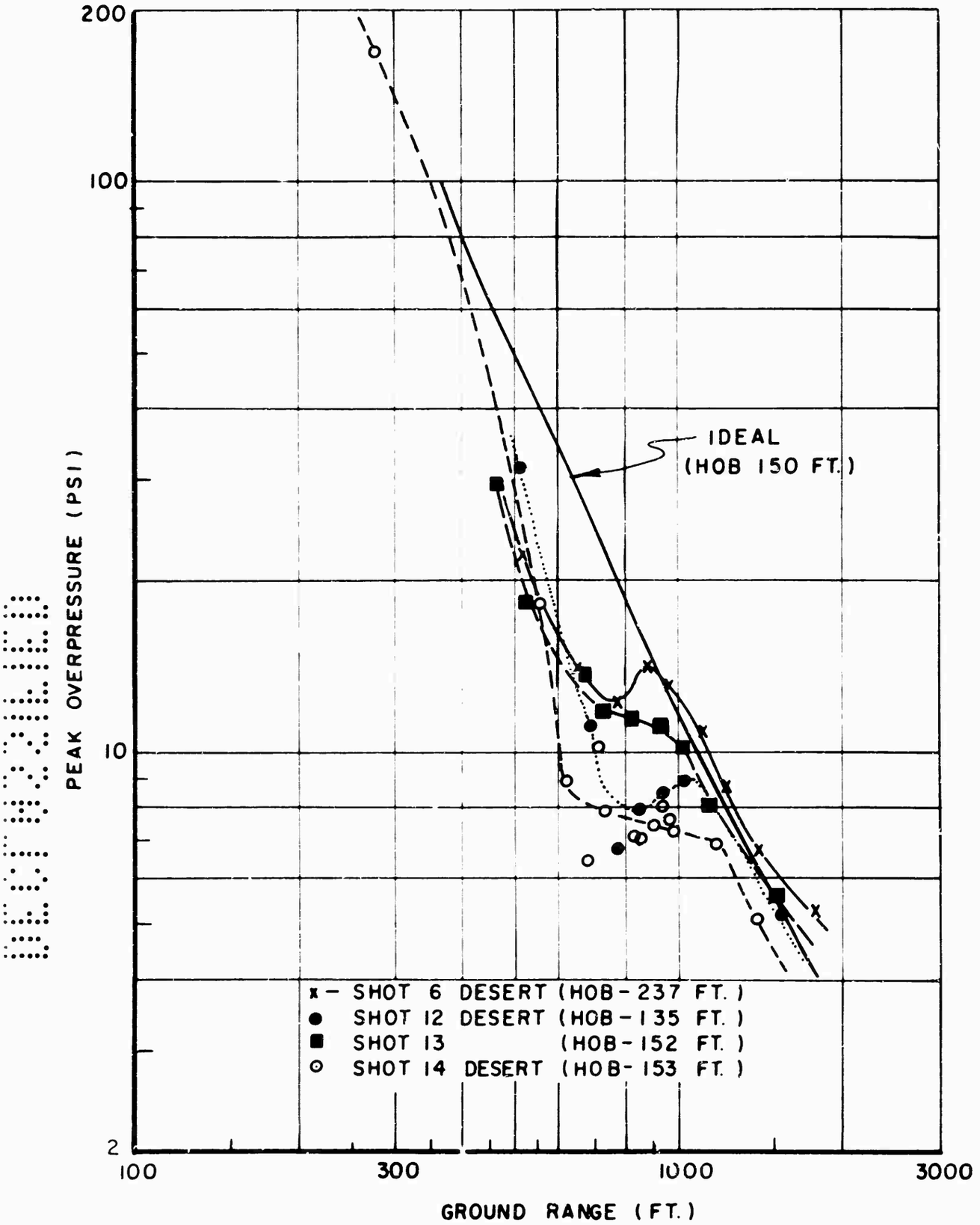

Fig. 4.9 Comparison of Peak Overpressure versus Ground Range for Shots 6, 12, 13 and 14, Desert Line. A-Scaled

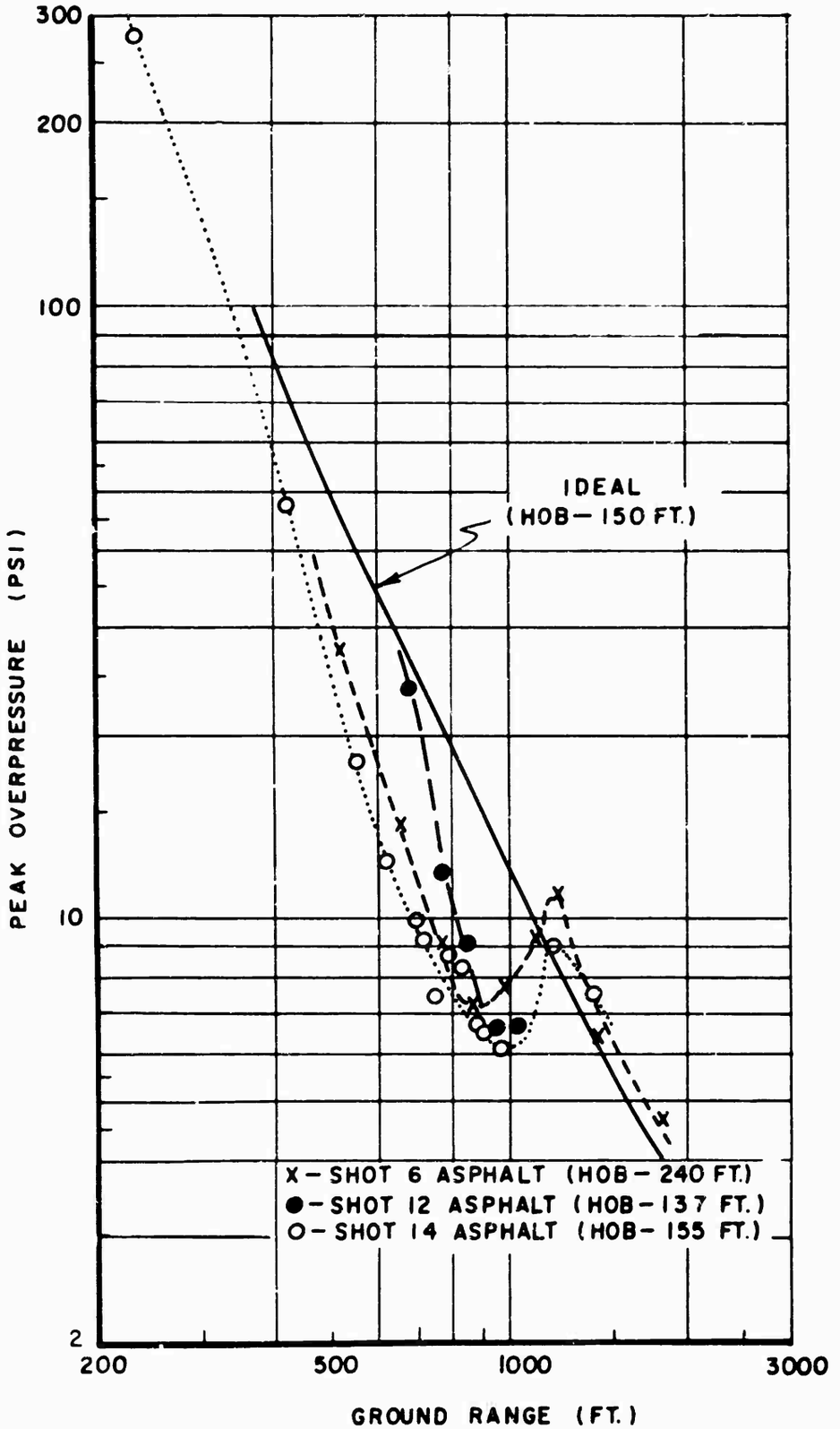

Fig. 4.10 Comparison of Peak Overpressure versus Ground Range for Shots 6, 12 and 14, Asphalt Line. A-Scaled

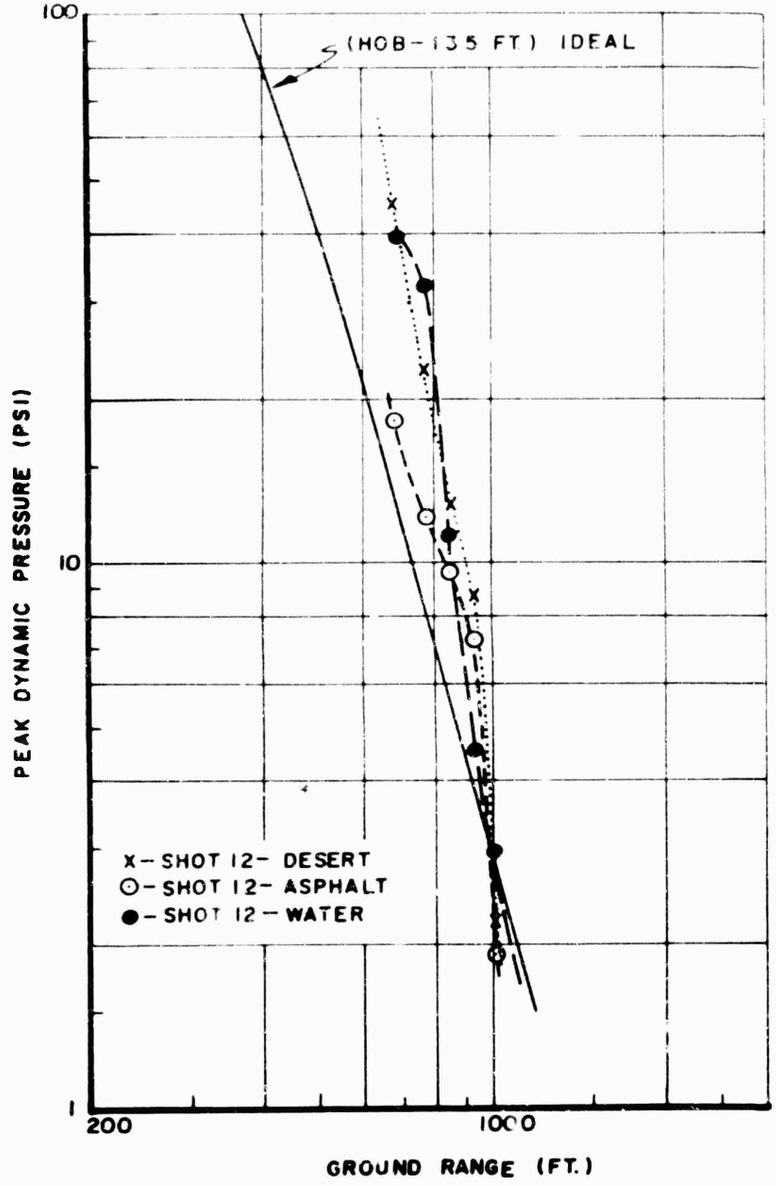

Fig. 4.11 Peak Dynamic Pressure versus Ground Range for Shot 12, Asphalt, Desert and Water Lines. A-Scaled

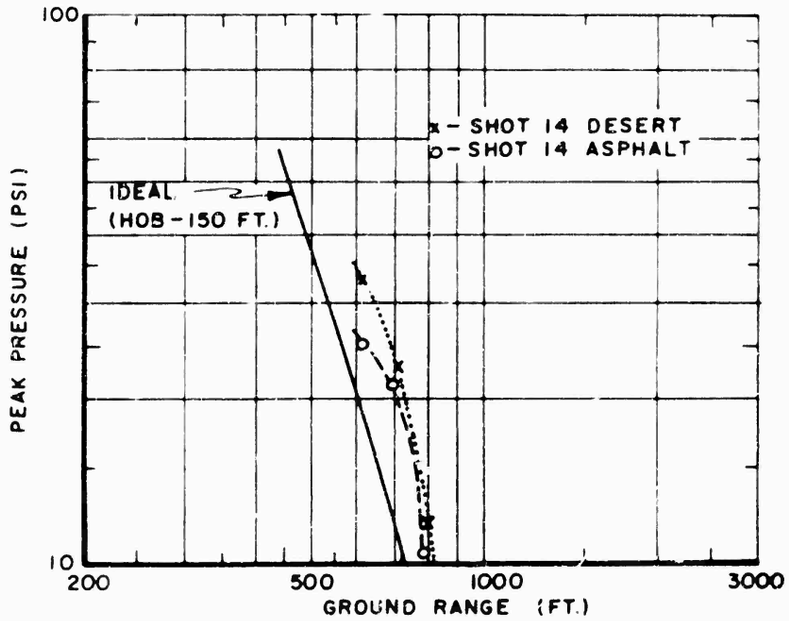

Fig. 4.12 Peak Dynamic Pressure versus Ground Range for Shot 14, Asphalt and Desert Lines. A-Scaled

The curves for A-scaled peak dynamic pressure versus distance are presented in the same manner as the peak overpressure curves and are shown in Figs. 4.11 to 4.18. On each of the figures an ideal dynamic pressure curve (Reference 4) is drawn for comparison with the measured values.

The values of dynamic pressure measured over the desert surface are, in general, greater than the values over the asphalt surface. Comparisons of these curves are shown in Fig. 4.11 for Shot 12, Fig. 4.12 for Shot 14 and Fig. 4.13 for Shot 6. Those values over the water surface correspond to the dynamic pressures over the desert surface, (See Fig. 4.11). The influence on dynamic pressure of dust-loading, water-loading and extraneous particle-loading noted on Shot 12 over the asphalt surface is uncertain.

A good correlation exists between the measured values of dynamic pressure and the ideal curve (Reference 4) on Shot 9, particularly in the Mach region. This comparison is shown in Fig. 4.14. Within the regular reflection region, the measured value of dynamic pressure is much greater than the ideal value. At the station in question, the time interval between the incident and reflected overpressure wave under ideal conditions should approximately be 4 msec at the 3-foot level. The wave form indicates the time interval between the initial rise and the second peak to be about 12 msec. The incident wave of overpressure recorded is 20 psi, which is the value predicted in free air. However, the reflected wave or the peak value is considerably less than either the value from the curve for the good surface condition or the ideal overpressure curve (See Fig. 4.6). Since a precursor was evident on this shot and because of its influence on the pressure measurements, it is likely that the value of dynamic pressure within the regular reflection region is real.

It is of interest to point out the results of the dynamic pressure measurements on Shots 2, 5, 8 and 11 which are shown in Fig. 4.15. Measured values, in general, are above the ideal curve. Outside the precursor zone there exists in a number of cases, a correlation between the measured dynamic pressures and calculated dynamic pressures using the Rankine-Hugoniot equation and the measured static overpressures. In addition, it appears that, on the basis of scaled values beyond the precursor zone, the lesser the yield the higher are the measured dynamic pressures.

The enhancement of dynamic pressure occurring in the precursor region becomes evident upon inspection of Fig. 4.16, which gives the results of Shots 3, 4 and 12 (desert). Shot 3 was the lowest yield weapon of the three shots and its overpressure-distance curve was not depressed to the extent of Shots 4 and 12. Also, the pressure-distance curve of Shot 4 was not depressed below Shot 12. Now, the measured dynamic pressures of Shot 3 correspond to the ideal curve and those of Shots 4 and 12 are above; Shot 12 has the highest measured values. It appears from this comparison that the overpressure-distance curve hav-

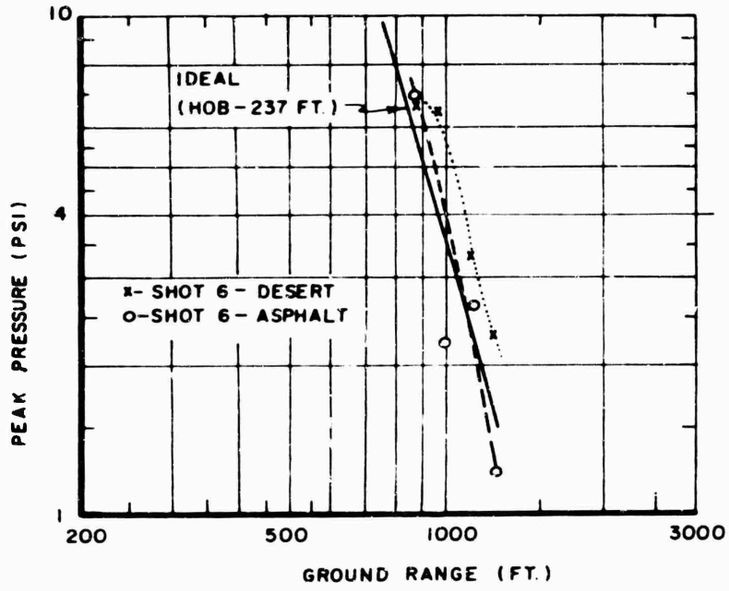

Fig. 4.13 Peak Dynamic Pressure versus Ground Range for Shot 6, Asphalt and Desert Line. A-Scaled

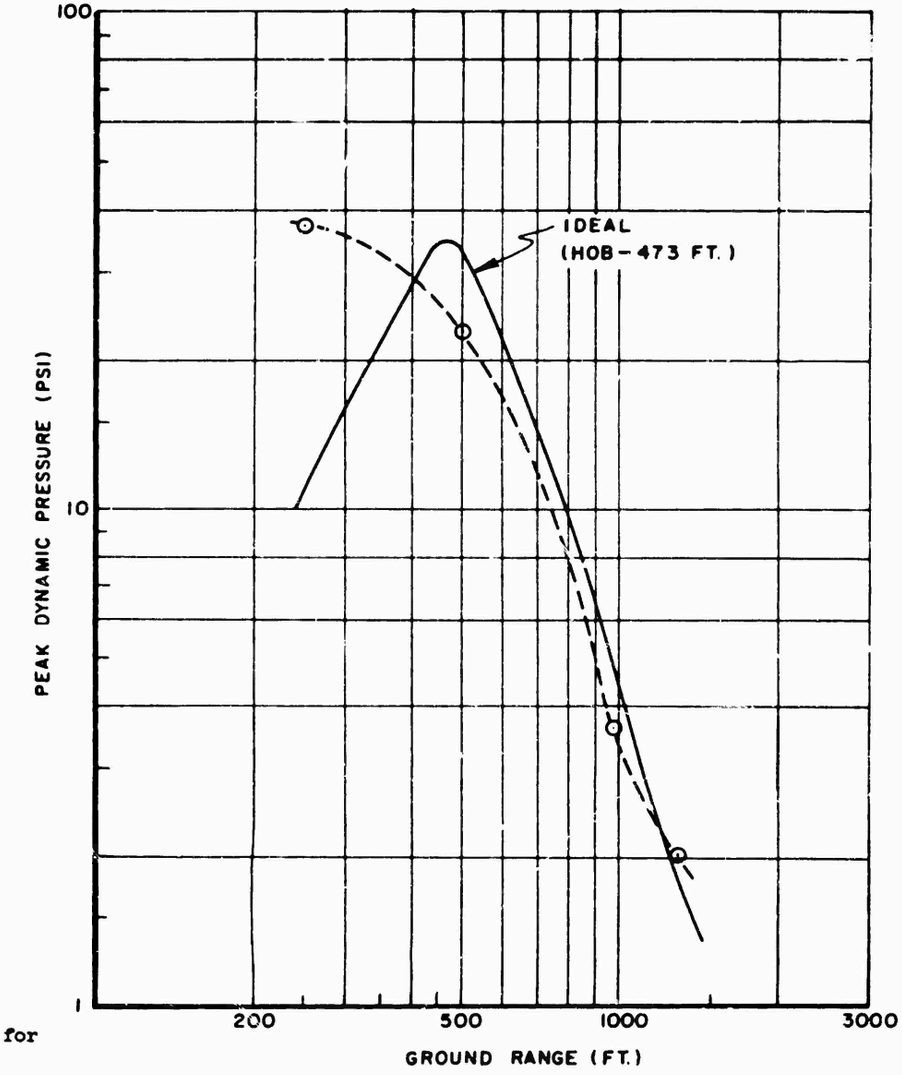

Fig. 4.14 Peak Dynamic Pressure versus Ground Range for Shot 9. A-Scaled

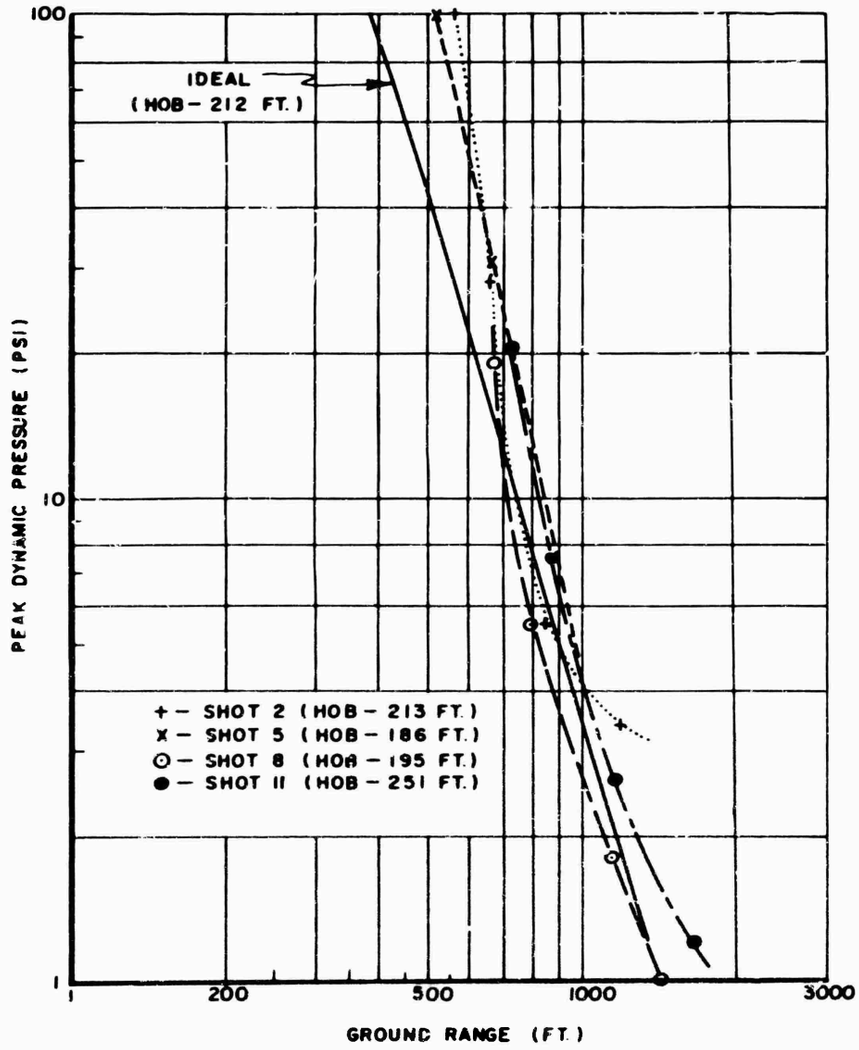

Fig. 4.15 Peak Dynamic Pressure versus Ground Range for Shots 2, 5, 8 and 11. A-Scaled

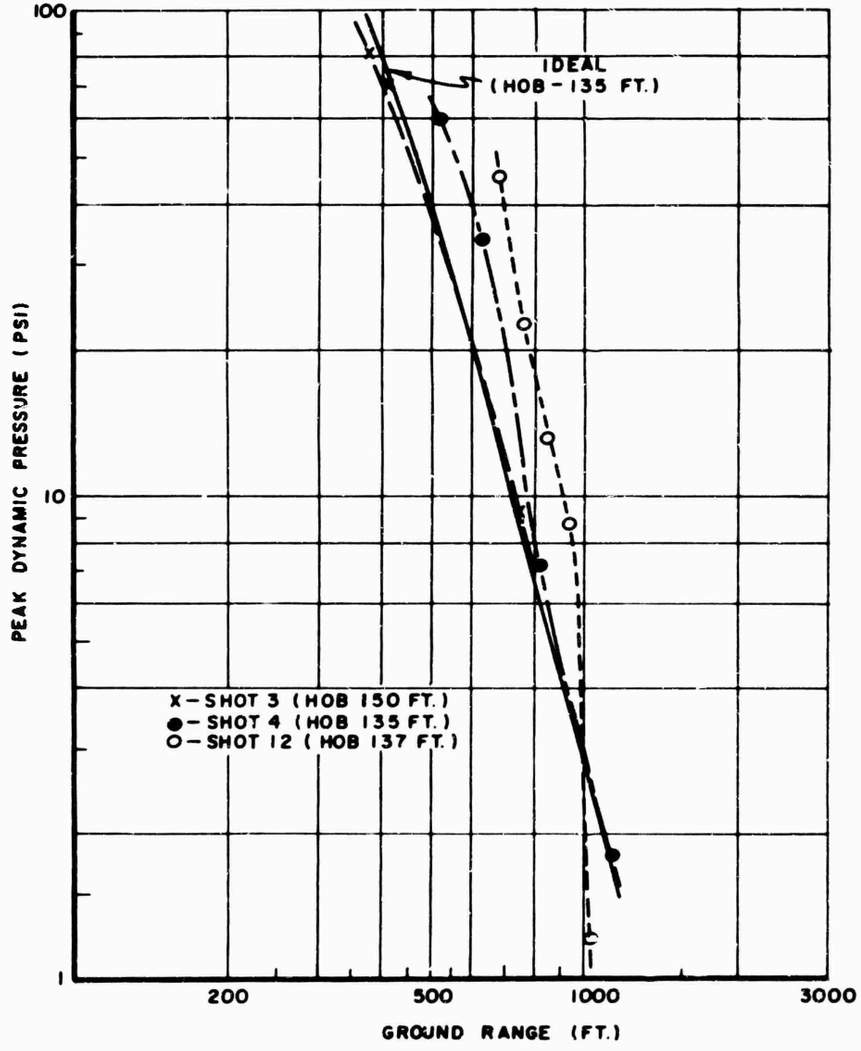

Fig. 4.16 Peak Dynamic Pressure versus Ground Range for Shots 3, 4 and 12 (Desert). A-Scaled

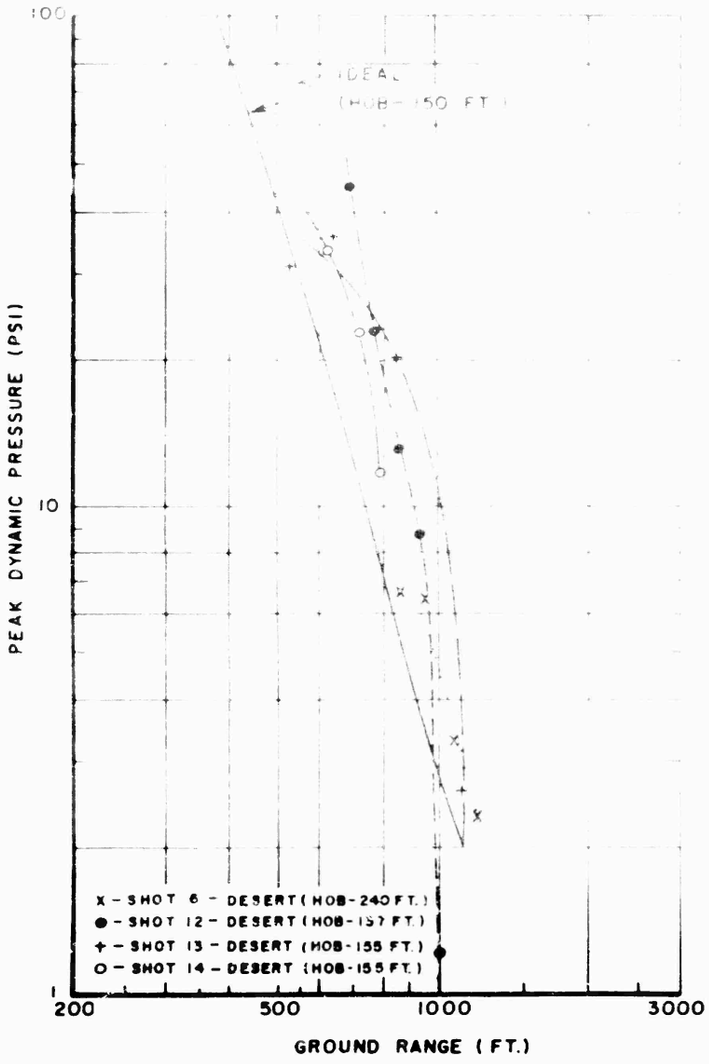

Fig. 4.17 Peak Dynamic Pressure versus Ground Range for Shots 6, 12, 13 and 14, Desert Line. A-Scaled

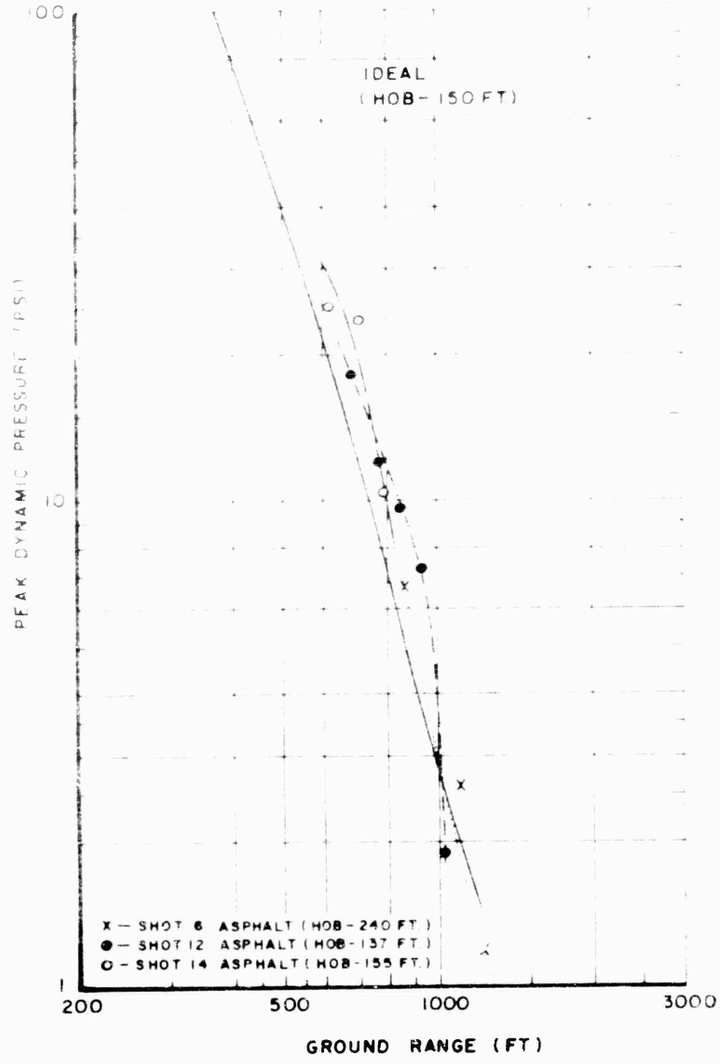

Fig. 4.18 Peak Dynamic Pressure versus Ground Range for Shots 6, 12 and 14, Asphalt Line. A-Scaled

ing the greatest depressions will have the highest values of dynamic pressure.

Comparisons of shots with similar surfaces are shown in Fig. 4.17 for the desert surface and Fig. 4.18 for the asphalt surface. Except for Shot 13 in Fig. 4.17, the dynamic pressure values on the desert surface as well as on the asphalt surface do not vary greatly from shot to shot for each type surface. It is to be noted that the shots having greatest depressions of the overpressure-distance curve have the highest values of dynamic pressure. However, it is not true for the overall dynamic pressure distance curve.

4.3 TIME OF ARRIVAL

The A-scaled time of arrival of the initial shock disturbance versus ground range is shown in Figs. 4.19 through 4.26. The curves drawn through the measured points were fitted by eye. The errors in the curve are primarily due to the time required for initiation of gage motors and the time required for the motors to reach constant speed. From tests conducted, the startup time and the time for the motors to reach constant speed was determined to be 64.7 msec with standard deviation of 11.3 millisec (See Appendix A). Maximum relative error will result for the low-yield devices and stations close to ground zero. The errors are inherent in all gages; hence, a relative comparison among shots can be made. The time of arrival from mechanical gages compared to electronic gages differs by about 18 percent at the close-in stations and about 1 percent at the fartherest station. This comparison is for the desert line on Shot 12.

Over the asphalt surface the initial shock disturbance advances ahead of the shock disturbances over either the water or the desert surface. The time-of-arrival data indicating this is shown in Figs. 4.19, 4.20 and 4.24 for Shots 12, 6 and 14, respectively. This increased rate of propagation is due to higher temperatures within the thermal layer formed over the asphalt surface. More thermal energy is absorbed by the asphalt surface than either the water surface or the desert surface resulting in higher temperatures.

The smoke generated on Shot 5 reduced the temperatures within the thermal layer formed, since there is a time lag of the initial disturbance on the smoke line as compared to arrival times on the clear line (See Fig. 4.21).

In view of the fact that more thermal energy can be expected from the higher yield burst than from the lower yield burst at the same scaled distance, it could be assumed that the scaled time of arrival of the low-yield burst would lag behind the high-yield burst. In the case of Shots 4 and 12, Fig. 4.23, and Shots 12 and 14, Fig. 4.26, the above statement holds, since Shots 4 and 14 were the larger yields and the time of arrivals are ahead of Shot 12. From the time-of-arrival data shown in Fig. 4.25 for Shots 2, 8, and 11, the reverse of the above seems to be true. Shot 8 was the larger yield of the three and the time of arrival of the initial disturbance lags behind that of Shot 2

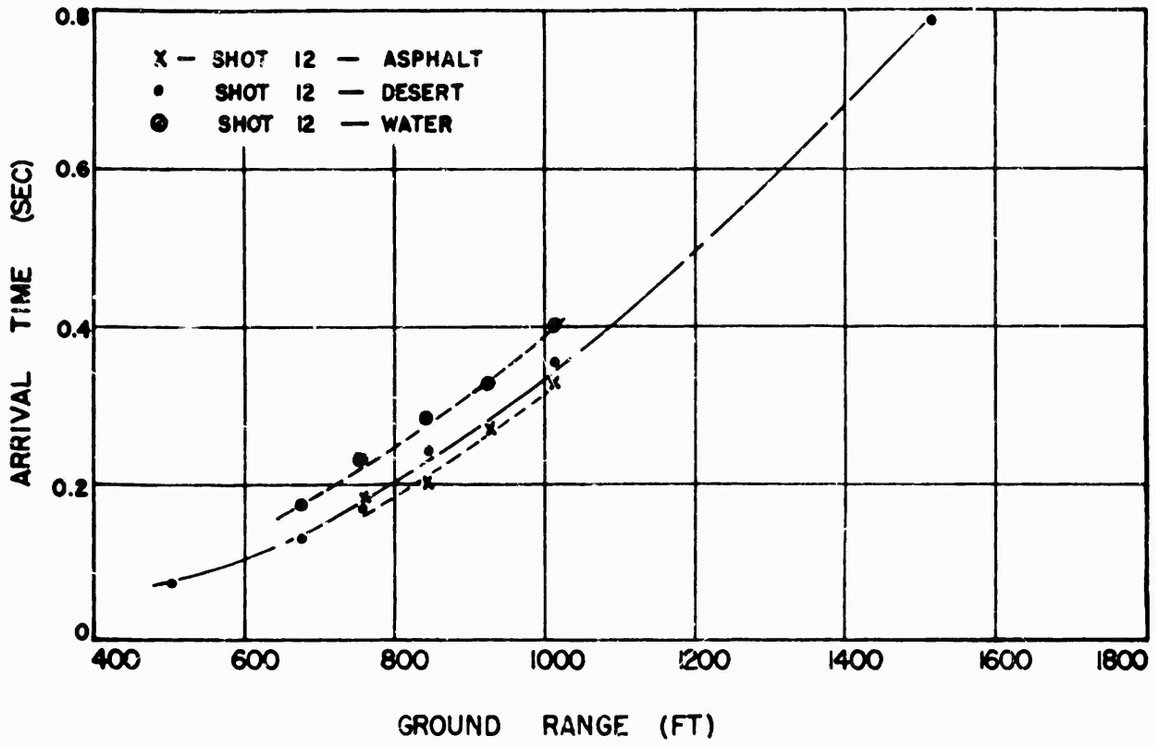

Fig. 4.19 Time of Arrival versus Ground Range for Shot 12, Asphalt, Desert and Water Lines. A-Scaled

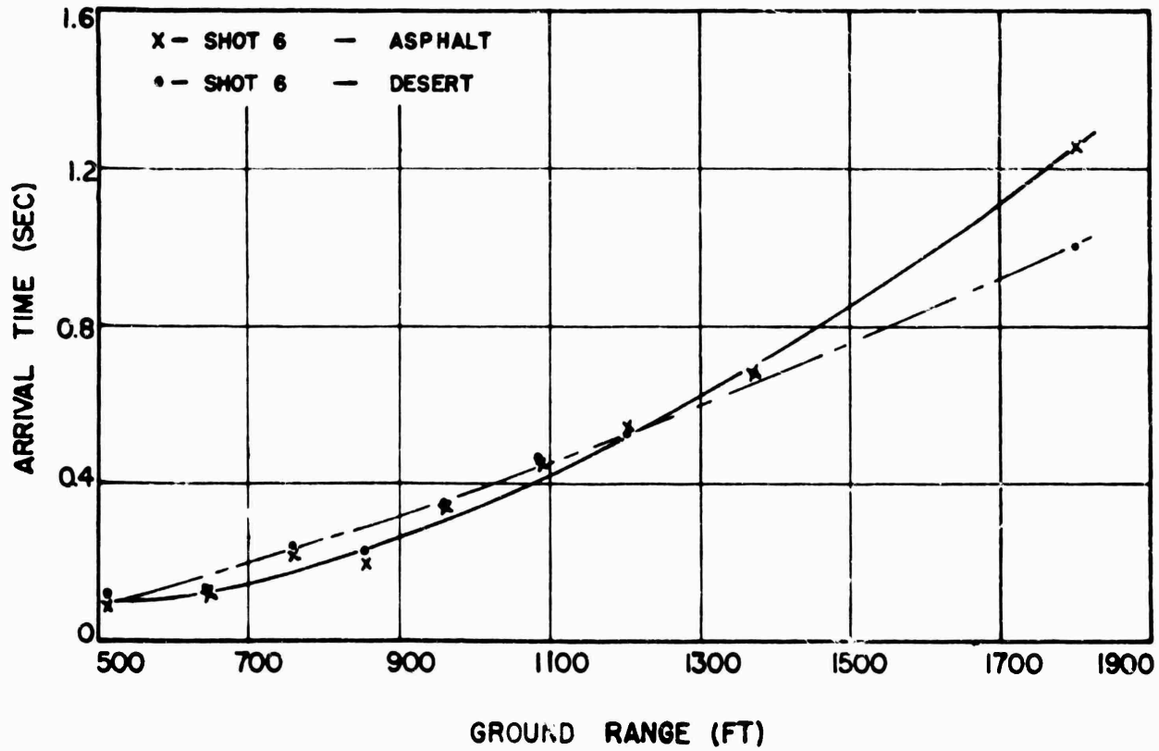

Fig. 4.20 Time of Arrival versus Ground Range for Shot 6, Asphalt and Desert Lines. A-Scaled

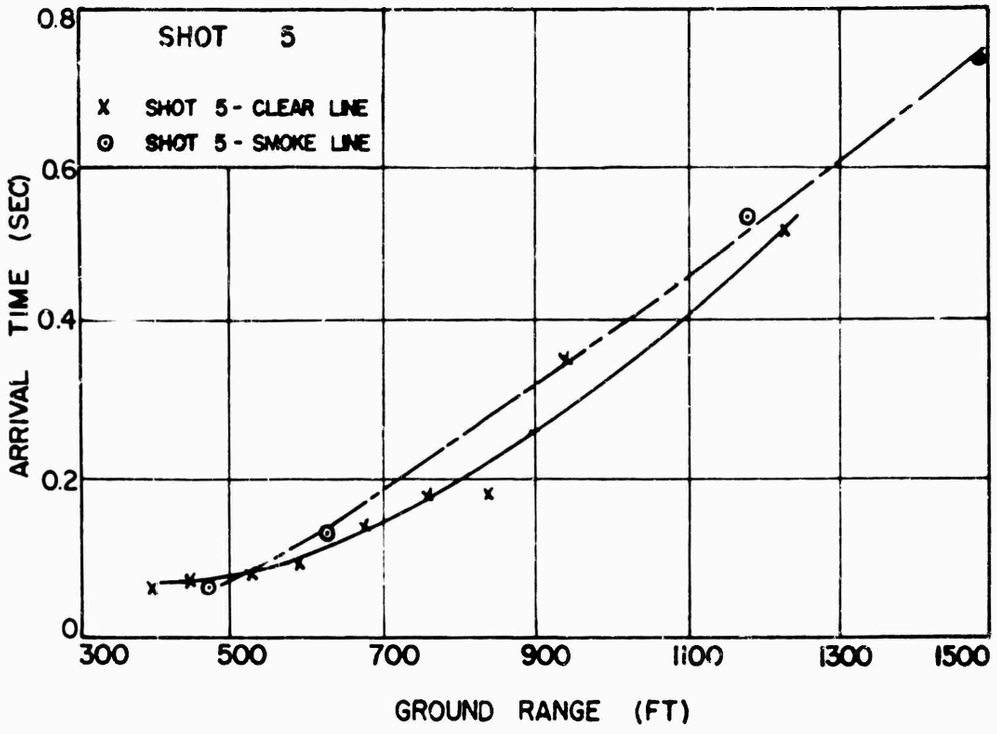

Fig. 4.21 Time of Arrival versus Ground Range for Shot 5, Clear and Smoke Line. A-Scaled

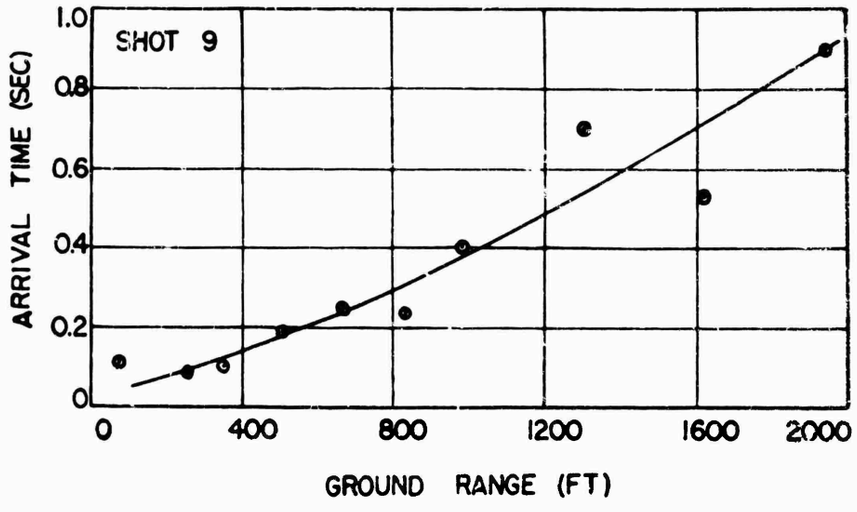

Fig. 4.22 Time of Arrival versus Ground Range for Shot 9. A-Scaled

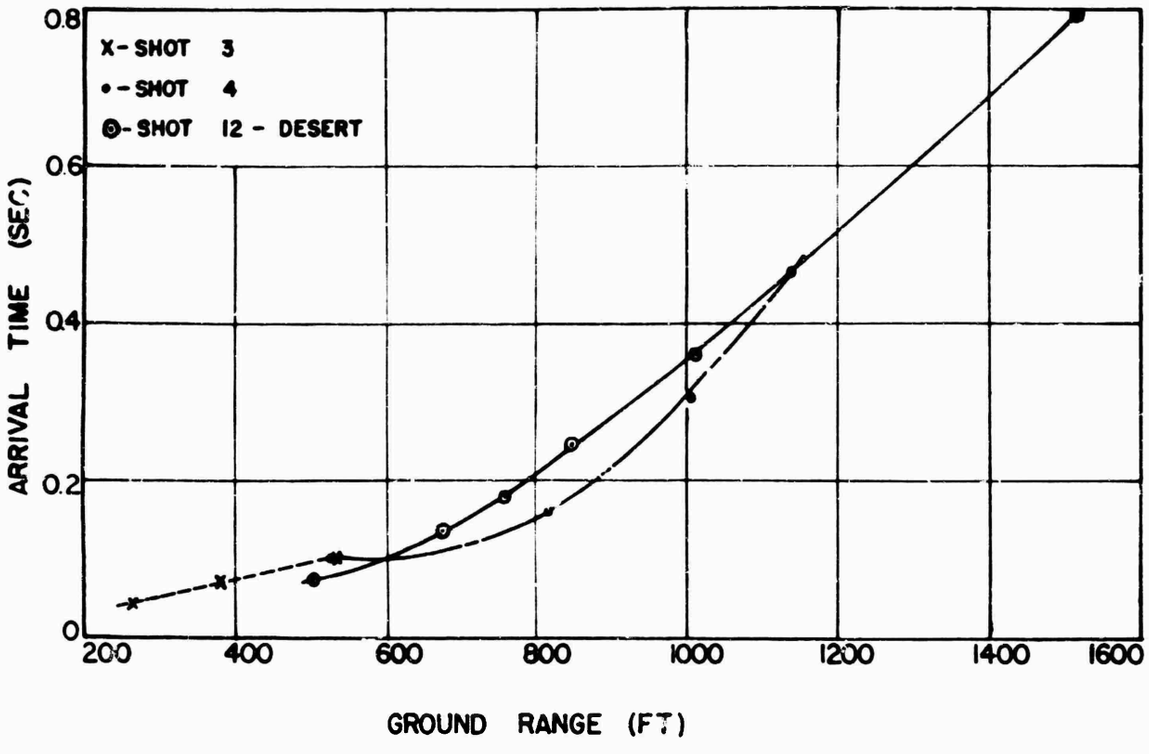

Fig. 4.23 Time of Arrival versus Ground Range for Shots 3, 4 and 12 (Desert). A-Scaled

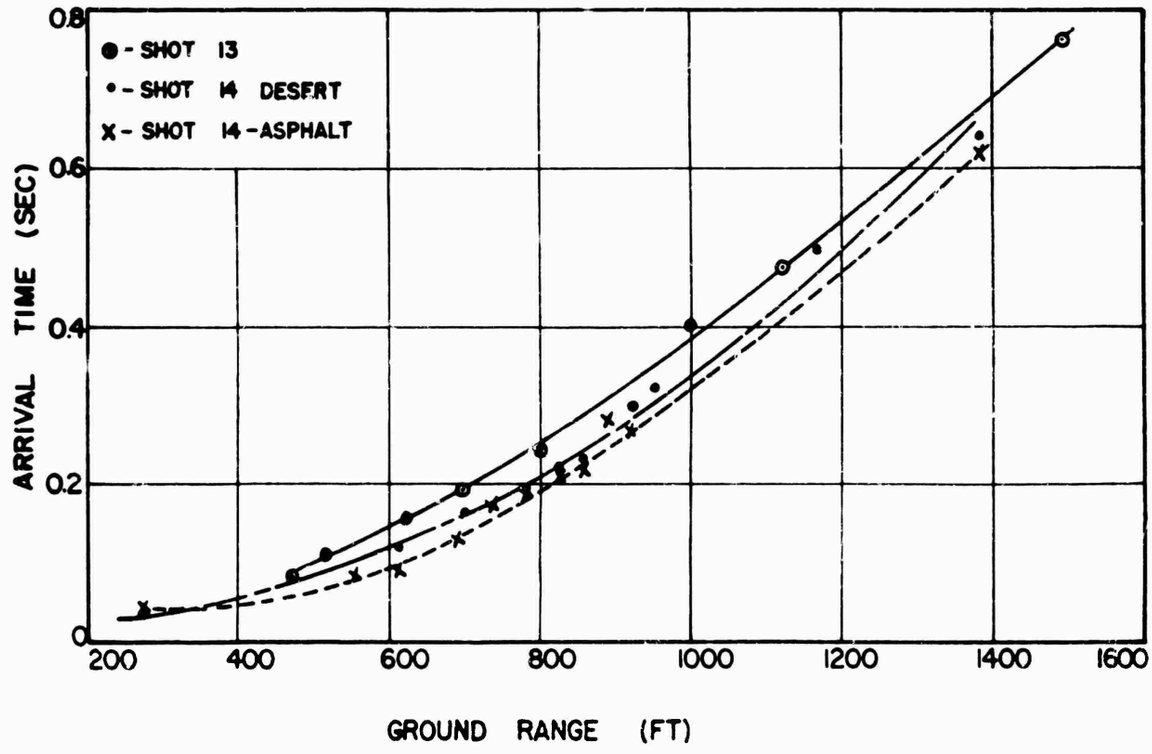

Fig. 4.24 Time of Arrival versus Ground Range for Shot 13 and Shot 14 (Asphalt and Desert Line). A-Scaled

and 11. No reason can be given for this discrepancy. The results of Shot 3 given in Fig. 4.23 are questionable, since a large error is introduced because of the proximity of the stations to ground zero.

The time of arrival data on Shot 13 lags the time of arrival on Shot 14, (See Fig. 4.24) even though the shot conditions for practical purposes were similar. Obviously certain factors causing the differences noted have not been considered.

4.4 POSITIVE PHASE DURATIONS VERSUS GROUND RANGE

The measured values of positive phase duration are shown in Figs. 4.27 through 4.36. Comparisons of the positive durations versus scaled ground range were made of shots with similar scaled heights of burst and/or shots with similar surfaces and are shown in Figs. 4.37 through 4.40.

The durations of Shot 12, Fig. 4.34 over the asphalt surface were longer than either over the desert and water surface. On Shot 6, Fig. 4.30 the durations were also longer on the asphalt surface than the desert surface. This is not,however, the case for Shot 14 as shown in Fig. 4.35. There is no particular trend to the data of Shot 14. This discrepancy may be attributed to the fact that the time lapse between activation of gages and detonation was approximately two weeks in which case the battery power supply for each gage could have lost some of its life in varying degrees. This could then cause the speed of motors to be erratic which in turn would yield durations in error by some unknown quantity.

The durations on the smoke and clear lines, Shot 5, are given in Fig. 4.29. The clear line has longer positive durations than the smoke line implying that the increase of positive duration results from more absorption of thermal energy by the surface.

The trend of the data also indicate to some degree that within the precursor zone the positive duration remains about constant. Since the absorption of thermal energy by the surface influences the positive duration it could be expected that with higher yields the positive duration would be increased at equivalent scaled ranges. This is not entirely borne out by the data obtained. Shot 12 has longer durations than Shot 6 but then Shot 4 being a larger yield weapon than Shot 12 has shorter durations than Shot 12.

4.5 PRECURSOR PHENOMENA

The wave forms for the surface overpressures on all shots show severe rounding, step shocks to two levels, or rounded double or multiple peaks (See Appendix E). Using these distortions as an indication of the presence of a precursor, then all shots instrumented had precursors, except for Shot 1. Only peak overpressures were obtained on Shot 1 and the wave shapes are unknown.

Figure 4.41 shows all the shots plotted on the chart for the pre-

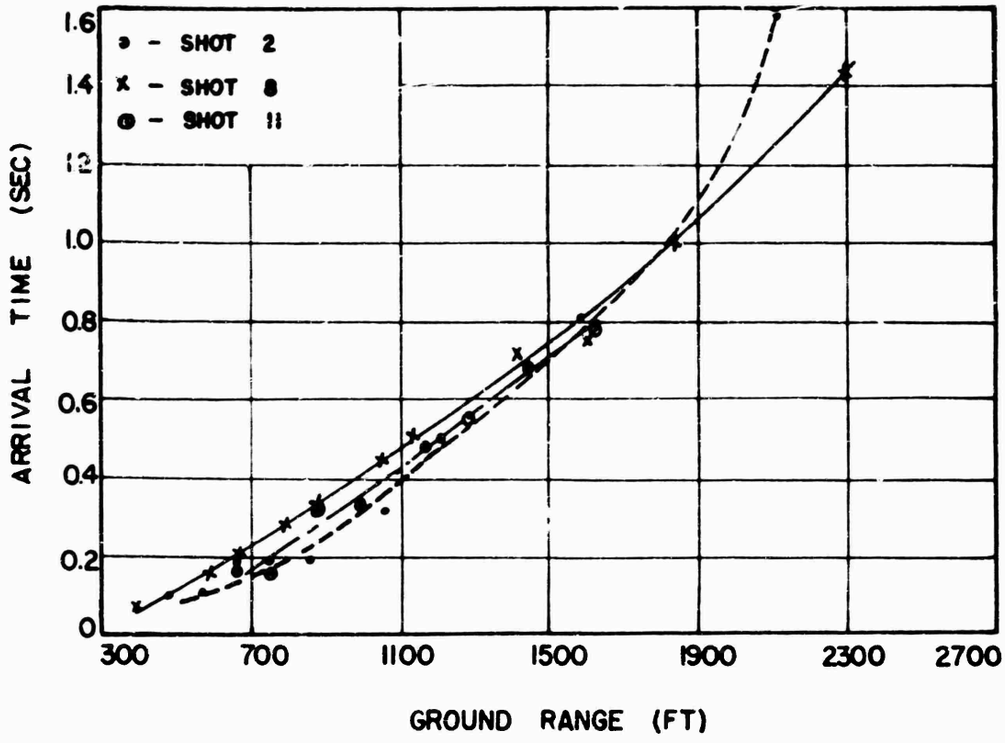

Fig. 4.25 Time of Arrival versus Ground Range for Shots 2, 8 and 11. A-Scaled

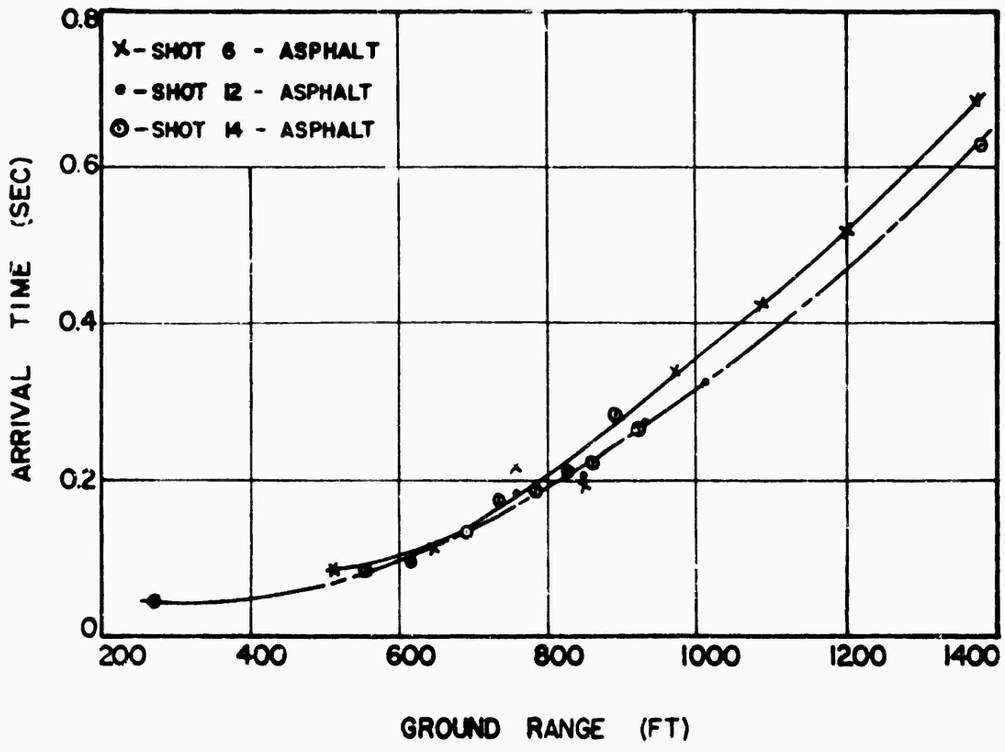

Fig. 4.26 Time of Arrival versus Ground Range for Shots 6, 12 and 14, Asphalt Line. A-Scaled

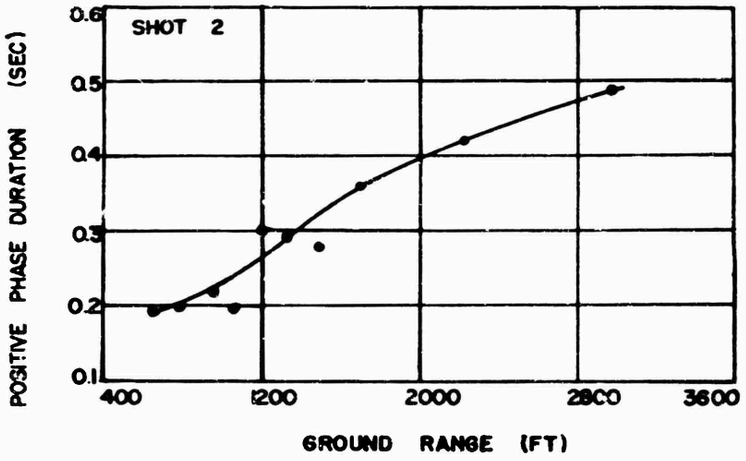

Fig. 4.27 Positive Duration versus Ground Range for Shot 2 (As Observed)

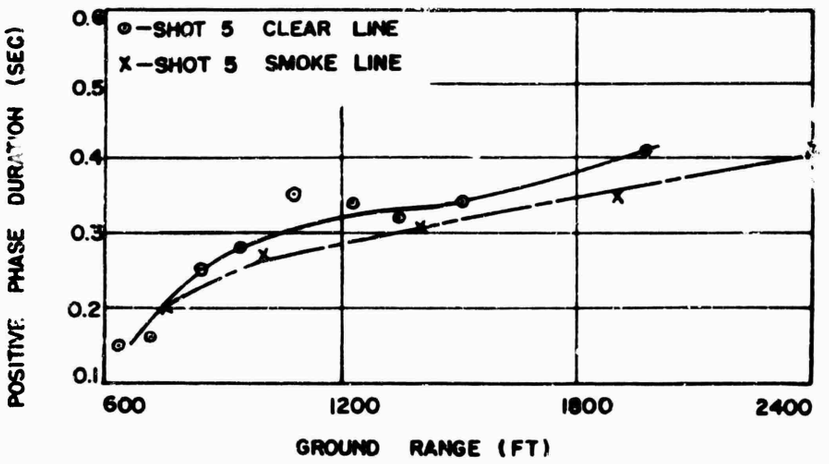

Fig. 4.28 Positive Duration versus Ground Range for Shot 4 (As Observed)

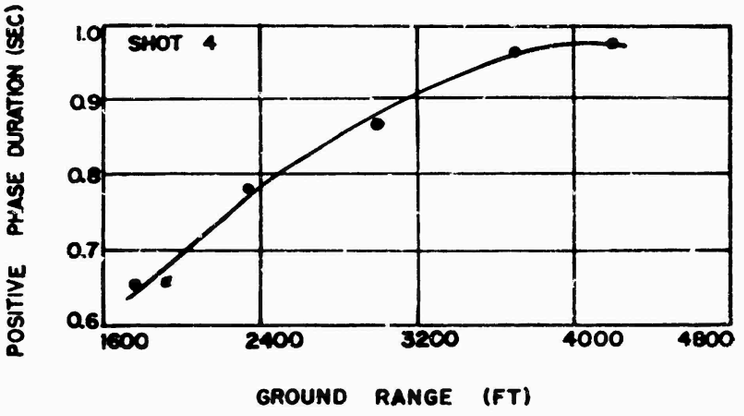

Fig. 4.29 Positive Duration versus Ground Range for Shot 5, Clear and Smoke Line (As Observed)

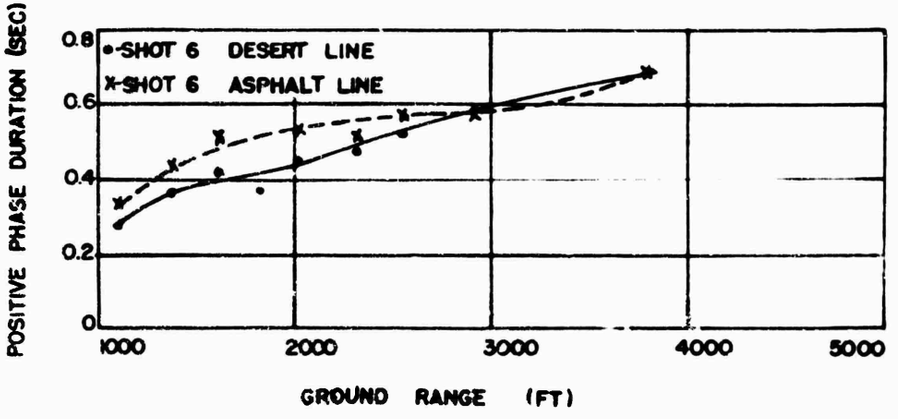

Fig. 4.30 Positive Duration versus Ground Range for Shot 6, Desert and Asphalt Line (As Observed)

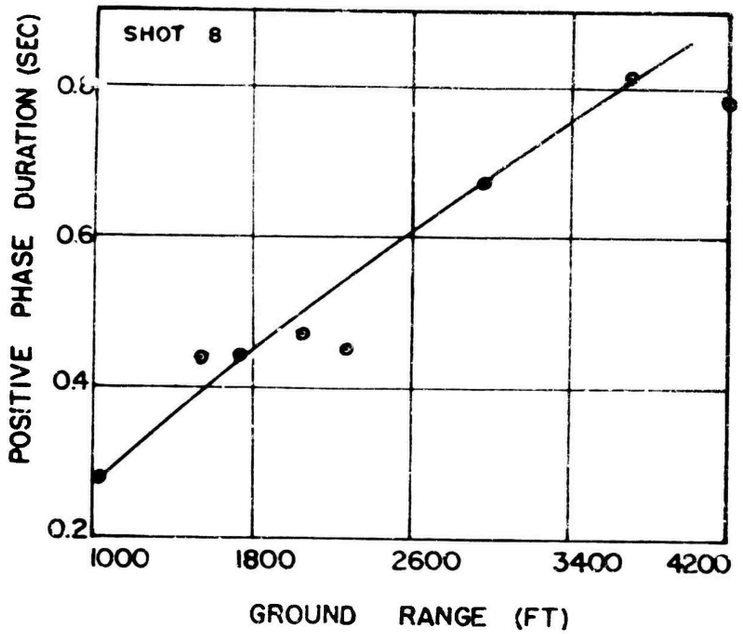

Fig. 4.31 Positive Duration versus Ground Range for Shot 8 (As Observed)

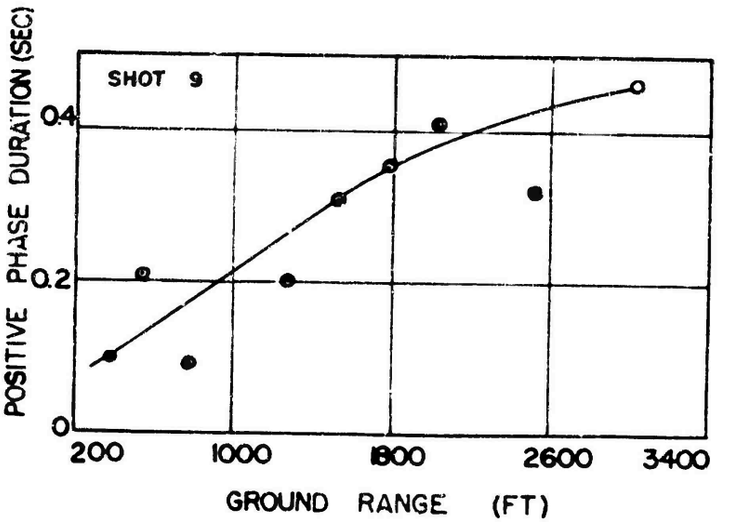

Fig. 4.32 Positive Duration versus Ground Range for Shot 9 (As Observed)

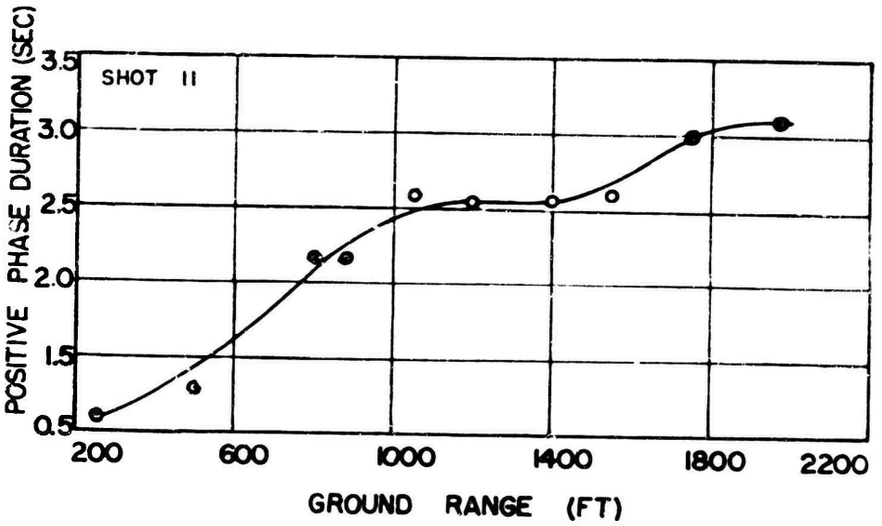

Fig. 4.33 Positive Duration versus Ground Range for Shot 11 (As Observed)

diction of precursor formation obtained by F. H. Shelton (Reference 5)

Three of the shots that had indications of a precursor fall completely outside the estimated error band. All other shots fall within the zone enclosed by the outer error band. The chart for predicting precursor formation given in Fig. 61 of TM 23-200 (Reference 2) predicted precursors on all shots except for Shot 1, including those which fall outside the error band on the chart by Shelton. The results suggest that the chart in TM 23-200 is more accurate for predicting precursor formation.

4.6 COMPARISON OF BRL DATA WITH SRI DATA FOR SHOT 12 AND SHOT 6

The results of Shots 6 and 12 obtained from the self-recording pressure-time and q-gages by BRL are compared to those obtained by SRI (Reference 5) with electronic gages. This comparison is tabulated in Tables 4.3 through 4.6, includes peak overpressure, peak dynamic pressure, time of arrival, and positive-phase duration. Comparisons of pressure-time histories for Shot 12 between BRL and SRI are given in Figs. 4.42 through 4.49. The dynamic-pressure comparisons are presented in Figs. 4.42 to 4.45 and the static pressure comparisons as obtained from the q-gage are presented in Figs. 4.45 to 4.49.

In the overall comparisons the agreement between the two types of gages is generally good. Over the asphalt surface, at ground level on Shot 12, the peak overpressures recorded by BRL are higher than the SRI and in some cases lower. Upon inspection of the wave forms, the maximum fluctuations in the comparison made occurs when oscillations are present on the records. If the oscillations were smoothed out, there would be a better agreement of values. The wave forms on the asphalt line of both BRL and SRI are smooth, so the comparison of the values agree very well.

Except for a few cases, there is also good agreement of the peak dynamic pressure values obtained by the two agencies on Shot 12. Again, when the agreement is poor, then the differences occur mainly because of oscillations, In smoothing through the curves, the agreement of dynamic pressure values will be better. The wave forms of the dynamic pressure records obtained by BRl do not differ too much with those records obtained by SRI. Main differences are in the latter portion of the records. Those of SRI do not decay as rapidly as those of BRL. No reason can be given for these differences.

The arrival times on all three surfaces of Shot 12 gives reasonable comparison. The BRL time-of-arrival data are lower than those of SRI. As for the positive-phase duration, the agreement is good for the water and desert surfaces. The agreement on the asphalt surface is not too good; however, only two values can be compared.

4.7 SUMMARY AND ANALYSIS

Many of the data discussed in this report have been observed previously and reported on in other operations, particularly Operation

TABLE 4.2 Summary of q-Gage Mount Failures

Shot No.	Distance (ft)	Scaled Distance (ft)	Surface	Remarks
2	795	564		Bent slightly back
4	1950	529		Bent back-30° from normal
5	840	522		Bent slightly back
12	2250	759	Water	Bent slightly back
12	2500	844	Desert	Knocked out of the ground by flying debris.
14	2300	706	Asphalt	Bent slightly back
14	2050	614	Desert	Knocked out of mount hole
14	2300	706	Desert	Knocked out of mount hole

TABLE 4.3 - Comparison of Peak Overpressure from BRL Data with SRI Data for Shot 12

Distance	Desert Surface (psi)		Water Surface (psi)		Asphalt Surface (psi)	
	BRL	SRI	BRL	SRI	BRL	SRI
SURFACE LEVEL						
1500	27.7	29.6				
2000	9.8	16.9	25.7	17.4	21.3	13.9
2500	7.0	7.4	12.0	11.8	8.0	6.6
3000	7.9	8.0	10.0	8.8	5.8	3.9
4500	4.7	4.6				
3 FOOT LEVEL						
2000	13.6	18.6	24.1	20.1	14.7	14.2
2500	9.0	9.0	9.8	13.2	8.2	8.5
2750	7.7	7.3	11.6	11.5	6.4	6.4
3000	8.0	8.3	10.5	10.5	5.6	4.9

TABLE 4.4 - COMPARISON OF PEAK OVERPRESSURE FROM BRL DATA WITH SRI DATA FOR SHOT 6 SURFACE LEVEL

DISTANCE (ft)	DESERT (psi)		ASPHALT (psi)	
	BRL	SRI	BRL	SRI
1300		14.1		10.1
1360	12.0		12.2	
1600	10.4		7.7	
1650		10.8		7.2
2000	11.2	11.4		4.2
2050			6.6	

TABLE 4.5 - COMPARISON OF PEAK DYNAMIC PRESSURE FROM BRL DATA WITH SRI DATA FOR SHOT 12 - 3 FT AND 10 FT LEVELS

DISTANCE (ft)	DESERT SURFACE (psi)		WATER SURFACE (psi)		ASPHALT SURFACE (psi)	
	BRL	SRI	BRL	SRI	BRL	SRI
2000	40.0	44.6	35.0	32.6	16.1	15.7
2500	11.3	10.2	10.0	5.6	8.5	9.9
2500	12.4*	14.6*	5.4*	4.5*	6.8*	11.2*
2760			4.0	4.6	6.4	
3000	1.1	1.8	2.6	3.1	1.7	0.8

* At 10 ft level

TABLE 4.6 - COMPARISON OF TIME OF ARRIVAL FROM BRL DATA WITH SRI DATA FOR SHOT 12

DISTANCE (ft)	DESERT SURFACE (sec)		WATER SURFACE (sec)		ASPHALT SURFACE (sec)	
	BRL	SRI	BRL	SRI	BRL	SRI
1500	0.225	0.265				
2000	0.395	0.453	0.525	0.589		
2250						
2500	0.725	0.781	0.845	0.914	0.615	0.674
2750			0.965	1.077	0.805	0.843
3000	1.065	1.192	1.205	1.246	0.965	1.034
4500	2.355	2.388				

TABLE 4.7 - COMPARISON OF POSITIVE PHASE DURATION FROM BRL DATA WITH SRI DATA FOR SHOT 12

DISTANCE (ft)	DESERT SURFACE (sec)		WATER SURFACE (sec)		ASPHALT SURFACE (sec)	
	BRL	SRI	BRL	SRI	BRL	SRI
1500	0.42	0.553				
2000	0.73	0.78	0.51	0.54		
2500	0.77	0.77	0.61	0.63	0.82	0.75
3000	0.76	0.86	0.68	0.73	1.03	0.7

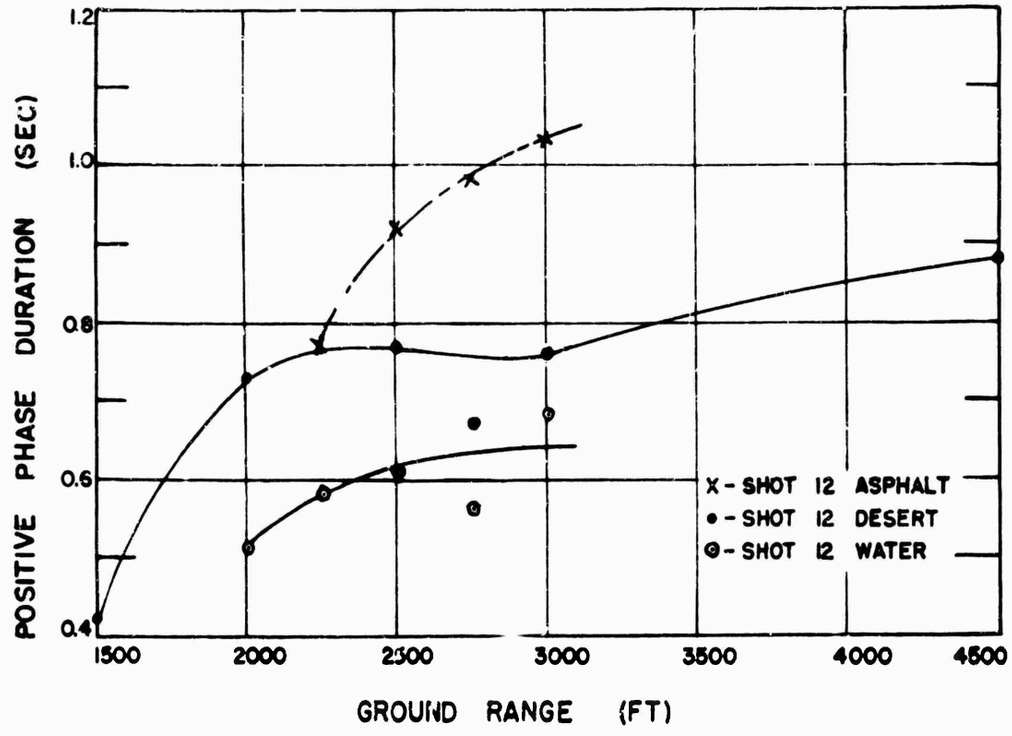

Fig. 4.34 Positive Duration versus Ground Range for Shot 12, Asphalt, Desert and Water Lines (As Observed)

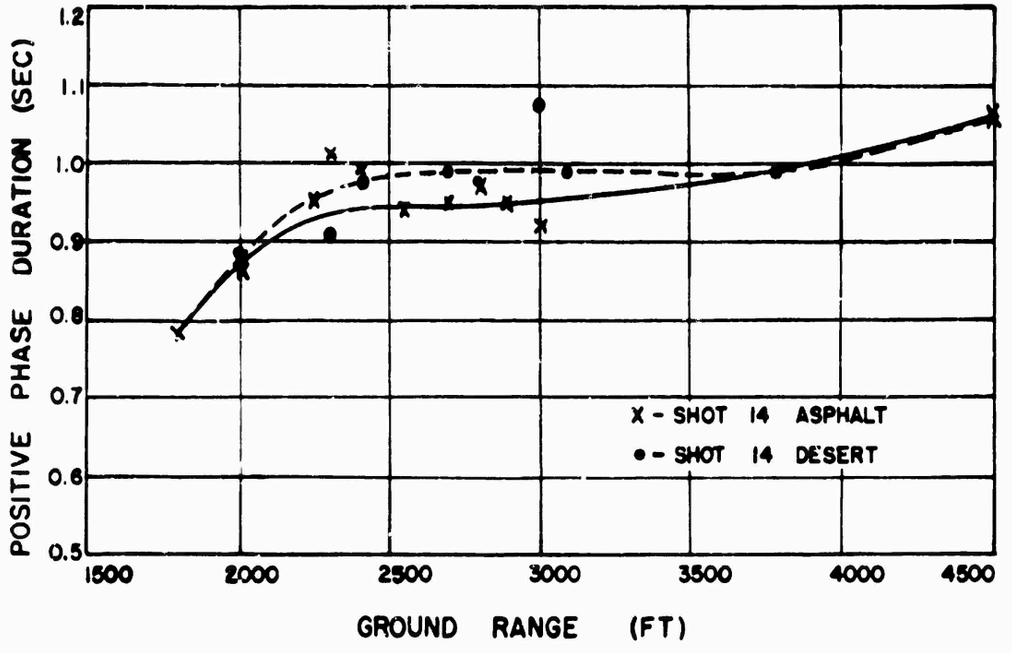

Fig. 4.35 Positive Duration versus Ground Range for Shot 14, Asphalt, and Desert Lines (As Observed)

UPSHOT/KNOTHOLE (References 7, 8,9). However, in this operation the measurements of dynamic pressure will supplement the data given in Ref. 9 and lend itself to a better understanding of the conditions existing in the presence of precursor formation.

In retrospect, the trends of the data noted and some of the observations made are summarized as follows:

1. The formation of a precursor will be a function of the surface conditions, height of burst, and yield of the nuclear device or weapon. In the presence of a precursor, the blast parameters (such as pressures, velocity of shock, positive phase duration) are affected. Also, a

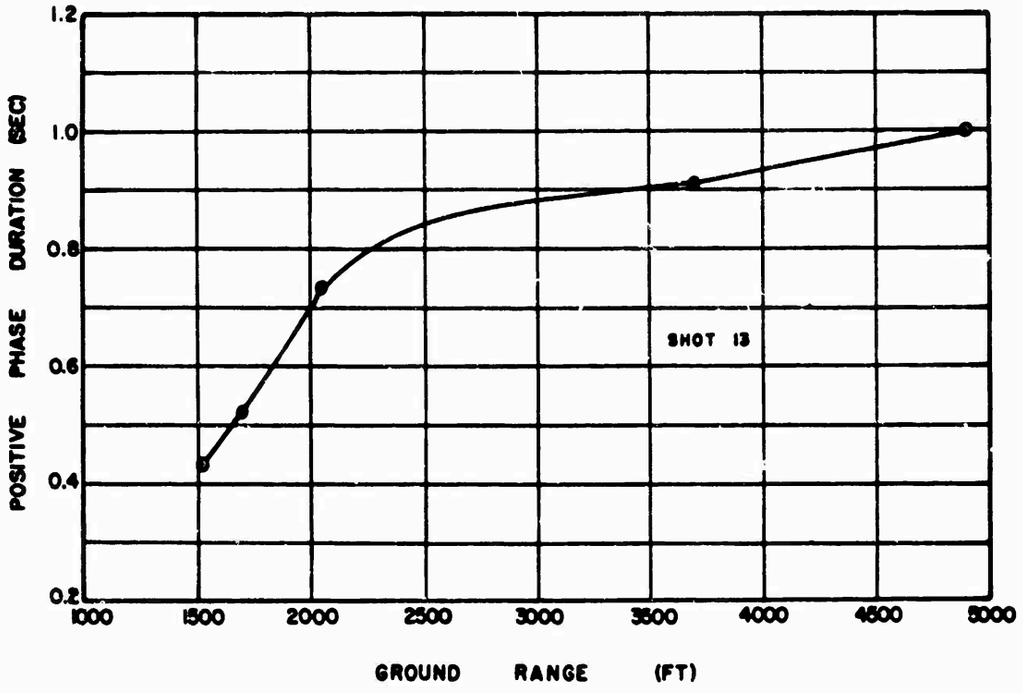

Fig. 4.36 Positive Duration versus Ground Range for Shot 13 (As Observed)

lowering or depression of the measured overpressure-distance curve below the ideal overpressure-distance curve (Reference 4) will result.

2. It appears that the greater the depression of the measured overpressure-distance curve the more pronounced is the precursor. This will also be dependent on the surface conditions and the height of burst and yield of the device.

3. As a corollary to Statement 2, it appears that the greater the depression of the overpressure-distance curve the greater is the measured dynamic pressure above the ideal dynamic pressure (Reference 4) in the precursor zone. The increase in dynamic pressure above the ideal values is further influenced by the surface conditions. Over a dusty region, the dynamic pressure will be greater than over a nondusty region, particularly at distances closer to ground zero. However, it

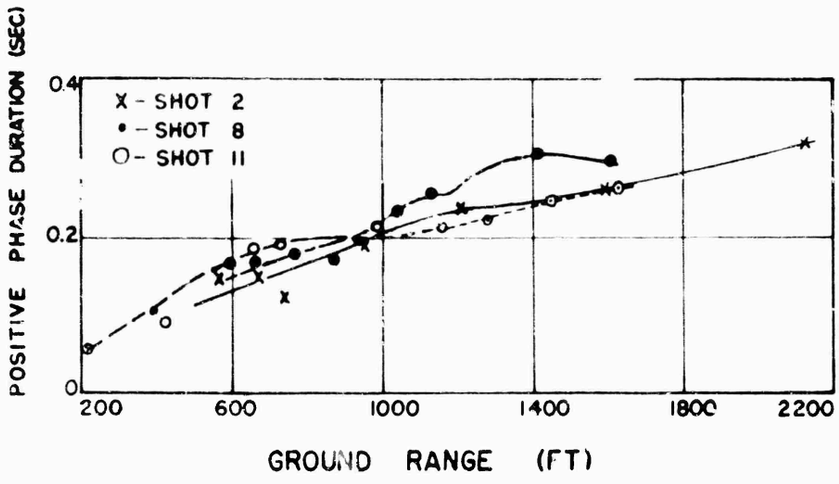

Fig. 4.37 Positive Duration versus Ground Range for Shots 2, 8, and 11. A-Scaled

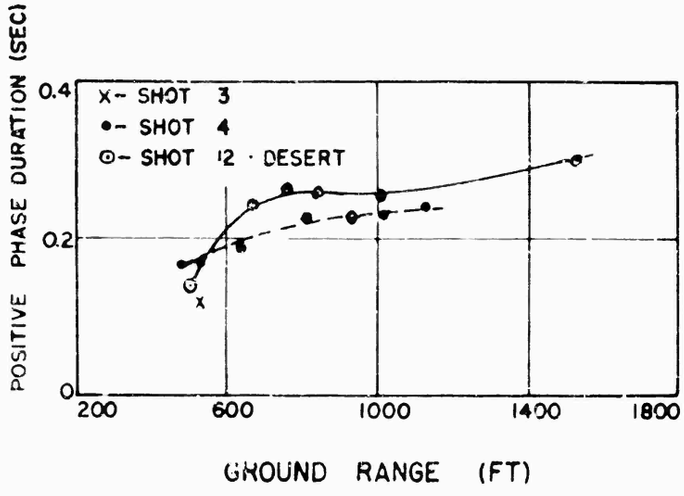

Fig. 4.38 Positive Duration versus Ground Range for Shots 3, 4, and 12 (Desert) A-Scaled

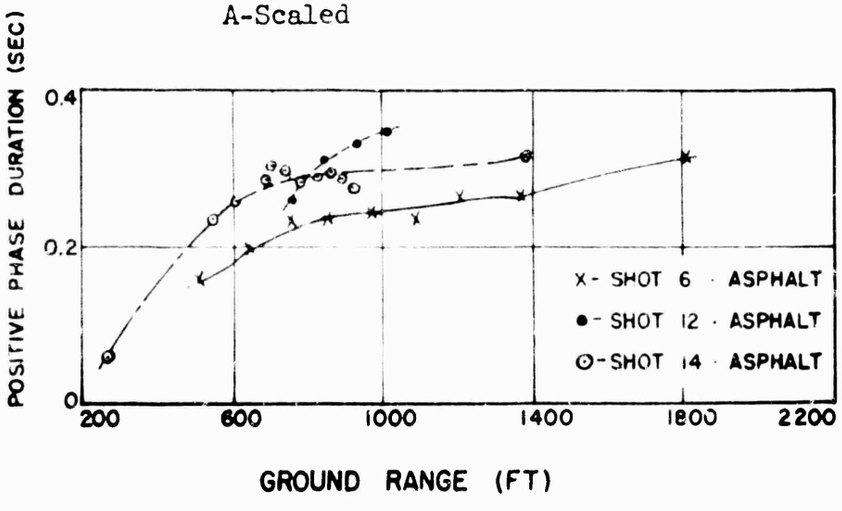

Fig. 4.39 Positive Duration versus Ground Range for Shots 6, 12 and 14 Asphalt Line. A-Scaled

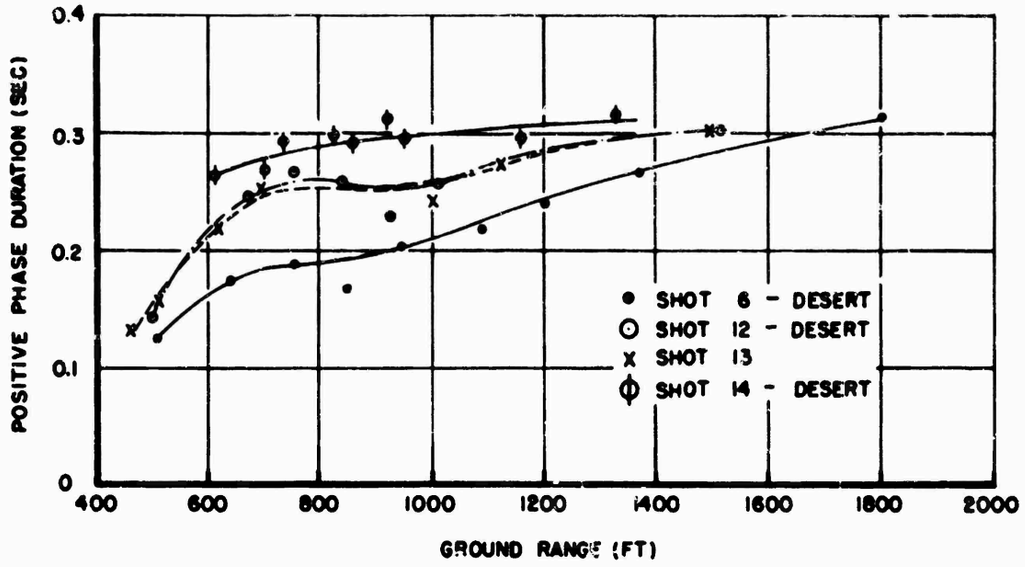

Fig. 4.40 Positive Duration versus Ground Range for Shots 6, 12, 13 and 14, Desert. A-Scaled

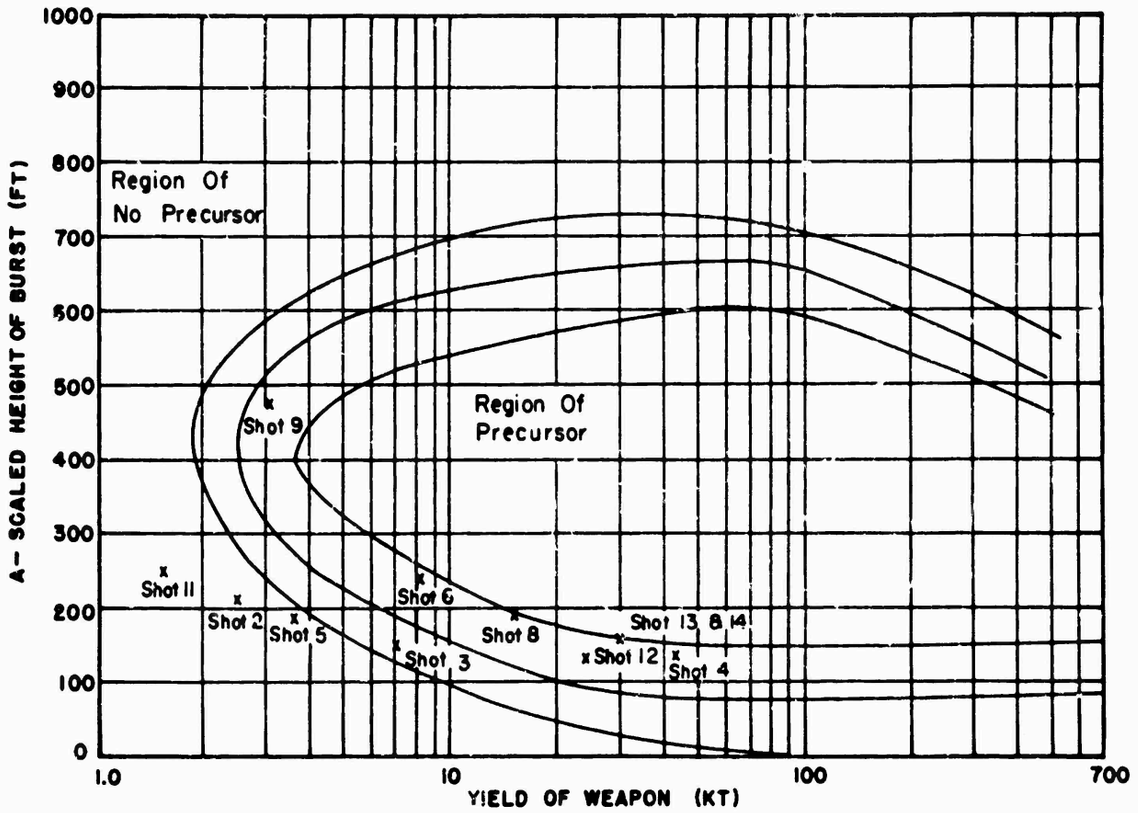

Fig. 4.41 Precursor Formation as a Function of Height of Burst and Yield

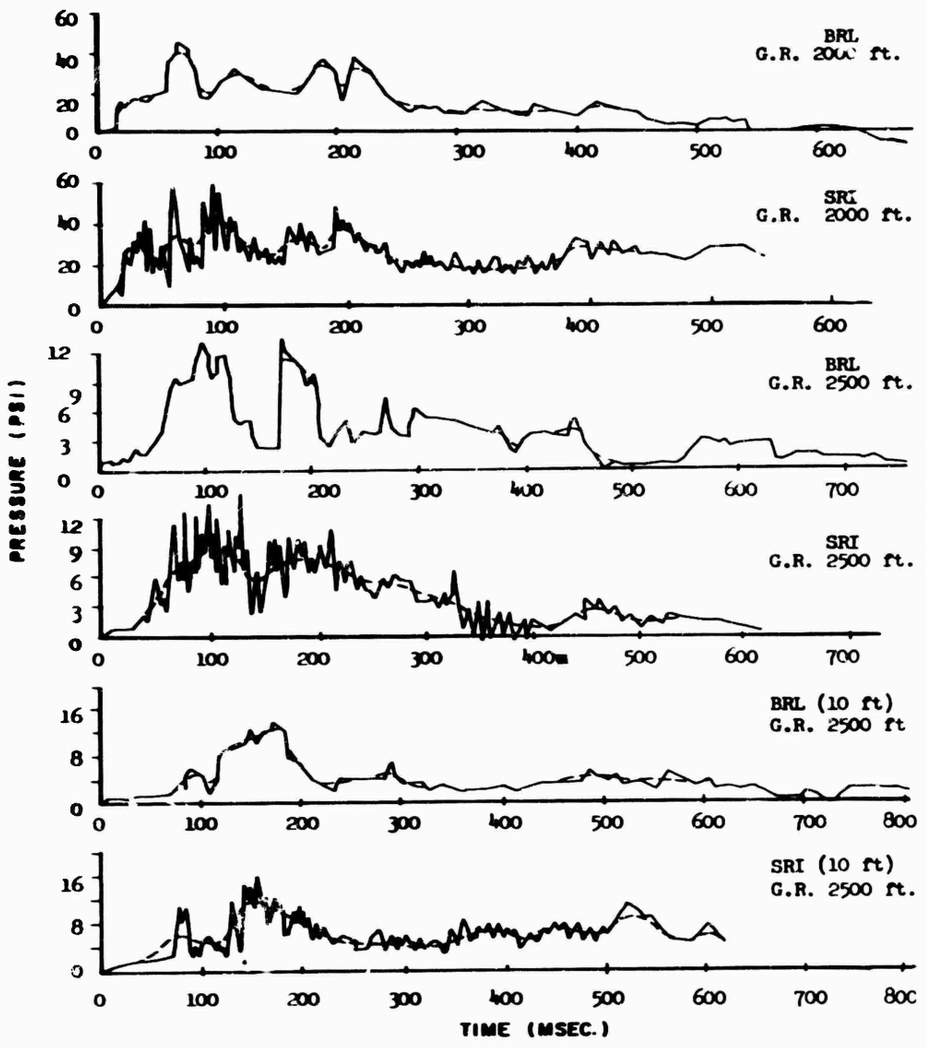

Fig. 4.42 Comparison of BRL with SRI Dynamic Pressure-Time Records for Shot 12. Desert Line

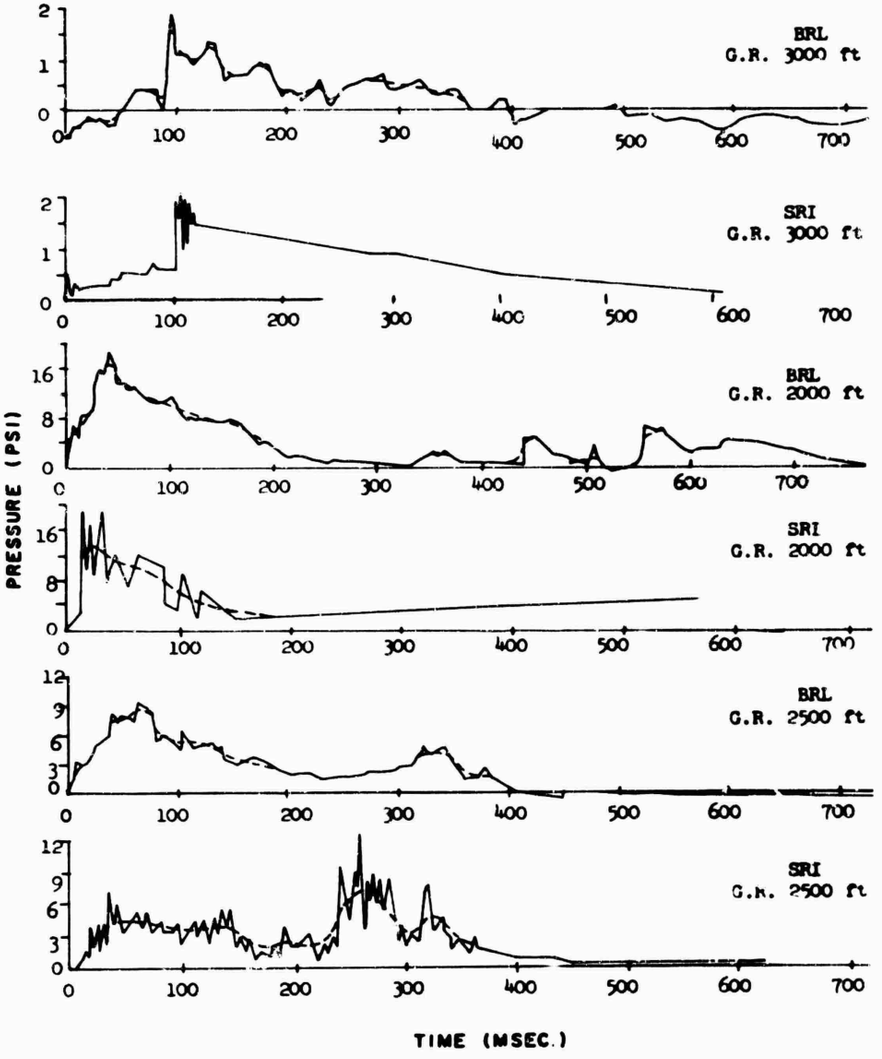

Fig. 4.43 Comparison of BRL with SRI Dynamic Pressure-Time Records for Shot 12. Desert Line (3,000 feet) and Asphalt Line (2,000 feet and 2,500 feet)

must be kept in mind that the measured dynamic pressure were uncorrected for compressibility and compared to the ideal curve. An appropriate correction factor for compressibility will reduce the measured values; the extent of reduction is unknown.

4. The velocity of the shock propagation is dependent upon the temperature within the thermal layer. The temperature, in turn, will depend on the amount of thermal energy absorbed by the surface and the thermal layer. Again, this is a function of surface conditions and the height of burst and yield of the weapon.

5. Another shock parameter that is a function of surface conditions and height of burst and yield of weapon is the positive-phase duration. When the temperature within the thermal layer is highest and the precursor formation is most pronounced the positive duration is longest.

For Shots 2, 5, 8, and 11 beyond the precursor range, the measured peak overpressures were equal to or above the ideal curve. For the larger-yield weapons, such as Shots 4, 12, 13, and 14, the measured values beyond the precursor zone correspond to the curve for good surface conditions or the ideal curve. A good surface curve falls below the ideal curve. The existence of the overpressure values above the ideal curve suggest that these increases may be attrituted to one or more of several factors. The possibility does exist that yield of weapon used in scaling distances for these shots is incorrect or that the efficienty of the blast energy is higher for the low-yield weapon. Another possibility is that when a precursor is formed and the depression of the overpressure-curve is least, the recovery or the clearing up of the precursor will result in higher overpressure values at ground level. This is further indicated in the comparison of pressure on the smoke and clear line of Shot 5. On the smoke line, the pressure-distance curve has a lesser depression than the clear line, and beyond the precursor zone the pressures on the smoke line are higher. Since the observation is made on the same shot, this would discount the possibility that the yield of weapon used in scaling is incorrect or that the efficienty of blast energy is higher for the low-yield weapon in explaining the existence of measured overpressures above the ideal. On the other hand, the influence of smoke on overpressures should not be disregarded. If smoke does influence the pressure obtained, then the factors mentioned above would be a consideration for the higher pressures measured.

It is evident that the data of Operation Teapot indicate a number of factors involved in affecting the blast-wave parameters. The most significant of these factors are surface conditions, height of burst, and yield.

4.7.1 Variations of Overpressure Measurements With Yield of Weapon

A number of shots of varying fields were detonated within a narrow range of heights of burst on Operation Teapot. This wide range of yields for a small variation in burst height suggested that yield de-

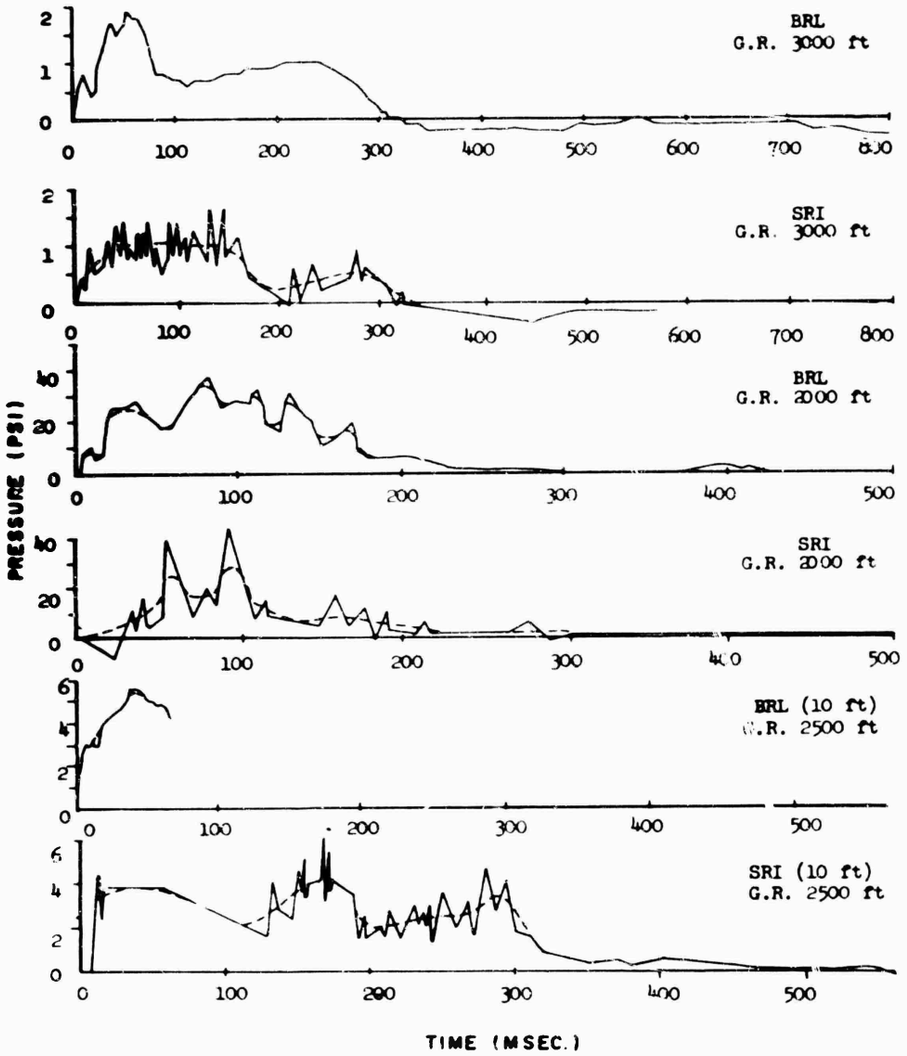

Fig. 4.44 Comparison of BRL with SRI Dynamic Pressure-Time Records for Shot 12. Asphalt Line (3,000 feet) and Water Line (2,000 feet and 2,500 feet)

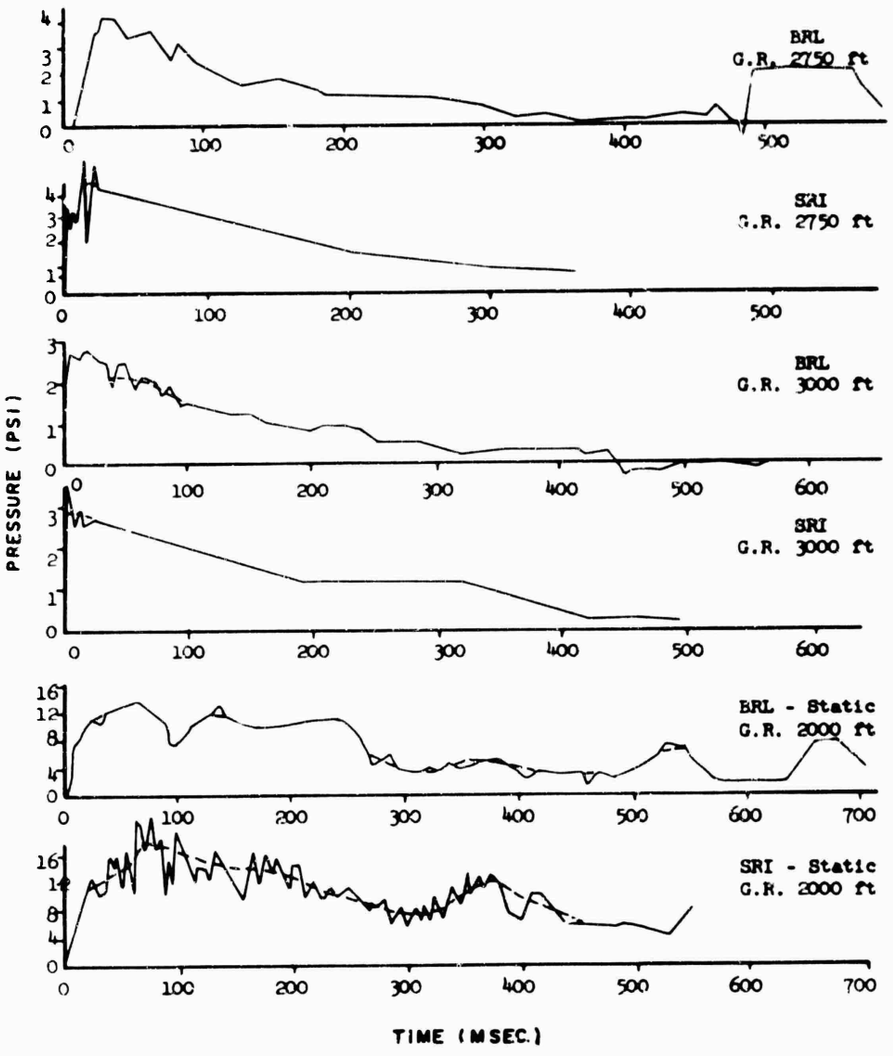

Fig. 4.45 Comparison of BRL with SRI Dynamic Pressure-Time Records for Shot 12. Water Line (2,750 feet and 3,000 feet) and Static Pressure-Time Records, Desert Line (2,000 feet) at 3-foot level.

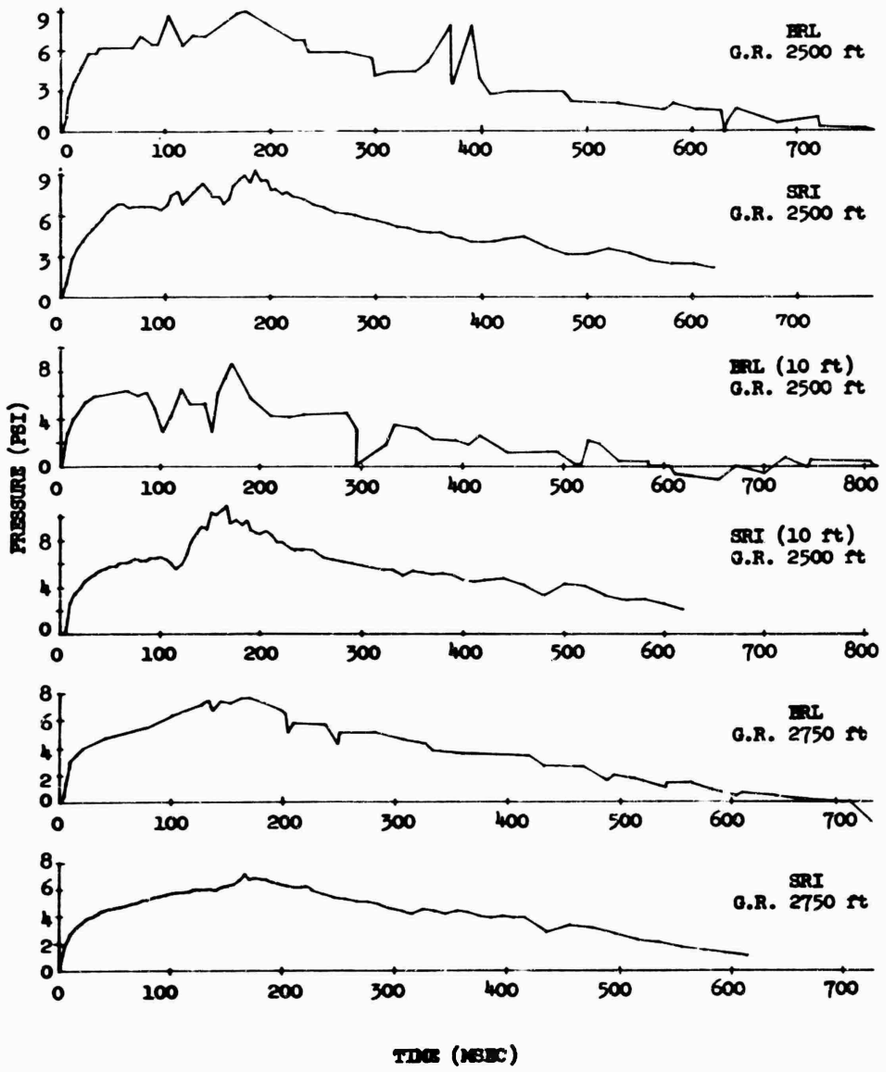

Fig. 4.46 Comparison of BRL with SRI Static Pressure-Time Records for Shot 12. Desert Line, 3-foot and 10-foot Level

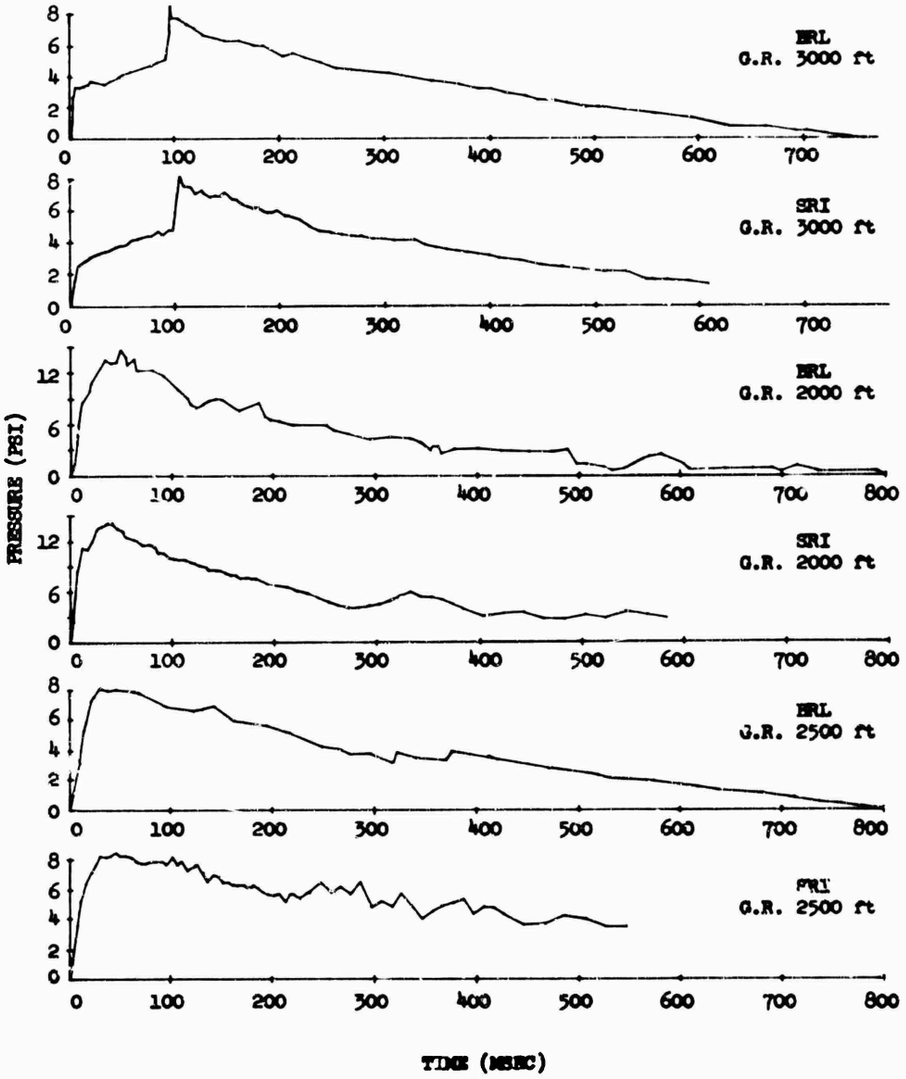

Fig. 4.47 Comparison of BRL with SRI Static Pressure-Time Records for Shot 12. Desert Line (3,000 feet) and Asphalt Line (2,000 feet and 2,500 feet) at 3-foot Level

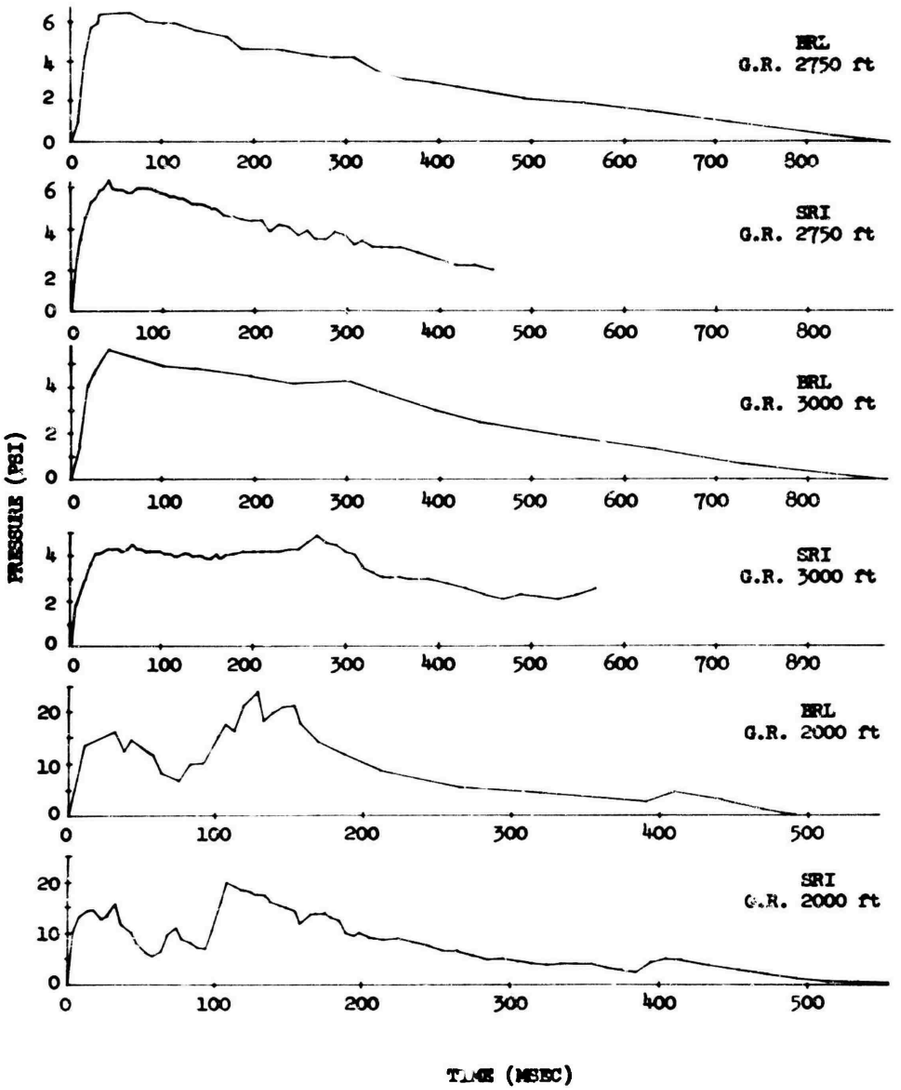

Fig. 4.48 Comparison of BRL with SRI Static Pressure-Time Records for Shot 12. Asphalt Line (2,750 feet and 3,000 feet) and Water Line (2,000 feet) at 3 ft Level

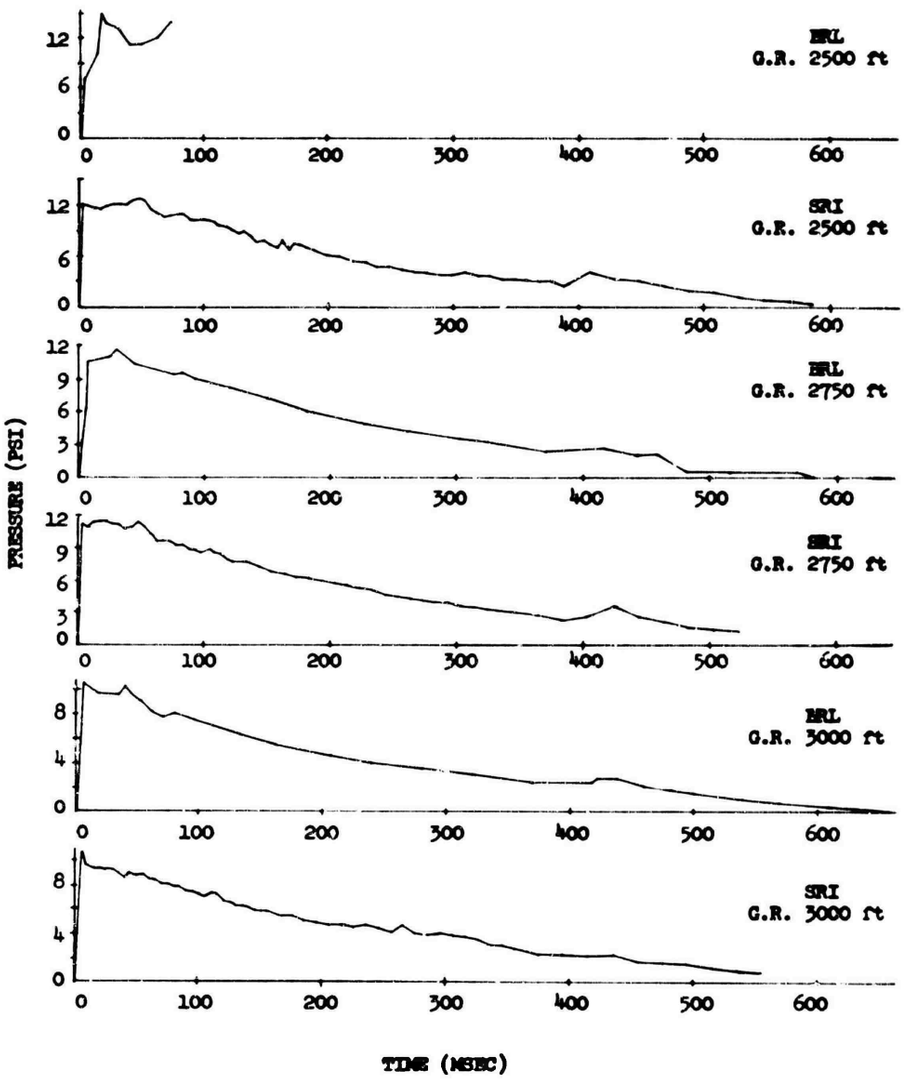

Fig. 4.49 Comparison of BRL with SRI Static Pressure-Time Records for Shot 12. Water Line at 3 foot Level

pendence not taken into account in the usual scaling laws might be demonstrable for a blast parameter.

The parameter investigated was the peak overpressure of the blast wave, irrespective of where the peak occurred in the time history of the blast wave. The measured peak overpressure values were scaled to 1 KT at sea level and then were compared to the ideal overpressure expected at the same ground range. The following factor was computed:

$$D = 100 \, (P_I - P_M) \, / \, P_I \qquad (4.1)$$

Where P_M = Scaled measured peak overpressure

P_I = Ideal overpressure at same scaled ground range

Then D is the percentage decrease of the measured overpressure below the ideal overpressure.

The value of D was computed for pressure levels from 5 to 60 psi, where data was available. The shots included in the comparison and their scaled heights of burst were as follows: Shot 2, HOB 213 ft; Shot 3, HOB 150 ft; Shot 4, HOB 136 ft; Shot 5, HOB 186 ft; Shot 6, HOB 237 ft; Shot 8, HOB 192 ft; Shot 11, HOB 248 ft; Shot 12, HOB 135 ft; Shot 13, HOB 152 ft; Shot 14, HOB 154 ft; Upshot/Knothole Shot 1, HOB 112 ft; and U/K Shot 10, HOB 204 ft. The criterion used for inclusion of these shots was that the ideal peak overpressure-distance curves for their range of heights of burst were essentially the same shape from 4 to 100 psi and differed only by slight shifts in ground range. Only pressures obtained over desert surfaces were used.

At a particular ideal overpressure level the values of D were plotted versus yield, and a curve was drawn by eye through the points. This was done for levels from 5 to 60 psi. The resulting lines were only slightly curved for levels from 6 to 40 psi plotted on semilog grid. Using these curves of D versus yield for various pressure levels, the curves shown in Fig. 4.50 were prepared for selecting yields. The values of D were used to determine $P_I - P_M$ for plotting. A curve indicating the ground range for this ideal overpressure is also given.

Fig. 4.50 indicates that a progressive lowering of overpressure below the ideal occurs as yield is increased over the range of data compared. A definite trend is shown from 6 to 40 psi, but below or above these values the curves intersect and become inconsistent. Above 40 psi the data points were widely scattered, and the approximating curves were of questionable shape and placement. The crossing of the curves at 5 psi depends on only a few data points and is also questionable.

The maximum decrease in overpressure below ideal of 50 KT is 65 percent at 21 psi and, for 2 KT, is 36 percent at 33 psi. The separation of the 2 KT and 50 KT curves from 6 to 40 psi averages about 40 percent. The maximum percentage increase above ideal for 2 KT is 45

percent at 5 psi.

A graph of height of burst versus yield for the comparison shots shows an average decrease from 200 feet at 2 KT to 120 feet at 50 KT. It seems unlikely that this change in height of burst can account for the large variation with yield indicated by Fig. 4.50.

The curves in Fig. 4.50 imply that an analysis of the measured peak overpressure in terms of the variables yield and height of burst would result in a significant relation between the decrease in overpressure below ideal and yield for a constant height of burst. Until such an analysis is conducted, the curves in Fig. 4.50 are considered reasonable averages of the results to be expected at the Nevada Test Site for scaled heights of burst from 100 to 250 feet.

4.7.2 Correction and Analysis of Dynamic Pressure Measurements. The comparisons of measured dynamic pressure with the ideal dynamic pressure is not quite valid, since the ideal pressures represent the

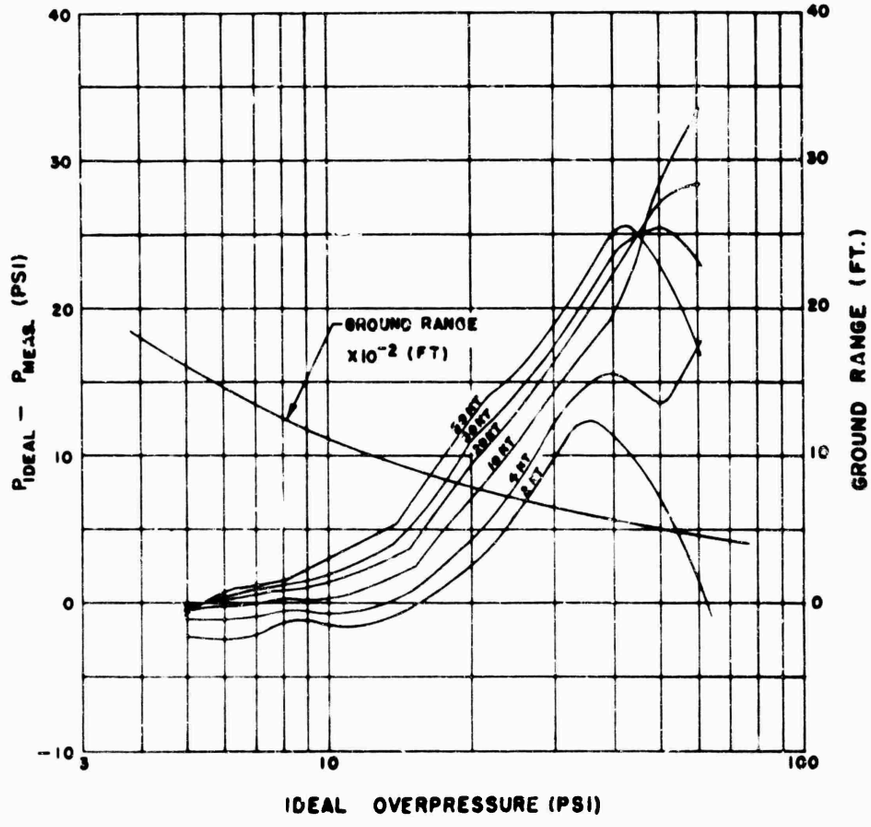

Fig. 4.50 Variation with Yield of ($P_{Ideal} - P_{Meas}$) Versus Ideal Peak Overpressure for Nevada Shots From 100 ft to 250 ft Height of Burst (1 KT at Sea Level)

free stream values and the measured dynamic pressures do not. The measured values have not been corrected for the Mach compressibility effect. By use of the pitot tube equations (Reference 10), Equation

4.2a and 4.2b, for correcting the readings measured by the q-gage the free stream values of dynamic pressure are obtained.

$$P_{dc_1} = (P_{ta} - P_{sa}) / (1 + \frac{1}{4} M^2 + \frac{1}{40} M^4 + ...) \qquad (4.2a)$$

or $$P_{dc_2} = \frac{\gamma}{2} M^2 P_{sa} \qquad (4.2b)$$

where: $P_{dc_1} = P_{dc_2}$ = dynamic pressure psi

P_{ta} = absolute total pressure, psia

P_{sa} = absolute static pressure, psia

M = Mach number, $\frac{u_1}{a_1} = \frac{\text{particle velocity, ft/sec}}{\text{local sound velocity ft/sec}}$

From the above equations it is seen that before the corrected dynamic pressure can be derived the Mach number, M, must be known. Now, it is known that the shock parameters within the precursor zone are not related through the Rankine-Hugoniot equations. Therefore, the Mach number cannot be calculated from Rankine-Hugoniot equation. To obtain the Mach number, recourse must be had to some other means. One such method by which the Mach numbers can be calculated is by use of the isentropic flow equations (Reference 10) given in Equation 4.3 and Equation 4.4.

$$\frac{P_{ta}}{P_{sa}} = (1 + \frac{\gamma-1}{2} M^2)^{\gamma/\gamma-1} \qquad \text{for } M \leq 1 \qquad (4.3)$$

and

$$\frac{P_{ta}}{P_{sa}} = \frac{(\frac{\gamma+1}{2} M^2)^{\gamma/\gamma-1}}{(\frac{2\gamma}{\gamma+1} M^2 - \frac{\gamma+1}{\gamma-1})^{1/\gamma-1}} \qquad \text{for } M \geq 1 \qquad (4.4)$$

By substituting the measured values of P_t, P_s and P_o in Equations 4.3 and 4.4 and solving the equations graphically the value M is obtained. Maximum recorded pressures as given in Chapter 3 were used in the calculations. The calculated Mach numbers and the corrected dynamic pressures for all shots are given in Table 4.8. Other pertinent information is also given in Table 4.8.

It is of interest to point out the error involved in calculating M

from q-gage measurements, which is given by Equation 4.5.

$$\frac{dM}{M} = \frac{\gamma - 1}{2\gamma \left(1 - \frac{P_{sa}}{P_{ta}}\right)^{\frac{\gamma-1}{\gamma}}} \left[\frac{dP_{ta}}{P_{ta}} - \frac{dP_{sa}}{P_{sa}}\right] \qquad (4.5)$$

Use was made of Equation 4.3 for $M \leq 1$ in deriving the above equation. When $\gamma = 1.4$ and the ratio $\frac{P_{ta}}{P_{sa}} = 2$ at which the Mach number, $M \cong 1$, Equation 4.5 becomes:

$$\frac{dM}{M} = 0.80 \frac{dP_{ta}}{P_{ta}} - \frac{dP_{sa}}{P_{sa}} \qquad (4.5a)$$

Similarly, when $\gamma = 1.4$ and the ratio $\frac{P_{ta}}{P_{sa}} = 1.1$ at which the Mach number, $M \cong 0.37$, Equation 4.5 becomes:

$$\frac{dM}{M} = 5.3 \frac{dP_{ta}}{P_{ta}} - \frac{dP_{sa}}{P_{sa}} \qquad (4.5b)$$

Hence, at increasing ratios of the total to the static pressure, the error in calculating the Mach number is decreased.

Also of interest are the errors involved in determining the corrected dynamic pressure. Equation 4.2a was derived by expanding in a power series the following expression, Equation 4.6:

$$P_{dc_1} = \frac{P_{ta} - P_{sa}}{\left[\frac{2}{\gamma M^2}\left(1 + \frac{\gamma - 1}{2} M^2\right)\right]^{\gamma/\gamma-1} - 1} \qquad (4.6)$$

The logarithmic derivatives of Equation 4.6 and Equation 4.2b

are respecitvely:

$$\frac{dP_{dc_1}}{P_{dc_1}} = \frac{dP_{ta} - dP_{sa}}{P_{ta} - P_{sa}} + 2 - \frac{\gamma M^2 \left(1 + \frac{\gamma-1}{2} M^2\right)^{\frac{1}{\gamma-1}}}{\left(1 + \frac{\gamma-1}{2} M^2\right)^{\gamma/M-1} - 1} \frac{dM}{M} \quad (4.7)$$

and:

$$\frac{dP_{dc_2}}{P_{dc_2}} = \frac{dP_{sa}}{P_{sa}} + 2\frac{dM}{M} \quad (4.8)$$

Equations 4.7 and 4.8 are equivalent. The error in the corrected dynamic pressure in Equatinn 4.7 as a function of Mach number is:

When: $\gamma = 1.4$ and $M = 0.1$

$$\frac{dP_{dc_1}}{P_{dc_1}} = \frac{dP_{ta} - dP_{sa}}{P_{ta} - P_{sa}} - 0.01 \left(\frac{dM}{M}\right) \quad (4.7a)$$

and when: $\gamma = 1.4$ and $M = 1.0$

$$\frac{dP_{dc_1}}{P_{dc_1}} = \frac{dP_{ta} - dP_{sa}}{P_{ta} - P_{sa}} - 0.47 \left(\frac{dM}{M}\right) \quad (4.7b)$$

It is seen from Equation 4.7a and Equation 4.7b that the error in the corrected dynamic pressure is a fraction of the error in the Mach number. The error in the corrected dynamic pressure in accordance with Equation 4.8 will be twice the error in the Mach number. Hence, the use of Equation 4.2a will reflect less error in terms of Mach number than Equation 4.2b. An interesting sidelight is the fact that, if the corrected dynamic pressures obtained from Equations 4.2a and 4.2b deviate from each other by large factors, it could be inferred that a large error exists in the value of Mach number. Both values of corrected dynamic pressures are given in Table 4.8

A cursory inspection of the wave forms of the pressure measurements indicate a trend which is worthwhile mentioning. Within the precursor zone high frequency and irregular oscillations are present on the wave forms. As the precursor is clearing up and out of the

TABLE 4.8 CORRECTED DYNAMIC PRESSURES

Ground (ft)	Total Pressure P_t (psi)	Static Overpressure P_s (psi)	Mach No. U/A	MEAS. Dynamic Pressure P_d (psi)	Corrected Dyanmic Pressure P_{dc_1} (psi)	Corrected Dynamic Pressure P_{dc_2} (psi)
SHOT 2						
940	38.5	15.0	0.98	24.0	19.0	18.6
1200	16.9	13.1	0.51	4.7	4.5	4.7
1700	11.1	8.2	0.51	2.9	2.7	2.6
SHOT 3						
760	120.2	46.1	1.15	70.0	51.0	54.2
830	100.0	35.0	1.19	60.0	42.9	46.9
1500	20.9	13.6	0.58	7.9	6.7	6.2
SHOT 4						
1950	75.1	18.1	1.34	50	32.7	38.7
2350	51.2	18.2	1.08	27.0	17.3	25.2
3000	12.9	6.1	0.68	6.0	5.4	6.0
4200	7.4	6.0	0.33	1.5	1.5	1.4
SHOT 5						
840	115.4	29.0	1.40	85.0	53.6	57.2
1080	46.6	16.5	1.07	27.0	20.4	23.3
1510	15.8	12.1	0.45	5.0	4.9	3.5
SHOT 6 - DESERT						
1825A	16.6	11.0	0.56	5.7	5.3	5.1
1825B	15.6	11.4	0.48	5.2	4.9	3.9
2050	16.0	10.7	0.55	5.5	5.1	4.9
2300	12.0	9.6	0.36	2.8	2.7	2.0
2550	9.5	7.3	0.36	2.2	2.1	1.8
SHOT 6 - ASPHALT						
1800	12.2	6.0	0.66	5.8	5.2	5.6
2050	6.9	5.1	0.36	1.9	1.6	1.8
2300	10.9	7.7	0.46	2.0	1.9	2.9
2550	9.8	7.8	0.36	1.0	0.97	1.9
SHOT 8						
1730	28.0	13.8	0.86	16.0	13.3	13.6
2040	17.5	13.6	0.45	5.5	5.2	3.6
2960	9.1	7.5	0.35	1.5	1.45	1.7
3700	6.0	5.4	0.31	0.8	0.78	1.1
SHOT 9						
780	35.2	21.1	0.72	19.0	16.7	12.2
1527	13.0	10.6	0.43	3.0	2.9	3.0
2026	8.6	6.9	0.36	1.7	1.6	1.8

TABLE 4.8 (Cont.)

Ground Range (ft)	Total Pressure P_t	Static Overpressure P_s (psi)	Mach No. U/A	MEAS. Dynamic Pressure P_d (psi)	Corrected Dynamic Pressure P_{dc_1} (psi)	Corrected Dynamic Pressure P_{dc_2} (psi)
SHOT 11						
880	30.7	14.2	0.86	17.3	14.4	13.8
1050	17.5	13.2	0.46	6.4	6.1	3.8
1400	11.3	8.4	0.43	2.2	2.1	2.7
1970	6.0	5.0	0.33	1.0	0.97	1.3
SHOT 12 - ASPHALT						
2000	31.6	14.7	0.85	16.1	13.5	14.0
2250	21.0	10.6	0.74	10.6	9.3	9.8
2500	17.4	8.2	0.73	8.5	7.5	8.3
2750	12.6	6.4	0.63	6.4	5.5	5.7
3000	7.4	5.6	0.38	1.7	1.6	1.8
SHOT 12 - DESERT						
2000	59.0	13.6	1.28	40.0	27.1	30.5
2250	34.6	14.3	0.93	20.0	16.2	16.4
2500	20.0	9.0	0.86	11.3	9.4	11.3
2750	15.8	7.7	0.70	7.7	6.8	7.1
3000	9.0	8.0	0.33	1.1	1.07	1.6
SHOT 12 - WATER						
2000	50.3	24.1	0.91	35.0	28.6	21.5
2250	39.0	14.2	1.0	28.3	22.2	19.0
2750	16.6	11.6	0.52	4.0	3.7	4.7
3000	13.2	10.5	0.38	2.6	2.5	2.5
SHOT 13						
1700	56.3	28.1	0.90	26.6	21.8	23.0
2650	30.7	13.1	0.96	17.0	13.6	16.4
3700	9.4	6.7	0.43	2.2	2.1	2.4
SHOT 14 - ASPHALT						
2000	37.4	15.8	0.93	21.0	17.0	16.9
2300	36.1	12.3	1.00	20.0	15.7	17.3
2550	19.2	8.6	0.78	8.7	7.5	8.9
SHOT 14 - DESERT						
2000	31.5	12.0	0.90	28.0	23.0	13.8
2300	29.3	10.0	0.98	19.0	15.0	15.1
2550	17.6	7.8	0.78	8.2	7.1	8.5

precursor zone the wave forms tend to smooth out. In the latter zone for some wave forms, spikes of short duration appear that would likely result from either overshoot of the capsule or in the difficulty of superimposing the static pressure-time curve on the total pressure-time curve from which the dynamic pressure-time history is obtained. By eliminating the short spikes in a number of cases, the dynamic pressures measured correspond to the values computed by means of Rankine-Hugoniot equation and the measured overpressure. These do not necessarily have to correspond to the ideal dynamic pressure, as was pointed out for Shots 2, 5, 8, and 11. In Shot 12 at the last station, 3000 feet, the peak dynamic pressure falls below the ideal value, but the measured value corresponds to the computed value, within experimental error. In the precursor zone of Shot 12, the initial portion of the measured dynamic pressure also corresponds to computed value using the Rankine-Hugoniot equation and measured values of the initial portion of overpressure. Thereafter, the dynamic pressure measured is higher than the computed value.

In an interim memorandum report (Reference 11) a method is presented that suggests an explanation for the differences between measured values of dynamic pressure and ideal dynamic pressure. The method describes the increase in flow resulting from secondary propagations being produced by a shock wave moving through a thermal layer.

The following analytical procedure to investigate the enhancement of dynamic pressure because of secondary propagations is due to C. W. Lampson of BRL. In the analytical procedure, use was made of adiabatic relations to describe the conditions instead of the Rankine-Hugoniot relations. However, the difference between these two relations can be neglected for the range of interest.

The particle velocity in an undisturbed compressional wave is given by Equation 4.9

$$u_1 = \frac{2}{\gamma-1}\, a_o \left[y_1^{\frac{\gamma-1}{2\gamma}} - 1 \right] \qquad (4.9)$$

where: $y_1 = \left(\frac{\rho_1}{\rho_o}\right)^{\gamma} = \frac{P_1}{P_o}$

u_1 = particle velocity, ft/sec

a_o = ambient sound velocity, ft/sec

and: P_1 = absolute static pressure, psia

P_o = ambient pressure, psia

As a result of the secondary propagation which will be a negative

pressure wavelet, the particle velocity is:

$$u_2 = \frac{2}{\gamma-1}\ a_1 \left[1 - \left(\frac{P_2}{P_1}\right)^{\frac{\gamma-1}{2\gamma}}\right] \qquad (4.10a)$$

or

$$u_2 = \frac{2}{\gamma-1}\ a_o \left[y_1^{\frac{\gamma-1}{2\gamma}} - y_2^{\frac{\gamma-1}{2\gamma}}\right] \qquad ,(4.10b)$$

where:

$$P_2/P_1 = \frac{P_o}{P_o}\ \frac{P_2}{P_o} = y_2/y_1$$

$$a_1 = a_o y_1^{\frac{\gamma-1}{2\gamma}}$$

a_1 = local sound velocity ft/sec

u_2 = particle velocity in rarefaction wave, ft/sec

and P_2 is the reduced absolute pressure, psia, resulting from the secondary propagations being produced.

The negative pressure pulse travels in the opposite direction of the initial shock wave, but the particle velocity travels in the same direction as the shock wave. The two particle velocities, one from shock wave and the other from the negative pressure, will reinforce each other giving rise to higher velocities. The equation relating the two particle velocities is given by:

$$u_1 + u_2 = \left(\frac{2}{\gamma-1}\ a_o\right)\left[2\,(y_1)^{\frac{\gamma-1}{\gamma}} - 1 - y_2^{\frac{\gamma-1}{2\gamma}}\right] \qquad (4.11)$$

Now, the dynamic pressure of the shock wave without disturbances is given by:

$$Pd_1 = \frac{1}{2}\ \rho_1\ u_1^2 \qquad (4.12)$$

The above quantity would then represent the ideal-dynamic pressure in the absence of a thermal layer. The dynamic pressure of a shock wave with disturbances or secondary propagations is given by:

$$Pd_2 = \frac{1}{2}\ \rho_2\ (u_1 + u_2)^2 \qquad (4.13)$$

This quantity is the resulting dynamic pressure when a thermal layer or when a precursor is formed. The ratio of these two dynamic pressure quantities is with the aid of Equations 4.9 and 4.11:

$$\frac{Pd_2}{Pd_1} = \frac{\rho_2}{\rho_1}\left(\frac{u_1 + u_2}{u_1}\right)^2 = \left(\frac{y_2}{y_1}\right)^{1/\gamma}\left[\frac{2\,(y_1)^{\frac{\gamma-1}{2\gamma}} - (y_2)^{\frac{\gamma-1}{2\gamma}} - 1}{(y_1)^{\frac{\gamma-1}{2\gamma}} - 1}\right] \quad (4.14)$$

Equation 4.14 is in the form which permitted comparing the computed ratios of dynamic pressure with the actual ratios.

Presented in Table 4.9 are the computations made for Shots 6, 12, and 14. On the asphalt line of Shot 12 the agreement between the computed and actual ratios is better, at least up to a ground range of 2,750 feet. Since it was assumed that large amounts of extraneous particles behind the shock wave were not present on the asphalt line, it could be expected that the agreement would be better on the asphalt line than on the desert line. The report of Reference 11 does not consider the effect of dust on the magnitudes of dynamic pressure. It is apparent from the table that the computed ratios on the desert line of Shot 12 do not agree with the actual ratios of dynamic pressure. However, the comparisons on the desert surface were for peak dynamic pressures of a relatively short duration.

If a line were drawn through the peak values, in effect smoothing out the pressure-time wave form, the ratios of the measured values of dynamic pressure to the ideal dynamic pressures would compare more favorably with the computed ratios. On Shot 14, on both surfaces, the asphalt and desert line, the agreement between the compared ratios is fair. Again, if a line were drawn through the oscillations present on the wave forms the agreement between the compared ratios would be improved.

The reason for the better comparison on the desert surface of Shot 14 than on Shot 12 desert surface may be due to the fact that at distances at 2,000 and 2,300 feet of Shot 14 the measured values of dynamic pressure are low. At these two stations each of the gage mounts were bent back or knocked out of the gage mount hole, therefore these two values are questionable. On the asphalt and desert line of Shot 6 and beyond 2,750 feet on the asphalt line of Shot 12, the agreement of the comparisons is not too good; but it would be suspected that, since these comparisons are made beyond the point of inflection on the pressure-distance curve, secondary propagations are no longer produced. At these distances, which may be considered the transition zone, differences exist between the ideal overpressures and measured overpressures, but the precursor is in the recovery or clearing up stage and the conditions other than that discussed in the memorandum report may prevail.

The method presented in Reference 10 does not accurately determine

TABLE 4.9 COMPARISON OF COMPUTED RATIOS WITH ACTUAL RATIOS OF DYNAMIC PRESSURE FOR SHOTS 6, 12 AND 14

Ground Range (ft)	Meas. Overpressure P_s psi	Ideal Overpressure P_s psi	Meas. Dynamic Pressure P_d psi	Corrected Dynamic Pressure P_{dc_1}	Ideal Dynamic Pressure P_{dI}	Actual $\frac{P_{dc_1}}{P_{dI}}$	Computed $\frac{P_{d2}}{P_{d_1}}$
			Shot 6 - Asphalt				
1800	6.0	14.2	5.8	5.2	4.9	1.14	1.73
2050	5.1	11.6	1.9	1.6	3.34	0.48	1.78
2300	7.7	9.2	2.0	1.9	2.17	1.38	1.23
2500	7.8	7.8	1.0	0.97	1.58	1.20	1.00
			Shot 6 - Desert				
1825A	11.0	14.2	5.7	5.3	4.9	1.08	1.26
1825B	11.4	14.2	5.2	4.9	4.9	1.00	1.26
2000	10.7	11.6	5.5	5.1	3.3	1.53	1.10
2300	9.6	9.2	2.8	2.7	1.6	1.69	1.00
			Shot 12 - Asphalt				
2000	14.7	24.0	16.1	13.5	12.54	1.08	1.35
2250	10.6	18.5	10.6	9.3	7.82	1.19	1.47
2500	8.2	14.8	8.5	7.5	[illegible]18	1.45	1.54
2750	6.4	12.2	6.4	5.5	3.6[illegible]	1.52	1.64
3000	5.6	10.3	1.7	1.6	2.62	0.61	1.66
			Shot 12 - Desert				
2000	13.6	24.0	40.0	27.1	12.54	2.1[illegible]	1.39
2250	14.3	18.5	20.0	16.2	7.82	2.07	1.24
2500	9.0	14.8	11.3	9.4	5.18	1.[illegible]	1.47
2750	7.7	12.2	7.7	6.8	3.61		1.[illegible]
3000	8.2	10.3	1.1	1.07	2.62	[illegible]41	1.28
			Shot 12 - Water				
2000	24.1	24.0	35.0	28.6	12.54	2.28	1.00
2250	14.2	18.5	28.3	22.2	7.82	2.84	1.24
2750	11.6	12.2	4.0	3.7	3.61	1.02	1.00
3000	10.5	10.3	2.6	2.5	2.62	0.95	1.00
			Shot 14 - Asphalt				
2050	15.7	26.2	21.0	17.0	15.24	1.12	1.34
2300	12.3	20.3	20.0	15.7	9.66	1.64	1.39
2550	9.6	16.3	9.7	7.5	6.47	1.16	1.54
			Shot 14 - Desert				
2000	12.0	26.2	28.0	23.0	15.24	1.51	1.39
2300	10.1	20.3	19.0	15.0	9.66	1.55	1.50
2550	7.8	16.3	8.2	7.1	6.47	1.10	1.60

the dynamic pressures resulting in the presence of precursor formation. Considering,however, the difficulty in measuring dynamic pressure as well as applying the proper correction for the Mach compressibility effect to obtain free-field dynamic pressure, it is felt that the method does give reasonable estimates. This method, along with the discussion on variations of overpressure measurements, will allow predictions of dynamic pressure to a reasonable degree of accuracy in the presence of precursor formation.

Chapter 5
CONCLUSIONS and RECOMMENDATIONS

5.1 CONCLUSIONS: INSTRUMENTATION

A high degree of success was achieved in the instrumentation of 12 shots in Teapot with the self-recording mechanical gages. The pressure-time gage and the dynamic pressure-time gage proved to be an ideal gage for use in a large-scale instrumentation program, particularly where the flexibility of the shot schedule required installation of blast lines on short notice.

The percentage of total record losses was very low. A major portion of gage failures resulted from pre-initiation on the first shot.

The design of the gages proved satisfactory. Although the arrival times and positive-phase durations compare well with SRI data, the addition of a timing system independent of motor characteristics is desirable for providing more-precise times of arrival and duration data. The peak overpressures and peak dynamic pressure obtained by the gages essentially agree with SRI data where comparisons can be made.

The shape of the pressure-distance curves obtained from the data indicate that relatively close spacing of gages on the blast line is necessary to properly define a pressure-distance curve within the radius of precursor action.

5.2 CONCLUSIONS: EFFECT OF PRECURSOR ON SHOCK-WAVE PARAMETERS

A great amount of data were obtained during Operation Teapot to give a better understanding of precursor formation and its relation to shock-wave parameters. The formation of a precursor will depend on the surface conditions, height of burst, and yield.

The chart in Reference 5 accurately predicted precursors for those shots on which they apparently occurred.

5.2.1 Peak Overpressure versus Ground Range. In the presence of a precursor, a lowering of overpressure will occur. The more-pronounced the precursor, the greater is the depression of the overpressure-distance curve. For a constant burst height and yield of weapon, the depression of the overpressure-distance curve is greater on an asphalt surface than on a desert surface. Recovery or clearing up of the presursor will be earlier on a desert surface than on an asphalt surface. The water surface used in these tests minimized the precursor effects.

The overpressure height-of-burst charts for good surface conditions and poor surface conditions contained in TM 23-200 generally bracket

the measured overpressure curves within the precursor zone. At the greater distances from ground zero beyond the precursor zone the pressures for the higher yield weapons (greater than 10 KT) fall on the good surface condition curves or on the ideal overpressure curves. The pressures from the lower-yield weapons (less than 10 KT) are above the ideal overpressure distance curves beyond the precursor zone.

Yield dependence of overpressures observed on Teapot can be shown when overpressures are referred to a height-of-burst chart that does not consider thermal effects.

5.2.2 Peak Dynamic Pressure versus Ground Range. The enhancement of dynamic pressure will depend on the surface conditions and is related to the depression of the overpressure-distance curve. The greater the depression of the curve, the greater are the measured dynamic pressures above the ideal dynamic pressure for the same type of surface. Over a dusty region the dynamic pressures will be greater than over a nondusty region.

Although peak dynamic pressures are of significance, it is questionable that they clearly represent the actual conditions existing throughout the precursor zone.

It is felt that the method given in Reference 11 gives a reasonable explanation for describing the differences between measured dynamic pressures and ideal dynamic pressures. This method can be useful in predicting dynamic pressures reasonably well in the presence of a precursor, although it will underestimate the magnitude of dynamic pressure over a dusty surface. To strive to predict dynamic pressure accurately from a military standpoint in the precursor zone seems somewhat unrealistic, in view of the fact that from the results obtained a change of 15 to 20 percent in ground range will result in a change of 100 to 400 percent in dynamic pressure.

5.2.3 Time of Arrival and Positive-Phase Durations versus Ground Range. When the precursor is most pronounced as was the case for the asphalt surfaces, the time of arrival of the initial disturbance will be least. The rate of propagation will be dependent upon temperature within the thermal layer. The higher the temperature the higher is the rate of propagation. Along with higher rates of propagation, the positive phase duration will be longer.

5.3 CONCLUSIONS: EFFECT OF SMOKE LAYER ON SHOCK WAVE PARAMETERS

Since the lowering of the overpressure-distance curve on the smoke line was less than on the clear line, it can be concluded that the thermal effects causing precursor formation were minimized because of the smoke. The time of arrival was longer and the positive phase duration was shorter on the smoke line than on the clear line, which further indicates that the smoke reduced the intensity of the precursor effect.

The effect of smoke on dynamic pressure cannot be determined, since no dynamic-pressure measurements were taken on the smoke line. However,

in view of the conclusions made about the precursor effect on dynamic pressure, it may be assumed that the dynamic pressure would be less on the smoke line than on the clear line within the precursor zone. On the other hand, beyond the precursor zone the overpressures on the smoke line are above the overpressures on the clear line; hence, the dynamic pressures may be assumed to be higher. This assumption follows from the comparisons of overpressure and dynamic pressure measurements of Shots 2, 5, 8 and 11.

5.4 RECOMMENDATIONS

It would be desirable to extend further the analysis, particularly in the field of the yield dependence on variation of overpressure and the relation of static-overpressure impulse to dynamic-pressure impulse. The latter would tend to eliminate the peaks of short duration on the pressure-time wave forms. Further, it is felt that dynamic impulse would be a more meaningful parameter from a military standpoint than peak dynamic pressure. This information combined with that already presented in this and previous operations would permit the prediction of the blast wave parameters for conditions similar to Operation Teapot.

Laboratory studies should be made to establish the effect of dust on dynamic pressure. An attempt should be made to correlate the effect of dust under laboratory conditions to field conditions. In line with the above, further tests should be conducted to determine the performance of the q-gage to dust-laden shock waves and to determine the correction factor for the Mach compressibility effect, so that the measurement of dynamic pressure can be corrected to free-field values. This should be extended to Mach numbers approaching one and above in dust free shock waves. The effect of orientation of q-gage with respect to direction of flow should be investigated.

Recommendations about the improvements of the instrumentation procedures are given in Appendix A. However, an additional recommendation is to improve the response time of the capsules or use capsules with similar response times in the q-gage to obtain a more-accurate record of dynamic-pressure versus time.

Appendix A
INSTRUMENTATION DESIGN

Self-contained, direct-recording gages for the measurement of air-blast pressures were first tested on a development basis by BRL during UPSHOT-KNOTHOLE. The results obtained were extremely promising. A full-scale project of measurement of air blast phenomena was undertaken for CASTLE 1/. The accelerated development program thus required, led to the production of a pressure-time gage, a dynamic-pressure gage, a peak pressure gage, and a very-low-pressure gage, all of which were used extensively and successfully during CASTLE. In addition, a prototype of a self-recording accelerometer was given a limited check with a moderate amount of success. Prior successes were further enhanced by continuing improvements to these instruments and resulted in a wealth of reliable pressure data being obtained on almost every shot of TEAPOT.

At the present time, due to this continuous program of development, a family of self-recording gages exists. These gages include: Pressure-time,standard; very-low-pressure-time,standard; peak-pressure, standard; differential-dynamic-pressure,development; accelerometer, development; displacement,development; and temperature,development.

A.1 PRESSURE-SENSING ELEMENTS

The basic component common to the pressure-time gage and the q-gage used by BRL during TEAPOT was a pressure-sensing capsule consisting of two concentrically convoluted diaphragms, nested together to reduce volume, and silver soldered together around their periphery. These capsules were essentially identical to those used in the various gages by BRL (Project 1.2b) during CASTLE. In brief, these capsules operate by an increase in outside air pressure entering through a small inlet hole, causing expansion of the diaphragms. A light spring stylus soldered to the center of the free diaphragm transmits this motion and produces a scratch on a coated-glass recording blank. The amplitude of this scratch is proportional to the movement of the diaphragm, which is proportional to the applied pressure. A sapphire-tipped phonograph needle, with a 1/2 mil radius tip soldered to the stylus arm is used to insure a very fine scratch. Ten ranges of capsules, from 0 to 1 psi to 0 to 400 psi, are in general use in BRL self-recording gages. The basic specifications of these are as follows:

Diaphragm material	NiSpanC (0 - 1 psi,phosphor bronze)
Deflection (at rated pressure)	0.020 in. min; 0.060 in. max.
Linearity	± 0.5%
Hysteresis	± 0.5%
Natural Frequency (undamped)	1400 - 2000 cps

Rise time	3 msec or less
Operating range	0 - 150# in. diameter
Pressure inlet opening Diameter	0.75 in. to 2.00 in. (depending on range)

Since the pressure capsules used on TEAPOT were of the same specification and ranges as those used on CASTLE, the same calibration methods and equipment were used (Reference 1).

The very-low-pressure gages use a single phosphor bronze, convoluted diaphragm, 5-3/4 inches in diameter. This diaphragm forms one side of the gage case. Any pressure differential existing between the inside and outside of the gage causes the diaphragm to deflect. This deflection is transmitted to and scratched on a coated-glass recording blank by a stylus soldered to the center of the diaphragm. The stylus point is the same as used on the pressure capsules. Reference 1 shows the various elements in Fig. C.1 .

The present pressure-sensing elements have proven themselves to be an accurate and reliable means of transmitting changes in pressure to a mechanically driven record. As in any research instrument, there is always room for improvement. A development program at BRL and a development contract with the U. S. GAGE Division of American Machinery and Metals Corporation is in progress to design even more satisfactory elements. A few desired improvements being investigated are as follows: (1) a welded construction to better resist salt water corrosion , (2) a more-satisfactory means of attaching the element to the gage to eliminate minor leakages and to make for more rapid changing of elements, (3) an all-metal stylus point which would compare in hardness to the present sapphire tip but would better resist shattering, which is presently experienced with excessive stylus pressure, (4) a better method of attaching the stylus arm to the movable shell. The present method of attachment allows the capsule to expand unevenly, and the stylus, instead of traveling in a straight line perpendicular to the mounting face, may go to the right or left in a straight or curved line or may lift from or dig into the recording surface. (5) a study is to be made to determine the optimum size inlet opening to provide sufficient damping to prevent excessive overshoot without the addition of damping material.

Further study is being given to the sensing element of the VLP gages. The present diaphragm has a usable range of 0 to 0.250 psi with a sensitivity of approximately 0.001 inches deflection per 0.001 psi overpressure and a natural frequency of approximately 50 cps. Due to the extreme sensitivity of this diaphragm, gusts of wind cause hash on the record if undamped. A 2-inch-thick section of a fiberglass filter reduces this effect by about 75 percent. An extremely steep fronted shock wave still causes excessive ringing of the element. Plans are being made to study these gages in a shock tube to determine a better means of damping. It is also thought to be possible to double the sensitivity by use of a capsule type element using two of the present

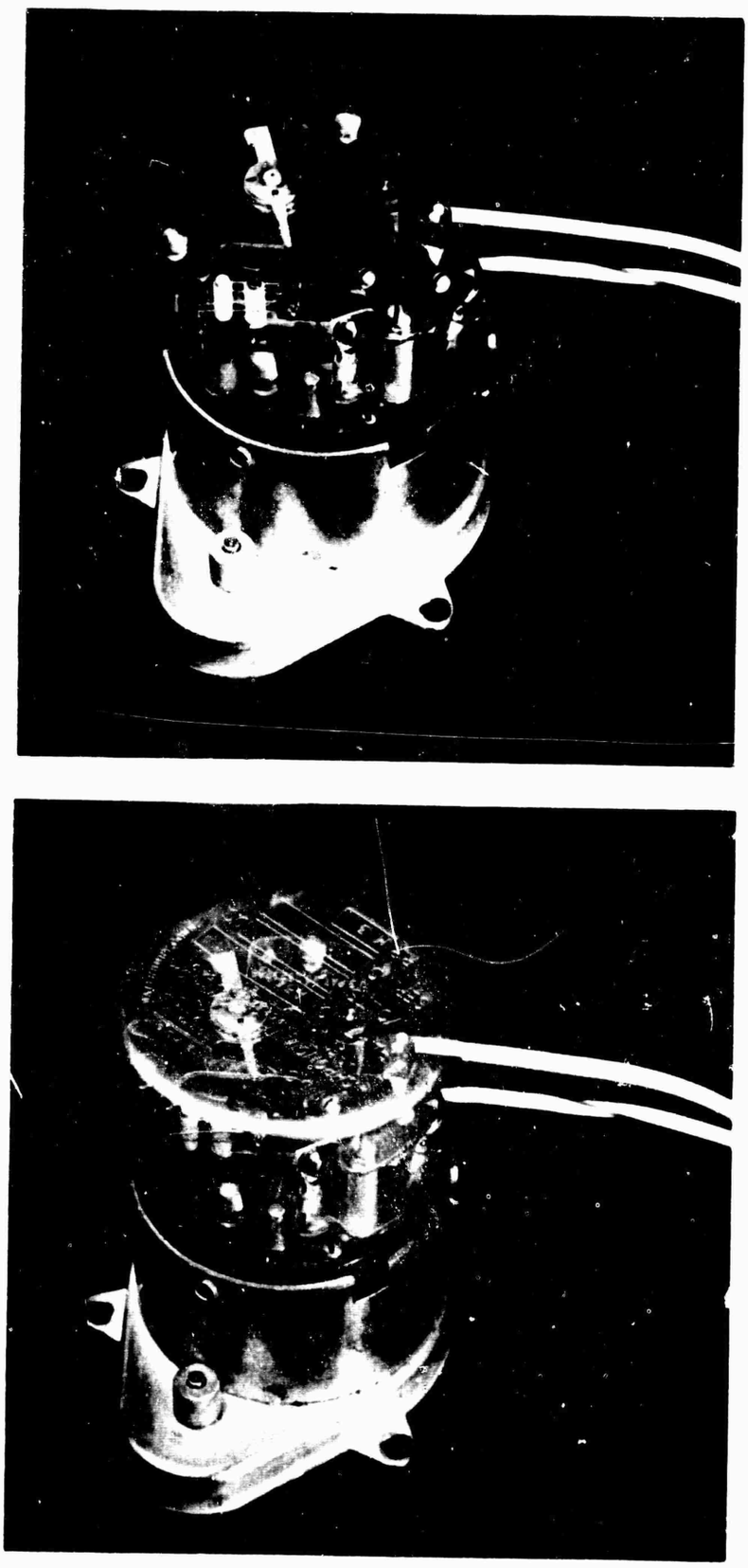

Fig. A.1 Mechanical Gage Chronometrically Governed D. C. Drive Motor

diaphragms.

A.2 RECORDING BLANKS

The recording medium of the scratch-type self-recording gages is a coated glass disc. A thin aluminum coating with approximately 15 percent light transmission is applied to one side of the disc by an evaporation process. Over thisathin coating of quartz is applied to protect the aluminum. This type of surface is less susceptible to damage from handling than the unprotected aluminum coating used by Project 1.2b on CASTLE. This coating however, has not proven entirely satisfactory. It was found necessary to apply excessive stylus pressure to produce an even and readable scratch. This was found to be especially true in the early days of the present series, when the ground temperature was low. This condition cleared up to a large extent with the coming of warm weather. It is felt that the hardness of the quartz coating is affected by temperature. Inconclusive laboratory tests appear to bear this out. Further tests will be conducted. Coating materials other than aluminum will be tried, including copper, silver, gold, and other metals. The present supplier of recording discs, Silver-Troy Corporation, is cooperating fully by supplying samples of various coatings for tests. It is hoped that eventually a coating material will be found that will be resistant to damage from handling and salt-water immersion and will produce a satisfactory scratch record with a nominal stylus pressure under all conditions of temperature and humidity.

A.3 DRIVE MOTOR

The heart of the time base in the pressure-time and q-gage is the A. W. Haydon Series 5600 motor used to drive the recording disk. The motor is a permanent magnet field style, requiring 7 to 9 volts D.C. for operation. An integral part of the motor is the chronometric governor. See Fig. A.1 . This governor operates by comparing the motor speed to that of a watch-type balance wheel and adjusting the motor current until both are identical. This results in rapid startup and accurate speed regulation. Laboratory tests upon sample motors give a startup time, i.e., the time difference between the actual time the current was turned on and a linear extrapolation to zero angle of rotation versus time, of 64.7 msec with a standard deviation of 11.3 msec. The data also showed that the motors reach 3 rpm within 130 msec after being turned on. Speed variations are less than 1 percent after full speed is attained. See Fig. A.2. The motors have been calibrated in the laboratory to within 0.1 percent of their rated rpm. According to the manufacturers specifications, the motor speed will not vary over 1 percent with up-to 10 G of acceleration at 10 to 300 cps. Laboratory tests show that the motors will stand up to 50 1g . impact with less than 10 msec.momentary deviation. The motor is operated at 8 volts by six Mallory MM-1R mercury cells. These cells give approximately 6 hours of operating time.

A.4 PRESSURE-TIME GAGE

The p-t gage used on TEAPOT is basically the same as that used by

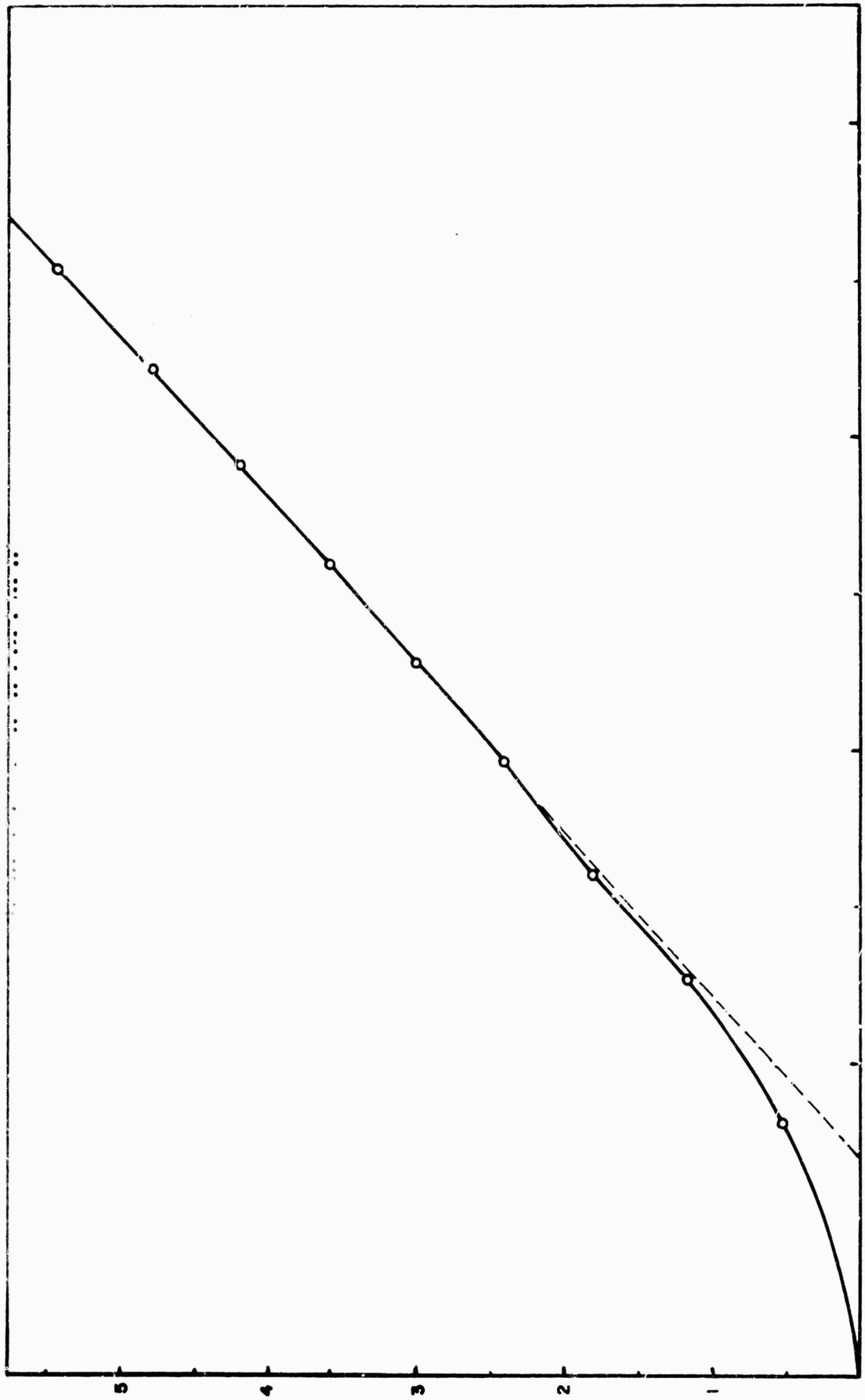

Fig. A.2 Starting Characteristics of Chronometrically Governed Motors

Project 1.2b on CASTLE; however, several modifications have been made. The capsules, stylii, and recording blanks have been modified to obtain a better, more-accurate record. The mechanical construction of the turntable and its coupling to the motor have been changed to eliminate the backlash and wobble previously encountered. A new photo-initiation circuit has been added to all gages to insure prompt and positive starting. In addition, a timing oscillator has been added to provide an additional check upon the motor for the determination of arrival times and phase durations.

These changes have enabled the p-t gage to become even more reliable and dependable, without sacrificing its portability, ease of installation, or ease of recovery. Due to the fact that is is entirely self-contained and self-powered, yet remaining small, light, and relatively inexpensive, it has shown itself to be an efficient gage for obtaining pressure-time data over a wide range of distances on almost every shot in the series.

A.4.1 Mechanical Construction. The p-t gage case consists of a 12-inch length of 5-inch diameter pipe closed at the bottom. A 3-inch pipe cap is welded to the bottom while a 1-1/4-inch flange is welded to the top. A 12-inch-diameter plate welded to a 3-inch pipe nipple, 12-inches long serves as a mount for the gage (see Fig. A.3). The gage unit is attached to an 8-inch-diameter plate which, in use, is bolted to the top of the flange. A rubber washer is used between the gage and its case to insure a pressure tight seal.

On the top of the gage is the photo cell with its mount and the "L" bar to support the thermal initiation link. The thermal link is hooked to a spring-loaded plunger. The photocell socket is rubber shielded and its lead is pressure sealed with a Condulet clamp. In field use, the photocell is covered with an optical filter held in place by a tubular fiber shield. 0.152-inch-diameter pressure orifice is near the center of the gage. The capsule-mounting screws extend through from the top and are pressure sealed with Permatex.

The interior of the gage has an 8-inch-long, 4-inch channel welded to the center of the top plate, with a 4-inch-square plate on the bottom (see Fig. A.3). At the center of the channel is the turntable-bearing housing, machined to a press fit. The turntable is mounted on two 5/8-inch-diameter ball bearings, each machined to a press fit in both the turntable shaft and housing. This completely eliminates any play in the turntables The turntable end of the bearing housing has been machined to clear the turntable by 0.003 inch , with the space filled with Dow-Corning Silicone Fluid DC-200 (viscosity 100,000 centistokes) to dampen the turntable and eliminate backlash. The motor is fitted into a hole in the end of the turntable shaft and fastened with two set screws. At the edge of the turntable is the limit microswitch cam. These limit switches are screwed to one side of the channel while on the other is the thermal initiator microswitch, directly beneath the plunger.

The motor driven batteries (6 Mallory RM-12) and the filament

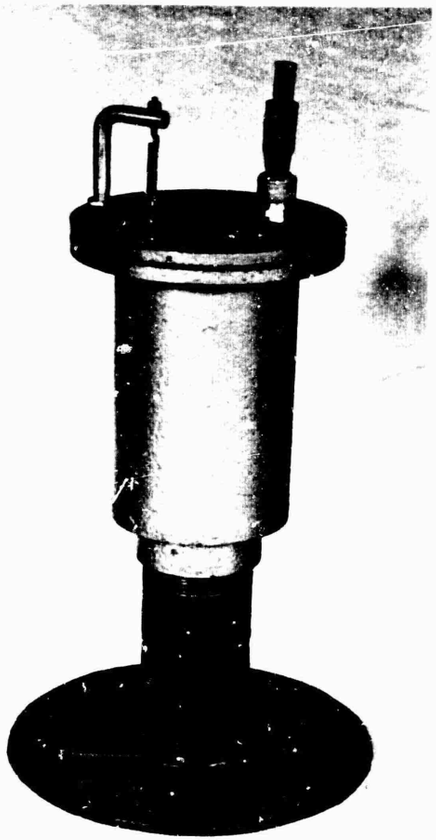

Assembled

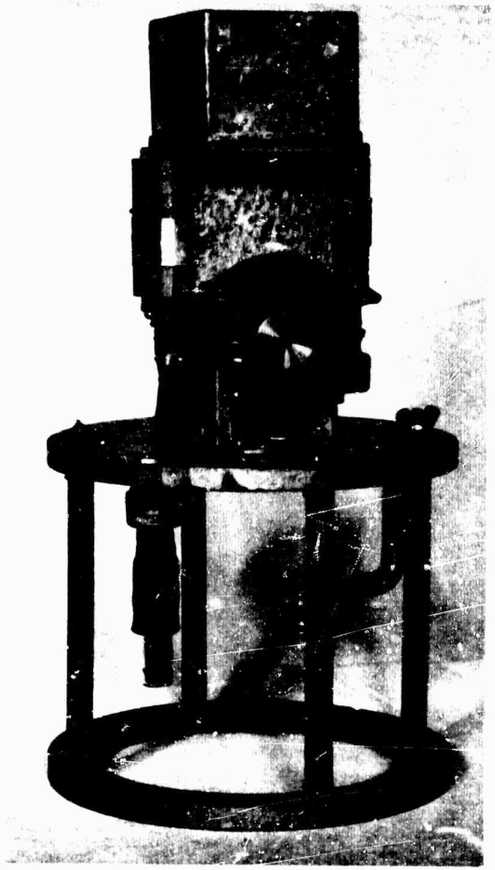

Recording Side

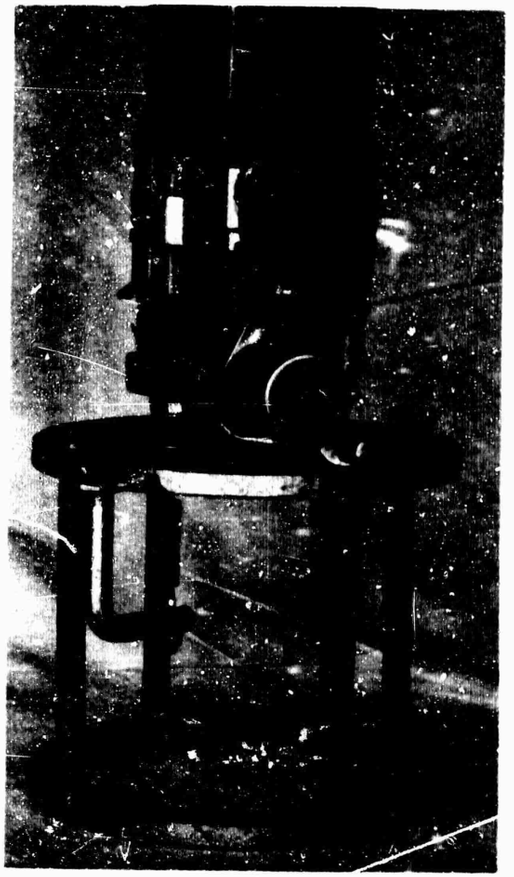

Drive Motor Side

Fig. A3 Mechanical Pressure-Time Gage

batteries (2 Mallory RM-42) are mounted in fiber tubes on each side of the channel. The timing subchassis is mounted to the hollow of the channel beneath the 16 contact plug. At the bottom of the gage is the main oscillator and photo-initiator chassis. Its connection to the gage by means of the 16 contact plug completes all connections at activation.

The pressure capsule is at the top of the gage, with its stylus projecting onto the recording disc. The timing stylus is directly below the pressure stylus, with the turntable brush extending along the record blank locking nut. A rubber and a paper washer are placed below the nut to keep the recording blank tight during use.

A.4.2 Initiation. The thermal initiator, used on all p-t gages, is the same as that used on CASTLE. Two strips of brass, 1/4 in. x 1-1/8 in. x 1/32 in., are overlapped 1/4 in., soldered with Wood's metal and then painted black. These strips hold the spring loaded plunger up (Fig. A.3); when the incident thermal radiation heats the Wood's metal to about 135°F., the link pulls apart allowing the plunger to drop and close the microswitch. This method is quite effective, although some failures have been noted at large distances on low yield shots and at extreme distances on large shots.

Photo initiators were also used on all p-t gages on TEAPOT. Figs. A.4 and A.5 show photographs of the chassis. The original circuit used on CASTLE is shown in Fig. A.6A. This consists of a photocell sensing element, a thyratron amplifier, and a relay actuator. The circuit works on light intensity. With sufficient light intensity, the phototube passes enough current to cause the voltage drop across the 22M resistor to exceed the firing potential of the thyratron (about 30V). The thyratron then fires, closing the relay which remains closed until the plate voltage is turned off.

New circuits were tried to produce an initiator that would be extremely reliable, but not susceptible to preinitiation. Fig. A.6B shows the first modification. This is similar to the first except that it requires a pulse of light to trigger it. This was successful but did not show the sensitivity desired.

The next attempts were made to find a method of initiation which did not depend on light. The circuit in Fig. A.6D was designed to initiate from the electromagnetic radiation pulse at zero time. This radiation would induce a voltage in the pickup coil, which would, in turn, fire the thyratron.

Fig. A.6E is a model designed to initiate from the gamma burst, as well as serve for a control in an experiment. The gage was normal except that no phototube was used.

An experimental test on the initiators was performed on Shot 3. Station No. 1, at 530 feet, and Station No. 4, at 1,070 feet, were equipped as per Fig. A.6E. Station No. 2 at 670 feet, and Station No.

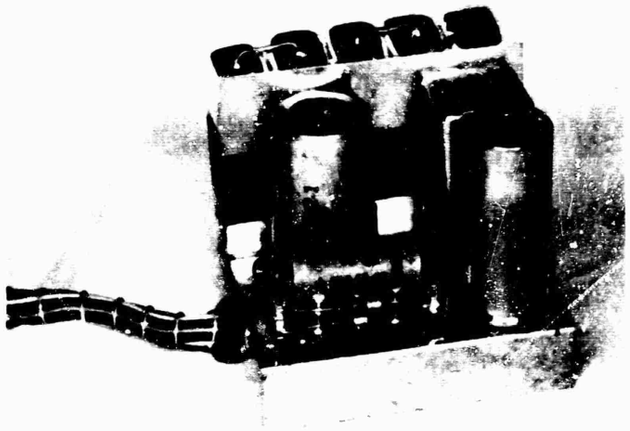

Fig. A.4 Photo Initiator and Timing Oscillator Chassis, Top View

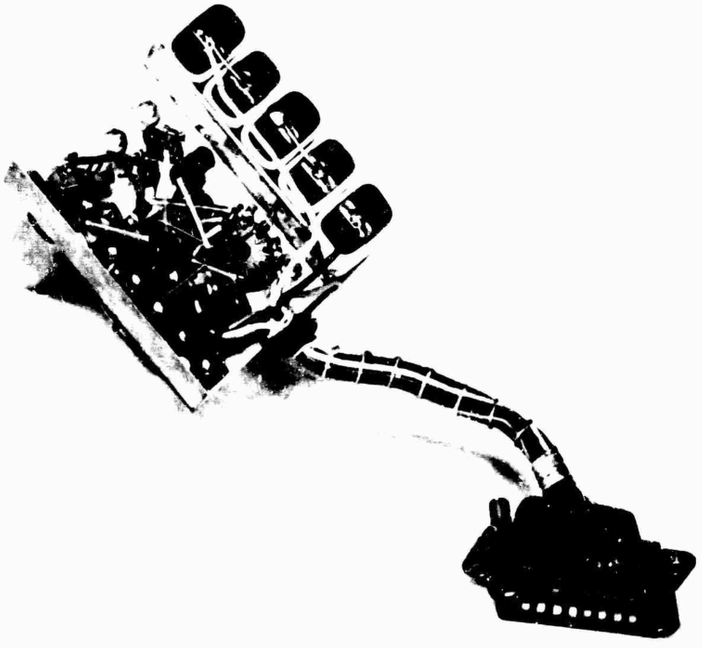

Fig. A.5 Photo Initiator and Timing Oscillator Chassis, Bottom View

5 at 1,500 feet, were equipped as per Fig. A.6D. Station No. 3, at 830 feet, was equipped as per Fig. A.6B. The first four initiators fired while the fifth did not. From this, one can only assume that the first four fired from the gamma burst, while the fifth was not sufficiently sensitive to operate at the distance selected.

Fig. A.6C shows the second modification in phototube circuits. This required a sharper pulse of light, but of less duration, than that of Fig. A.6B. This circuit proved quite successful.

Filters were used over the phototubes to reduce their sensitivity so that sunlight would not trip the gage or saturate the phototube. The photo initiators set off the gages prematurely on Shot 1 due to the failure of completely covering the phototube. This was corrected and caused no trouble on later shots. Original filters were made from film at BRL and had an optical density of 2.8. This was too dense for the outlying gages on Shot 4. Experiments were performed to determine the optimum density (See Fig. A.7). The filters selected had a density of 2.4. This requires a light intensity of about twice that of bright sunlight, and yet will work in the daytime or at night. This is optimum for pulse circuits also.

The circuit shown in Fig. A.6F is designed to get an initiator which is highly sensitive to the flash from A-bombs only. Field tests have not been conducted as yet, but laboratory tests show this circuit cannot be tripped by brilliant sunshine, but can be tripped by a 20 watt second electronic flash unit at 3 feet.

A.4.3 Timing. The timing marks on the p-t gage records are furnished by an oscillator and a pulse forming network. A typical pressure-time record with timing marks is shown in Fig. A.8. The complete circuit is shown in Fig. A.9. The oscillator, in the main chassis, furnished a 50 cycle signal to the pulse former, located in the subchassis. These current pulses are then put through the recording disc by means of the timing stylus. These current pulses have sufficient energy to burn holes in their aluminum coating, leaving a trace widened at the timing intervals.

The timing signals are furnished by a modified Wein bridge oscillator that has been calibrated to 50 + 2 cycles. These signals trigger a self-extinquishing cold cathode thyratron to produce 600 ma current pulses to the timing stylus. The timing stylus is constructed from a fine needle and has a tip diameter of 0.0002 inches. An extremely fine stylus tip is required to obtain a high voltage gradient at the point of contact, insuring that the pulse will leave a mark on the record. Large variations in mark diameter are noticed, mainly due to variations in thickness of the aluminum coating, and also the protective silica coating. All blanks used for timing traces had been immersed in water for a minimum of 30 minutes to remove as much of the protective coating as possible (data from manufacturers). It has been originally intended to put the timing marks on with the pressure stylus, however, this was discarded due to stylii difficulties, as well as the lack of

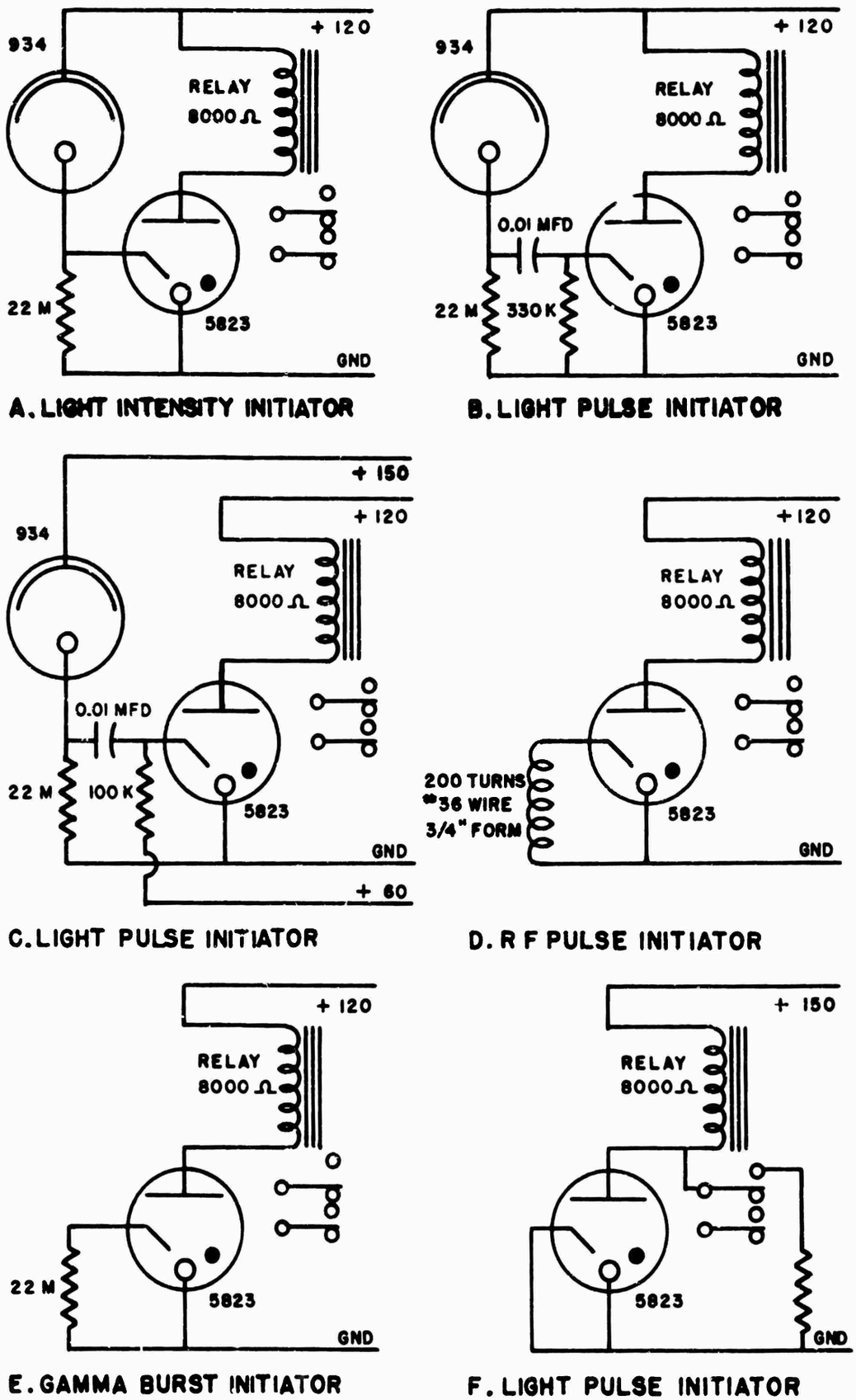

Fig. A.6 Schematics of Various Photo-Initiator Circuits

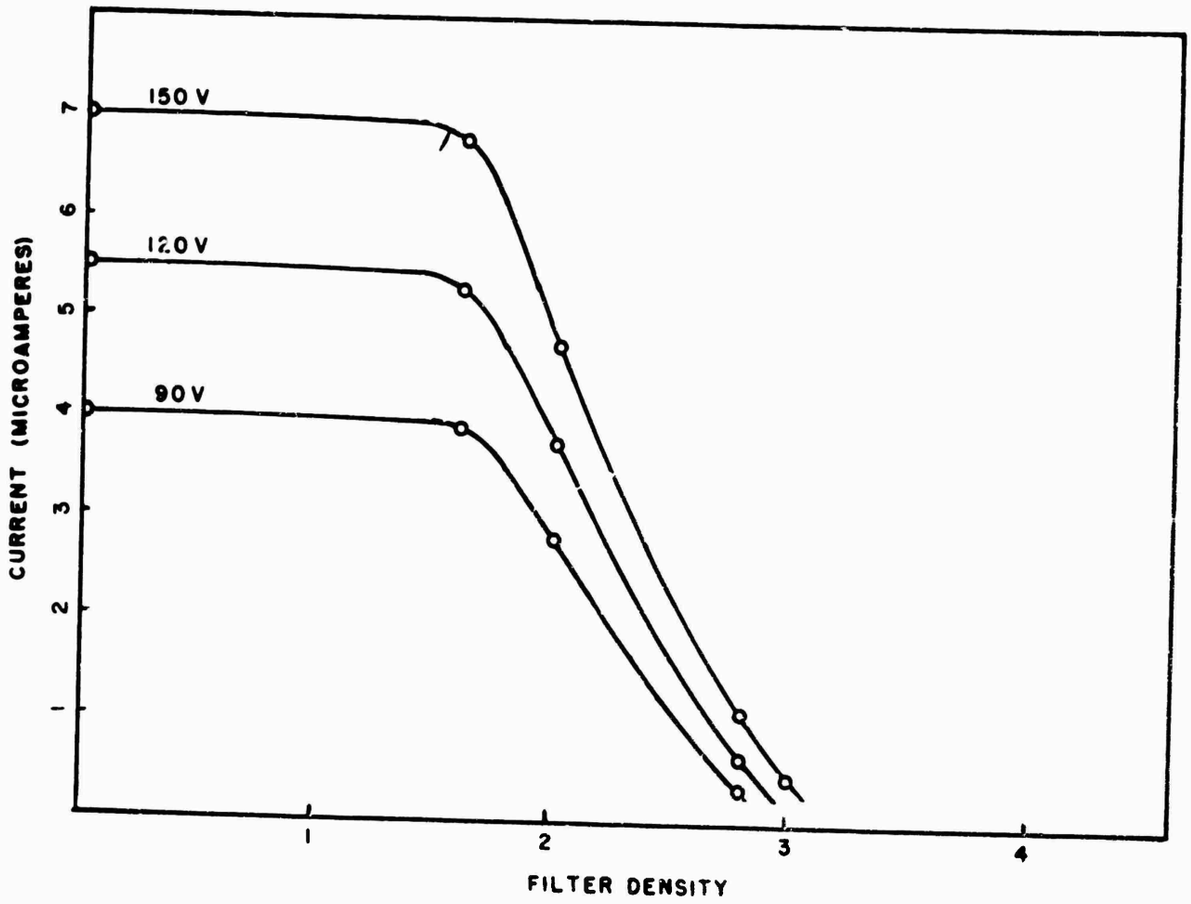

Fig. A.7 Photo Cell Currents vs Filter Density

Fig. A.8 Typical Pressure-Time Record w/Timing Record

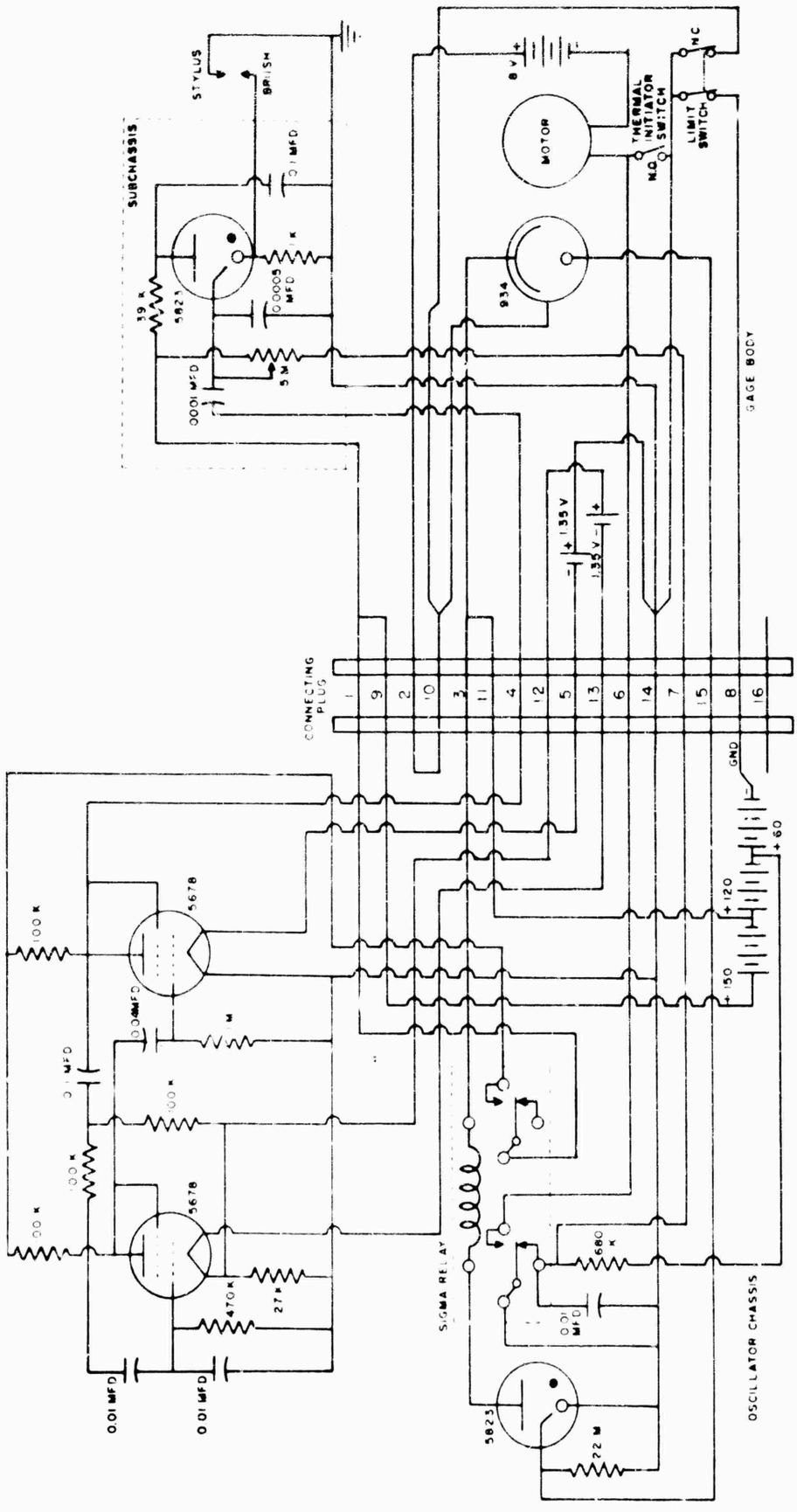

Fig. A.9 Schematic of Electrical Circuit of p-t Gages

resolution that it would give the pressure record.

An electronic delay circuit has been incorporated to prevent the timing marks from overlapping at the start of the record and becoming indistinquishable. This circuit introduces an inherent inaccuracy, as it delays the start of pulses, rather than the oscillator itself. Plate power for the oscillator is turned on at zero time in order that calibration accuracy is not destroyed by battery discharge. However, filament power is turned on when the gage is activated. The filament batteries used have a life of about 40 hours.

A.4.4 Installation and Recovery . Prior to actual installation, each p-t gage is completely checked out. The timing oscillator is calibrated to 50 + 2 cycles by means of the oscillator calibration circuit (See Fig. A.10) and a Hewlett Packard Model 524B frequency time interval counter. Then the entire gage is attached to the final

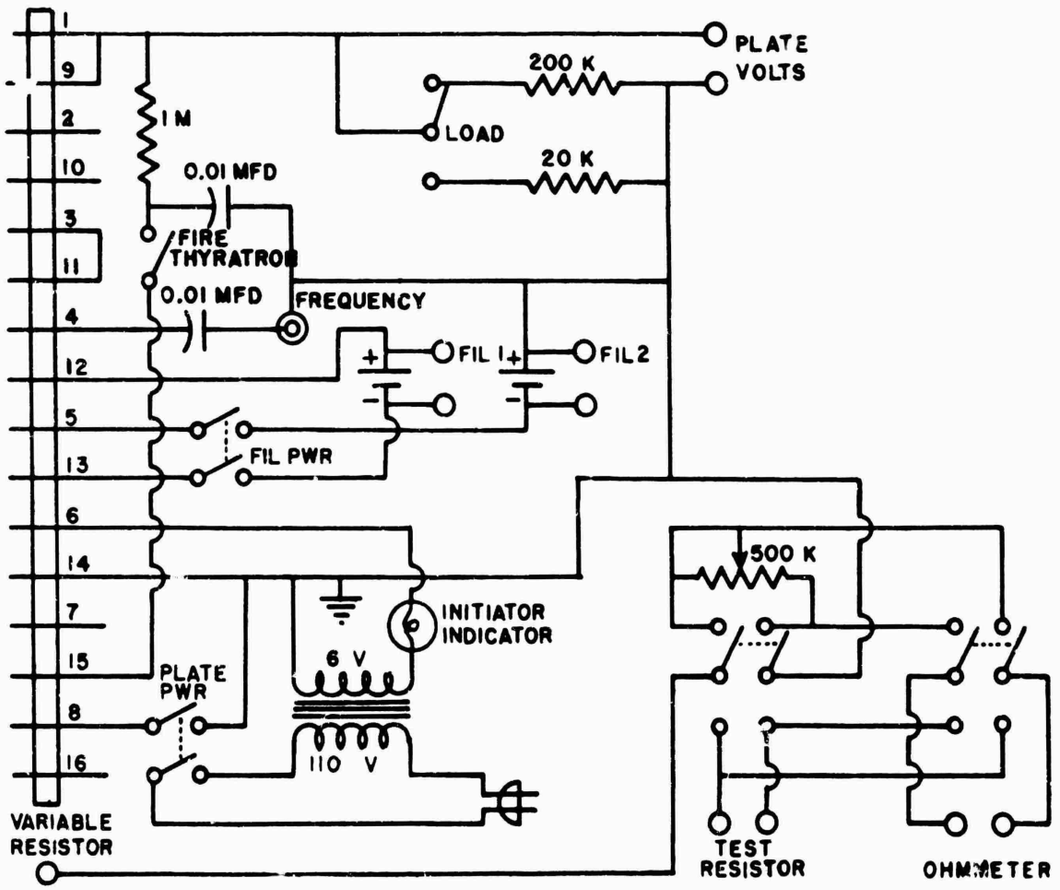

Fig. A.10 Schematic of Oscillator Calibration

checkout panel (See Fig. A.11 and A.12) and checked again. The battery voltages are checked and the oscillator frequency measured. The photo initiator is tested with an electronic flash bulb. The pulse forming thyratron is adjusted to its triggering level and the time delay measured. All pertinent data are scribed on the recording blank and the blank is installed. Activation is not completed at this time, how-

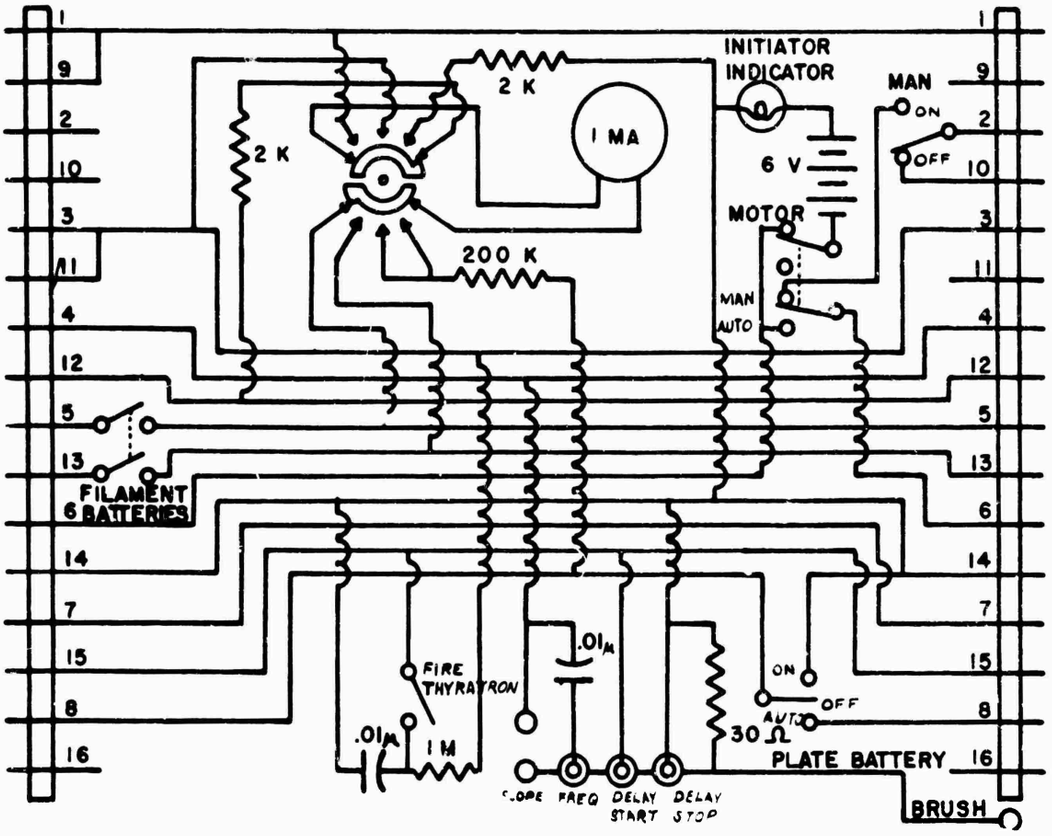

Fig. A.11 Schematic of Pre-installation Check Panel

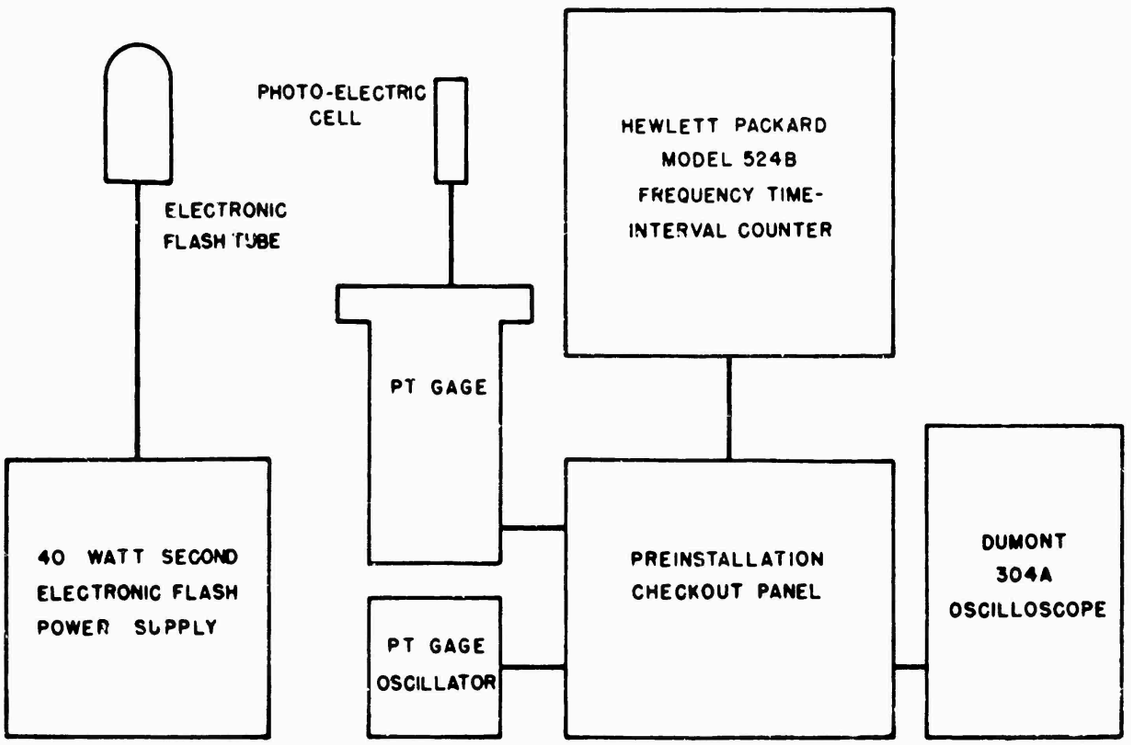

Fig. A.12 Block Diagram of Final Check System

ever, in order to conserve filament battery life.

Field installation installation is greatly simplified by use of the hole drilling rig (See Fig. A.13). Then, with a small amount of manual labor, the hole is ready for the gage (See Fig. A.14). The gage, with base, is set in the hole such that the top is level with the ground and the hole backfilled.

The gage is given a final visual check (See Fig. A.15) mainly to check the initiator switches, and then the 16 contact plug is inserted (See Fig. A.16). On gages with timing, activation is completed as late as possible (usually around midnight) to conserve the life of filament batteries. Cancellation of individual shots necessitates deactivation and reactivation due to the limited life of the filament batteries. After activation, the gage is put in its case and bolted down (See Fig. A.17). The ground around it is smoothed and the unit is ready for operation (See Fig. A.18 for a typical installation).

When the radiation level is sufficiently low, gages are recovered. A large pair of tongs is placed around the gage flange (See Fig. A.19). Next, the entire unit is pulled from the ground with a winch (See Fig. A.20). The gage is then opened and a base line run on the disc. Record blanks are then removed for reading.

A.4.5 Conclusions. The p-t gages used on TEAPOT have shown their reliability and versatility as was evidenced on CASTLE, yet with improved records (See Fig. A.8). Pressure-time records were obtained from over 95 percent of the stations installed. However, certain improvements can be suggested:

1. Recording blanks can be improved and made more uniform so that better timing traces can be obtained.
2. Simpler battery brackets should be devised for greater ease in battery installation.
3. Timing stylii and brushes should be modified for simpler record blank installation without scratching.
4. Limit switches should be changed to give more positive action, and possibly give more than one revolution. Two revolutions would eliminate base time shift.
5. A different mounting for the phototubes should be manufactured to eliminate complete replacement for every installation.
6. The timing circuits should be improved to give better and more reliable timing marks.
7. Filament battery turn-on should be changed to eliminate late activation.

A.5 DYNAMIC PRESSURE GAGE

The dynamic pressure gage or q-gage is a self-initiated, self-recording gage for measuring dynamic pressure. Static pressure and stagnation pressures are recorded on a single aluminized glass disc by

Fig. A.13 Drill Rig Operation for p_t Gage Stations

Fig. A.14 Installation of p_t Gage

Fig. A.15 Inspection of Initiators

Fig. A.16 Activation of Gage Circuits

Fig. A.17 Final "Button Up"

Fig. A.18 Typical p_t-gage Installations

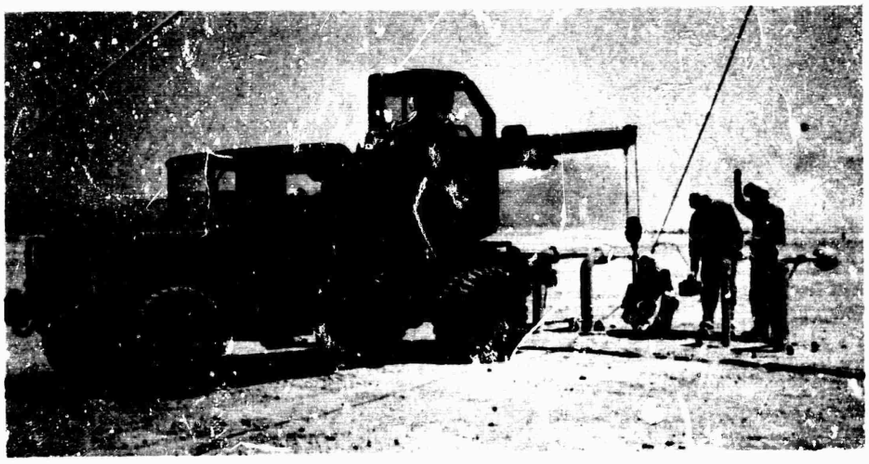

Fig. A.19 P_t Gage Recovery w/ 3/4 Ton Wrecker - Preparation

Fig. A.20 P_t Gage Recovery w/ 3/4 Ton Wrecker - Pulled Out

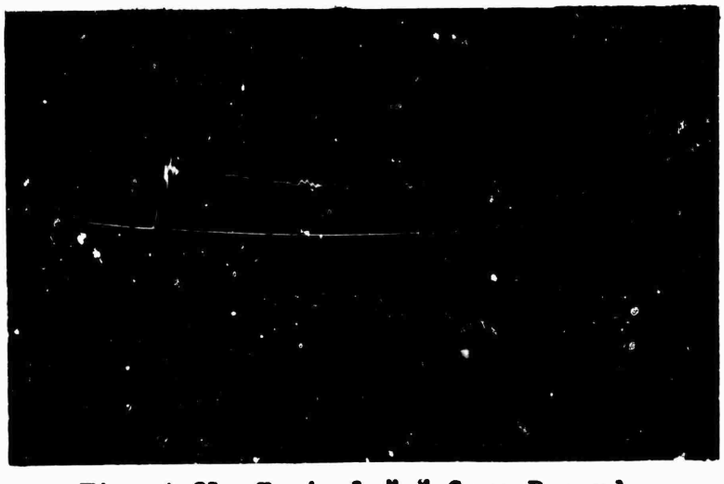

Fig. A.21 Typical "q" Gage Record

the action of two pressure sensing capsules. A typical record is shown in Fig. A.21.

The gage is 38 inches long and 3.8 inches in diameter with a hemispherical nose. The static pressure inlet is 12-3/8 inches from the front of the gage and has a diameter of 0.15 inches. The stagnation pressure inlet is 11 inches long with a diameter of 1/4 inch, except for the first half inch from the front which is choked down to 3/16 inch. Two 3-inch female pipe weldolets are welded to the bottom of the gage for mounting. Six-inch nipples of 3-inch pipe are screwed in the weldolets. To facilitate rapid recovery, a pipe union is used to secure the gage to the mount. Projecting laterally from the rear of the gage are a phototube and a fusible link for initiation of the gage.

A.5.1 Recording System. The pressure sensitive capsules are mounted with the axis of each 90° apart in a plane through the surface of the recording disc. The capsules are positioned such that the stylii will scratch concentric traces 1-13/16 inch and 1-5/8 inch in diameter on the aluminized coating on the disc.

Rigid mounting and precision machining are critical in the recording drive unit which consists of the turntable and shaft, shaft bearings, gear drive, and motor mounting (See Fig. C.10 CASTLE). The turntable is driven at 5 rpm through 2-to-1 reduction gears by the 10 rpm A. W. Haydon chronometrically governed D C motor. This rpm gives a recording speed of approximately 0.5 in/sec for the stagnation element and approximately 0.45 in/sec for the static element. In certain cases where a shock wave of short duration was expected, a 40 rpm motor was used to give a recording speed of 4 times the above values. This gives a more accurate time base and better resolution of the record.

A.5.2 Control System. The control section, consisting of an 8-volt mercury-cell battery unit for the motor power supply, a 45-volt battery for the photo-initiator, and the photo-initiator circuit, is mounted in the center of the gage.

The gage can be initiated by either a thermal link or a photoelectric unit. The thermal switch and the phototube are located on the rear chamber of the gage and are connected to the control section through a pressure-tight connector. The thermal switch is held open by the thermal link which is supported in a glass tube. The switch completes the circuit for the motor drive. Paralleling the thermal switch is the photoelectric circuit consisting of a 91° phototube, a sensitive-plate relay (Sigma type 16000 SP), an adjustable potentiometer, and a mechanical latching relay (Allied type 654B). This circuit operates on an intensity basis. The sensitive relay closes when the light becomes sufficiently intense to allow 400 microamps of current to pass through the phototube, potentiometer, and sensitive relay. This closure completes the solenoid circuit of the latching relay, which closes the drive motor circuit. A combination of a neutral density filter over the phototube and potentiometer setting is selected to give about half the relay closure current in bright sunlight. A filter density of between

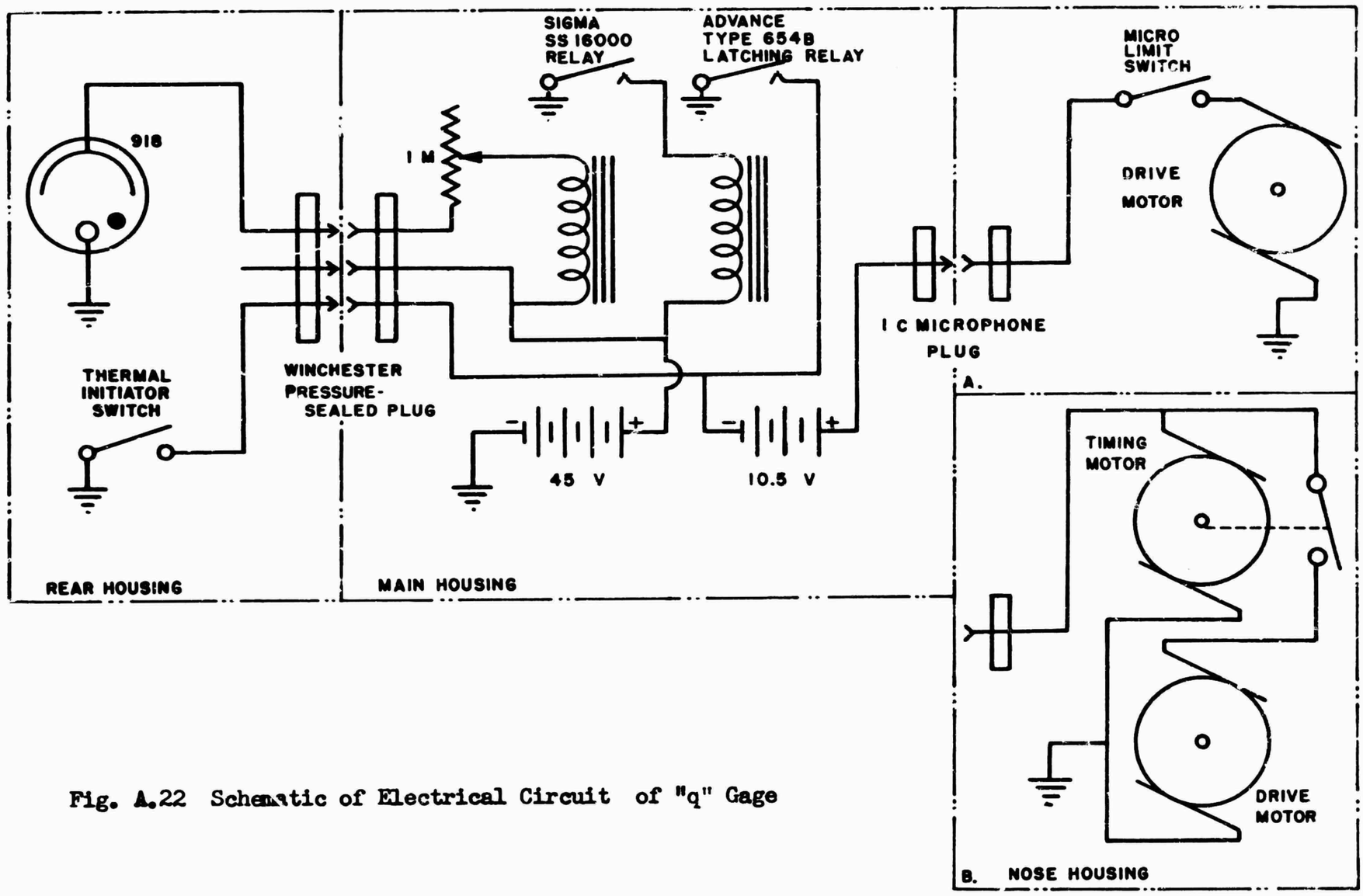

Fig. A.22 Schematic of Electrical Circuit of "q" Gage

0.7 and 0.8 has been found satisfactory for use at the Nevada Test Site. These filters are made by exposing a 4 x 5 in. cut film and developing to the desired density.

On TEAPOT one revolution of the record disc, or 10 plus seconds, was found to be sufficient recording time for all gage positions. A cam soldered on the underside of the turntable actuated a miniature microswitch cutting off the drive motor. By use of an auxiliary timing motor a recording time of up to 30 seconds is obtainable (See CASTLE Reference1)

A.5.3 Gage Mounts. The 3 foot mounts for the q-gages consisted of two parallel extra strong 3 inch pipes, each pipe connected to the gage through a union and 6-inch nipple. Below the unions were four cross-pieces, two perpendicular to the pipe and two at a 45-degree angle to the pipe. These cross pieces caused the mount to act as a rigid frame which enabled it to take a much higher bending moment than if two unconnected parallel pipes had been used. The pipes extended 3 feet into the ground where they were set in a concrete mix. A typical 3-foot mount with gage installed is shown in Fig. A.23.

In the first field installations of the 3-foot mounts, one bag of a quick setting cement, Cal-Seal, was mixed for the foundation. This mixture covered about 1-1/4 foot of the pipes and a loose earth fill was used to fill the rest of the hole. A slight shifting of the mounts was noted on the first few shots. The top of the mount was moved back from 4 to 10 inches. This was due to the rotation of the mount and foundation as a unit. An example of this condition is shown in Fig. A.24.

Shifting of the mount as described above occurred on the following shots; on Shot 5, approximate dynamic pressure 77 psi, on Shot 4, approximate dynamic pressure 62 psi, and on Shot 2, approximate dynamic pressure, 86 psi.

At the closest q-gage mount to ground zero on Shot 5, the most serious failure of a mount occurred. There the front pipe pulled part way out of the concrete and was bent into an arc. The rear pipe was bent, but not pulled out of the concrete. No lateral motion of the mount was noticed. It is estimated that the dynamic pressure was about 120 psi at this point although no record was obtained and this pressure is only a rough estimate. This gage mount is shown in Figure A.25.

Two changes were made in the placement of the mounts on the later portion of the tests. First, two bags of Cal-Seal were used for each mount, filling up the entire foundation hole with concrete mix. This was done to reduce the possibility of shifting of the foundation in the soil. Second, pieces of scrap metal were welded across the two pipes at the bottom of the mount to give better bond between the concrete and the mount. This was done to prevent the pipe from pulling out of the foundation. After these modifications were made no further difficulty was experienced with the mounts.

On Shot 12 there were two other failures of the 3 foot mounts. On

Fig. A.23 3' "q" Mount with Gage Installed

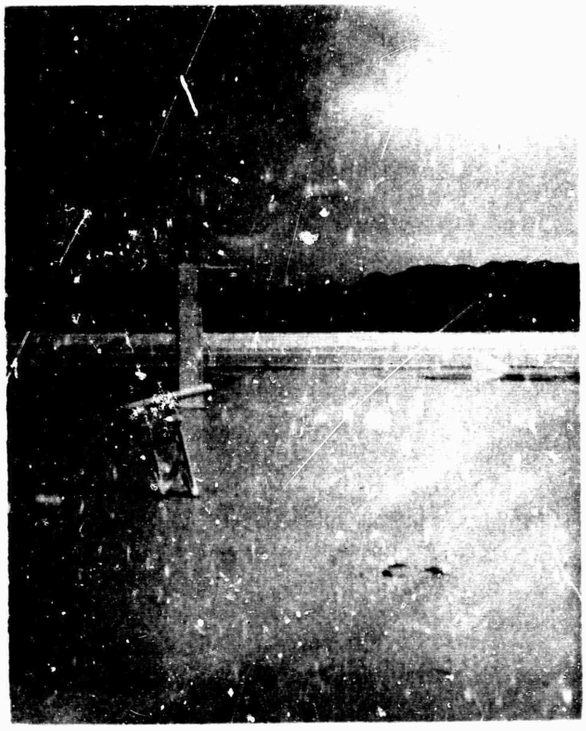

Fig. A.24 3' "q" Mount Displaced by Blast

Fig. A.25 3' "q" Mount Bent by Blast

the desert line the mount at the 2,500-foot station (dynamic pressure 12.4 psi) was completely torn from the ground, Fig. A.26. This mount was apparently hit by parts of a dismembered jeep. On the water line, the 3-foot mount at the 2,250-foot station (Dynamic pressure 14.5 psi) was rotated backwards about 12 inches. This failure was similar to failures which occurred on earlier shots and shown in Fig. A.24. In this case, the earth around the foundation was apparently softened by water seepage which permitted the movement of the mount. Closer to ground zero where the pressure was higher there was no failure of the 3-foot mounts.

The highest pressure at which any 3-foot mount stood without any sign of damage was 43.4 psi dynamic on the Shot 12 desert line.

The 10-foot mounts were similar to the 3-foot mounts in construction. A union and nipple were used to connect the pipe to the gage. The two parallel 3-inch extra strong pipes were connected by cross bracing for the above ground portion of the mount. The pipes extended 4 feet into the ground and were set in a concrete mix. Three guy wires were used to give added rigidity to the 10-ft mount, one to the rear and the other two orientated 45° to the right and left of the forward direction. The cables were attached to 10-inch expanding anchors buried about 4-feet in the ground. To improve the holding action of the anchor at least one bag of cement mix was poured into each anchor hole after it had been placed. A typical 10-foot mount with gage installed is shown in Fig. A.27.

Only four 10-foot mounts were used. On Shots 1 and 9, one mount was exposed twice to dynamic pressures of 4.0 and 14.3 psi. On Shot 12, one 10-foot mount was used at the 2,500-foot station on each of the three lines. Both the water and desert line mounts received some damage. On the desert line (dynamic pressure 12.4 psi) both front guy wires were severed and the mount deflected to the rear for about 6 inches. On the water line (dynamic pressure 10 psi) the right front guy wire was severed and the mount deflected about 3 feet to the left rear. Both of these mounts were in a region of flying vehicle parts and in all likelihood these missiles caused the severance of the guy wires. The damage to the desert line mount is shown in Fig. A.28.

A.5.4 Orifice Size and Damping. In the development of the q-gage a series of tests were run at the BRL Shock Tube to determine optimum dimensions and damping of the orifices. These tests covered static pressures from 3 to 30 psi. Various sizes of stagnation pressure orifices, damped and undamped, and varying quantities of damping material in the static and stagnation pressure inlets were tested. From these tests, it was concluded that optimum results would be obtained using a stagnation pressure inlet of 1/4 inch diameter with a 3/16 inch diameter choke, 1/2 inch long in the nose. The static pressure inlet was placed 12-5/8 inches from the nose and has a diameter of 0.152 inch and a length of 1/2 inch.

A.5.5 Experimental Models. Two experimental models were made in the field by modifying the present q-gage in an attempt to provide a

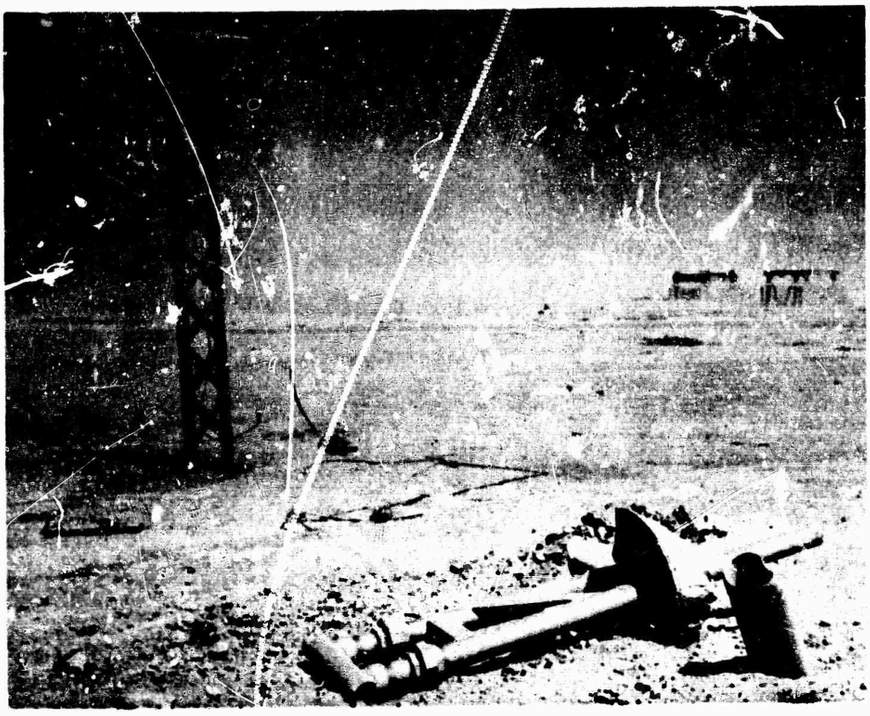

Fig. A.26 3' "q" Mount Hit By Flying Vehicle Parts

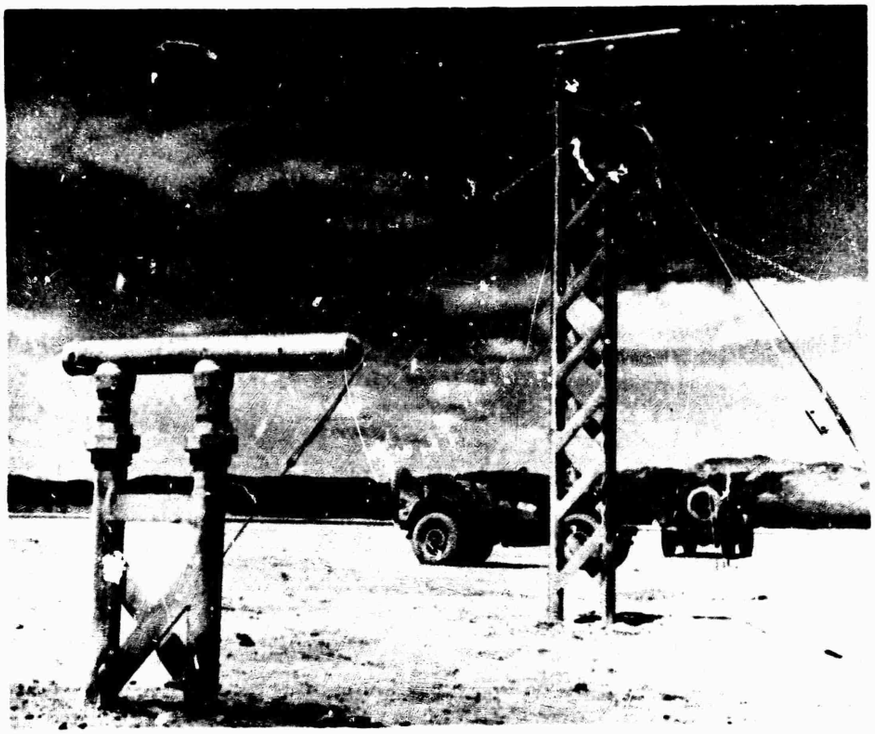

Fig. A.27 10' "q" Mount with Gage Installed

gage which will be both simpler to assemble and to provide a single scratch record giving differential pressure directly. This would eliminate the necessity of reading two records and subtracting the static pressure from the stagnation pressure. The disadvantage of this is that no static pressure record is provided by this gage. In practice, however, a standard p-t gage, surface mounted, is placed along side the q-gage.

The first model tried used a differential capsule system consisting of four capsules. The capsules are connected in two groups of two capsules each in series so that two of the capsules respond to the

Fig. A.28 10' "q" Mount with Guys Cut and Displaced by Flying Vehicle Parts

stagnation pressure, the other two to the static pressure. The two groups are connected by means of a short link which supports the stylus arm. In this manner one group opposes the other group and the resultant is the differential pressures. The capsules used gave a deflection of approxiately 40 mils at 16 psi differential pressure. The calibration curve was extremely linear. A disadvantage of the model is the bulk of the capsule system and the difficulty of attaching it to both the stagnation and static openings. Further development should alleviate these disadvantages.

A second experimental model that also shows much promise is simpler in construction. A single capsule is connected to the stagnation pressure inlet. A large static pressure inlet hole is located at the

same position as the static capsule on the standard gage. This allows the static pressure to fill the entire recording chamber and thus applies this pressure to the exterior of the stagnation element. In this manner the capsule responds to the differential pressure, and the standard calibration curve for an element of any range may be used. On the present model a 1/4-inch-diameter static pressure inlet hole is used. Shock tube tests to determine the optimum size opening will be made. This model has the advantage of using only one standard capsule and will make for simpler installation of the recording disc and drive unit. A minor modification to seal off the recording chamber is the only other change necessary.

A.6 VERY LOW-PRESSURE GAGE

The very-low-pressure gage is a modification of the VLP gage used on CASTLE by Project 1.2b. The basic ideas of the gage are the same, but through experience and laboratory tests it has been modified to correct difficulties previously experienced and to widen its uses. These include a better construction of the case, a variety of recording speeds, the addition of a wind and damping baffle, and a photo initiation system to be used in conjunction with the gage. A timing circuit was also incorporated into the gage, but did not prove too successful due to the excessive stylus pressure required for recording.

The VLP gage is self-contained and self-recording and is capable of measuring pressure differentials in the 0-to-0.500 psi range with a sensitivity of 0.0001 psi.

A.6.1 Description. The VLP gage itself consists of five major parts:

1. A pressure-sensing diaphragm that consists of a single phosphor-bronze convoluted diaphragm, 4-3/4 inches in diameter, having a stylus arm with a sapphire tipped needle soldered to the center of the diaphragm to transmit the motion of the diaphragm to the recording disc.

2. The recording disc, which is a 5-inch-diameter glass disc, 1/16 inch thick, with an aluminized coating and a quartz film to protect the coating. A trace less than one mil wide and approximately 4-3/4 inches in diameter (varying slightly with the gage), is recorded.

3. The drive motor of which there were four to choose from, directly turned a turntable that held the recording disc. The available motors were a 6-volt dc , chronometric-governed motor providing a recording speed of 3 rpm, or one of three spring drivenchart drive motors giving recording speeds of one revolution per 4 hours, one per 12 hours, and one per 24 hours.

4. The gage case, which is a 9 in. x 7 in. x 1/8 in. thick steel box with a removable cover. The front and top of the case were machined to permit sealing of the diaphragm and the cover to make the box air-tight. A sponge rubber gasket was used to seal the lucite

cover. The assembled gage is shown in Fig. A.29.

5. A wind and damping baffle that consisted of a 2 inch thick spun glass air filter in a 6 in. x 7 in. sheet metal case. This is fastened to the outside of the case in front of the diaphragm, Fig. A.29.

A.6.2 Initiation. These gages could be initiated either manually or by means of a photoelectric system. Figure A.30 shows the gage and photo initiator. The standard method for initiation was manual and consisted of throwing a switch which completed the motor drive circuit and started the recording mechanism. This was done at zero time along with the closing of the relief screw, which had been left open prior to this time to permit pressure equalization.

The photo-initiation system was used at stations where it was impossible for personnel to man the gages. The circuit (See Fig. A.31) consisted of a sensitive photocell circuit closing an electrical latching relay, providing a closed circuit to the motor drive circuit and also to a Cramer timer. The timer was set to open the relay, which opened the motor drive circuit, after the pressure wave had passed. The flash was focused into the cell by means of a ground lens mounted with the photocell in a fiber tube so that it could be adjusted to see the flash. The photoinitiation system proved to be very successful. The only failure experienced was a preshot initiation apparently due to a passing car's headlights.

A.6.3 Calibration. The calibration of the VLP gage consisted of removing the baffle and placing a pressure chamber in its place (See Fig. A.32). A water tube manometer was used in setting the pressures. The calibration was recorded on a regular recording disc in steps of 1 inch of water in the low pressures and 5 inches of water in the higher pressures. The gages were calibrated to 40 inches of water which corresponds to 0.5688 psi. Two calibrations were run on each gage to check the calibration curve and in all cases they were identical.

The procedure of calibration was to seal the case and then apply the pressure and record it. The pressure was then released and the gage unsealed to record a zero. This was done with each calibration step to simulate actual field conditions. A typical VLP gage calibration curve is shown in Fig. A.33.

A.6.4 Discussion and Conclusions. For an inexpensive, self-recording, sensitive pressure-time gage the VLP gages have proven themselves to be reliable and accurate. Being simple and of few parts they record directly and do not require the additional calibration of amplifiers and recording equipment used with electronic equipment. There are still many improvements and experiments to be made on these gages, some of which are:

(1.) improve damping overshoot and ringing of the element; (2.) increased sensitivity of the sensing element; (3.) sideways restraint

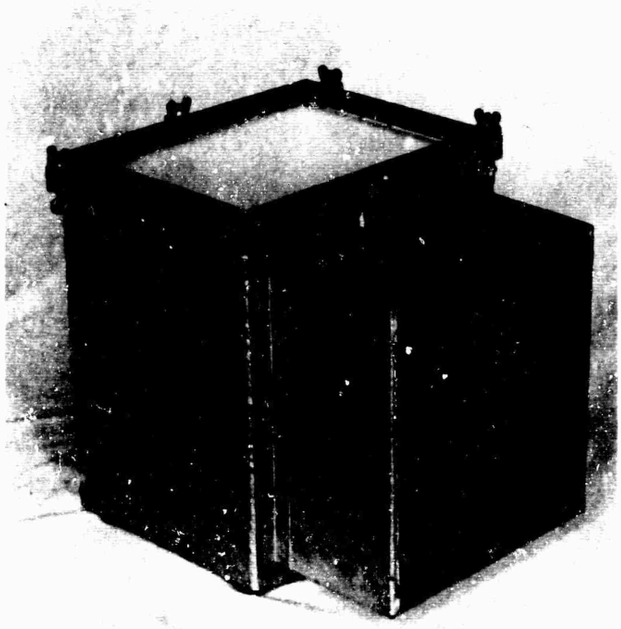

Fig. A.29 VLP Gage

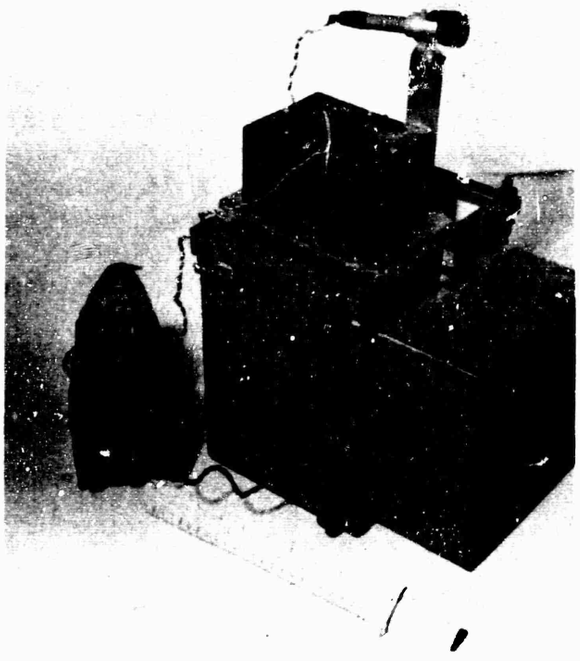

Fig. A.30 VLP Gage and Photo Initiator

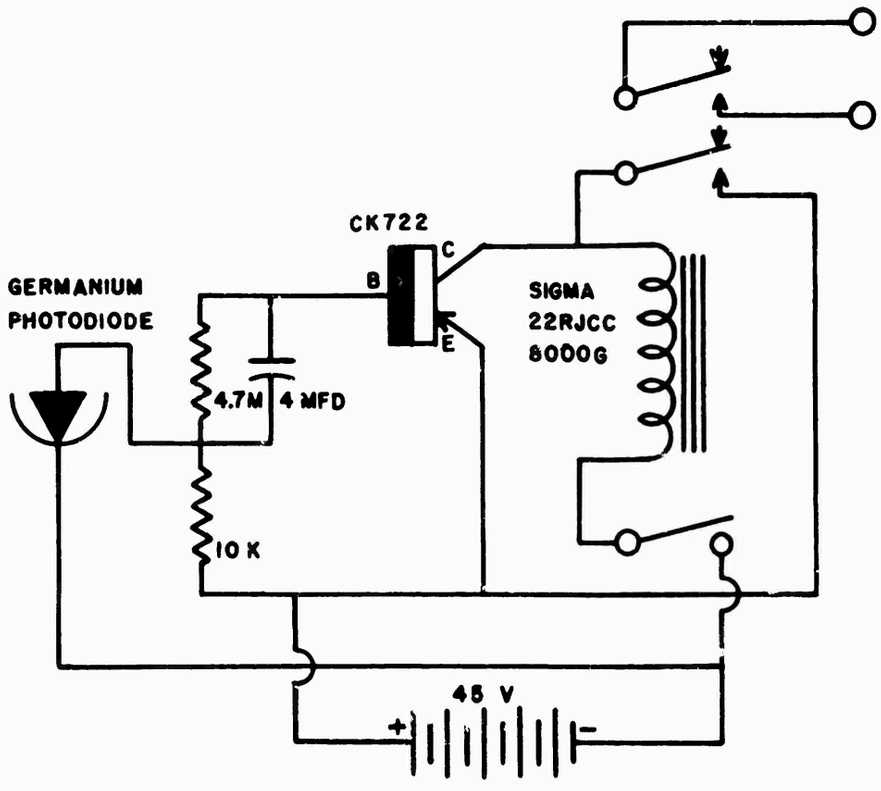

Fig. A.31 Schematic of Photo Initiator Circuit for VLP Gage

of the stylus arm to assure a record movement vertical to a tangent to the base line; (4.) an improved timing circuit and better means of applying timing marks to the record; and (5.) a means of applying a zero time mark.

Some experiments on damping and timing were tried on several shots on TEAPOT, but more work will be done in the laboratory and shock tube.

Continued development of the VLP gage should result in an even more reliable and accurate inexpensive gage, useful to establish damage

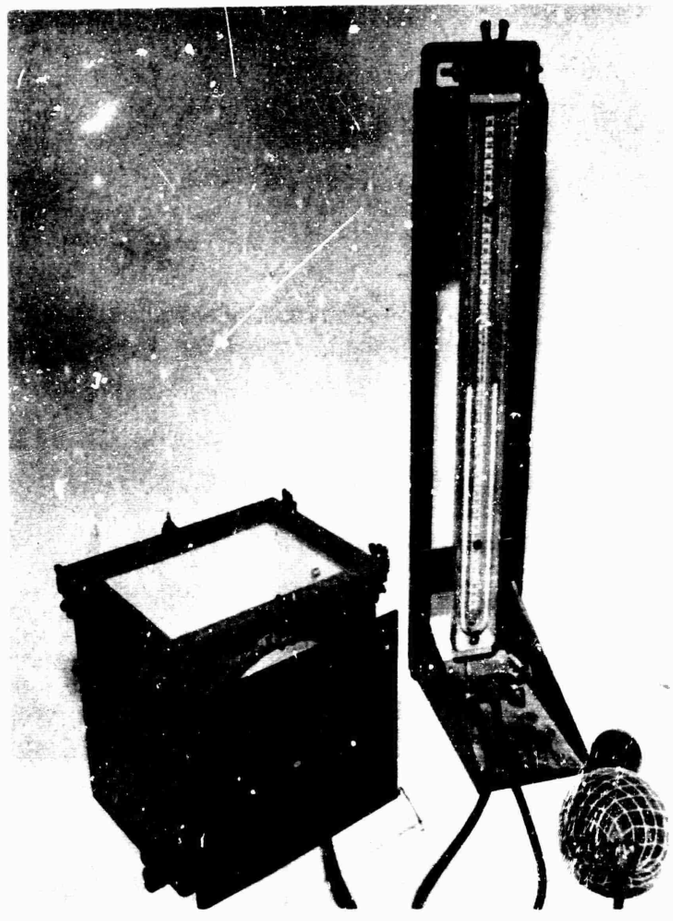

Fig. A.32 Calibration of VLP Gage

criteria from shock waves at considerable distances from a detonation.

A.7 SHOCK-TUBE CALIBRATION OF THE q-GAGE

In order to properly interpret the dynamic pressure measurements obtained in Operation TEAPOT, it was necessary to determine the response of the q-gage to known input conditions. Of particular interest was the response of the static pressure capsules to known static pressure values and the mach compressibility factor for the gage as a whole.

The test section of the BRL shock tube chosen for calibration of

the gage was 78 feet from the diaphragm. This section was chosen specifically because accurate knowledge of the waveshape was desired. The gage mount was so constructed that the gage was situated at the center of the tube. Three piezo-electric gages and one consolidated gage were used to determine the shock strength along the wall of the shock tube. One piezo gage and one consolidated gage were placed approximately 2 feet upstream of the nose of the q-gage. It was assumed that these gages would be relatively free of effects from the q-gage. A second piezoelectric gage was placed 2 feet behind the nose or approximately 1 foot behind the static pressure inlet. The purpose of this gage was to record the strength of the reflections or turbulence caused by the q-gage. The third gage was placed 5 feet behind the nose. This gage was also used to determine possible reflections from the q-gage. A fourth piezo-electric gage was mounted in the nose of the q-gage itself approximately 1/2 inch in front of and at an angle of approximately 90 degrees away from the static opening. This gage was used to compare waveforms obtained from the static pressure capsule. A velocity system was set up such that it would span the entire installation.

An additional factor for consideration in calibrating the q-gage was the choking effect. Choking is a phenomena related to pressure and cross-sectional area, and has not been investigated previously in the shock tube. By introducing the q-gage the cross-sectional area of the BRL shock tube was reduced by 7 percent. Comparison of the waveforms taken during the calibration to the waveforms obtained after the q-gage was removed indicated choking effects at pressure levels greater than 25 psi. It appeared as a rather considerable pressure rise beginning approximately 30 msec behind the initial rise. It was decided that choking would not affect the measurements of the initial rise.

Four pressure capsules including two ranges, 0 to 15 psi and 0 to 25 psi, were used. The first set being used for the pressure range from 0 to 20 psi and the second set being used for the pressure range from 20 to 30 psi. The waveforms of the 15 psi capsules were good under dynamic loading. Oscillations occurred, as was to be expected, however they were easily read with the help of the piezo and consolidated gage waveforms. The 25-psi capsule set, on the other hand, was poor. These capsules were overstressed in past experiments. The waveform moreover had obvious lateral movement along with the vertical movement. Because of this, and the fact that insufficient needle pressure could not be obtained, the records above 20 psi on the total pressure capsule were lost.

As a first step in investigating the response of the q-gage, a comparison was made between pressures as measured by the pressure capsule and the piezoelectric gages. The variation in pressure measurements from the four piezoelectric gages used was $\pm$ 5 percent.

Tabulated values of pressure measurements from the capsules denot-

ed as P_q and values from the piezo gages located on the q-gage denoted as P, $_q$ are shown in Table A.1. The plot of these values is shown in Fig. A.34. The solid line represents the ideal relation between the static pressure measurement of the piezo gage and the pressure capsule. The dotted lines represent the ± 5 percent error in the piezoelectric gage readings. Points are scattered on both sides of the ideal curve and outside of the ± 5 percent error band. The pressure readings from the 0 to 15 psi capsule are in general reading low while

TABLE A.1 Pressure Measurements from q-Gage and Piezoelectric gage in BRL Shock Tube

Shot No.	Capsule Range	Static Pressure P_q (psi)	Static Pressure P_{pE} (psi)	Total Pressure P_t (psi)
1	0-15	10.68	11.56	13.37
2	0-15	10.76	11.43	13.81
3	0-15	5.47	5.87	6.71
4	0-15	5.31	5.28	7.08
5	0-15	15.91	15.88	20.97
6	0-15	15.99		21.94
7	0-15	21.28		31.10
8	0-15	21.84	21.65	31.51
9	0-15	10.84	12.13	14.10
10	0-25	21.68	19.23	31.10
11	0-25	30.73	25.73	49.00
12	0-25	27.54	35.47	
13	0-25	31.19	30.13	
14	0-25	32.40	27.55	
15	0-25	27.04	26.88	

the results of the 0 to 25 psi capsules are much too erratic to draw any conclusions. Another means of representing the data was to compute the mach number from Eq. A.1 using the pressure readings of the piezo gage and the q-gage capsule.

$$M = \frac{5\ z}{\left[7\ (z + 1)\ (z + 7)\right]}^{1/2} \qquad (A.1)$$

where: $M = \frac{u}{a}$ - mach number

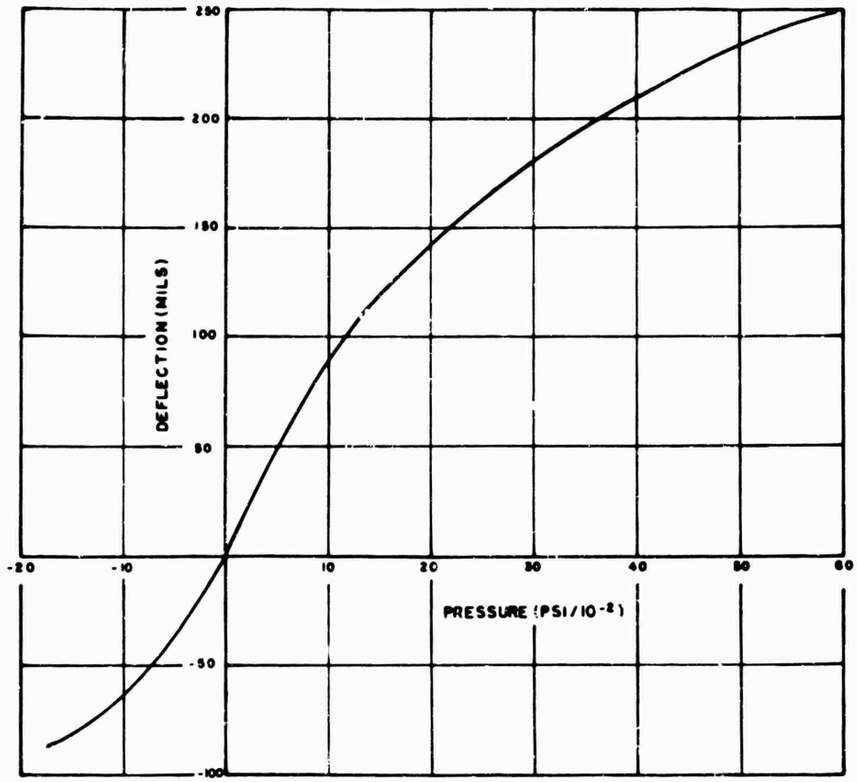

Fig. A.33 Typical VLP Gage Calibration Curve

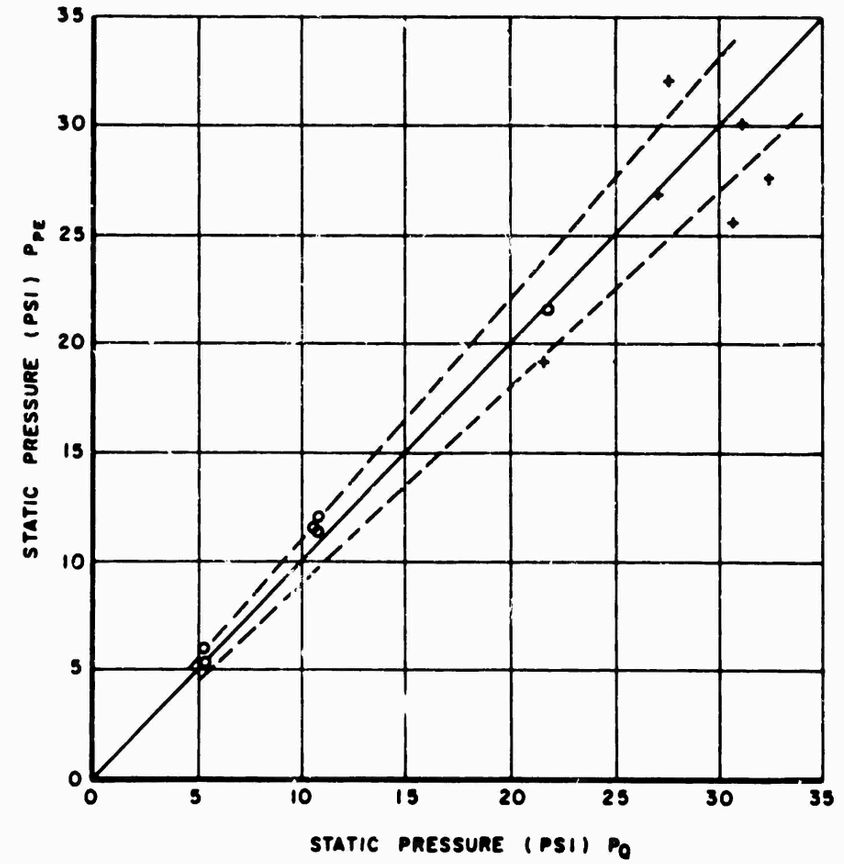

Fig. A.34 Static Pressure, Piezo-Gage versus Static Pressure, q-Gage, (Measured Values)

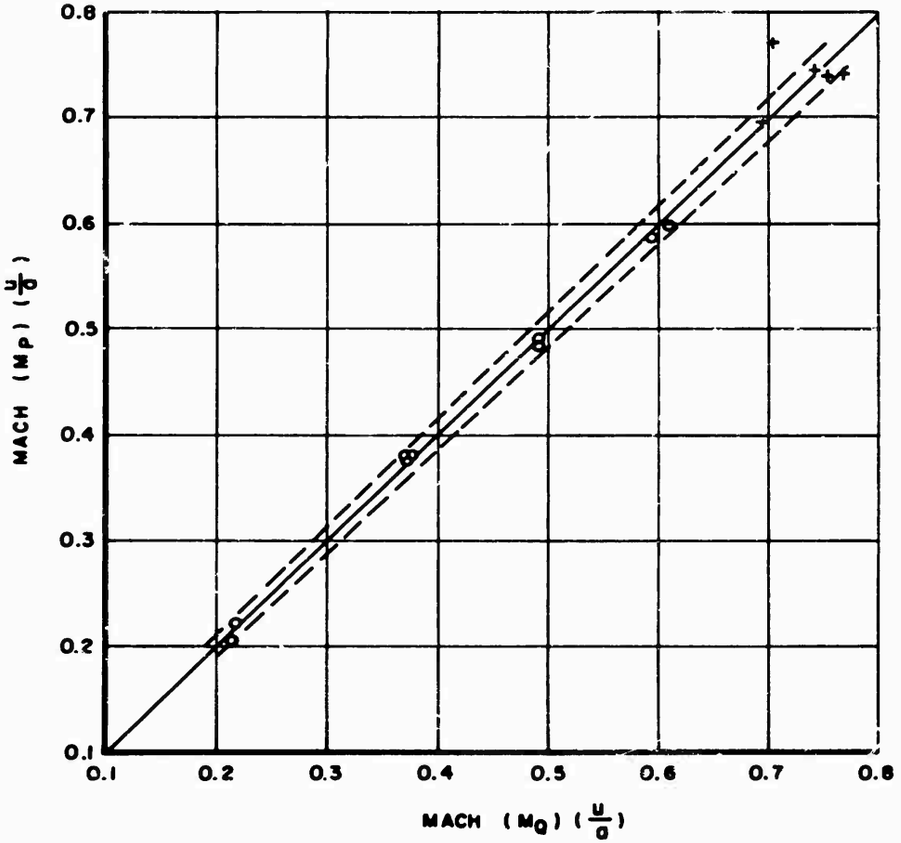

Fig. A.35 Mach Number, Piezo-Gage versus Mach Number, q-Gage, (Computed Values)

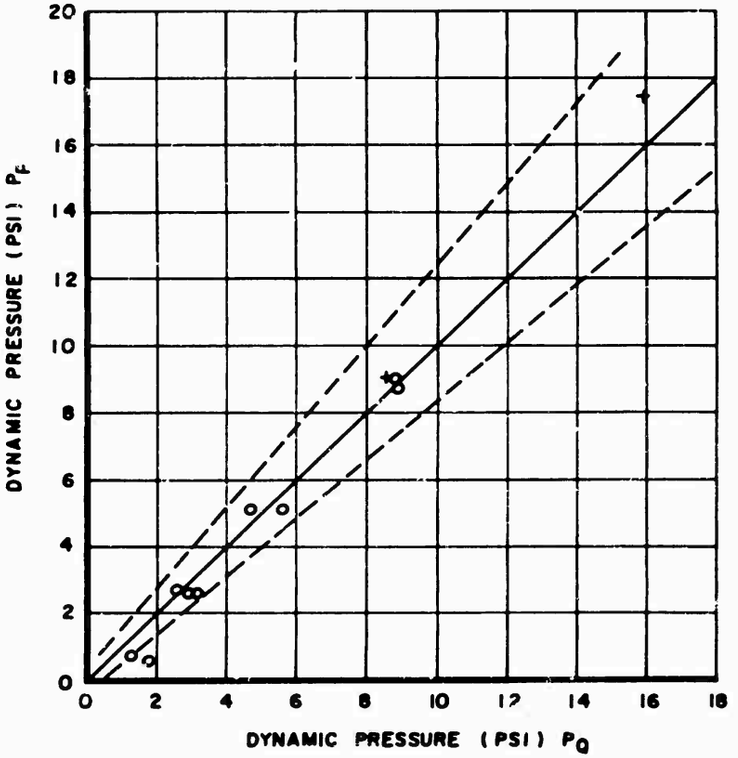

Fig. A.36 Dynamic Pressure, Piezo-Gage (Computed from Rankine-Hugoniot Equation) versus Dynamic Pressure, q-Gage (Corrected)

$$z = \frac{P_s}{P_o}$$ - ratio of shock strength

and: u = particle velocity behind shock - ft/sec

a = local sound velocity - ft/sec

P_s = shock overpressure - psi

P_o = ambient pressure - psi

This plot is shown in Fig. A.35. The solid line represents the ideal relation between the two readings and the dotted lines represent an assumed 5 percent error in the pressure readings. The calculated probable error (Reference 12) in the mach number is given by the following relation

$$\Delta M = \frac{\partial M}{\partial P_s} \Delta P_s = \frac{\partial M}{\partial z} \Delta z$$

and $$\Delta M = \frac{140z + 245}{(7z^2 + 56z + 49)^{3/2}} \qquad (A.2)$$

To determine the mach compressibility factor for the BRL q-gage, the normal pitot-static tube equations (Reference 10) for dynamic pressure were used and compared to the theoretical values of dynamic pressure derived from the Rankine-Hugoniot relation. The dynamic pressure from the q-gage is:

$$P_d = \frac{P_t - P_s}{(1 + 1/4\ M^2 + 1/40\ M^4 + \ldots.)} \qquad (A.3)$$

where: P_d = dynamic pressure - psi

P_t = total or stagnation pressure - psi

P_s = static pressure - psi

$M = \frac{u}{a}$ - mach number

The quantity in the denominator of Eq. A.3 is the normal correction for the mach compressibility factor. The plot of the corrected dynamic pressure values versus the theoretical values are shown in Fig. A.36 with the ideal curve and a $\pm$ 5 percent error band.

Although the test of the q-gage was limited to pressure range of

30 psi, it can be concluded that at least up to 20 psi the correction for static pressure measurements of the q-gage need not be applied while above this pressure range no definite conclusions can be made. As for the mach compressibility correction factor, since all but one point is within the probable error band, the normal pitot-static equation can be used for correcting the dynamic pressures measured by the BRL q-gage.

Appendix B

BLAST ASYMMETRY

The Ballistic Research Laboratories proposed to check the asymmetries of the blast wave resulting from Shots No. 12 and No. 14, on Operation TEAPOT. Instrumentation for these tests were the BRL self-recording pressure-time gages, with a zero time fiducial, positioned on the circumference of a semi-circle inscribed about the shot tower. It was hoped that such an array of gages would provide information pertinent to the parameters influencing the asymmetries in the blast wave resulting from nuclear explosives.

The test data show the blast wave to be very asymmetrical at the 2500 foot range and the pressure-time records show the wave in many shapes and varying pressures. Gages not more than 100 feet apart show marked differences in wave character and arrival time. Fig. B.1 and B.2 show the field layout with the gage positioning and figures B.3 and B.4 are plots of the inverse of the arrival time. The latter plots are indications of the wave velocity and illustrate the effect of the surface condition on arrival time. Note that greater velocities are obtained over the asphalt pad and are in agreement with the experiment design. The geometry of the blast circle on Shot 14, Fig. B.2, indicates that every gage should record a different arrival time. The time resolution of the P-t gages was such that these differences would not be observed, however it was felt that a distinct difference in arrival time would be observed between the extremes of the circle. Fig. B.5 and B.6 are plots of the arrival time at the stations. On Shot 12 in the desert sector the blast wave had double peaks which are also plotted from zero time (Fig. B.5).

The pressure data in general were good and are shown in Fig. B.7 and B.8. On Shot 12 (Fig. B.7) a line joins the points indicating the pressure maximums and for those waves with double peaks a second point indicating the strength of the initial maximum is shown. Note the highest pressures without the double peaks occur over the water sector. Comparing this curve with the arrival time plot (Fig. B.5), notice that the highest pressures are associated with the longest arrival time. No double peaks occur in the asphalt region, however stations on either side of the sector exhibit the double peaked character.

Shot 14 showed no evidence of double peaks and no distinct difference in blast wave front. The wave shape throughout the blast circle has the same general character, however pressures are lower in the immediate vicinity of the black topped region (Fig. 4.8).

Figs 4.9 and B.10 show the positive phase duration for the two shots. In the asphalt region on Shot 12 there is a significant in-

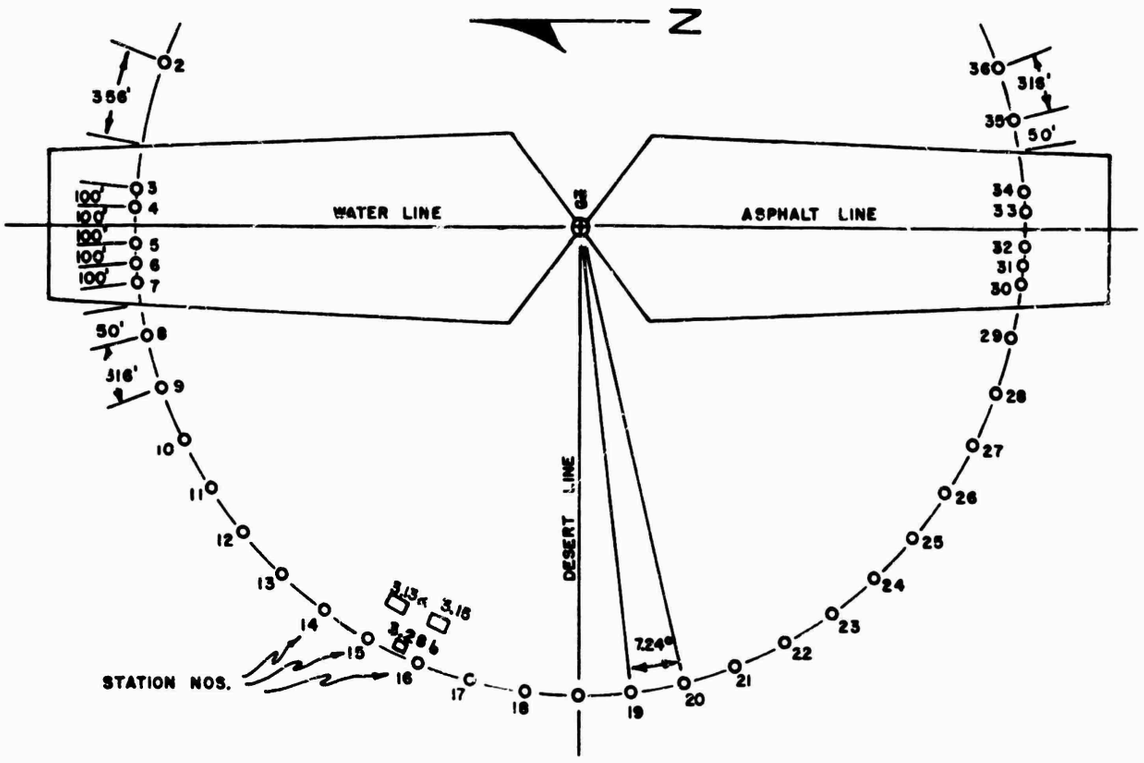

Fig. B.1 Gage Layout Shot No. 12

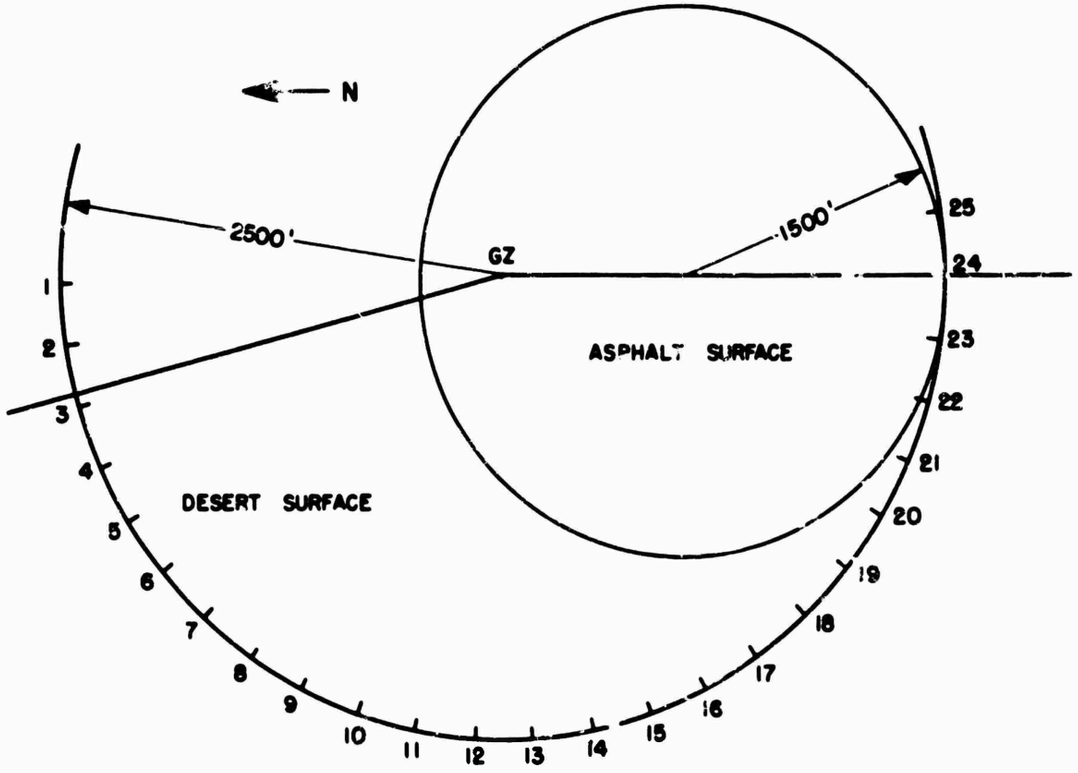

Fig. B.2 Gage Layout Shot No. 14

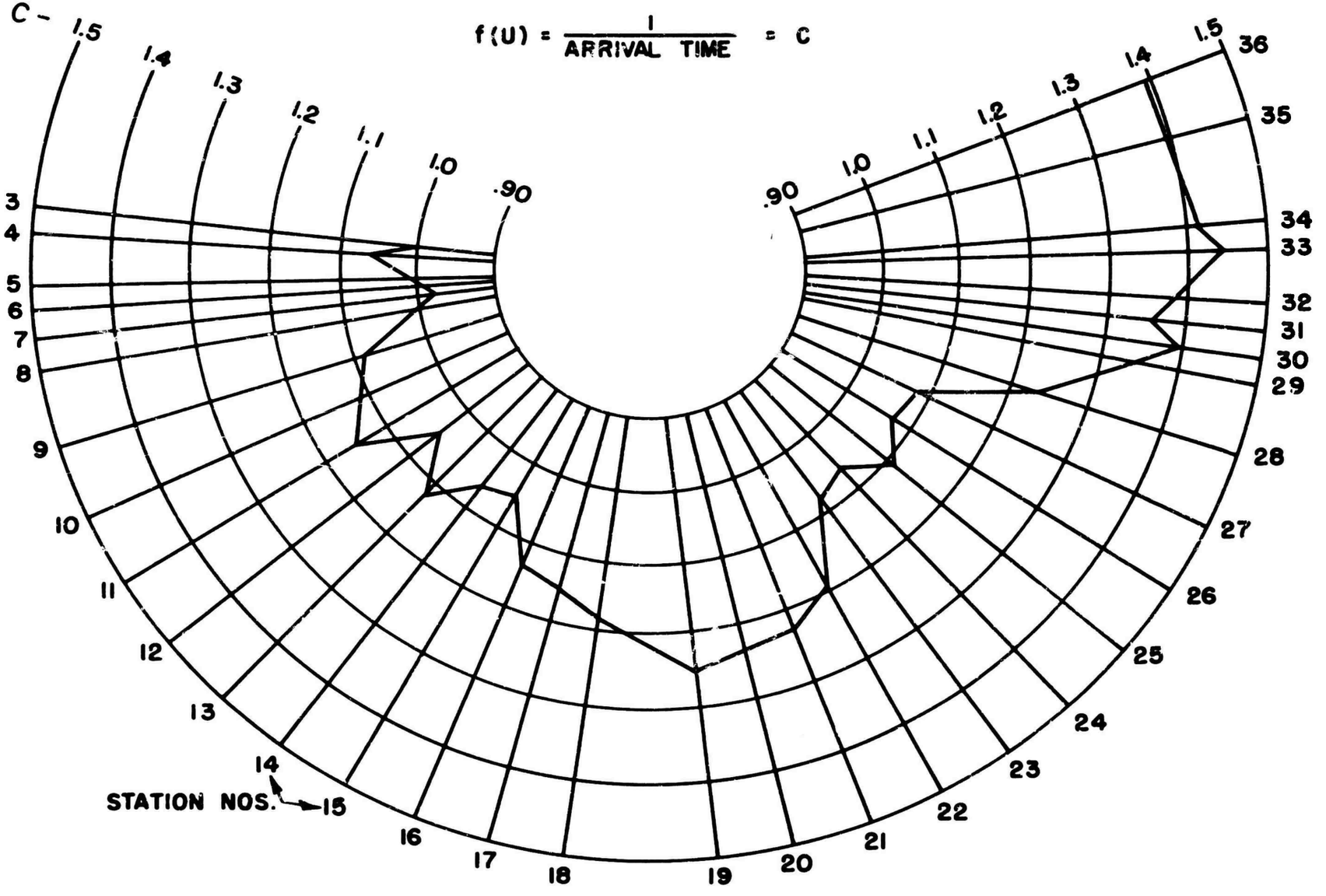

Fig. B.3 Velocity Profile for Shot 12, Gage Position versus C, 2,500 foot Circle C= 1/t

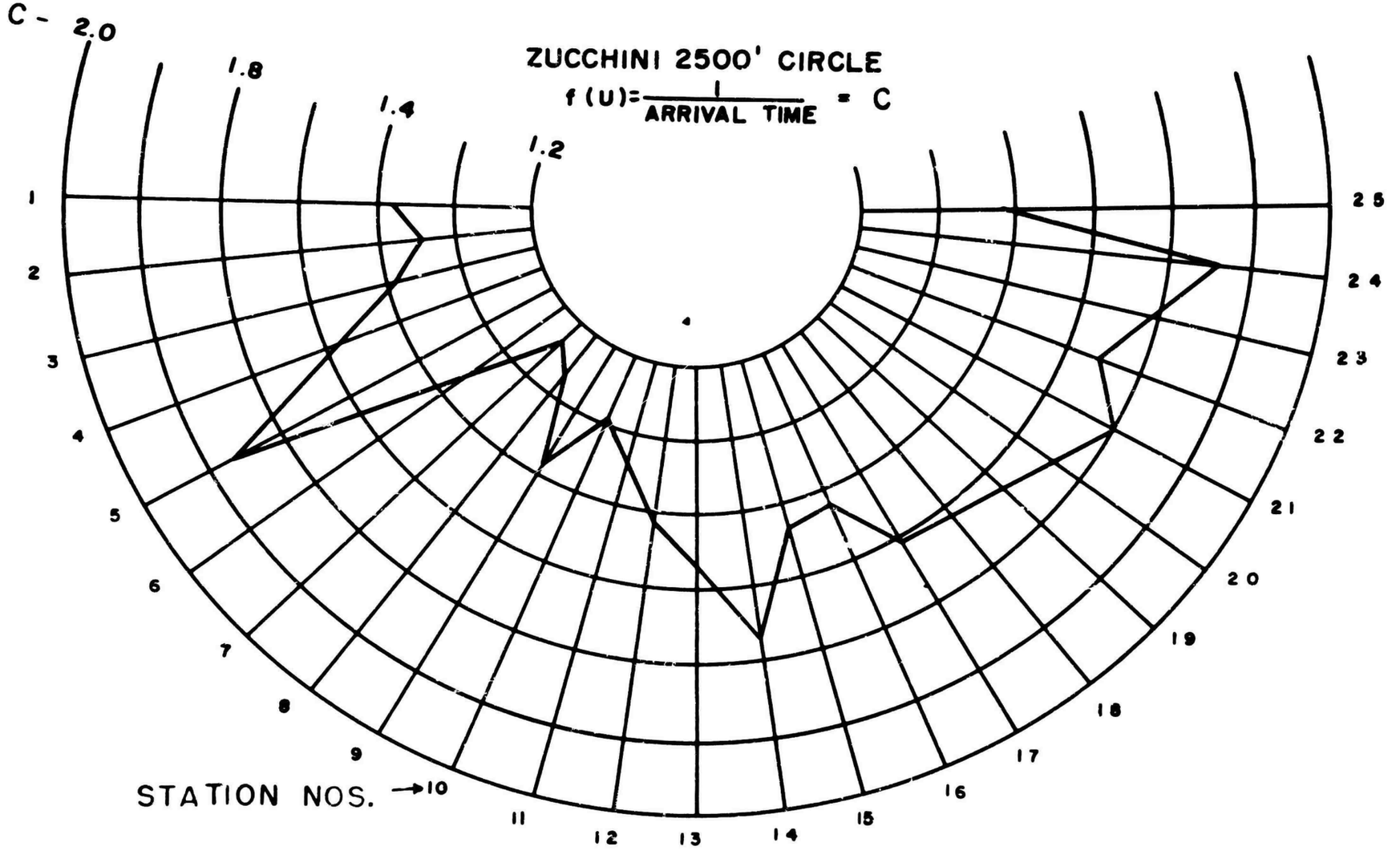

Fig. B.4 Velocity Profile for Shot 14, Gage Position versus C, 2,500-foot Circle C = 1/t

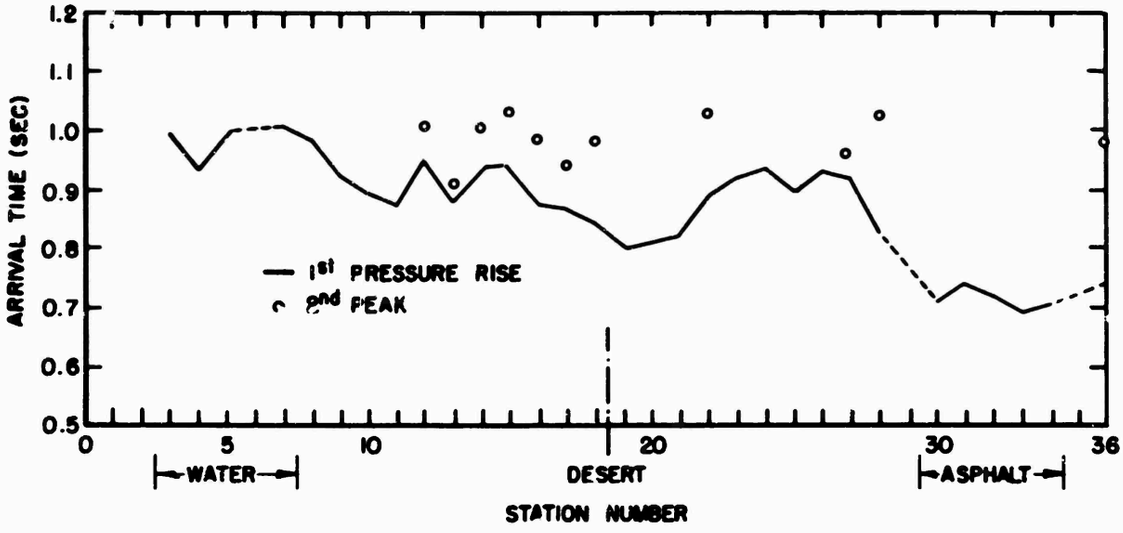

Fig. B.5 Arrival Time at Gage Circle Stations, Shot 12

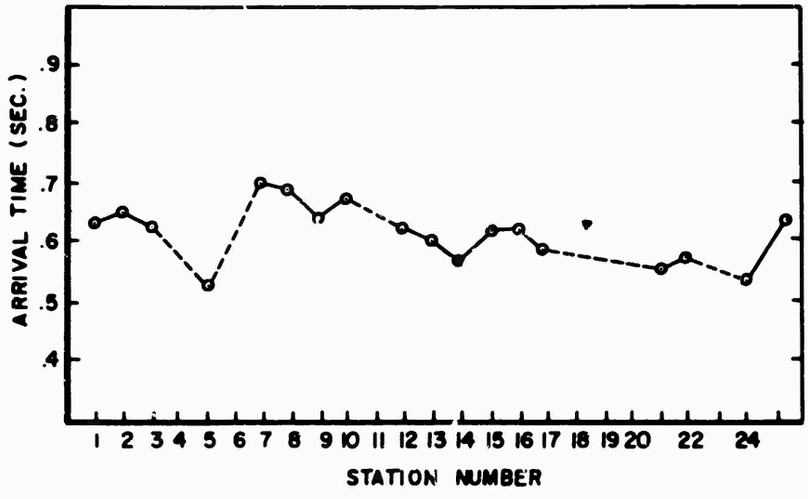

Fig. B.6 Arrival Time at Gage Circle Stations, Shot 14

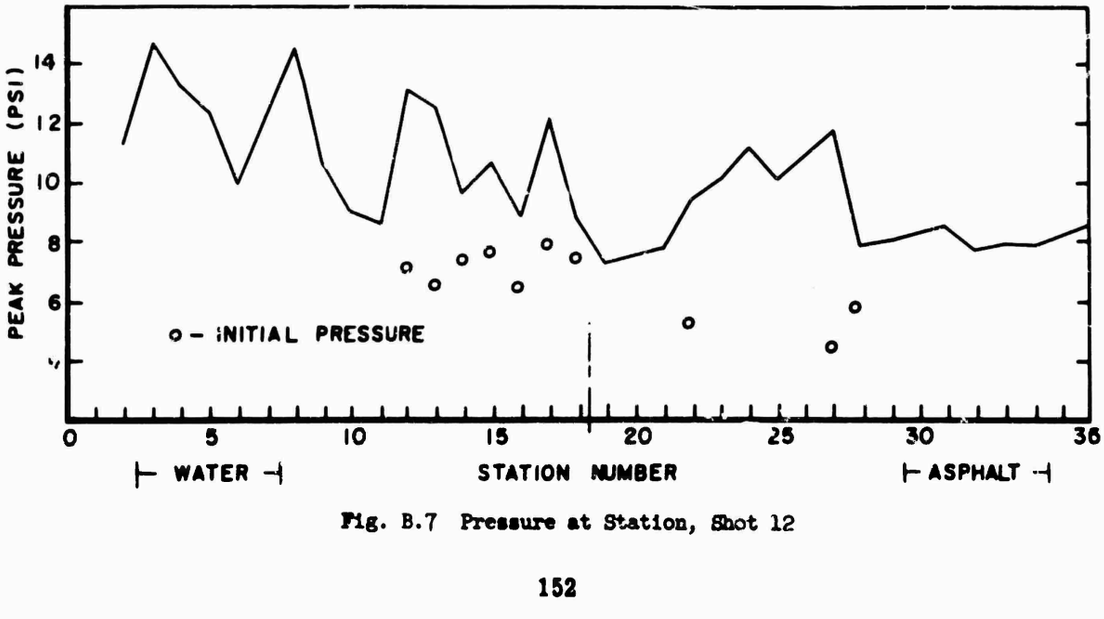

Fig. B.7 Pressure at Station, Shot 12

crease in positive phase duration, which is accompanied by a decrease in overpressure.

On Shot 14 however such a correlation cannot be readily made, but trends can be noted in the data. It must be remembered that the instrumentation on Shot 14 was at a shorter scaled range. Arrival times on this shot were several hundred milliseconds less than those on Shot 12 and hence there was less time for the velocity differences to show their effect on an arrival time plot. The shorter scaled range placed the gage circle in a region of greater thermal flux and hence delayed the so-called precursor clean-up stage. This perhaps accounts for the absence of double peaks at the 2500 foot range. Blast lines measurements however show double peaks at the 4500 foot range.

Fig. B.11, B.12, and B.13 are photographs of the pressure-time curves obtained from Shots 12 and 14 and the tabulated data pertinent to the shots are listed in Tables B.1 and B.2.

These experiments are not sufficient to formulate a theory for blast wave behavior, however there is sufficient data to assume that arrival times over surfaces with distinct thermal reflecting properties may change 25% and that pressure may change 25%. It is also reasonable to assume that the section of the wave that arrives at a station after traversing many hundreds of feet of asphalt was spilled into adjacent sectors to mix eventually with a wave that has traveled directly to the adjacent sector. This presents the possibility that there are regions of strong transverse flow and may account for some of the anomalies in the pressure-time curves. Again it is difficult to say with any degree of certitude that surface conditions only are instrumental in causing pressure and arrival time irregularities.

The many variables that could perhaps influence the symmetry of a blast wave are not dwelled upon because of the limited knowledge of their importance when integrated with other effects. For instance, there is much thought as to the effects of the tower guy wires on the blast wave asymmetry. Photographs of the fireball growth show jets extending down the guy cables. This phenomena would most certainly cause an irregular blast wave profile in the immediate vicinity of the cables, however the circle of gage instrumentation is 2500 feet from the tower while the guy wires extend no greater than 500 feet. This leaves 2000 feet for recovery to occur. The tendency for recovery will be effected by the ground surface conditions which are different in the immediate vicinity of 3 of the 4 cables on Shot 12. So it might be expected that if recovery times are long, then different arrival times and pressure profiles might be expected at stations on the same radii as the cables.

However, is it reasonable to assume that recovery times are long? Blast line stations only several hundred feet apart quite often show very different pressure profiles, indicating that wave shapes changes can occur in small fractions of the time allowed by the 2000 foot gap between the guy cables and the instrumented circles. There appears

TABLE B.1 Gage Circle Results For Shot No. 12

Station	Precursor (psi)	Peak (psi)	Arrival Time (sec)	Duration (sec)
2	-	11.3	-	0.590
3	-	14.8	0.992	0.577
4	-	13.2	0.937	0.581
5	-	12.5	0.995	0.611
6	-	10.0	-	0.601
7	-	-	1.021	-
8	-	14.0	0.985	0.586
9	-	10.7	9.922	0.642
10	-	9.1	0.890	0.664
11	-	8.7	0.877	0.675
12	7.1	13.3	0.955	0.651
13	6.8	12.9	0.888	0.628
14	7.4	9.7	0.935	0.703
15	7.7	10.8	0.945	0.710
16	6.5	8.7	0.880	0.527
17	7.9	12.2	0.875	0.680
18	7.5	8.9	0.841	0.733
19	-	7.4	0.802	0.757
20	-	7.5	-	0.736
21	-	7.9	0.832	0.763
22	5.2	9.7	0.893	0.696
23	-	10.1	0.923	0.647
24	-	11.3	0.580	0.623
25	-	10.1	0.700	0.627
26	6.0	11.0	0.770	0.678
27	4.5	11.9	0.550	0.677
28	5.8	7.8	0.825	0.740
29	-	8.2	0.670	0.886
30	-	8.2	0.780	0.916
31	-	8.6	0.720	0.901
32	-	7.8	0.780	0.888
33	-	8.1	0.780	0.817
34	-	8.0	0.820	0.897
35	-	-	-	-
36	-	8.7	0.740	0.713

TABLE B.2 Gage Circle Result for Shot No. 14

Station	Peak (psi)	Arrival Time (sec)	Duration (sec)
1	7.6	.636	1.00
2	7.1	.650	.98
3	7.2	.623	1.02
4	6.7	-	-
5	6.7	.536	1.00
6	7.8	-	-
7	6.5	.697	.98
8	7.0	.683	.95
9	8.5	.630	.96
10	8.4	.671	.94
11	-	-	-
12	7.1	.618	.91
13	7.3	.597	.99
14	-	.565	-
15	6.4	.613	1.05
16	7.4	.616	1.01
17	7.9	.584	.97
18	-	-	-
19	8.8	-	-
20	-	-	-
21	9.8	.558	1.03
22	8.0	.574	1.03
23	6.7	-	1.04
24	6.1	.537	1.02
25	5.7	.631	.96

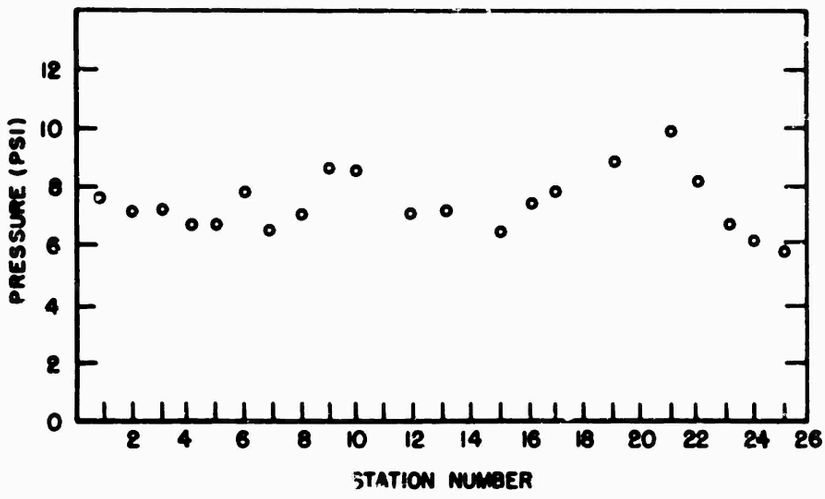

Fig. B.8 Pressures at Stations, Shot 14

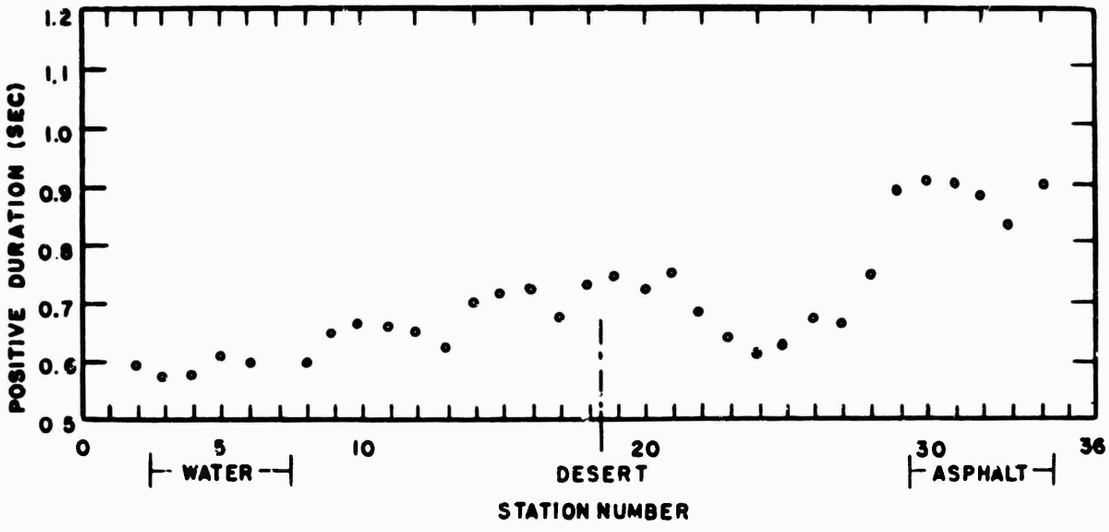

Fig. B.9 Positive Phase Duration at Stations, Shot 12

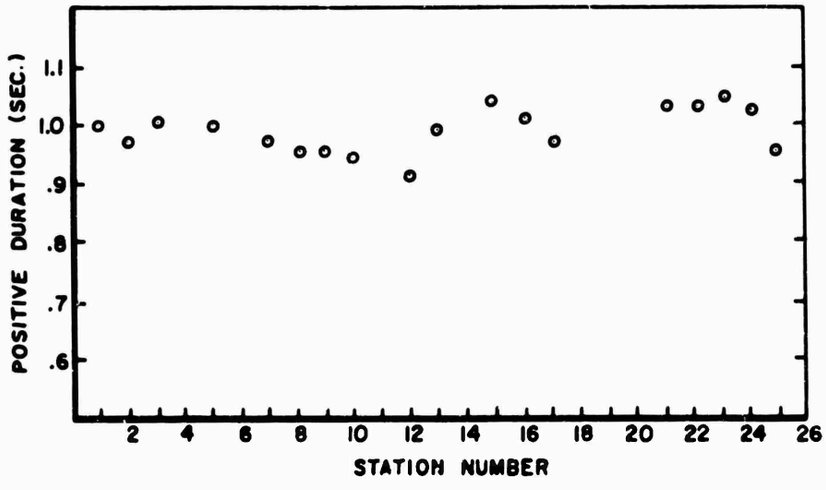

Fig. B.10 Positive Phase Duration at Stations, Shot 14

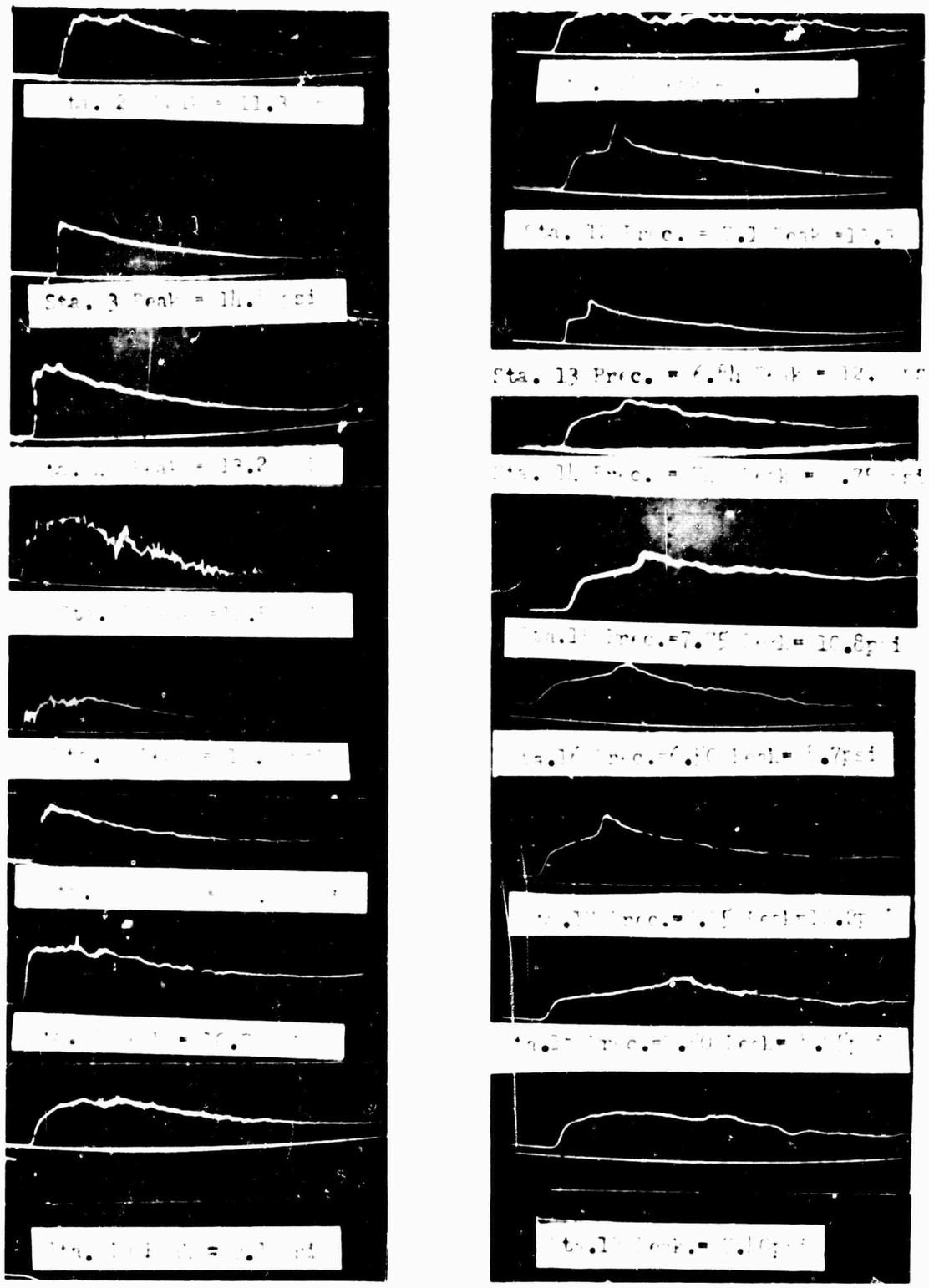

Fig. B.11 Record Photographs, Gage Circle, 2,500 ft Radius, Shot 12

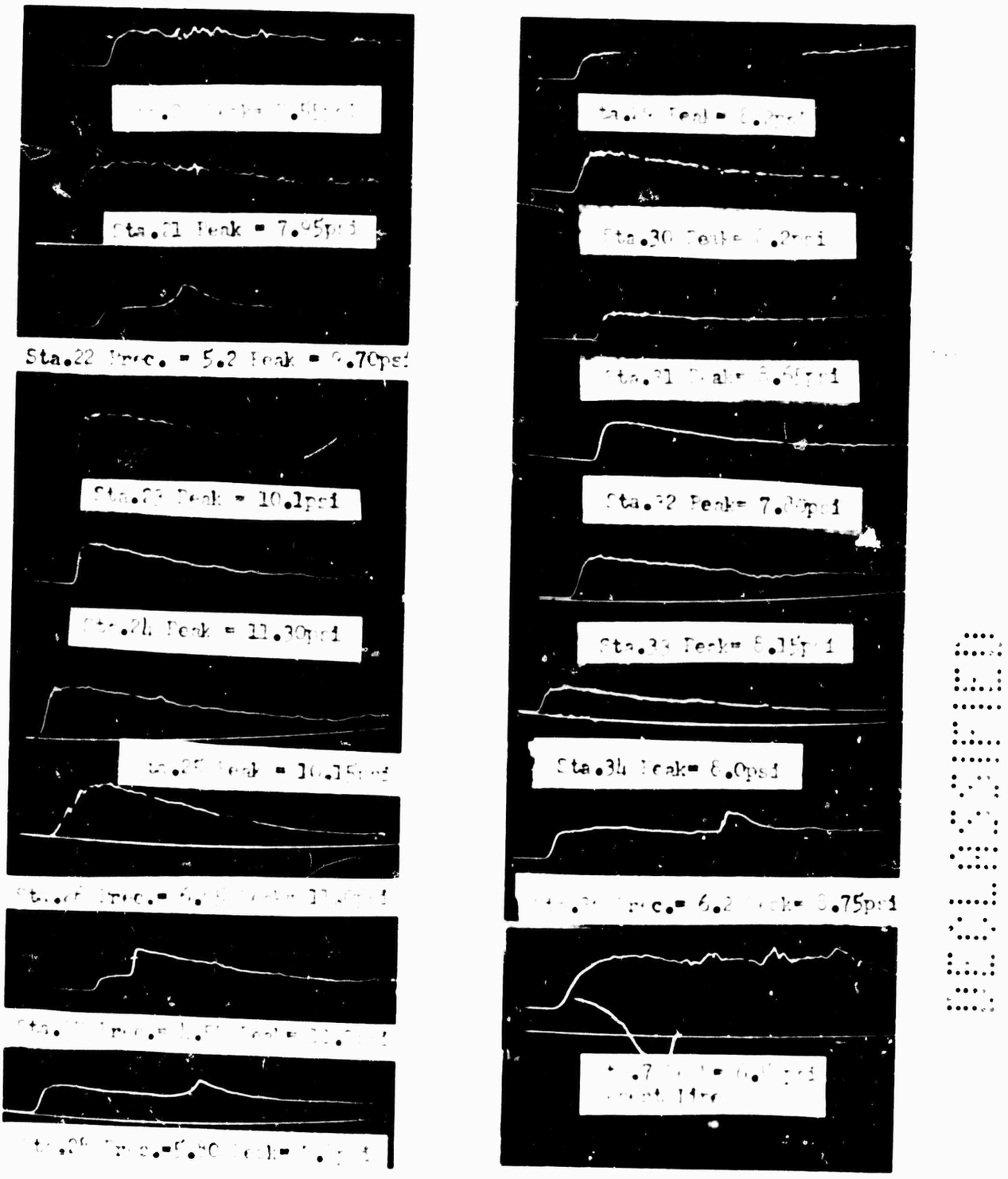

Fig. B.12 Record Photographs, Gage Circle, 2,500 ft Radius, Shot 12

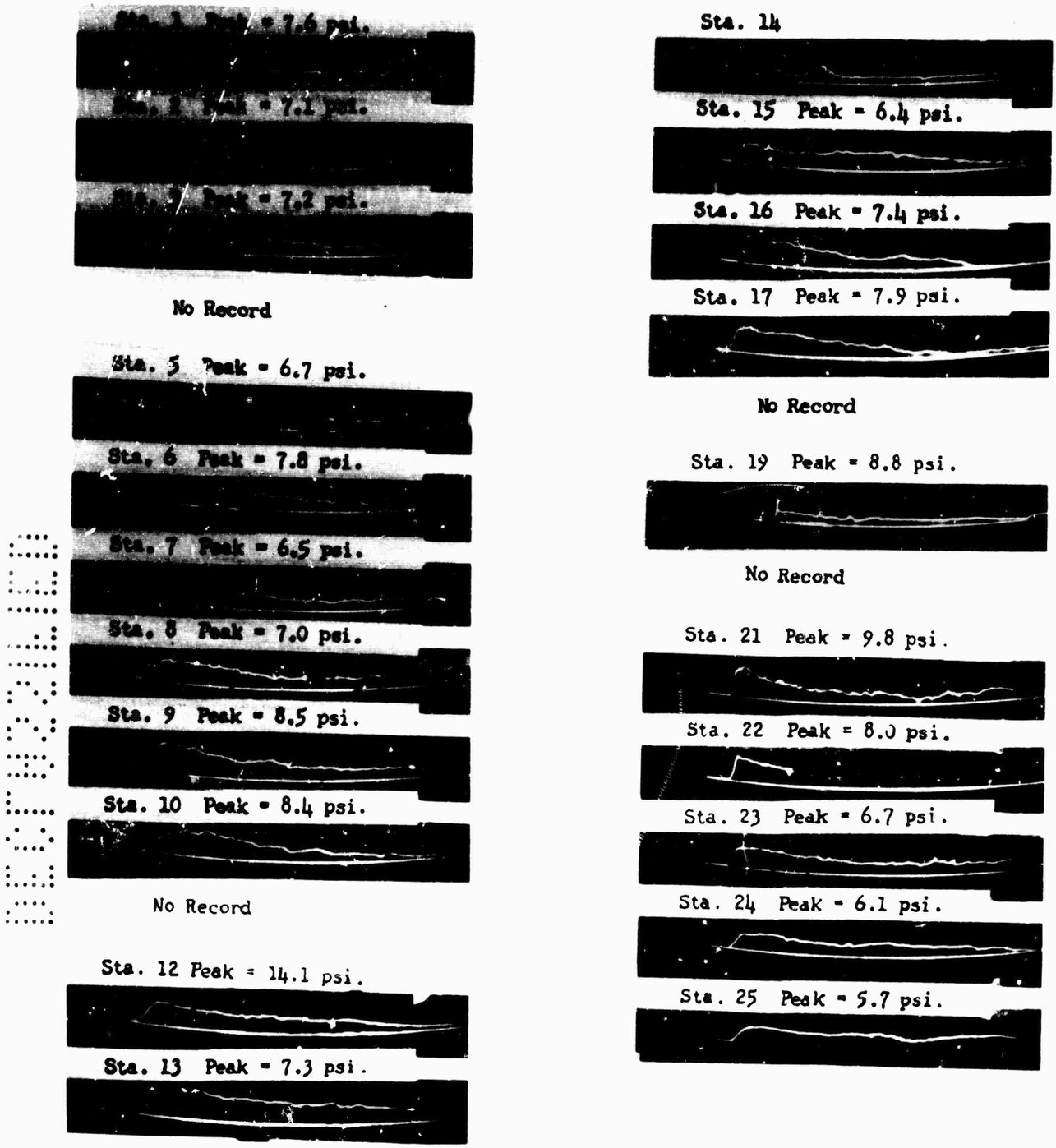

Fig. B.13 Record Photographs at Gage Circle, Shot 14

to be some phenomena more important than the guy cables. Surface conditions alone however could not account for the asymmetries indicated on the arrival time plots because of the great variations in arrival times on the same surfaces.

It is felt that a more fundamental investigation of nuclear blast wave asymmetry is needed to resolve some of the questions presented in this paper. Such an investigation should consider the type of device to be tested; i.e., for optimum data evaluation a standard device with symmetrical surroundings. There should be no radiation shields or large masses in close proximity to the weapon. If possible, there should be no tower or guy wires, however the point of detonation should be accurately predetermined.

Ground surface conditions should be identical throughout the entire region of measurement. When the above conditions are met and an asymmetrical pattern is obtained, then the experimenter looks toward the device and the symmetry of the detonation. Photographs of the fireball may be compared with the blast patterns. Irregularities in the fireball growth are quite often observed.

The instrumentation for such an investigation should be pressure-time recording with a zero-time fiducial. A semicircle of gages is considered adequate encompassment, however there should be three such semicircles: one in the precursor region; one in the precursor clean-up region; and one at a position such that a classical wave might be expected. An equal number of gages should be located on each circle and positioned such that one gage from each circle be on a radii. Such an array of gages would permit the experimenter to observe changes in the blast pattern and hence aid in tracing the history of pressure anomalies.

Appendix C

PRESSURE MEASUREMENTS for VARIOUS STRUCTURES PROJECTS

Part of the data required by certain projects necessitated the measurement of the pressure acting on various structures. These data were obtained using the BRL self-recording pressure and dynamic pressure gages described in Appendix A.

Since analysis of the data is to be done by the projects concerned the individual project reports should be consulted to determine the significance of the data.

C.1 PRESSURE MEASUREMENTS IN FIELD FORTIFICATIONS

In order to determine the effectiveness of various types of field fortifications as protection from air blast, 11 of the fortifications constructed by the Engineer Research and Development Laboratories (ERDL) were instrumented with pressure-time gages. Gages were located within the structure at the positions indicated in Fig. C.1. Each gage was placed on the floor of the structure and held in place with sand-bags as shown in Fig. C.2. Photographs of the records obtained are shown in Fig. C.3 and the maximum pressure recorded by each gage together with the positive duration of the record listed in Table C.1.

C.2 PRESSURE MEASUREMENTS ON STRUCTURE 3.6A1

Data needed by Project 3.6 to determine the effectiveness of earth cover in protecting above ground buildings from blast damage required the measurement of the force acting on the outside of the earth berm of Structure 3.6A1. This was accomplished by placing nine pressure gages on the center line of the structure as shown in Fig. C.4.

The data obtained from these gages are listed in Table C.2 and reproduced in Fig. C.5. Gages 4, 5 and 8 were not located after the shot; hence, no records are available from these gages.

Because of interest in the diffraction effects on this structure and as an aid in selecting the proper gage ranges, a model study was conducted in the BRL Shock Tube. Results of this investigation are discussed in Section C.6.

C.3 PRESSURE MEASUREMENTS FOR PROJECT 3.8

To determine the pressure affecting the two fixed-end concrete panels constructed for Project 3.8, two pressure gages were used with

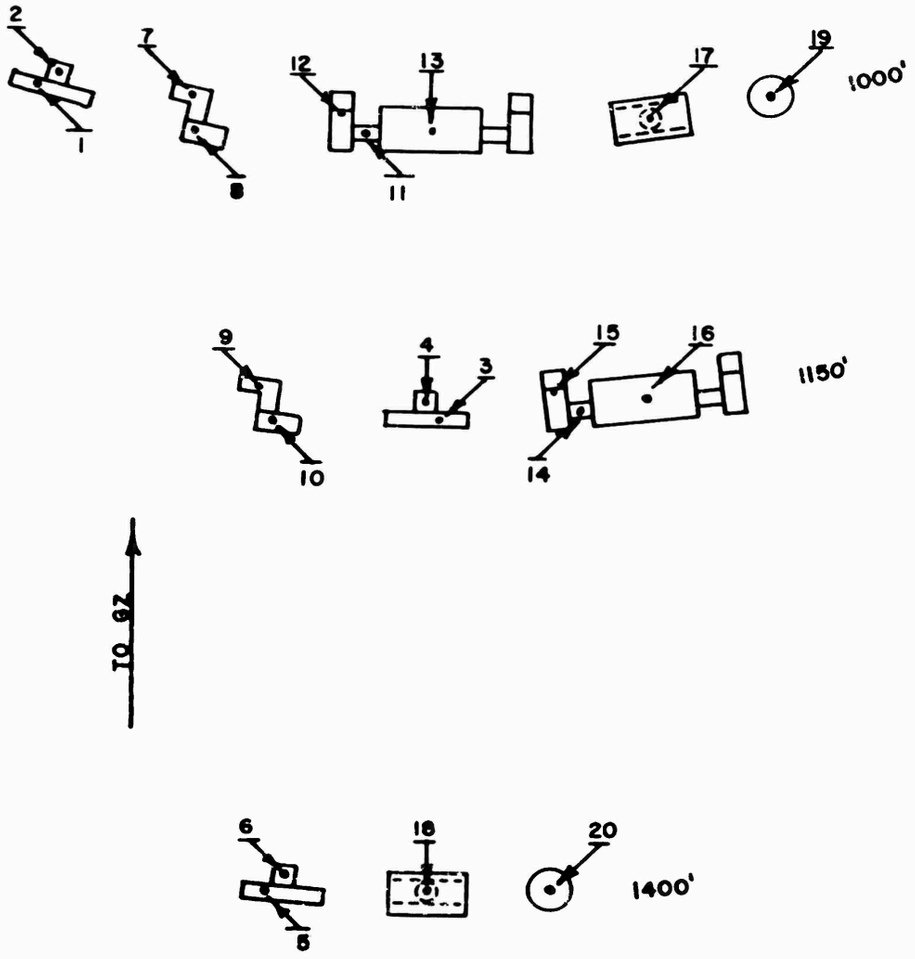

Fig. C.1 Location of Pressure Gages in Field Fortifications

Fig. C.2 Pressure Gage Mounted in Field Fortification

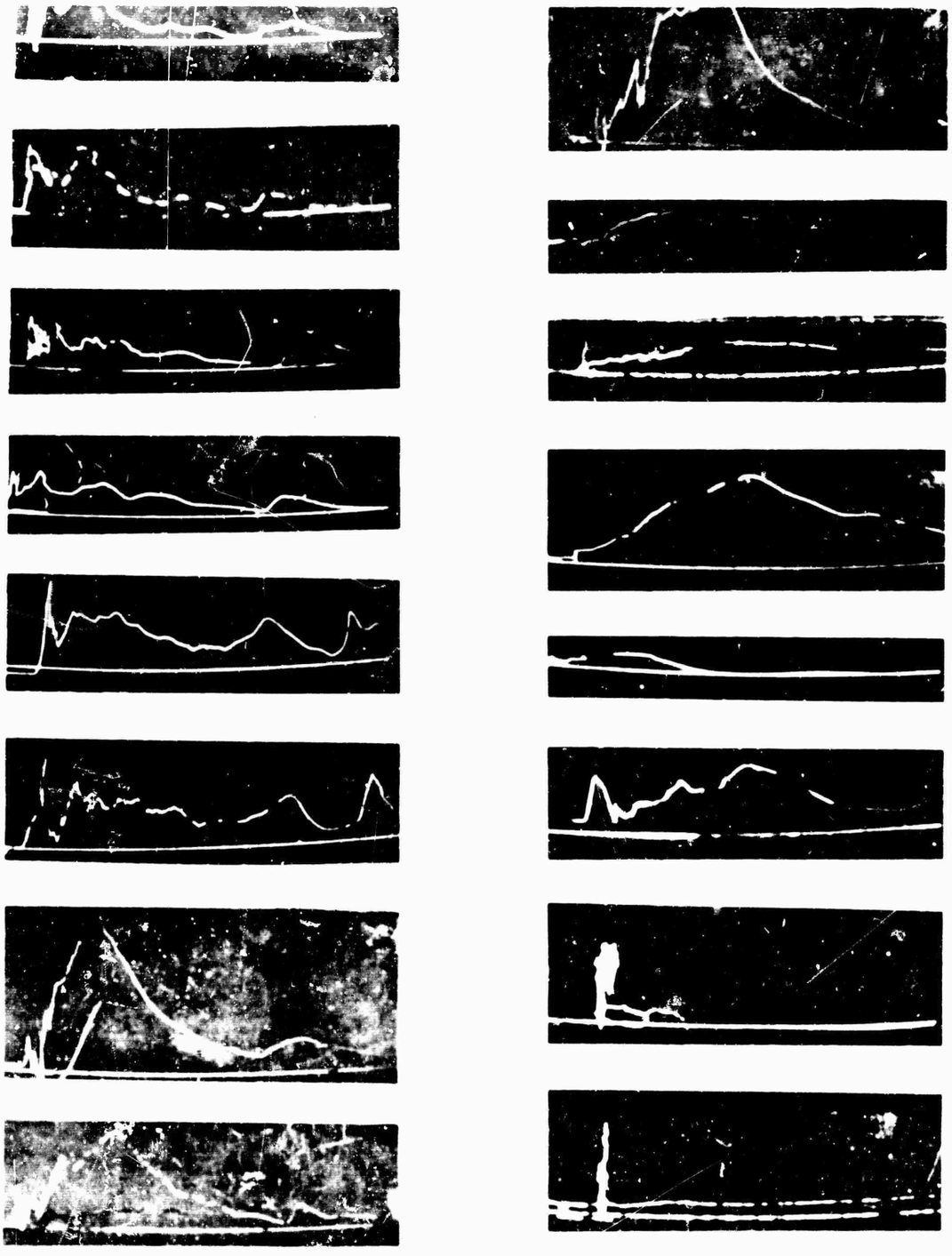

Fig. C.3 Records Obtained in Field Fortifications

TABLE C.1 Data Obtained in Field Fortifications

Gage No.	Structure Type	Ground Range (ft)	Peak Pressure (psi)	Positive Duration (sec)
1	A	1000	49.9	0.401
2	A	1000	40.0	0.398
3	A	1150	30.8	0.422
4	A	1150	22.8	0.432
5	A	1400	16.3	0.482
6	A	1400	15.0	0.497
8	B	1000	38.5	0.471
9	B	1150	30.6	0.482
10	B	1150	33.0	0.462
11	D	1000	15.0	0.508
13	D	1000	14.6	*
14	D	1150	13.4	*
15	D	1150	19.0	*
16	D	1150	16.3	0.574
17	F	1000	50.0	0.228
18	F	1400	27.1	0.546
19	H	1000	46.8	*
20	H	1400	14.3	*

* Unreadable

TABLE C.2 Data Obtained on Structure 3.6A1

Gage No.	Peak Pressure (psi)	Positive Duration (sec)
1	62.0	0.494
2	57.8	0.488
3	60.0	0.478
6	18.0	0.546
7	11.4	0.552
9	19.8	0.606

each panel. In each case, one gage was placed at the surface of the ground near the panel and the other beneath the panel.

The records obtained from these gages are reprod ced in Fig. C.6 and the data tab ulated in Table C.3. Gages 1 and 3 were those at the ground surface at the distances indicated and gages 2 and 4 were those beneath the panels.

The record from gage 4 was too small to be of significance when photographed and hence is not shown.

C.4 MEASUREMENTS FOR PROJECTS 3.2 AND 3.7

A pressure gage was placed at the ground surface between structures 3.2A1 and 3.2A2 for correlation with records obtained by the project from gages on the str ctures. This gage produced the record shown in Fig. C.7. This record indicates a peak overpressure of 7.9 psi which is slightly lower than the pressure recorded at the same distance

TABLE C.3 Data Obtained for Project 3.8

Gage No.	Ground Range (ft)	Peak Pressure (psi)	Positive Duration (sec)
1	3600	7.4	0.815
2	3600	2.20	0.867
3	4850	3.95	0.872
4	4850	0.15	*

* Unreadable

on the desert blast line. This difference in pressure can be explained by the asymmetries noted in Appendix B. Figure B.2 gives a good picture of the amount of variation in pressure for a given radial distance that can be obtained at different azimuths. The gage at this particular location started with the shock wave and thus the arrival time was lost. The positive duration required correction for the start up time of the motor in order to be valid. The corrected value of 0.56 sec. for positive duration may be in error as much as + 20 percent. The record has a very thin trace which increased the reading accuracy. The re-

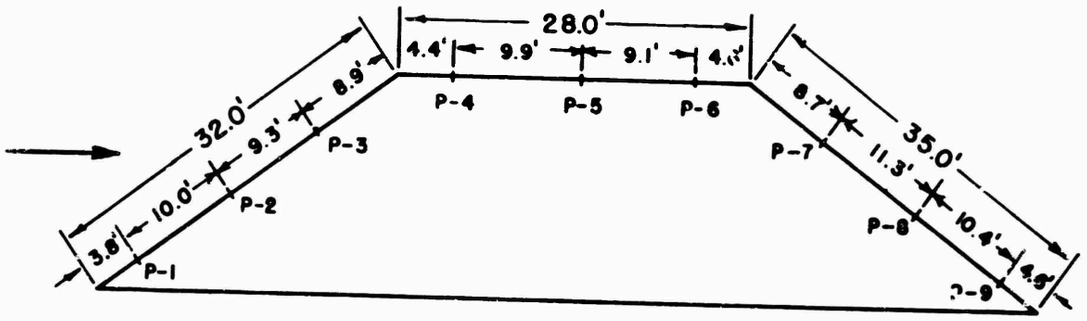

Fig. C.4 Pressure-Time Gage Locations on Structure 3.6A1

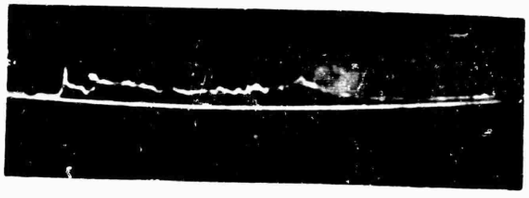

SRI-1, 1500', 62 psi

SRI-6, 1500', 18.0 psi

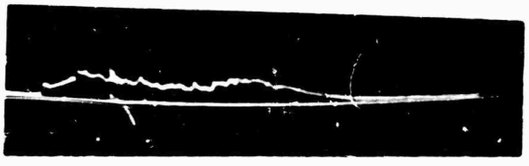

SRI-2, 1500', 57.8 psi

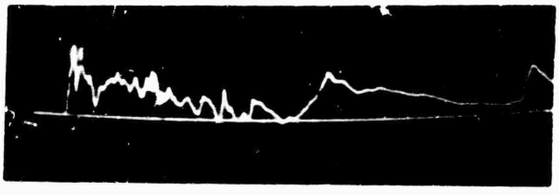

SRI-7, 1500', 11.4 psi

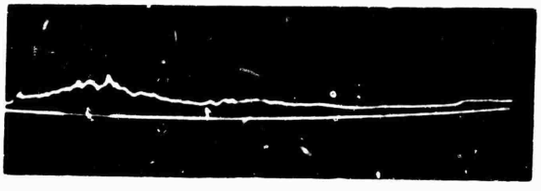

SRI-3, 1500', 60.0 psi

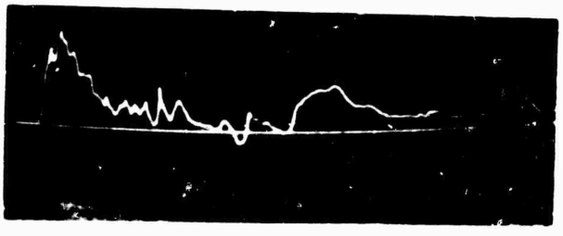

SRI-9, 1500', 19.8 psi

Fig. C.5 Records Obtained on Structure 3.6A1

BuD-1, 3500', 7.4 psi

BuD-3, 4850', 3.95psi

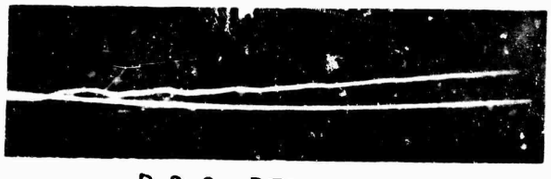

BuD-2, 3500', 2.2 psi

Fig. C.6 Records Obtained for Project 3.8

Fig. C.7 Record Obtained for Project 3.2

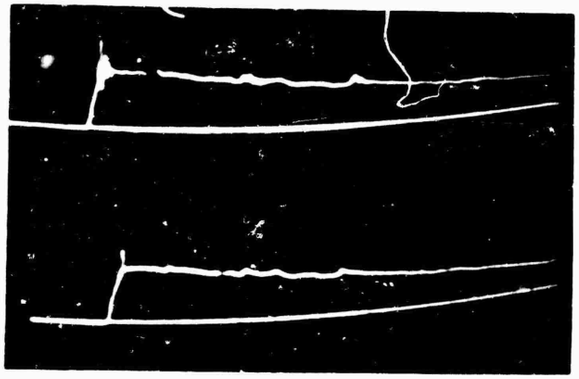

Fig. C.9 Record Obtained at Structure 3.7B1

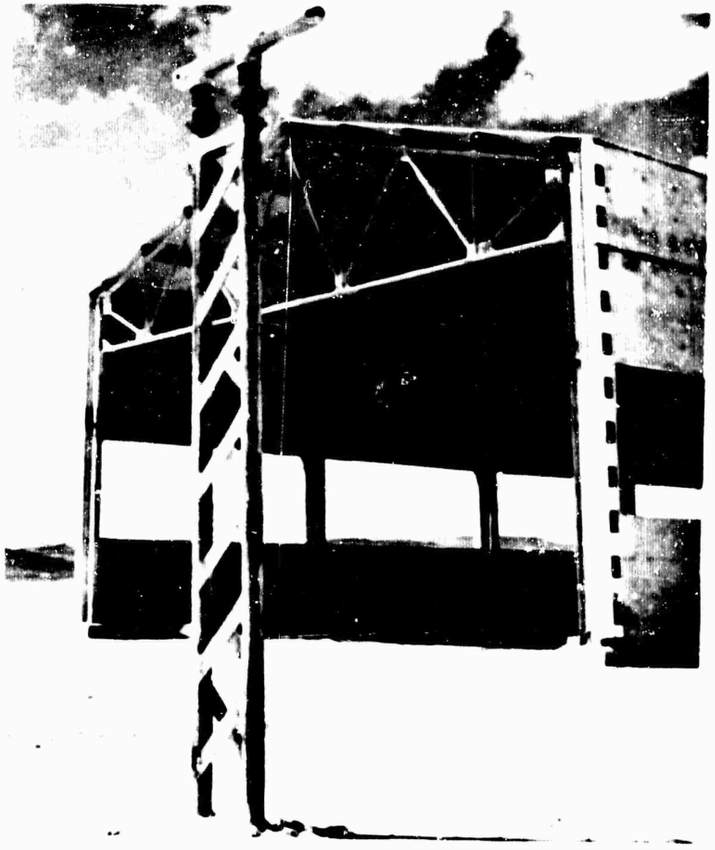

Fig. C.8 Dynamic Pressure Gage Mounted at Structure 3.7B1

cording speed of this record was at 3 rpm which gives approximately 400 msec of the initial portion of the record in the photograph.

To determine the dynamic pressure at Structure 3.7B1 a self-recording q-gage was mounted 10 feet above the ground near one end of the structure as shown in Fig. C.8. The record obtained from this gage is shown in Fig. C.9; the upper trace being the total pressure and the lower the static pressure. This record shows a peak dynamic pressure of 0.30 psi with a positive duration of 0.95 seconds.

C.5 MODEL STUDIES FOR STRUCTURE 3.6A1

An extensive model program has been under way for the past two years at the Explosion Kinetics Branch of the Terminal Ballistics Laboratory of BRL. Several technical notes have been published showing the comparison between the pressure-time records obtained from gages on structures in the field and those obtained by placing a scaled model in the shock tube. The object of this section is to present in this report pressure-time curves which were obtained prior to this operation from a 1/120 scaled model of the 3.6 structure.

Miniature piezoelectric gages were used to record the pressure at the various positions on the model. These gages have a linear response for the pressure used in this experiment. A calibration of the gages was taken both before and after being used in the model. In Fig. C.10 the nine gage locations and model dimensions are given. Two photographs of the steel model used in the shock tube and the mounting plate are shown in Fig. C.11.

Section C.3 of this report summarized the field results for the field structure and the records from the model are given in Figs. C.12-C.20. The air blast loading curves of pressure versus time are prepared for each gage position. The pressure measured on the walls of the structure is designated as P_w and is presented in psi. Since these curves are to be compared with curves obtained in the field at a different atmospheric pressure, the pressures obtained on the model are expressed in terms of the incident overpressure. The second scale in the figures is the ratio of the pressure on the wall (P_w) to the incident pressure (P_1). This ratio is multiplied by 100 and presented as percent.

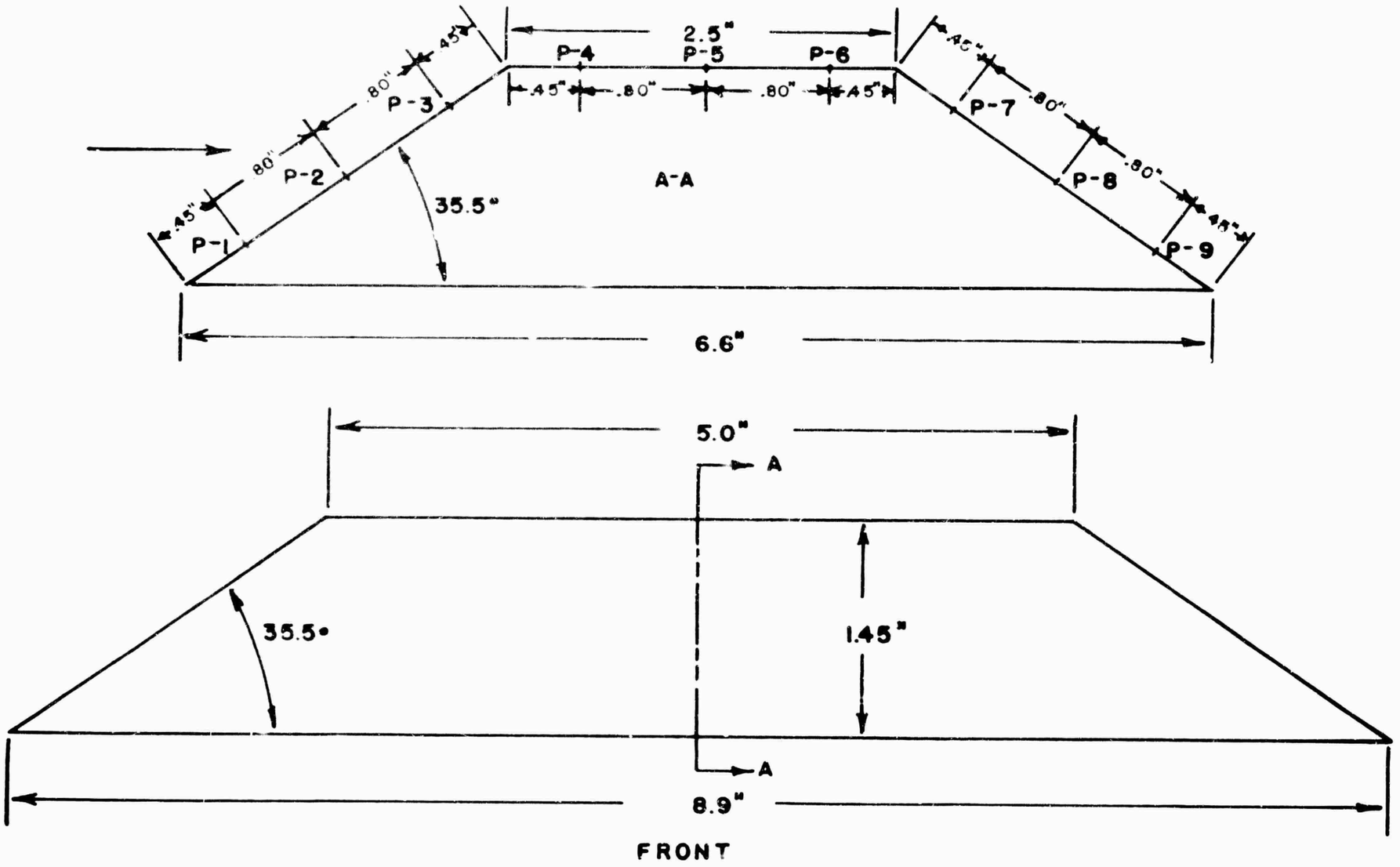

Fig. C.10 Scaled Model Dimensions and Gage Positions

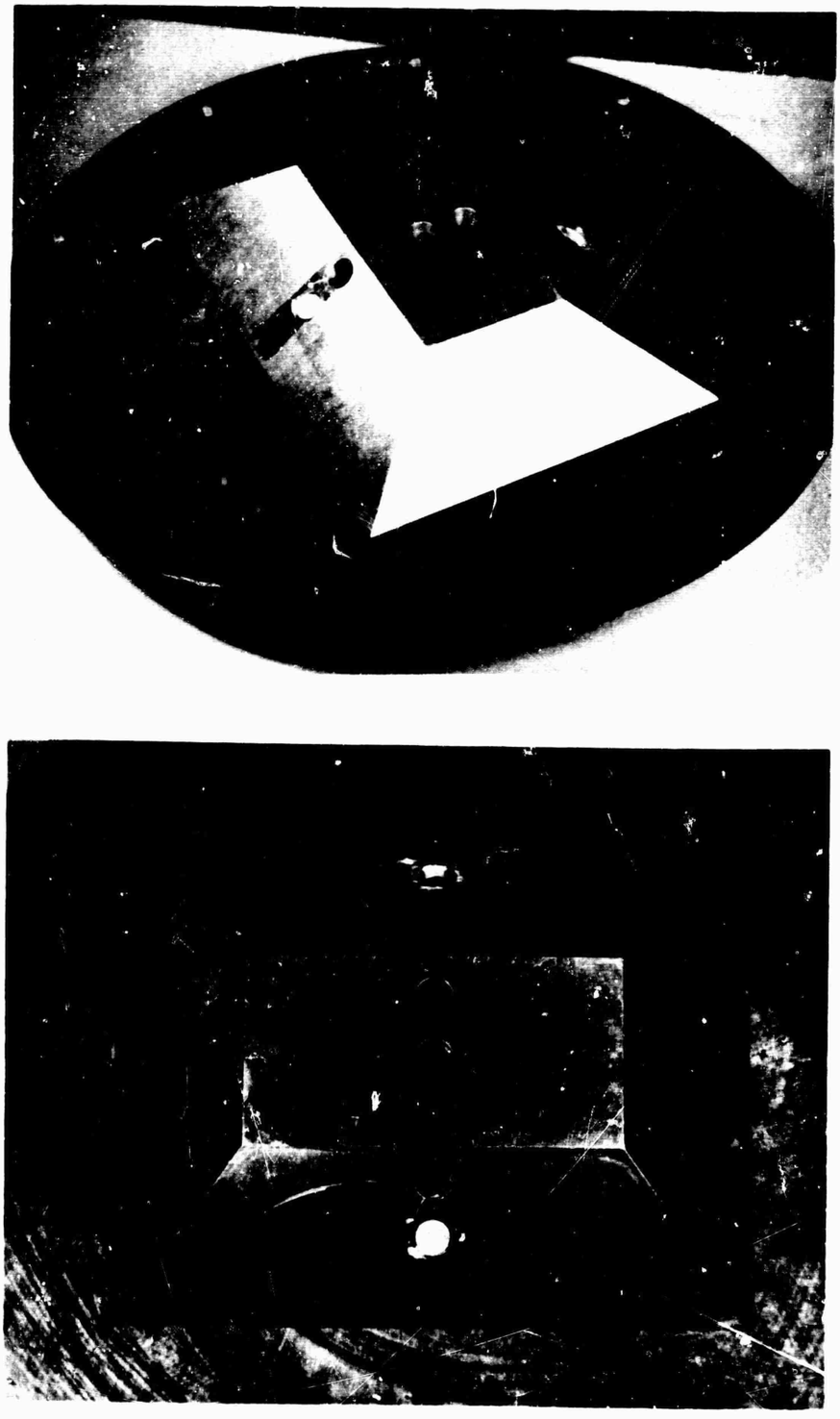

Fig. C.11 Photographs of the 1/120 Scaled Model of the 3.6Al Structure

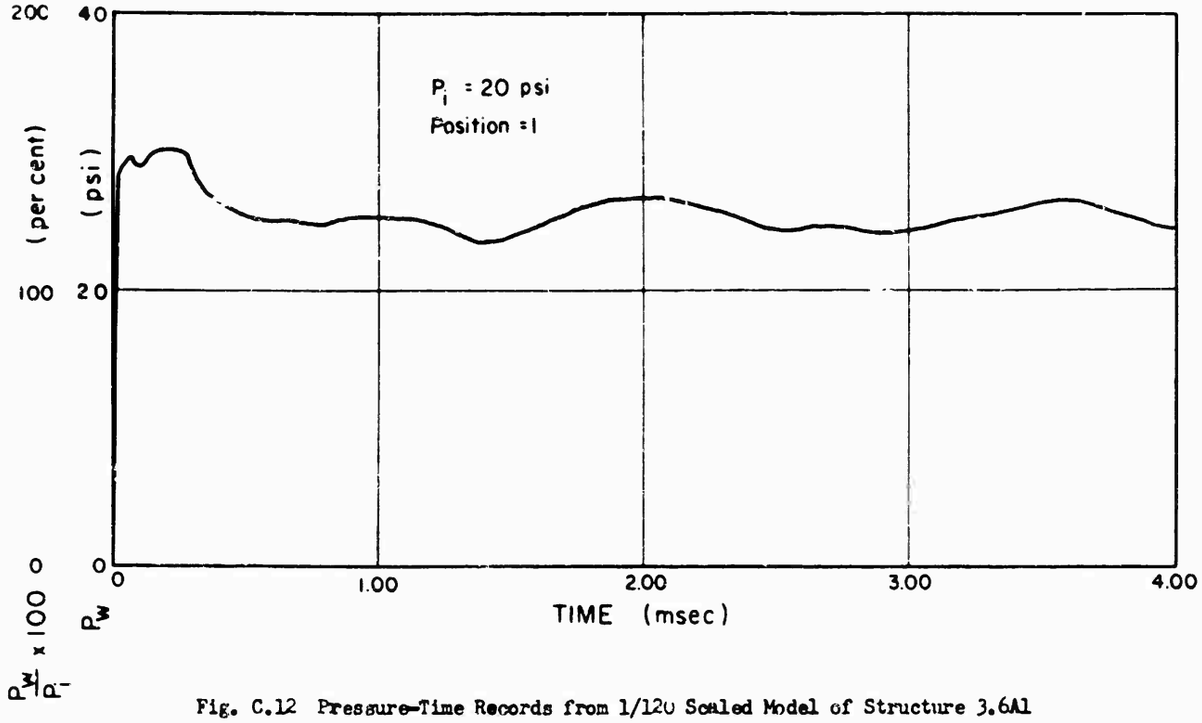

Fig. C.12 Pressure-Time Records from 1/120 Scaled Model of Structure 3.6A1

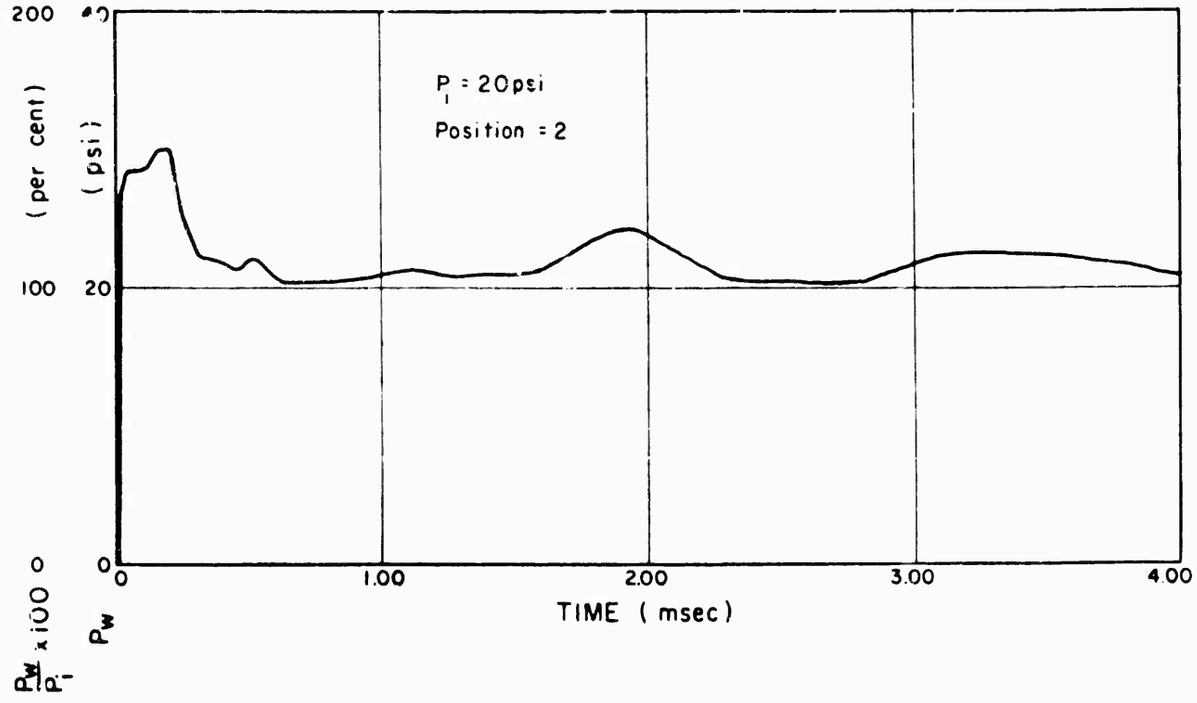

Fig. C.13 Pressure-Time Record from 1/120 Scaled Model of Structure 3.6A1

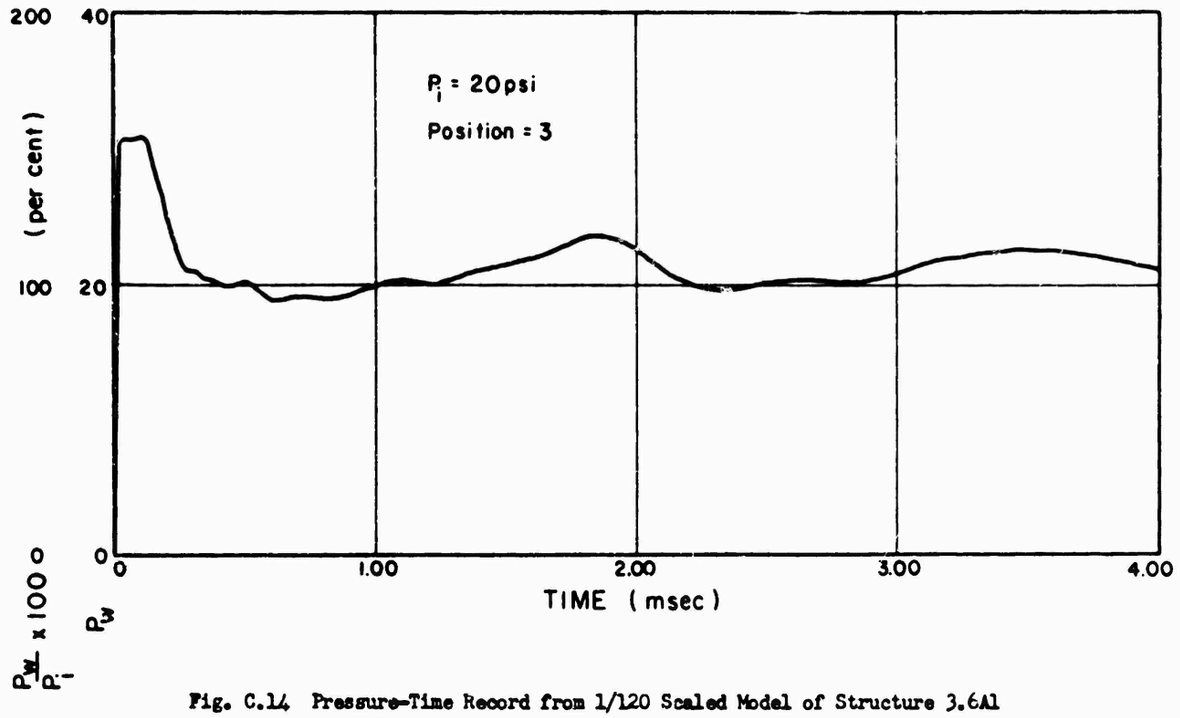

Fig. C.14 Pressure-Time Record from 1/120 Scaled Model of Structure 3.6A1

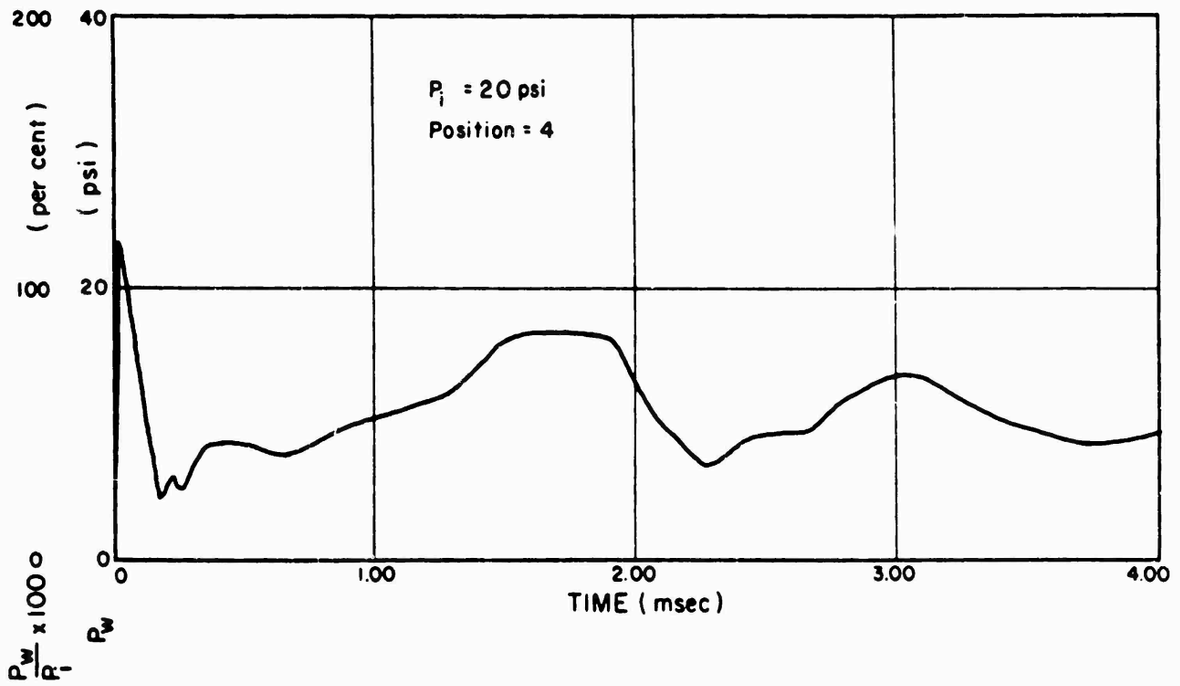

Fig. C.15 Pressure-Time Record from 1/120 Scaled Model of Structure 3.6A1

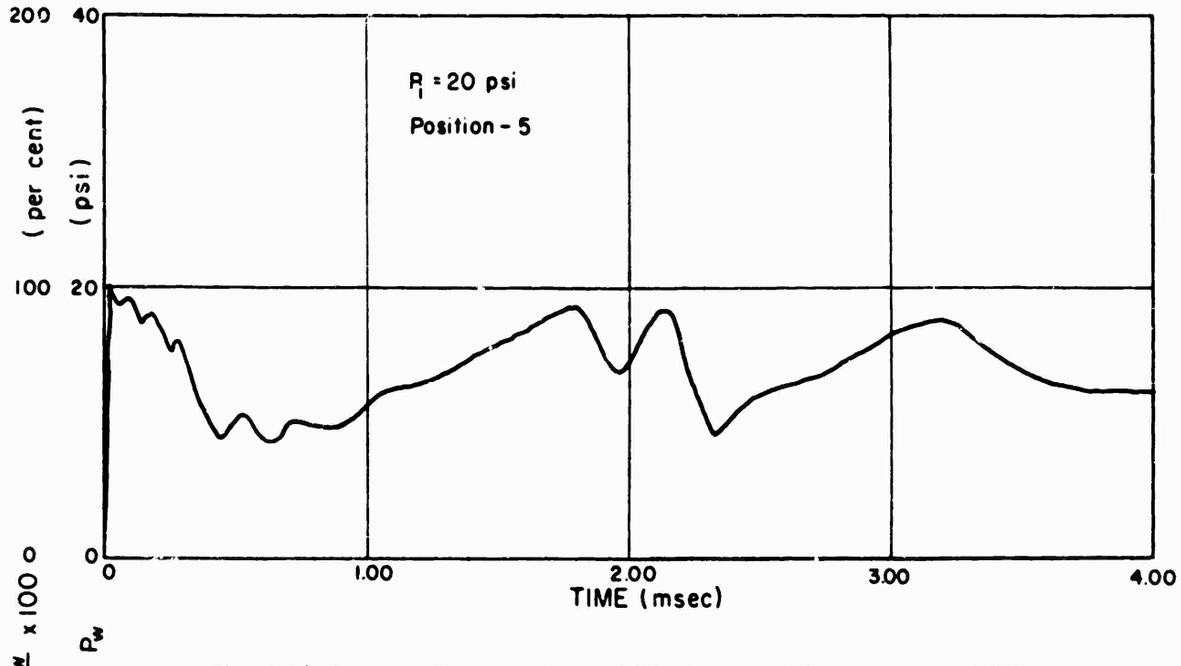

Fig. C.16 Pressure-Time Record from 1/120 Scaled Model of Structure 3.6A1

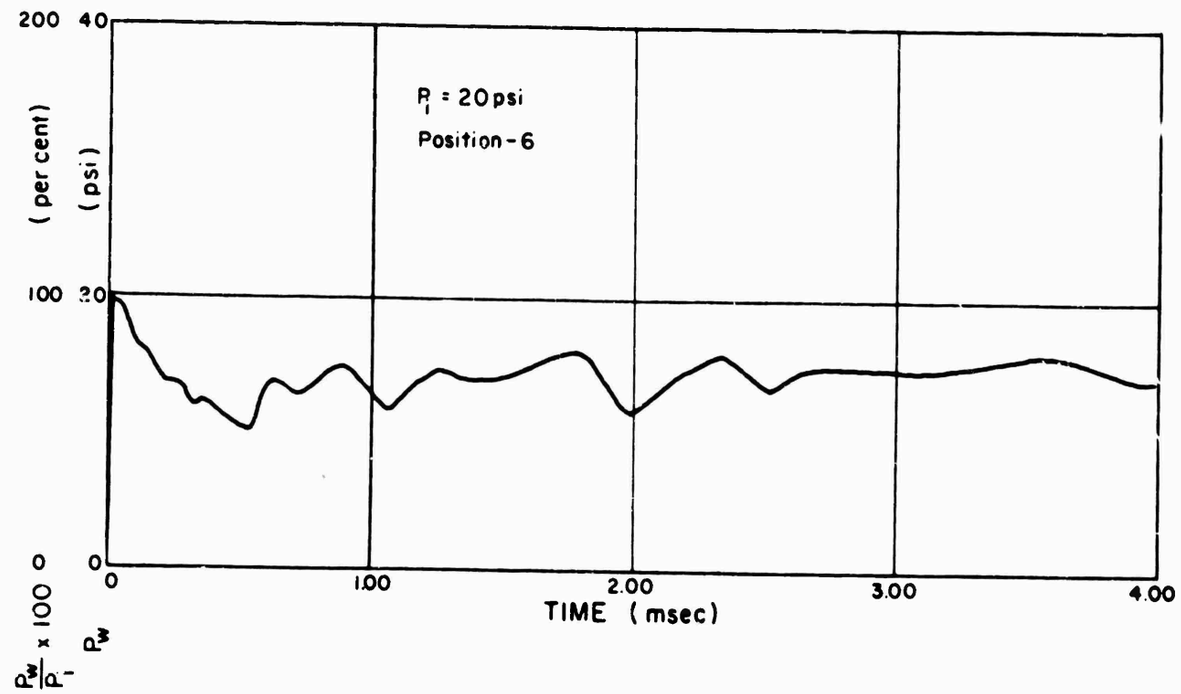

Fig. C.17 Pressure-Time Record from 1/120 Scaled Model of Structure 3.6A1

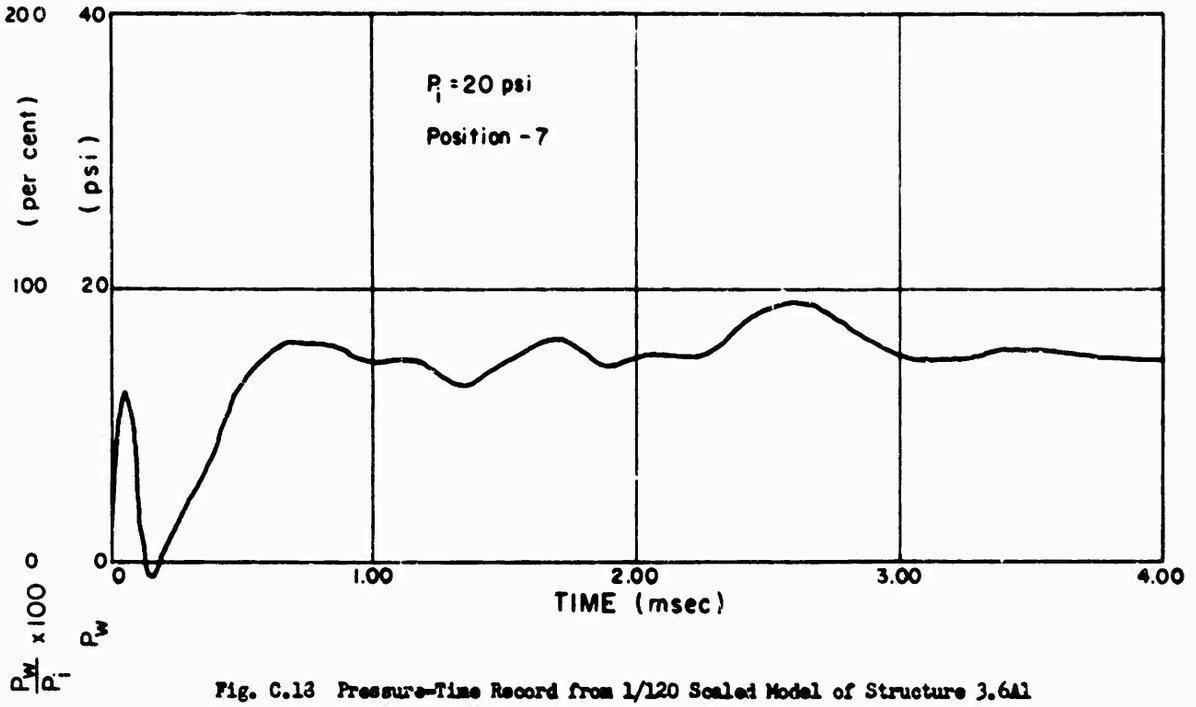

Fig. C.18 Pressure-Time Record from 1/120 Scaled Model of Structure 3.6A1

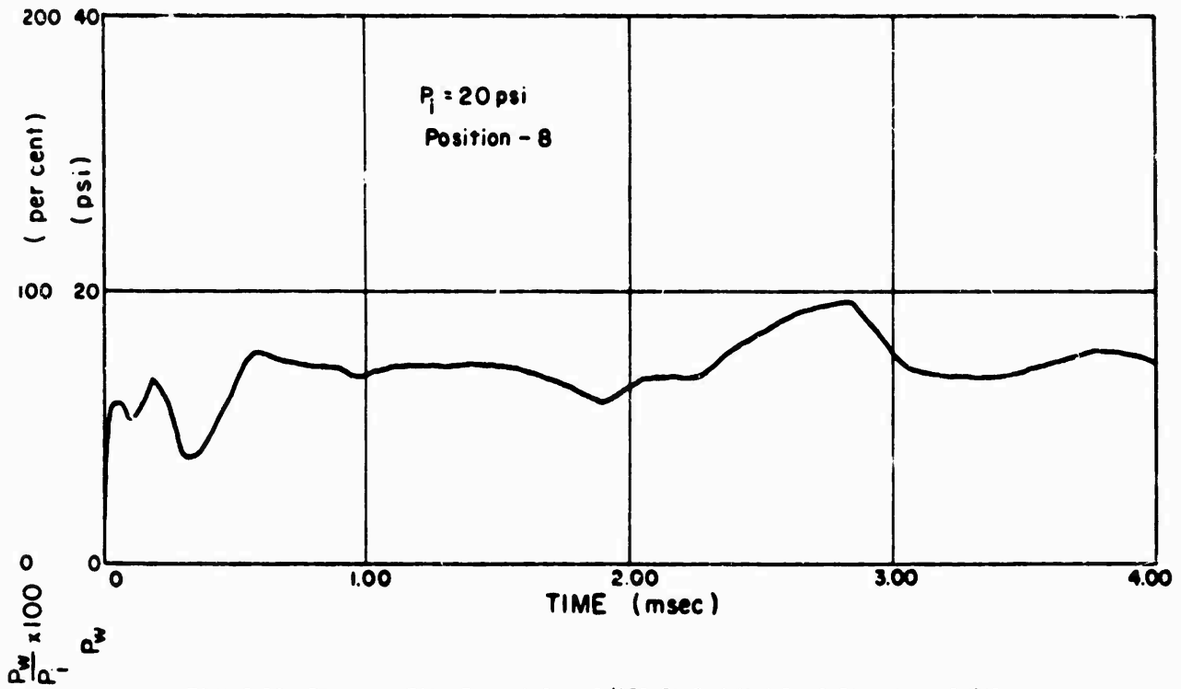

Fig. C.19 Pressure-Time Record from 1/120 Scaled Model of Structure 3.6A1

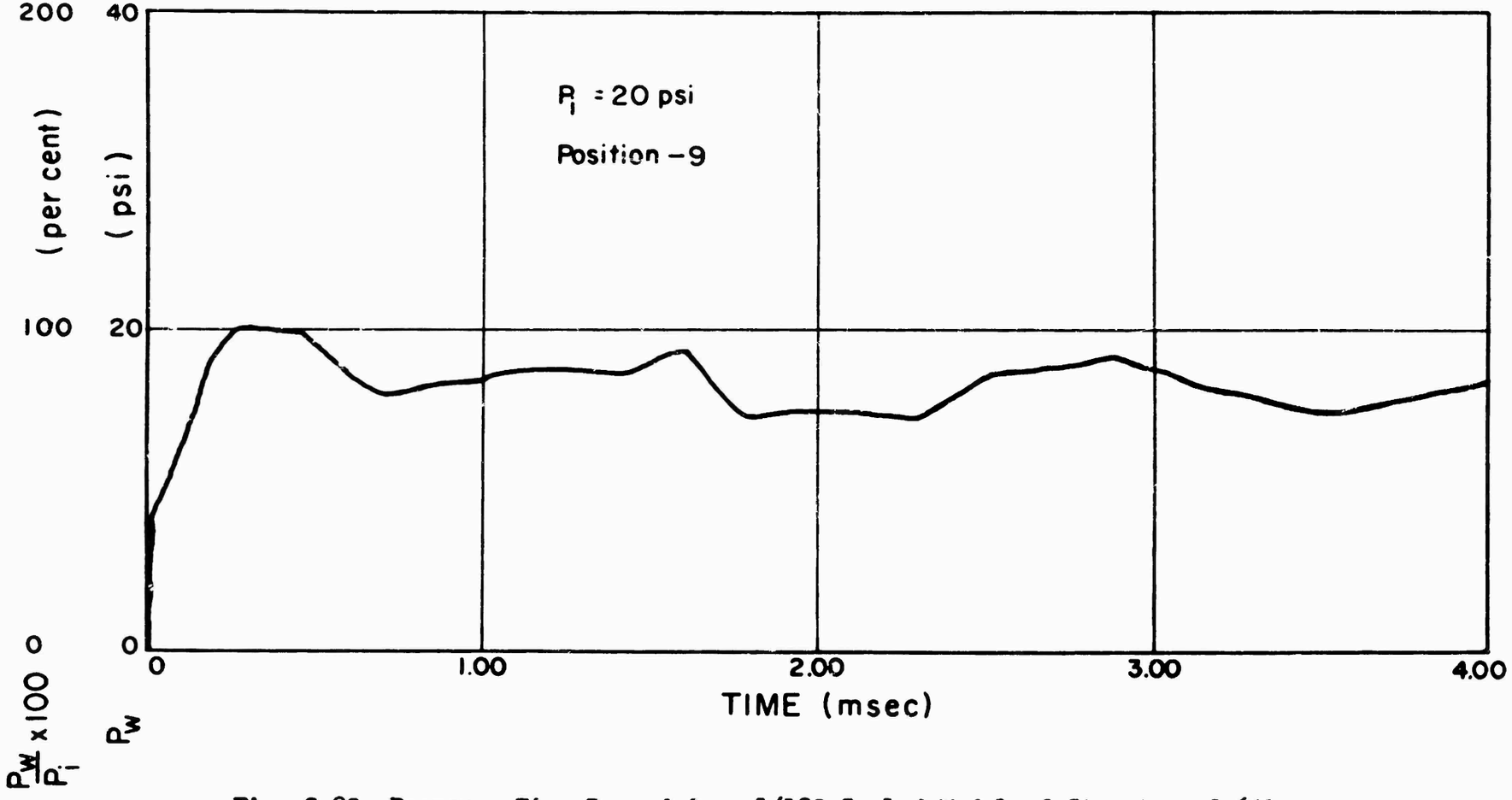

Fig. C.20 Pressure-Time Record from 1/120 Scaled Model of Structure 3.6A1

Appendix D

VERY-LOW-PRESSURE-GAGE RESULTS

The very-low-pressure gages were used for recording pressure-time phenomena at distances from 7 to 20 miles from the detonation point. A total of 49 measurements were made during the operation to obtain data on nine shots. These measurements were made at the Control Point, Camp Mercury, Indian Springs Air Force Base, and various locations on Shot 10. The gages were placed beside Sandia Corporation's microbarograph stations on all instrumented shots except Shot 10. Two gages were used in most cases to check data, and at various stations and shots modified gages were used. Although these measurements are still being made with experimental gages, the results appear to be accurate. A description of the gage itself along with a discussion of its shortcomings and an outline of improvements to be incorporated before the next operation will be found in Appendix A.

On Shot 10, VLP gages were used upon the request of the Sandia Corp. to obtain measurements at three remote stations, located as shown in Fig. D.1. Safety considerations prevented the use of Sandia's manned instruments at these locations. At stations 7W and 7E, two gages were placed atop a 60 foot pole and two others at the base of the pole. The 7N station consisted of two gages at ground level. Photographs of the stations are shown in Figs. D.2 and D.3. All gages were placed side-on to the blast and were initiated by means of a photo-initiation system.

Seven out of 10 gages on Shot 10 gave excellent pressure-time records with arrival times. Of the three gage failures only one appears attributable to the gage mechanism. The two gages at the North station were initiated preshot, apparently by the headlights of a passing vehicle on a nearby road. Due to the design of the gage, however, acceptable peak pressure records were obtained from all three of these gages. Typical records from the shot are shown in Fig. D.4, and Table C.1 gives the results.

On several shots, more than one gage was placed at a station for the purpose of checking damping devices, effect of gage orientation, and consistency of wave shapes. A typical example of such a station was on Shot 5, where three gages were placed at a single location. The consistency of the wave shapes can be seen in the enlarged photographs of the gage records shown in Fig. D.5. Data from these three gages are given in Table D.2. Gage 4 had the normal 2-inch layer of fiber glass damping material, gage 5 had a 4-inch layer, and gage 6 had the normal 2-inch layer but was oriented face-on to the blast, which resulted in a slightly higher overpressure.

Table D.3 is a table of results from 10 representative records

taken at various locations on several shots. Figure D.6 shows a wave shape with one major peak and one negative phase. Figure D.7 shows a wave with two cycles. Figure D.8 shows photomicrographs of the initial portion of two gages at each of two stations on Shot 12. One station was at the Control Point and the other at the observation point near the Mercury gate. Although these stations were at approximately the same distance from GZ, a great dissimilarity of wave shapes can be seen, probably due to meteorological and geographical conditions.

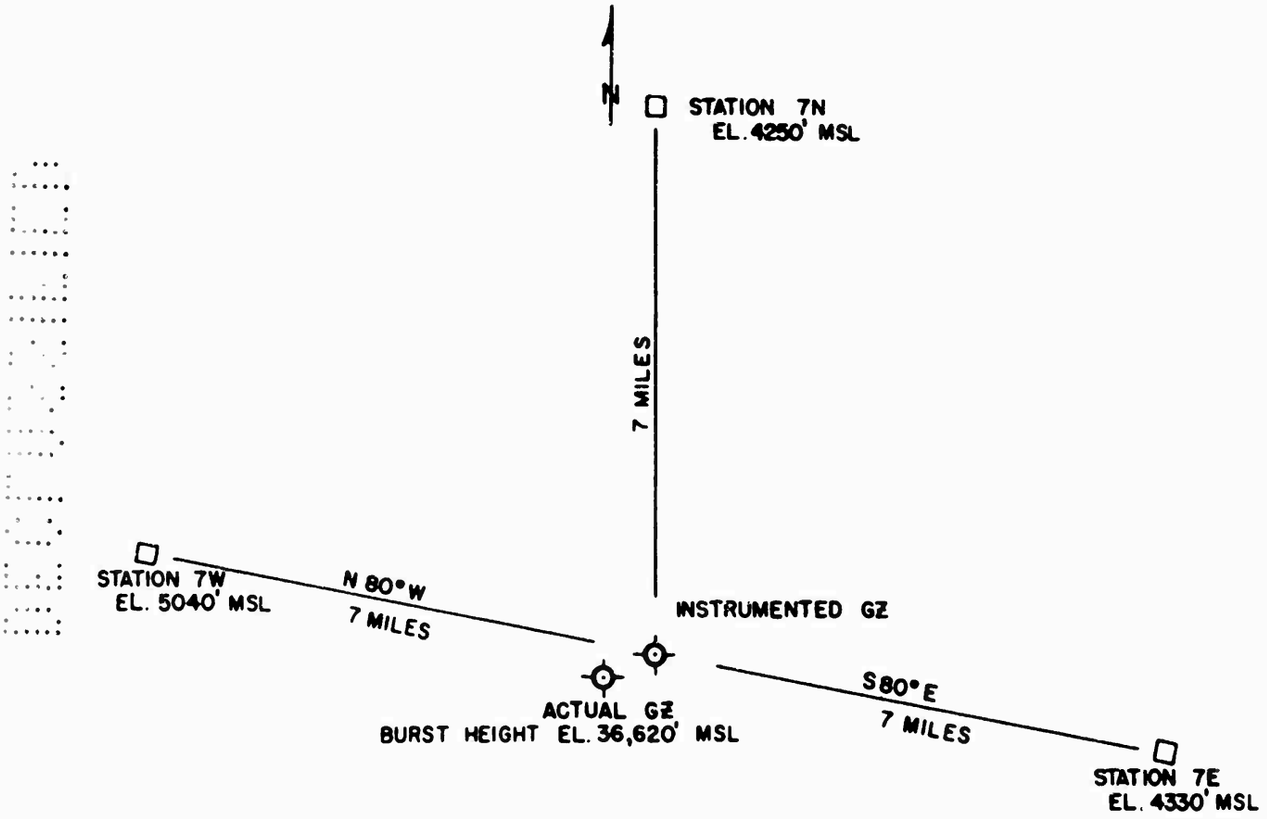

Fig. D.1 Gage Layout for Shot 10

TABLE D.1 Results of Shot 10

Station	Position	Gage No.	P_1 Peak Overpressure* (psi)	P_2 Peak Overpressure* (psi)	P_3 Peak Overpressure* (psi)	Max. Negative Pressure (psi)	Duration D_1* (sec)	Duration Positive Phase (sec)	Duration Negative Phase (sec)	Shock Arrival Time (sec)	Remarks
7E	60 ft Pole	10	0.059	0.045	0.098	0.047	0.0611	1.156	2.472	46.1	Good Pressure-time Record
7E	60 ft Pole	1	-	-	0.095	0.045	-	-	-	-	Did Not Run - P. P. Only
7E	Ground	8	-	-	0.099	0.051	-	0.975	2.522	45.9	Good Pressure-time Record
7E	Ground	3	-	-	0.106	0.052	-	1.385	2.690	46.2	Good Pressure-time Record
7N	Ground	7	-	-	0.100	-	-	-	-	-	Did Not Run - P. P. Only
7N	Ground	4	-	-	0.093	-	-	-	-	-	Did Not Run - P. O. Only
7W	60 ft Pole	2	0.045	0.043	0.085	0.046	.0843	1.354	2.056	47.8	Good Pressure-time Record
7W	60 ft Pole	9	0.045	.039	0.095	0.047	.0833	1.445	2.146	45.2	Good Pressure-time Record
7W	Ground	5	-	-	0.089	0.028	-	.851	1.750	44.8	Never got up to speed
7W	Ground	6	-	-	0.075	0.044	-	1.315	2.423	47.9	Extra damped - Good Record

* Values read from gage record

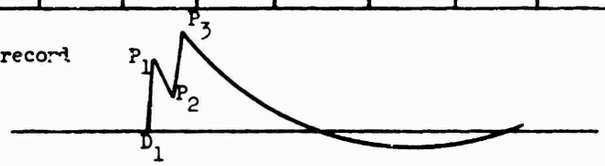

TABLE D.2 Results of Shot 5

Gage No.	Operating Agency	1st Peak Overpressure (psi)	2nd Peak Overpressure (psi)	Max. Negative Pressure (psi)	Duration Positive Phase (sec)	Duration Negative Phase (sec)	Shock Arrival Time (sec)	Remarks
3	Shaw & Estes	0.265	0.090	0.068	1.172	1.888	34.320	Good Pressure-time Record
4	BRL	0.278	0.079	0.054	1.48	2.27	None	Good Pressure-time Record
5	BRL	0.275	0.078	.056	1.33	2.24	None	Good Pressure-time Record
6	BRL	0.304	0.067	.050	1.48	2.22	None	Gage Face-on to Blast-Good Record
	Sandia Corp. Microbarograph	0.116	0.090	0.075	1.17	2.20	34.31	Good Pressure-time Record

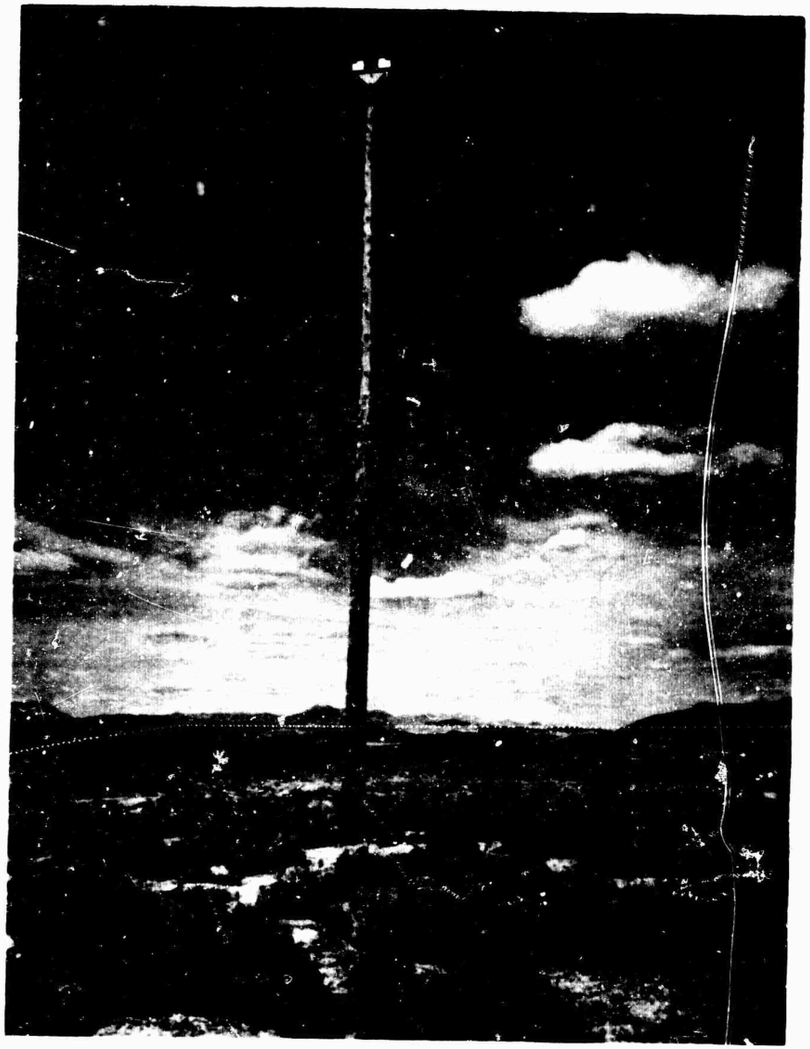

Fig. D.2 Typical Installation on 60' Pole for Shot 10

Fig. D.3 Typical Ground Station for Shot 10

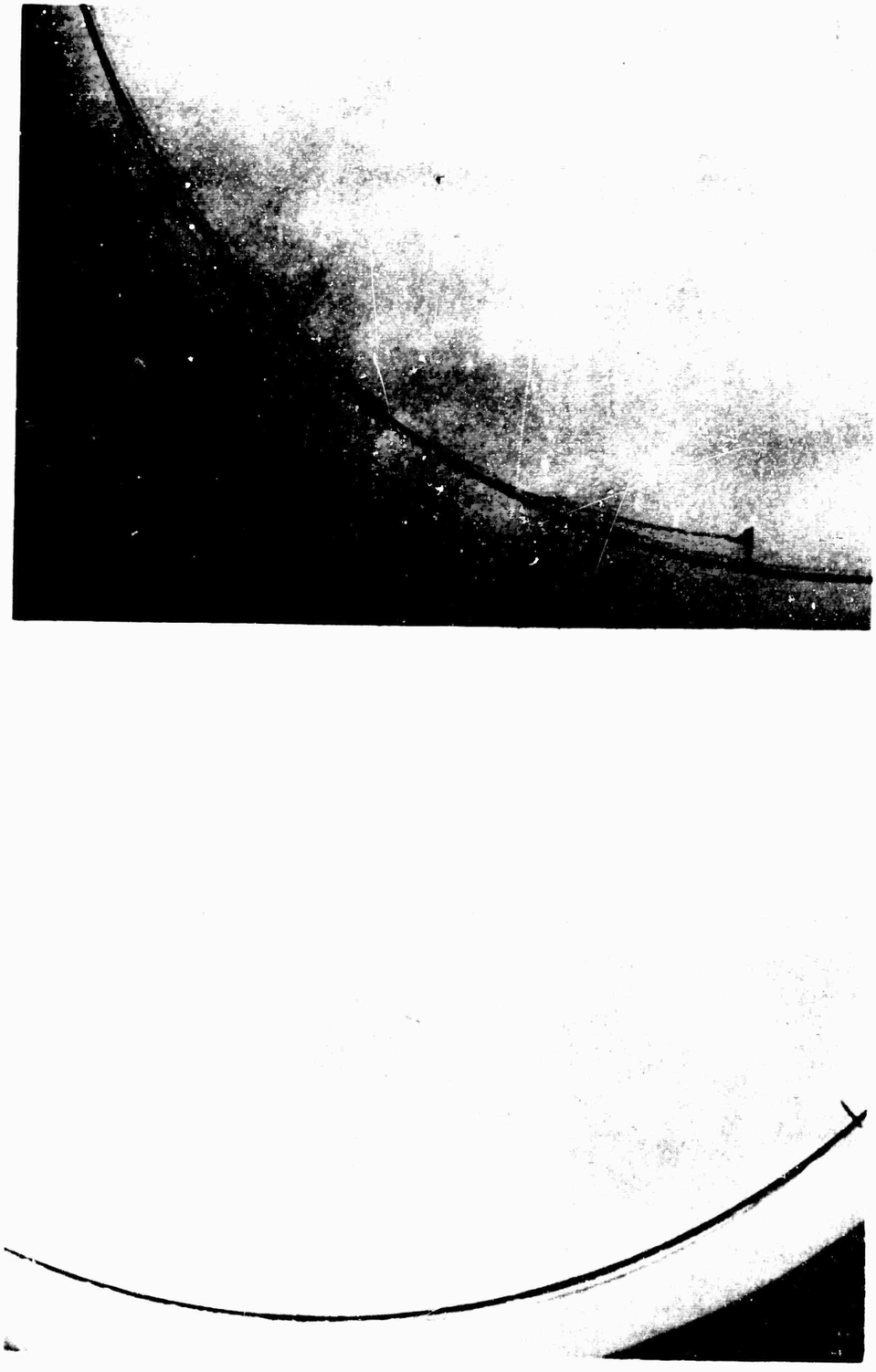

Fig. D.4 Typical Records from Shot 10

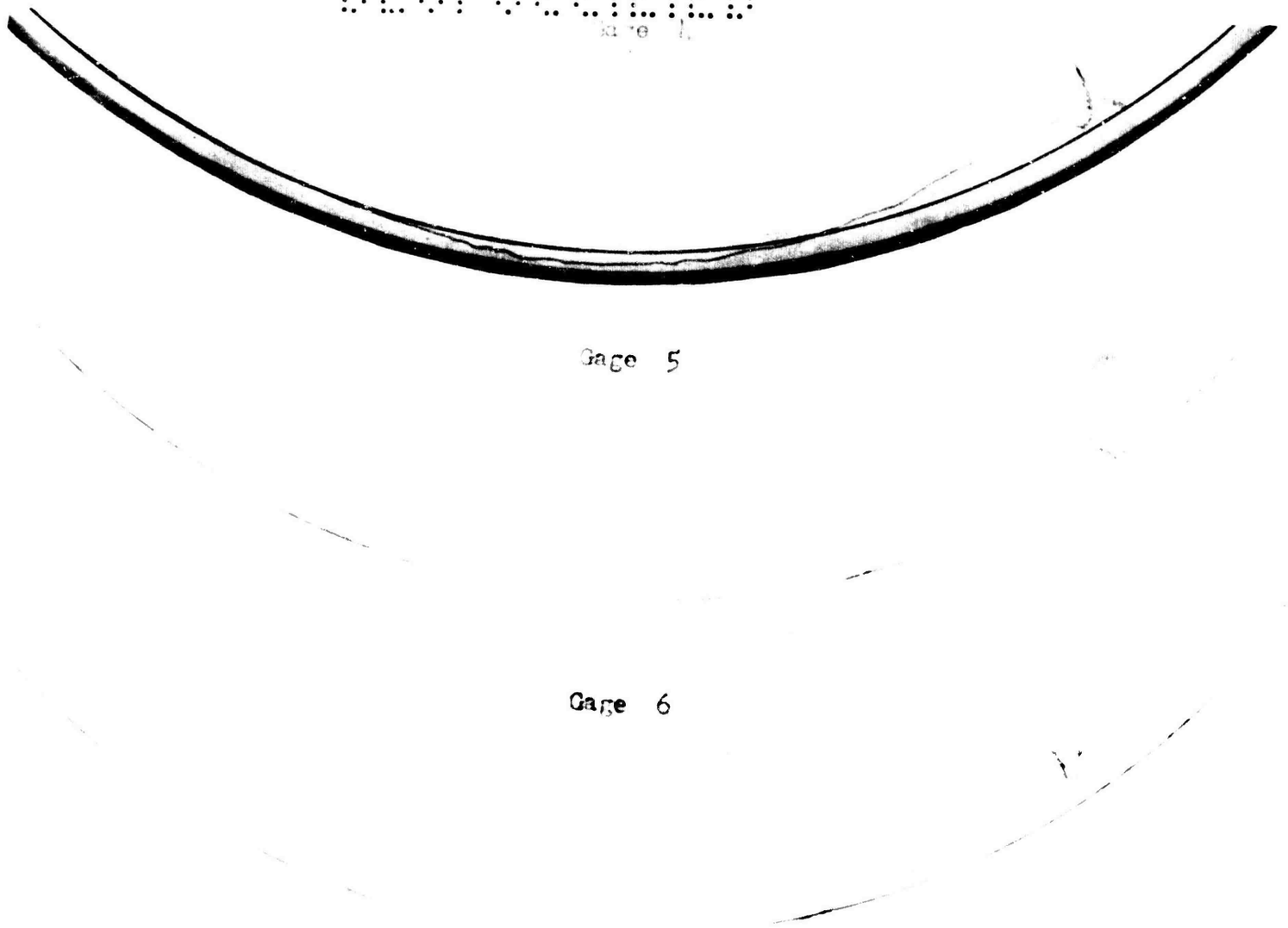

Fig. D.5 Comparison of Records from Three Gages at One Location on Shot 5

TABLE D.3 Typical VLP Gage Results

Shot	Station	Gage	Figure	Time A* (sec)	Time B* (sec)	Time C* (sec)	Time D* (sec)	P_1 Peak Overpressure* (psi)	P_2 Maximum Negative Pressure* (psi)	P_3 Peak Overpressure* (psi)	P_4 Negative Pressure* (psi)
3	CP	4	2	.270	.117	.117	.297	.120	.022	.040	.007
4	CP	4	1	2.483	2.988	-	-	.520	.027	-	-
6	ISAFB	4	2	.898	2.180	1.554	.475	.036	.013	.025	.003
6	Q-20	5	1	1.373	2.410	-	-	.700	.022	-	-
8	ISAFB	4	2	2.027	3.005	1.649	-	.026	.005	.004	-
8	Q-20	7	1	3.681	2.888	-	-	.010	.012	-	-
8	CP	9	2	3.311	3.492	3.756	-	.043	.040	.009	-
9	CP	2	2	.631	.751	.998	1.251	.018	.005	.004	.004
12	Obs. Ar.	6	1	1.993	3.923	-	-	.169	.049	-	-
12	CP	8	1	1.649	3.336	-	-	.096	.026	-	-

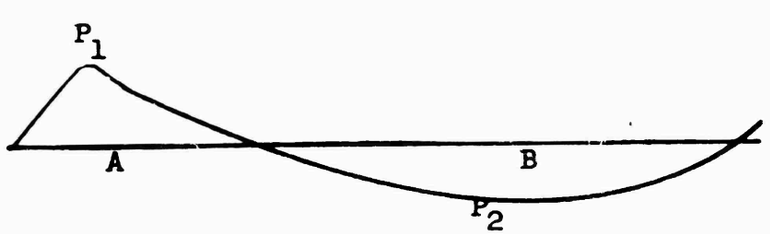

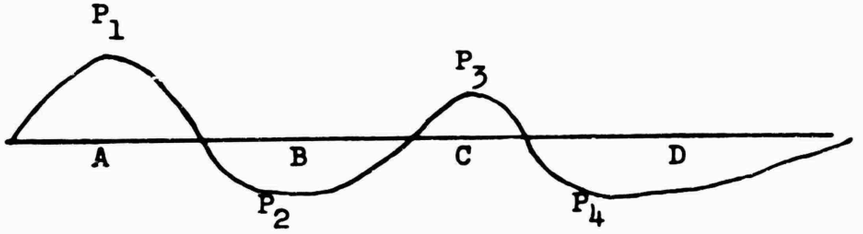

Fig. D.6 Illustration of VLP Record with One Positive Peak

Fig. D.7 Illustration of VLP Record with Two Positive Peaks

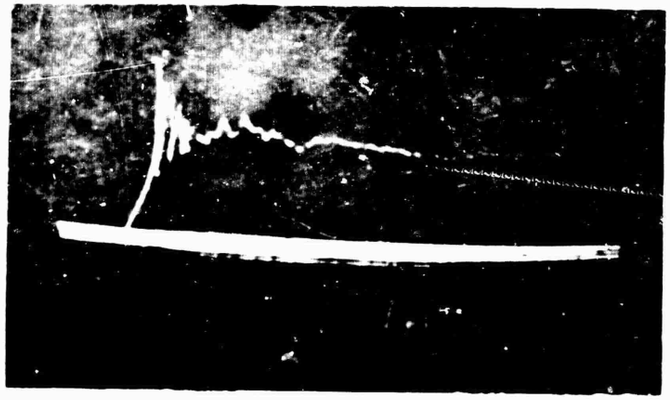

Control Point Gage 2

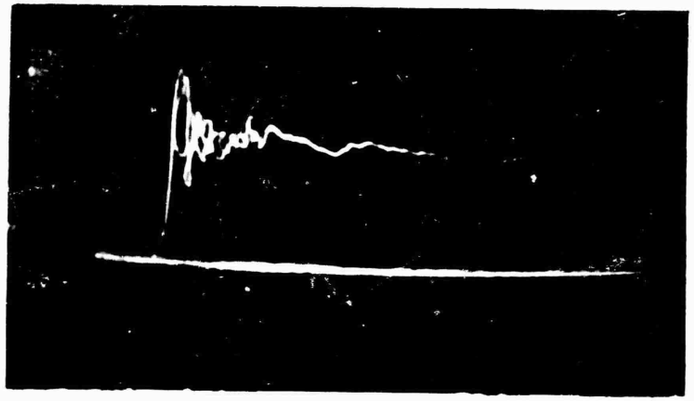

Control Point Gage 8

Observation Point for Shot MET Gage 4

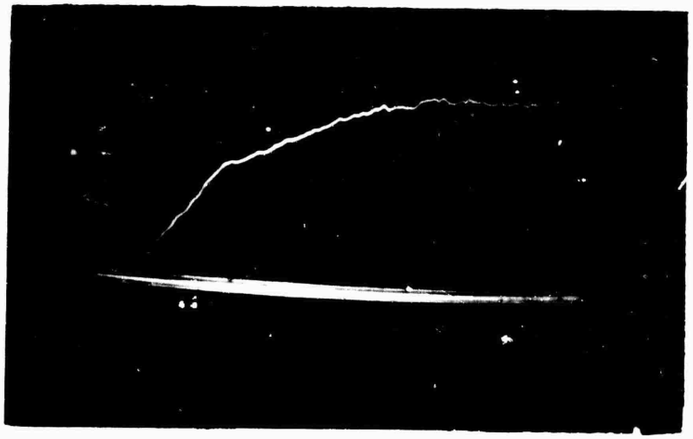

Observation Point for Shot MET Gage 6

Fig. D.8 Photomicrographs of Initial Portion of Four VLP Gages of Two Widely Separated Locations on Shot 12

Appendix E

RECORD PRESENTATION

All records from p-t gage and q-gage which could be reduced to pressure-time are presented in this appendix.

The first series of records in Fig. E.1 through Fig. E.32 are from the q-gages. These are arranged by shot and by distance from ground zero. For each station the total and static pressure-time records are given along with the dynamic pressure-time records. Unless otherwise indicated the q-gage records are for the 3-foot level. The surface level pressure-time records are given in Fig. E.33 through Fig. E.55. These are arranged first by shot then by distance from ground zero. Some attempt was made in smoothing through the irregular oscillations of the pressure-time records. This is indicated by dotted lines drawn through the record. It was difficult to determine which pressure record should be smoothed through and which record should be left as read.

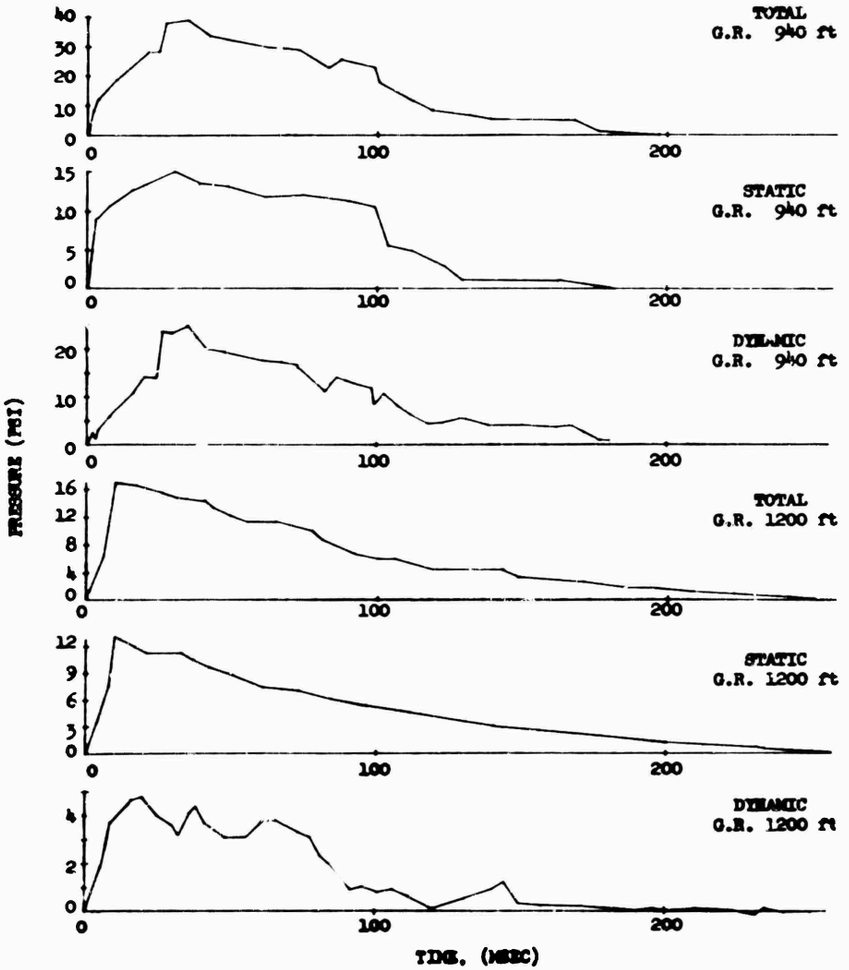

Fig. E.1

Pressure-time Records from q-Gage for Shot 2

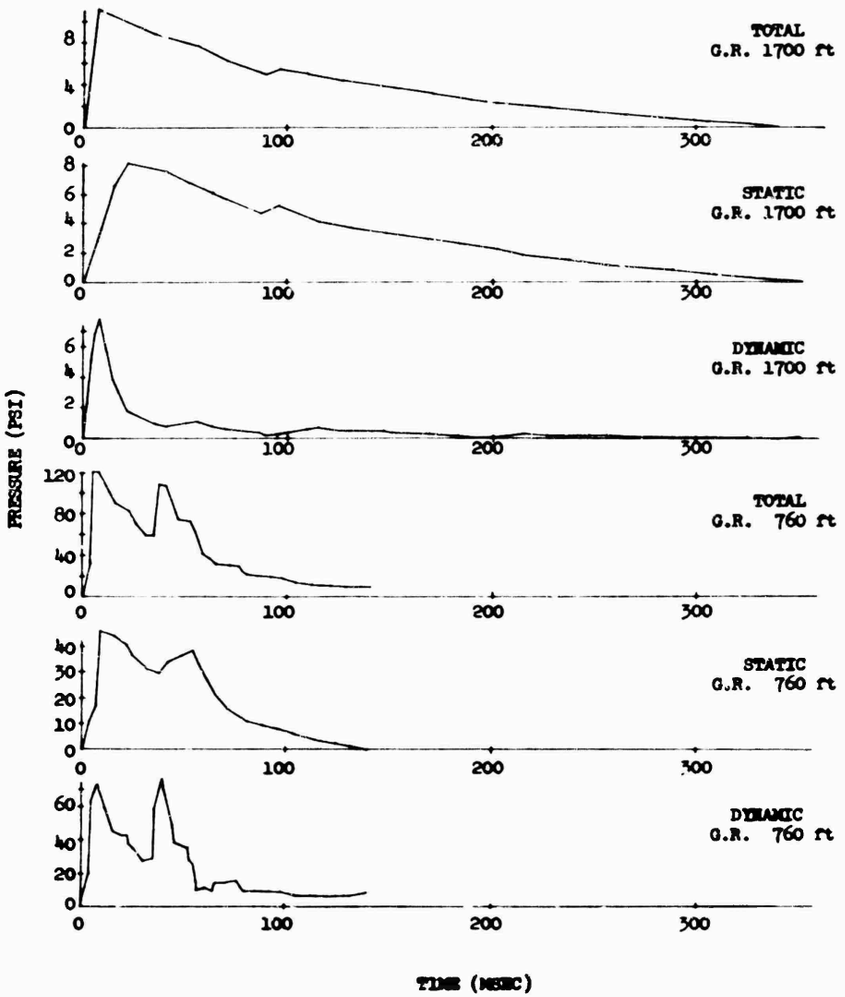

Fig. E.2

Pressure-Time Records from q-Gage for
Shot 2, (GR 1700 ft) and Shot 3, (GR 760 ft)

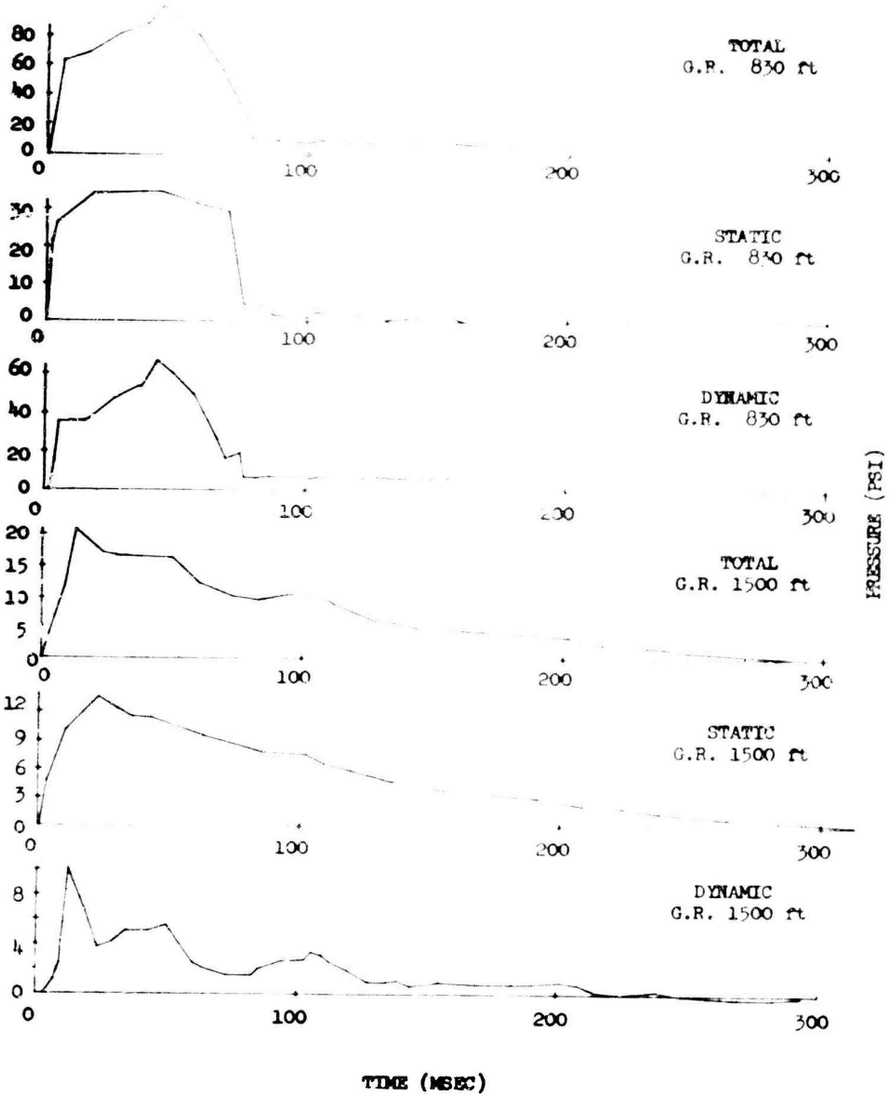

Fig. E.3 Pressure-Time Records from q-Gage for Shot 3

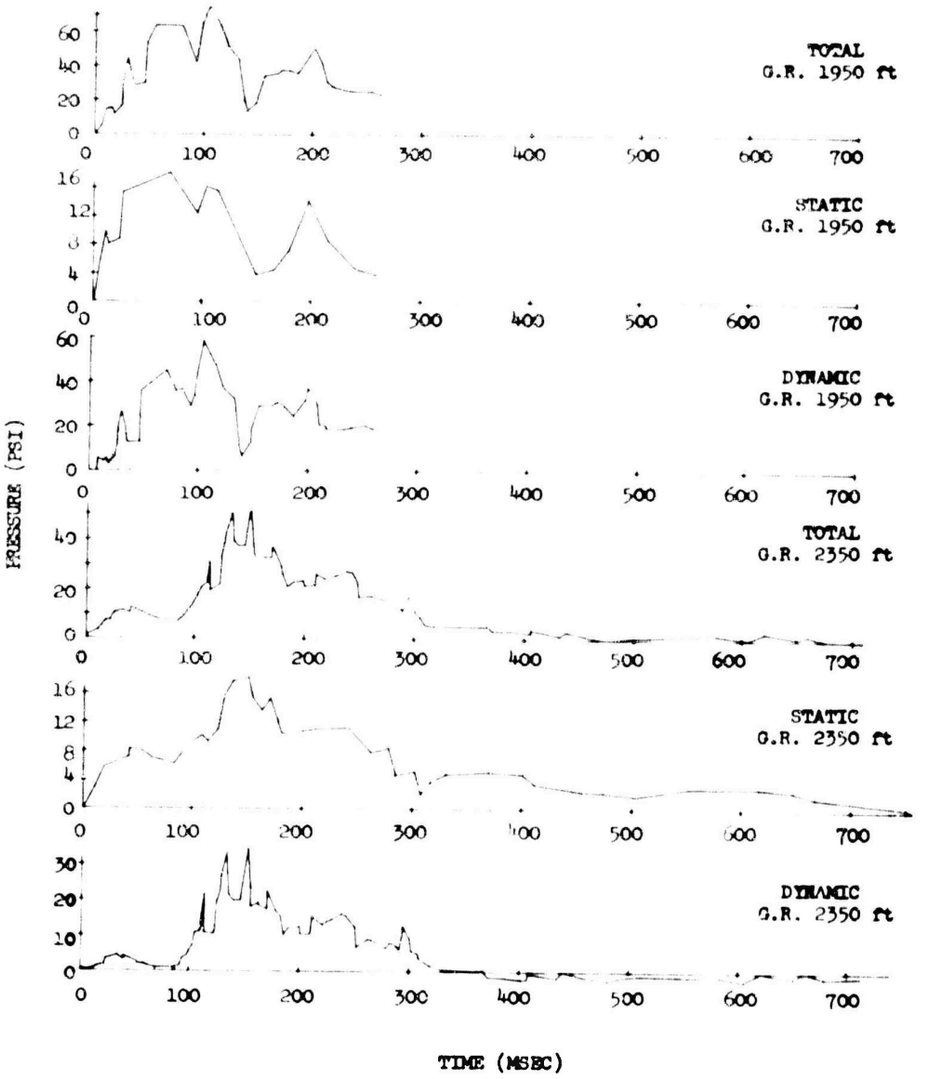

Fig. E.4 Pressure-Time Records from q-Gage for Shot 4

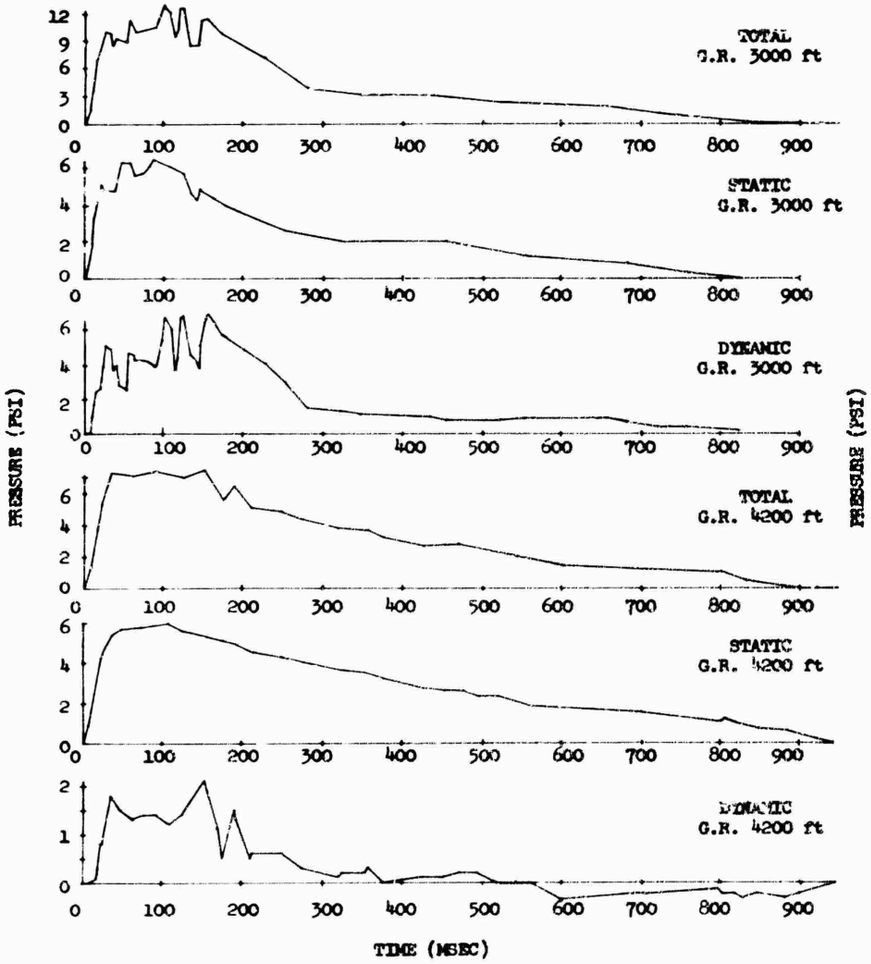

Fig. E.5 Pressure-time Records from q-Gage for Shot 4

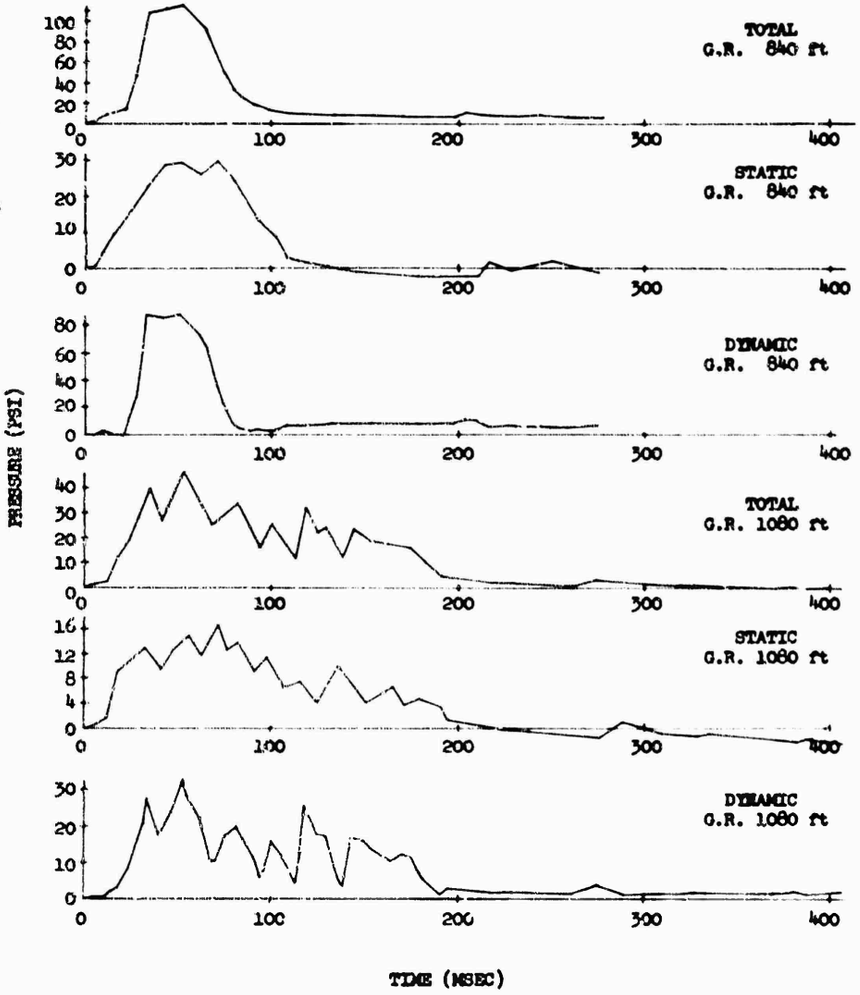

Fig. E.6 Pressure-Time Records from q-Gage for Shot 5

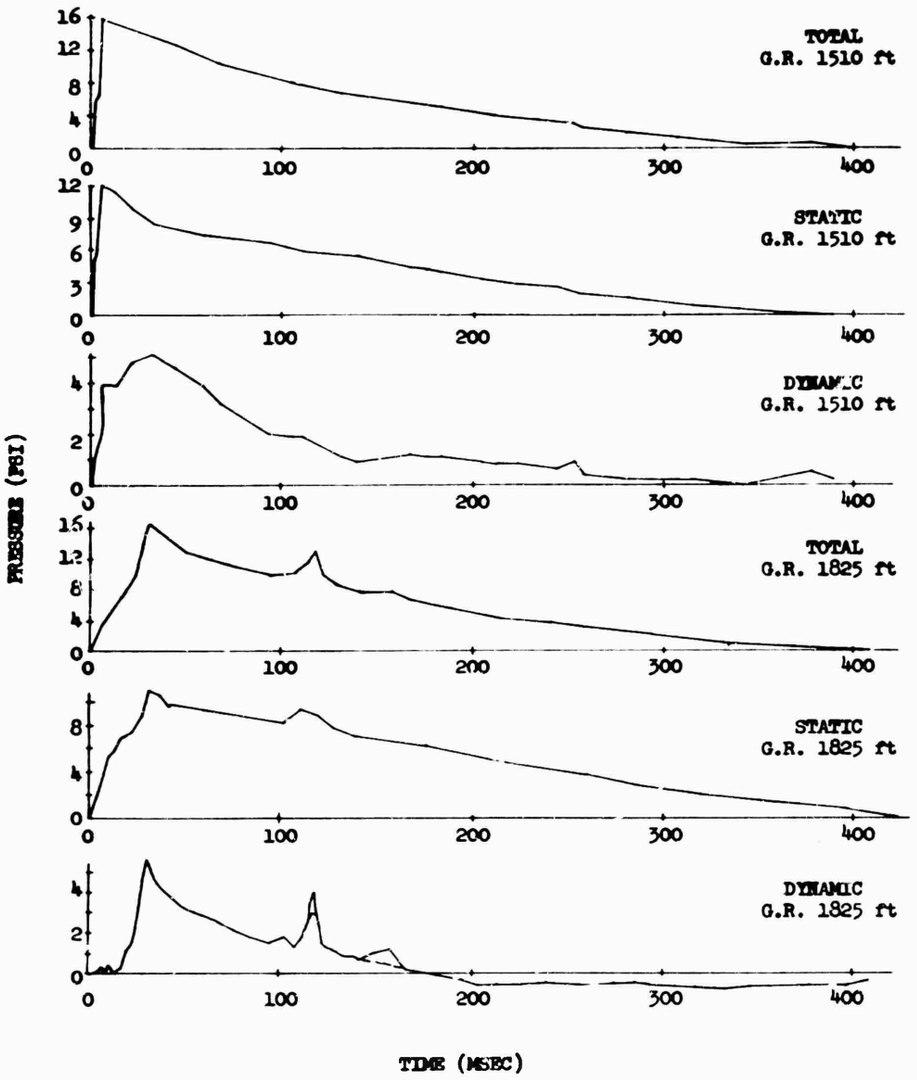

Fig. E.7 Pressure-Time Records from q-Gage for Shot 5, (GR 1510 ft) and Shot 6, Desert Surface (GR 1825 ft)

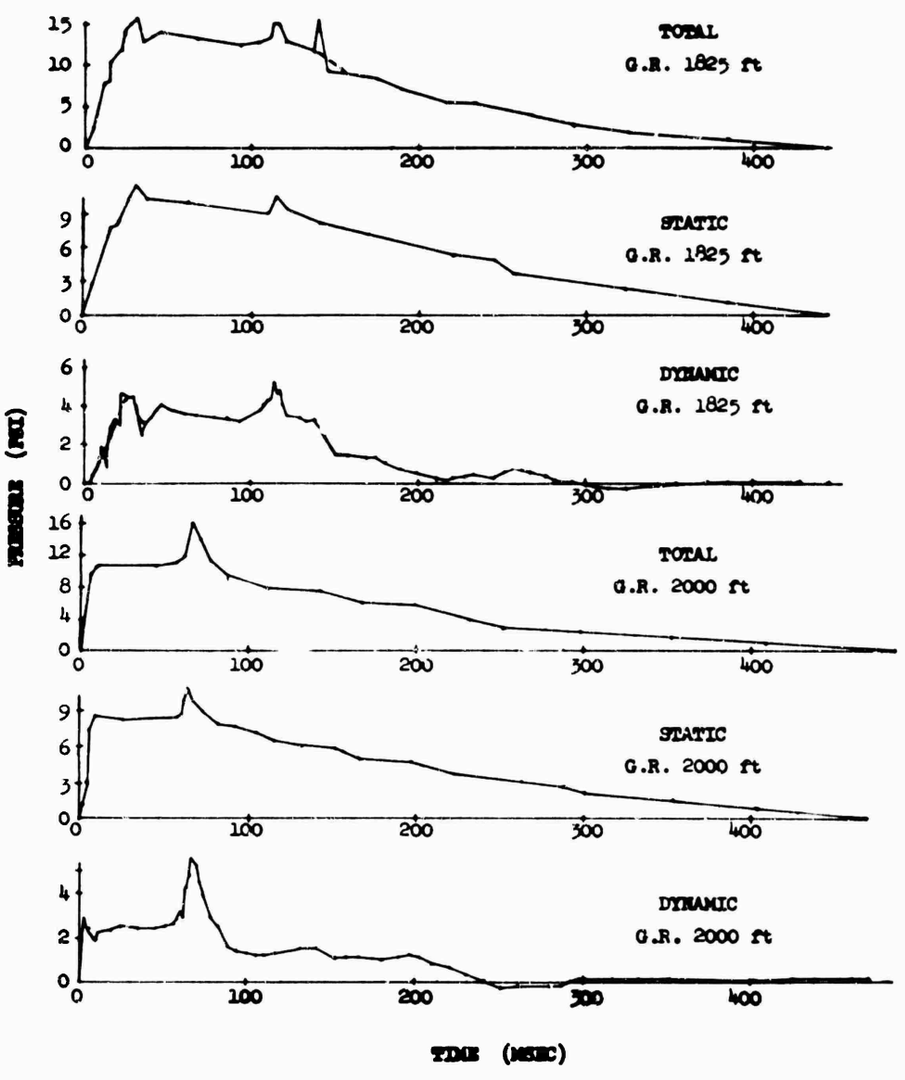

Fig. E.8 Pressure-Time Records from q-Gage for Shot 6, Desert Surface

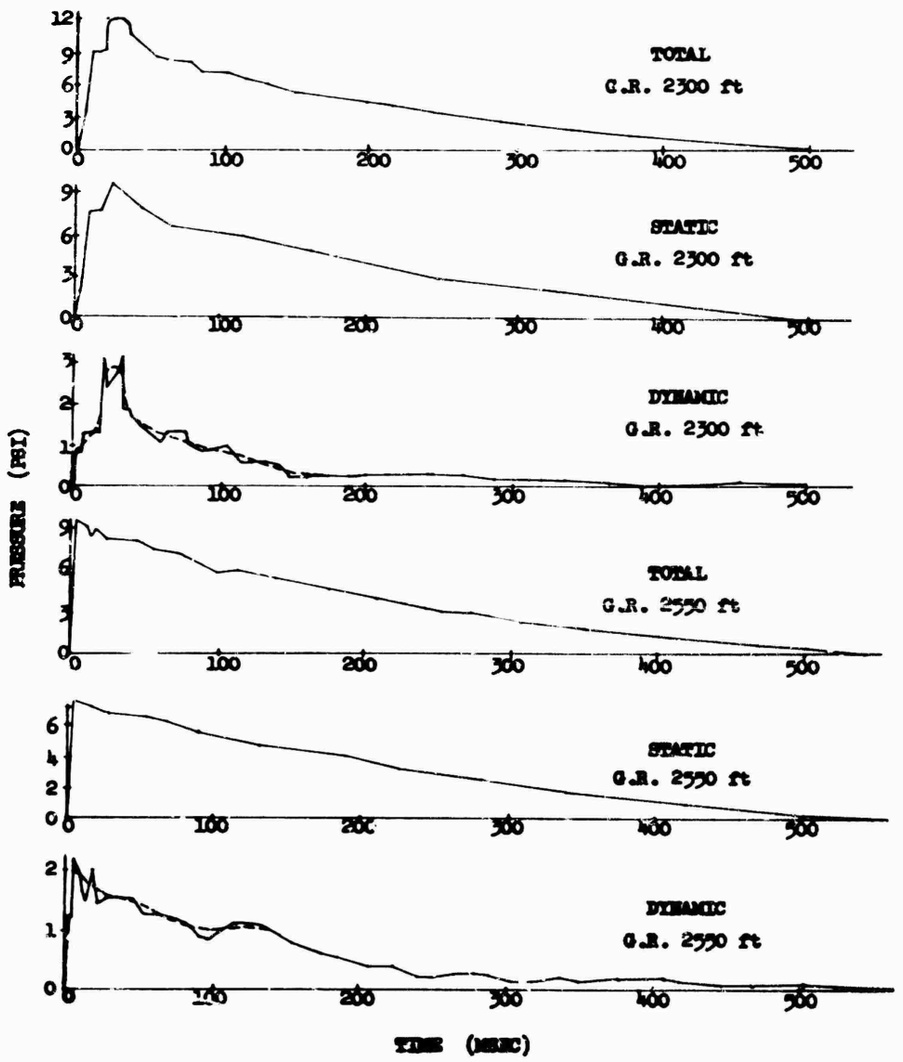

Fig. E.9 Pressure-Time Records from q-Gage for Shot 6, Desert Surface

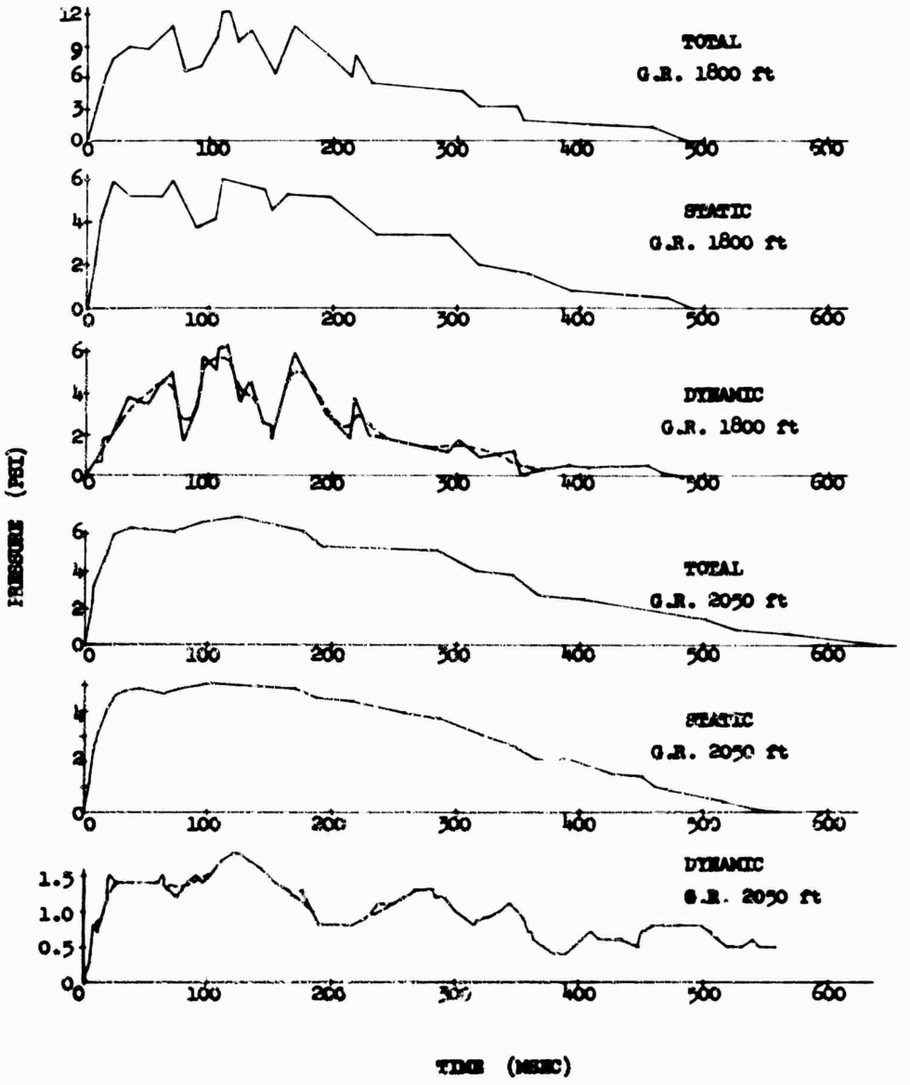

Fig. E.10
Pressure-Time Records from q-Gage for Shot 6, Asphalt Surface

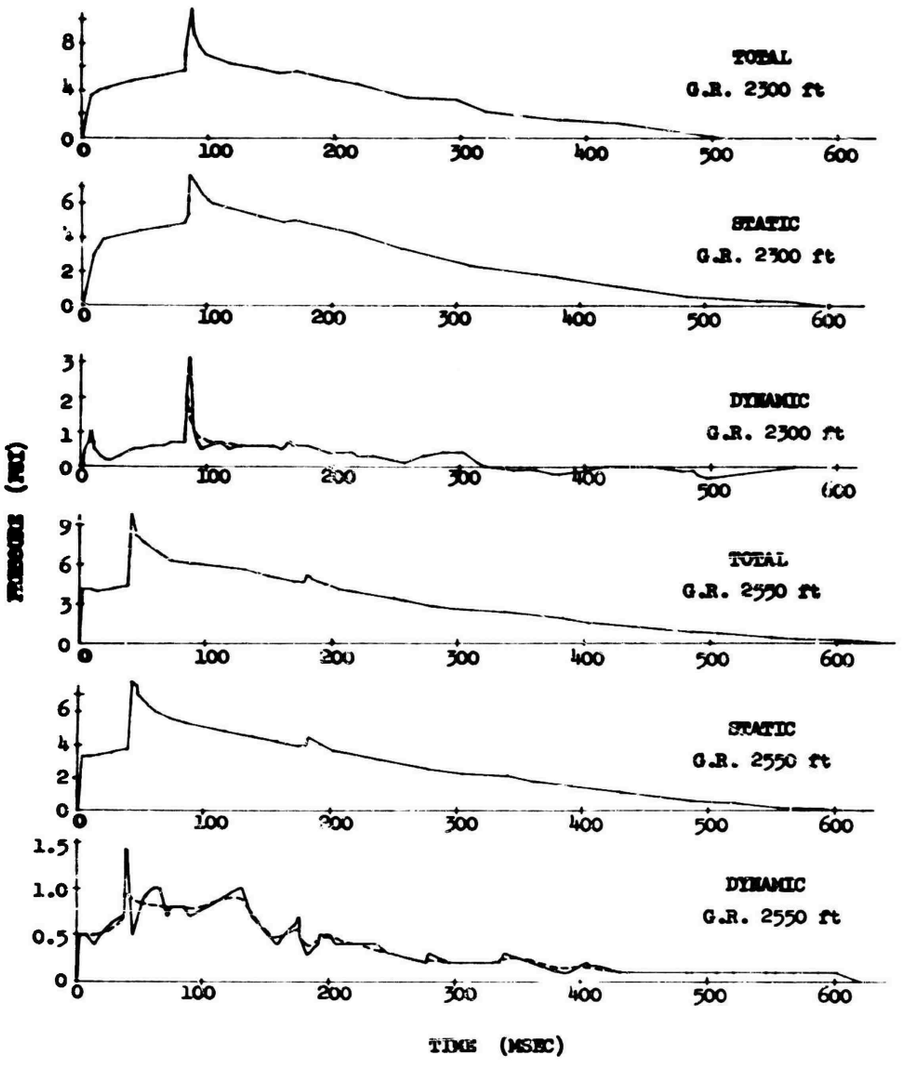

Fig. E.11
Pressure-Time Records from q-Gage for Shot 6, Asphalt Surface

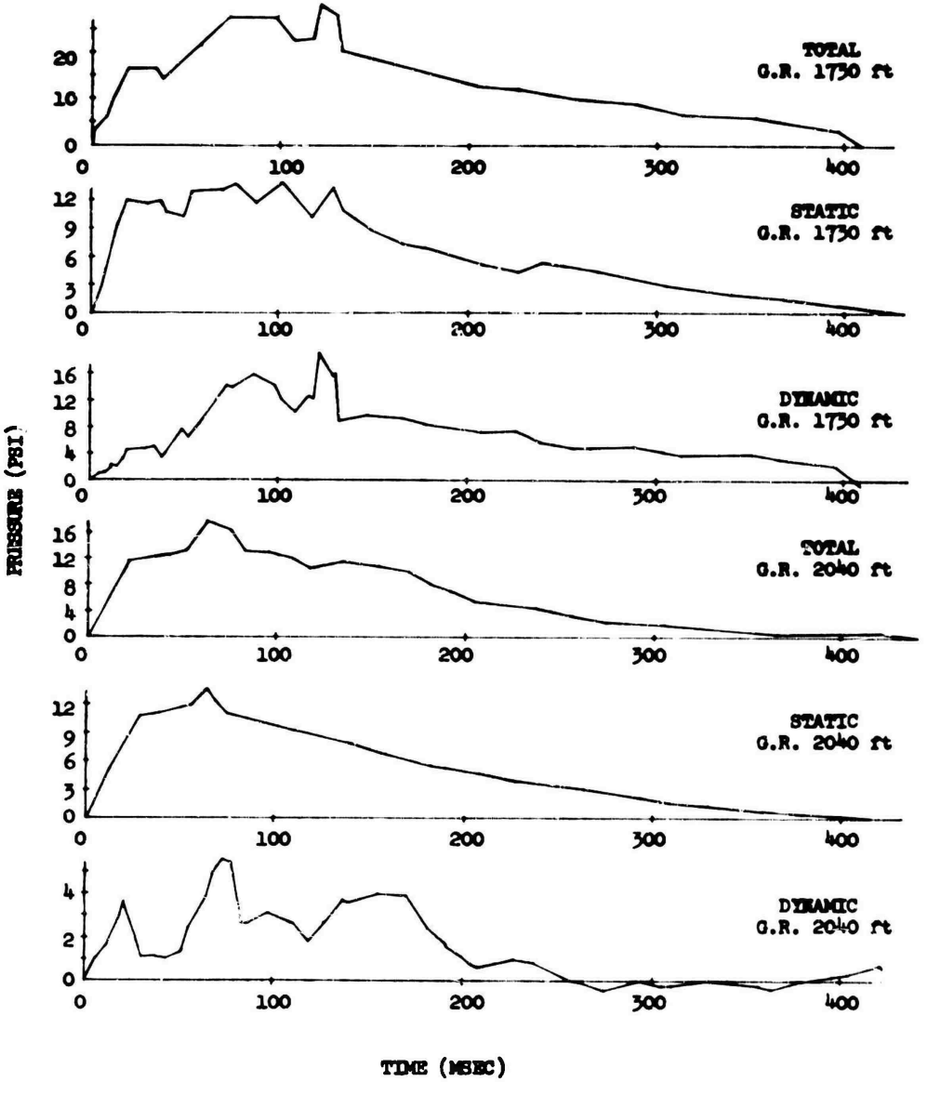

Fig. E.12 Pressure-Time Records from q-Gage for Shot 8

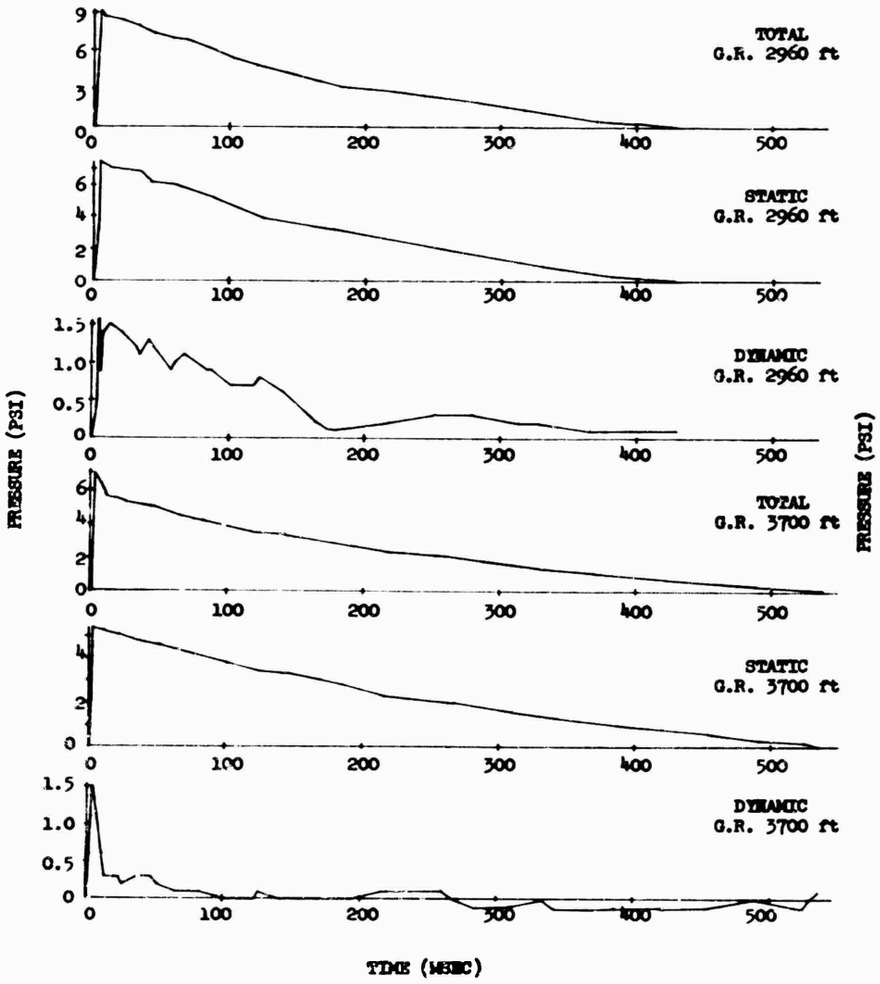

Fig. E.13 Pressure-Time Records from q-Cage for Shot 8

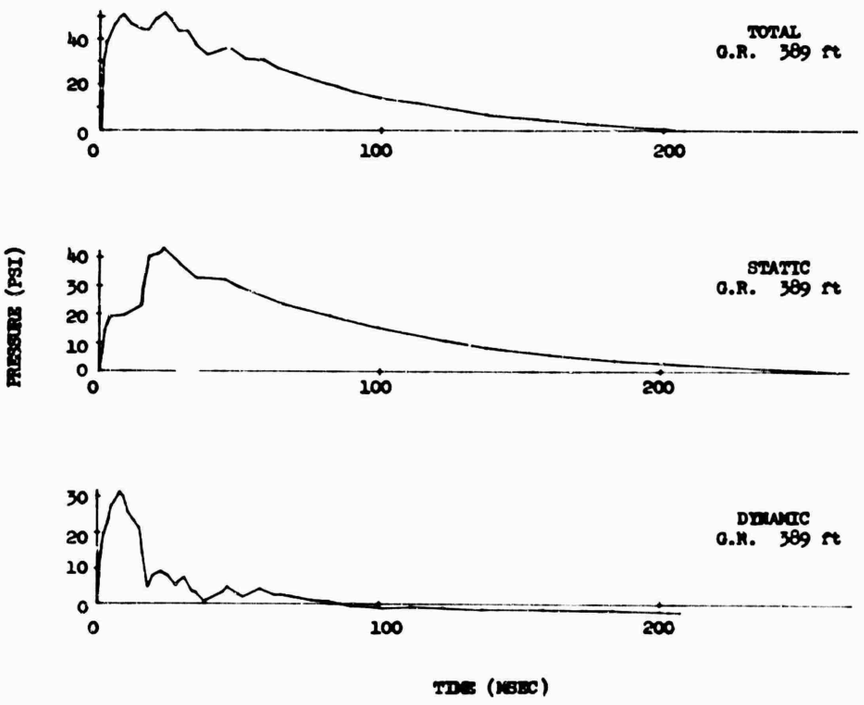

Fig. E.14 Pressure-Time Records from q-Cage for Shot 9

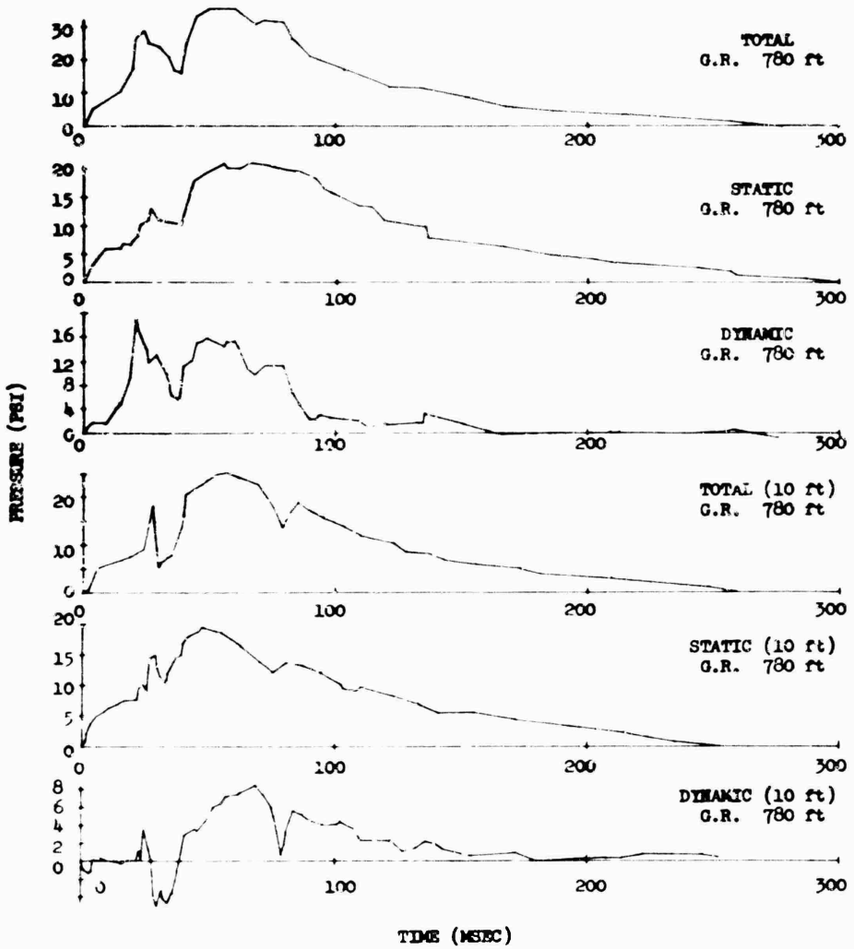

Fig. E.15 Pressure-Time Records from q-Gage for Shot 9

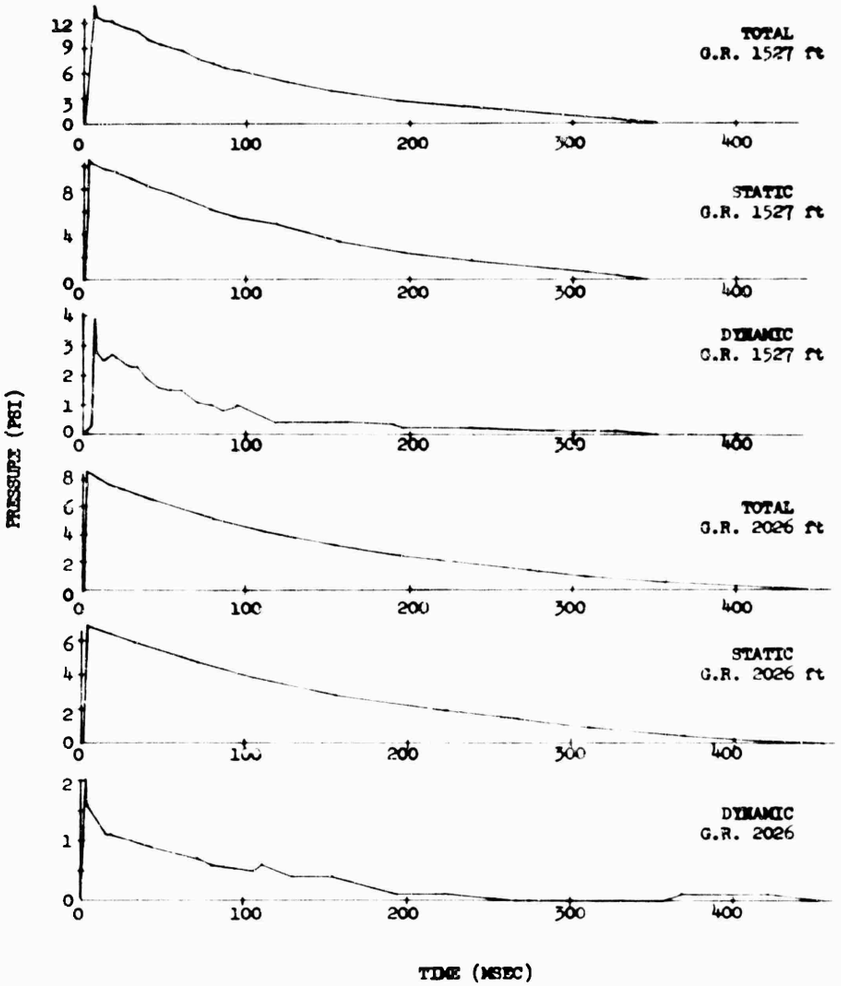

Fig. E.16 Pressure-Time Records from q-Gage for Shot 9

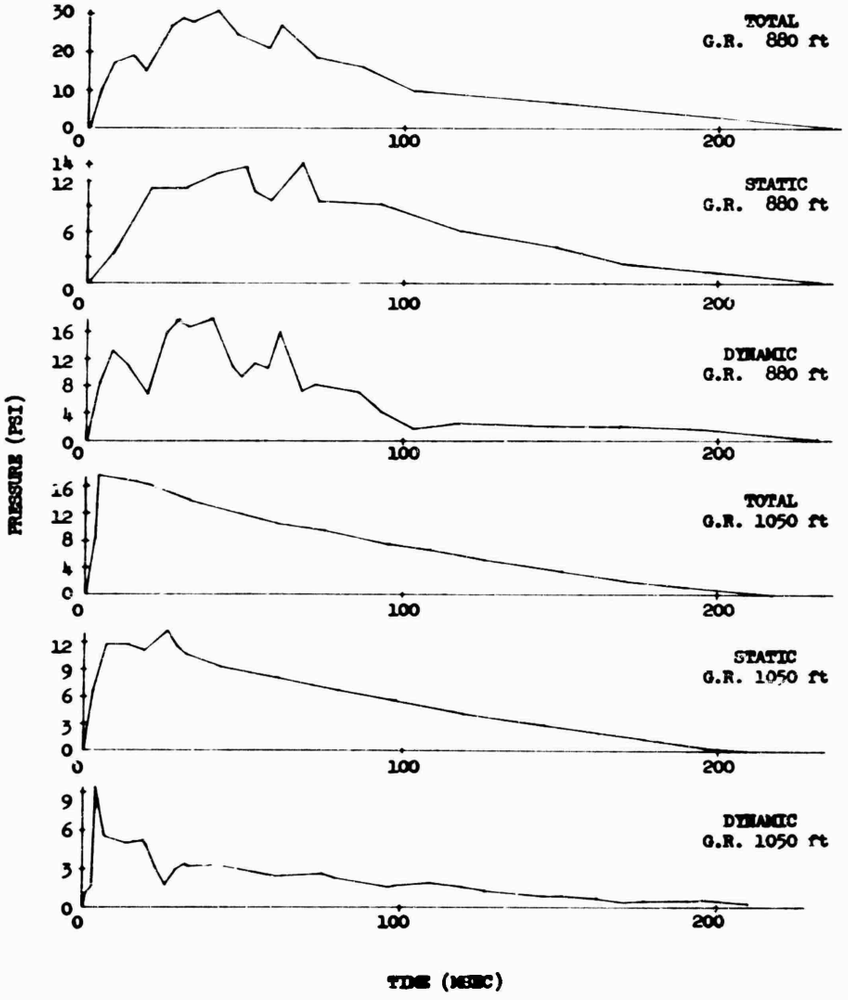

Fig. E.17 Pressure-Time Records from q-Gage for Shot 11

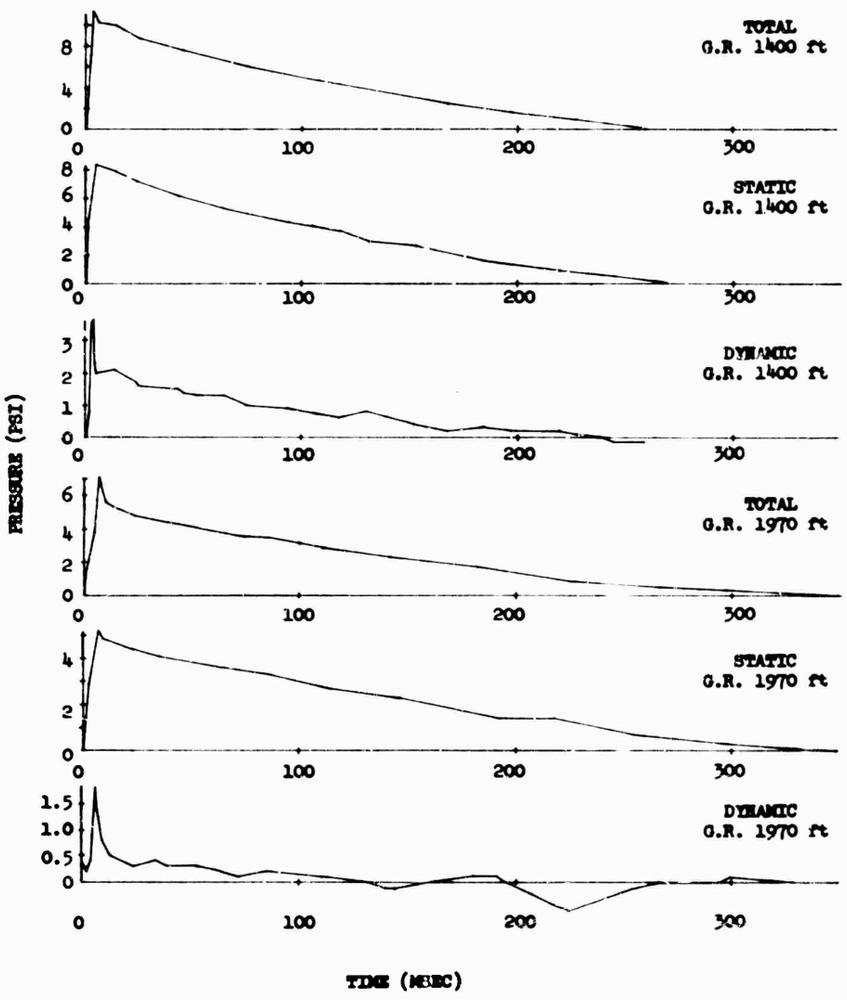

Fig. E.18 Pressure-Time Records from q-Gage for Shot 11

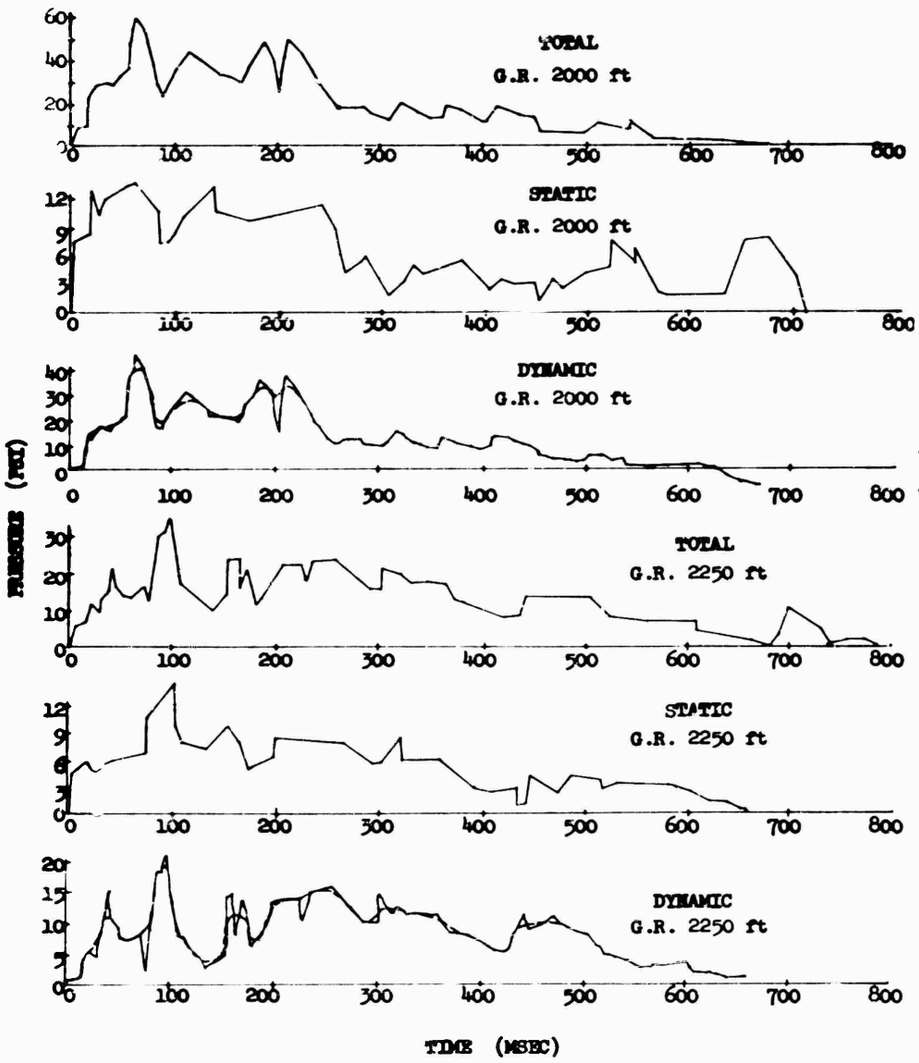

Fig. E.19
Pressure-Time Records from q-Gage for Shot 12, Desert Surface

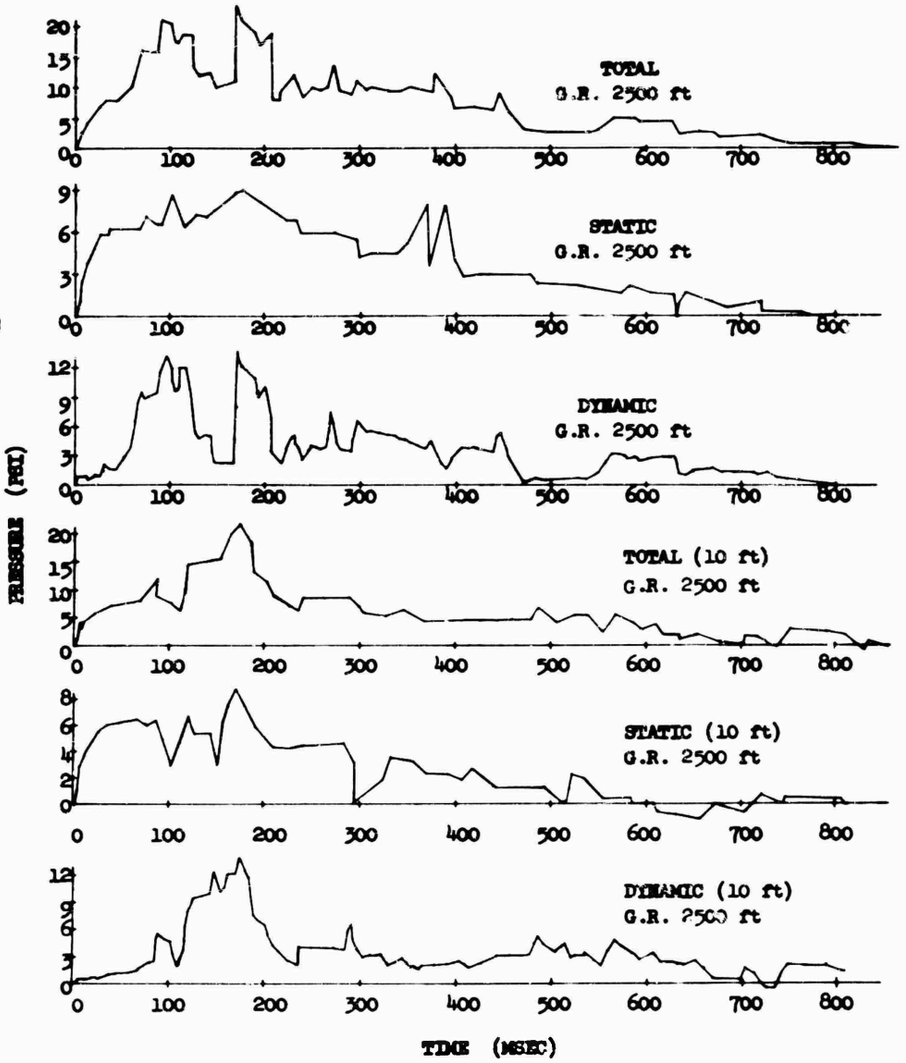

Fig. E.20
Pressure-Time Records from q-Gage for Shot 12, Desert Surface

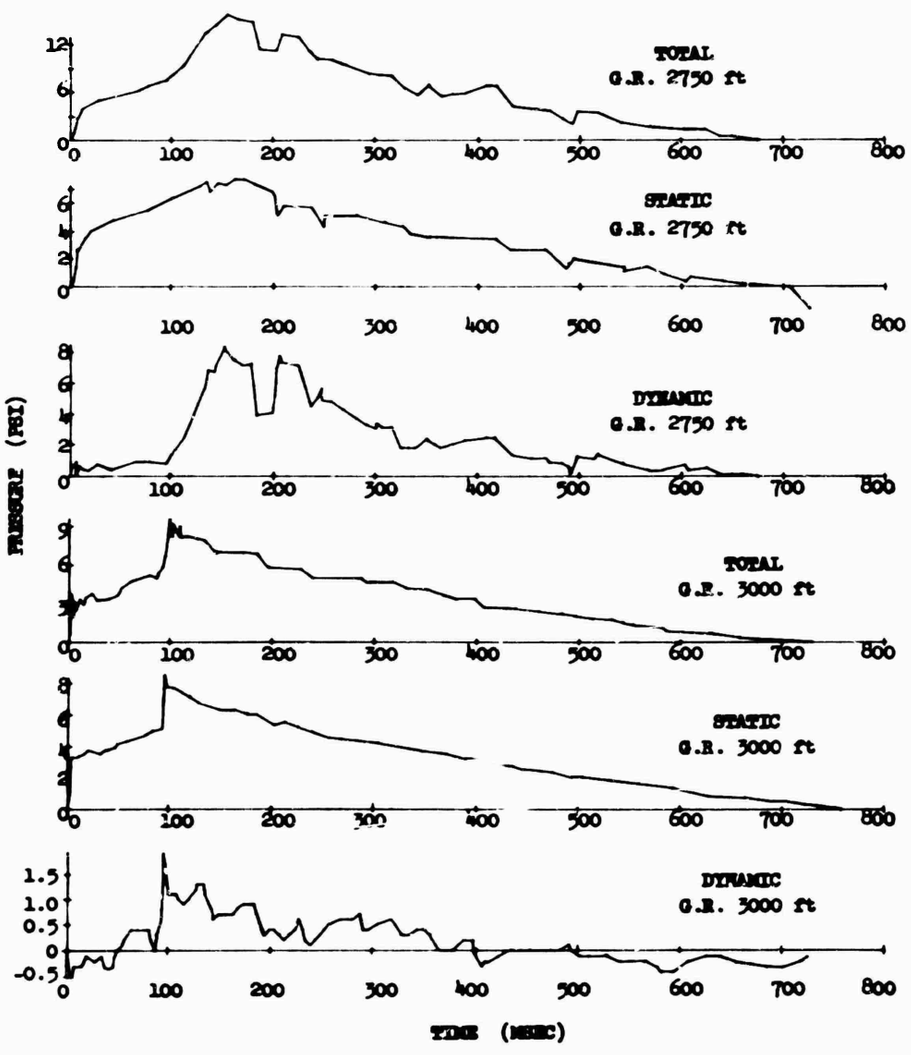

Fig. E.21
Pressure-Time Recorus from q-Gage for Shot 12, Desert Surface

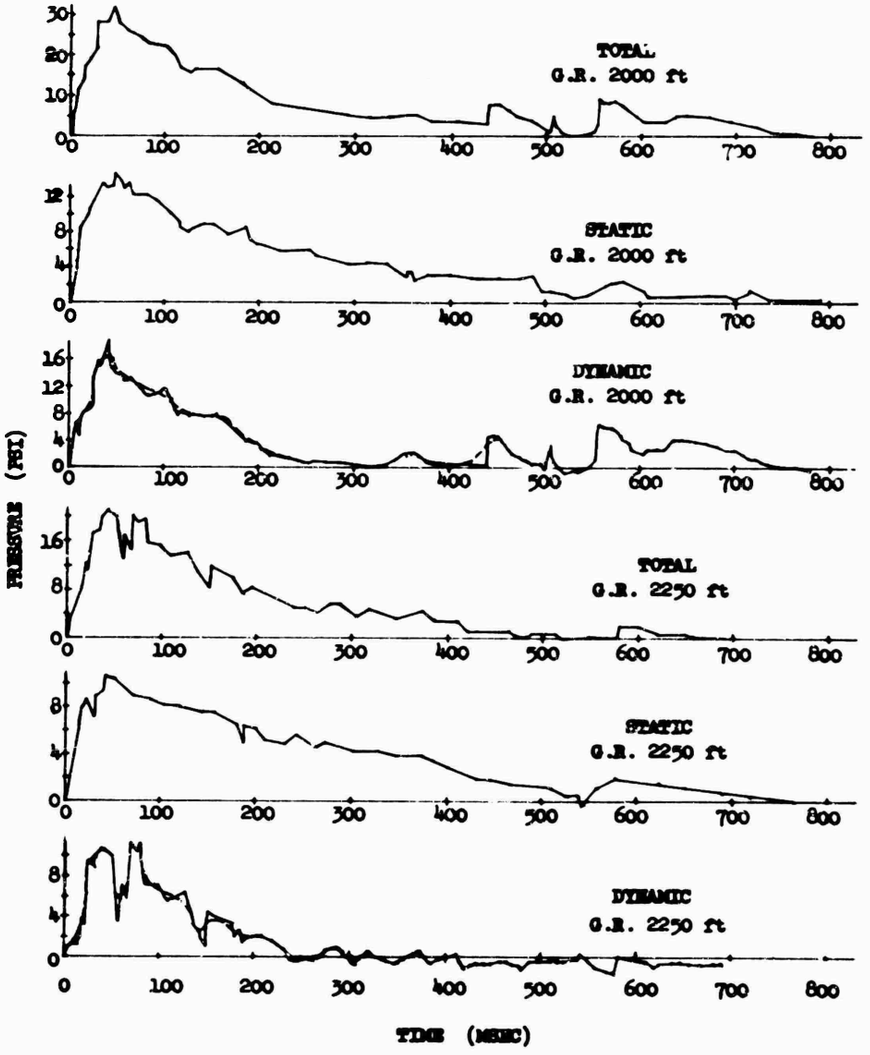

Fig. E 22
Pressure-Time Records from q-Gage for Shot 12, Asphalt Surface

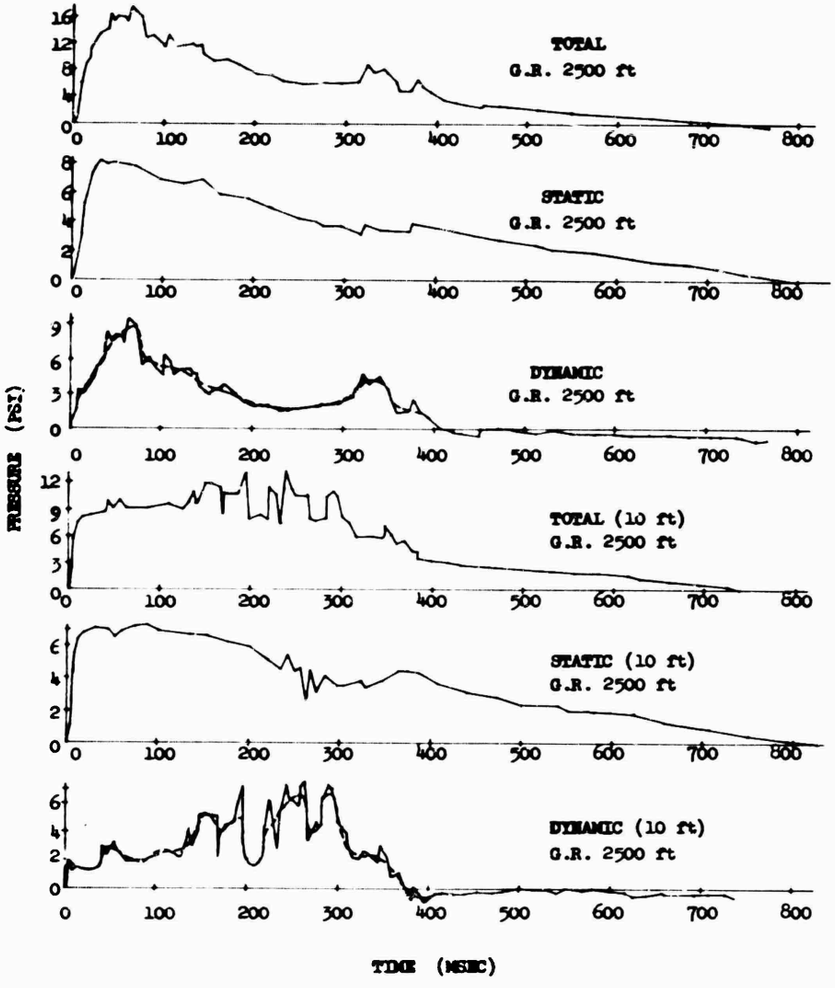

Fig. E.23
Pressure-Time Records from q-Gage for Shot 12, Asphalt Surface

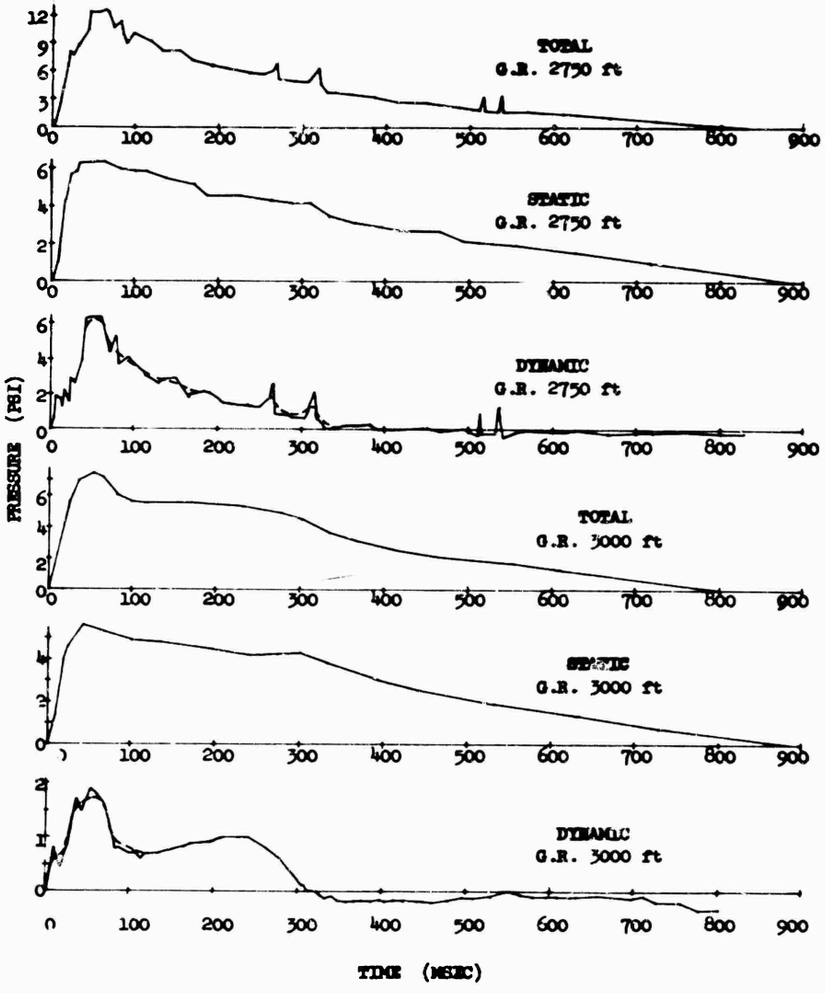

Fig. E.24 Pressure-Time Records from q-Gage for Shot 12, Asphalt Line

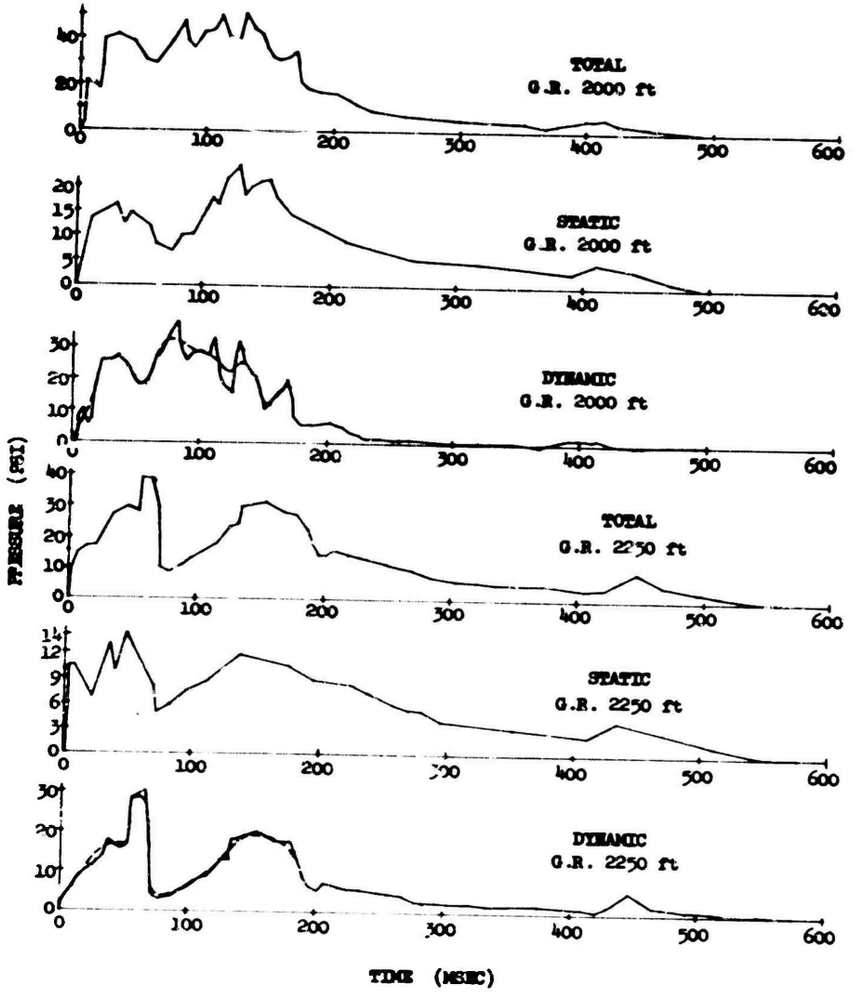

Fig. E.25
Pressure-Time Records from q-Gage for Shot 12, Water Line

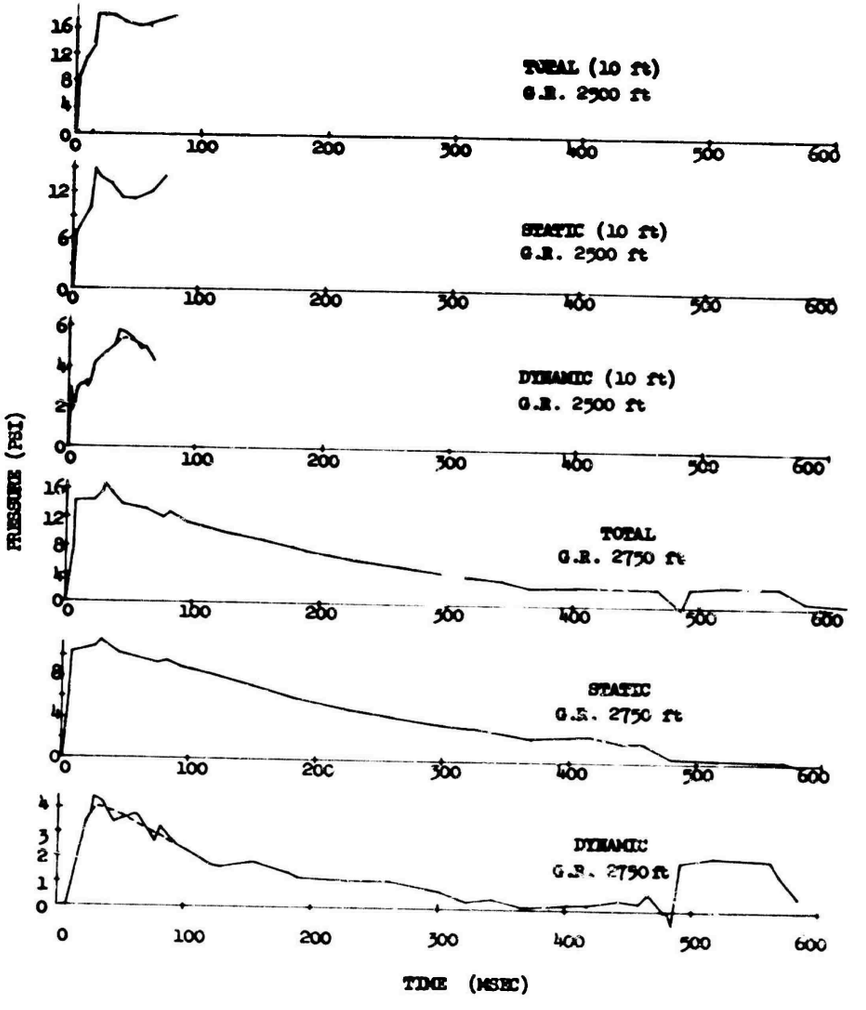

Fig. E.26
Pressure-Time Records from q-Gage for Shot 12, Water Line

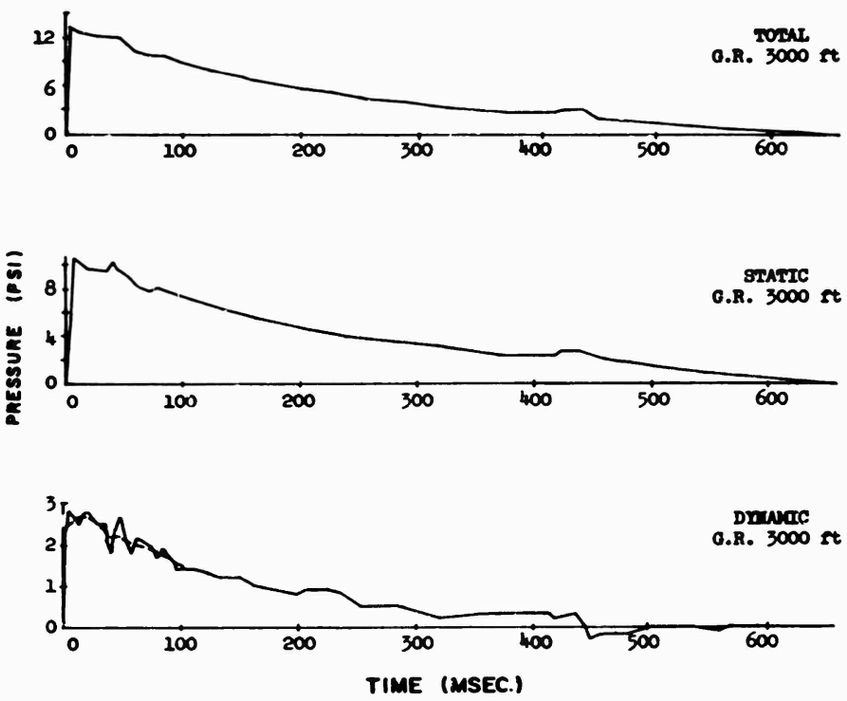

Fig. E.27
Pressure-Time Records from q-Gage for Shot 12, Water Line

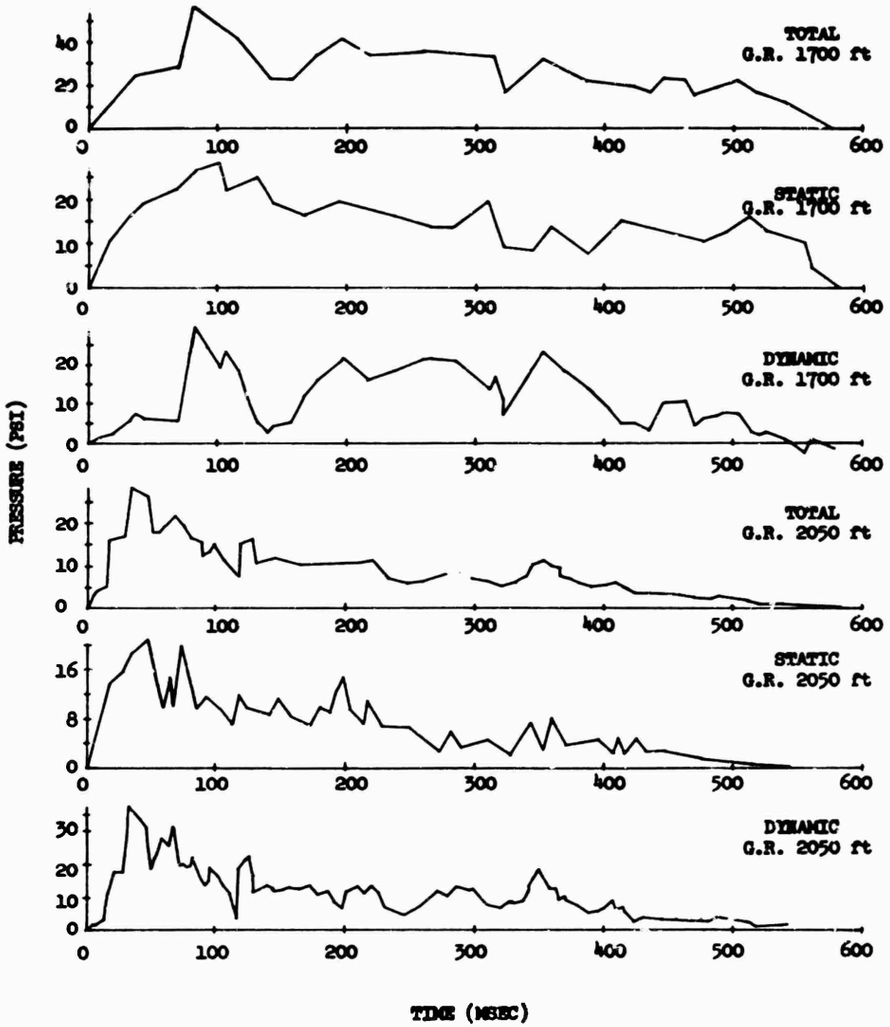

Fig. E.28 Pressure-Time Records from q-Gage for Shot 13

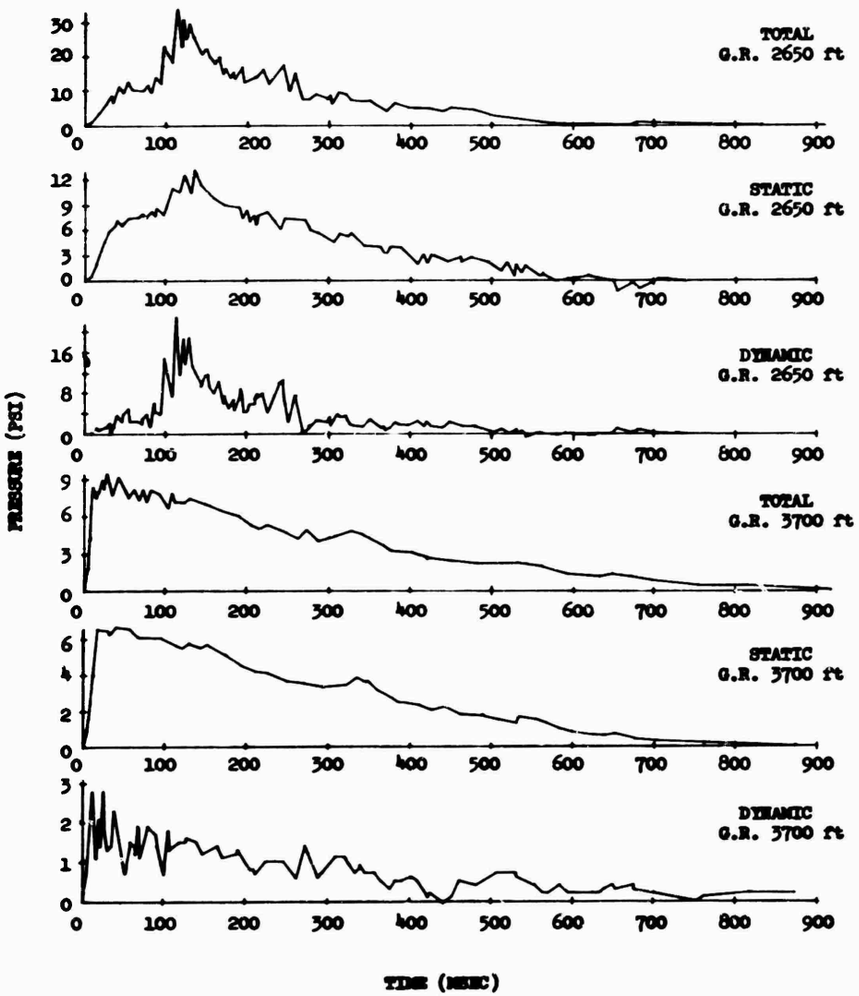

Fig. E.29 Pressure-Time Records from q-Gage for Shot 13

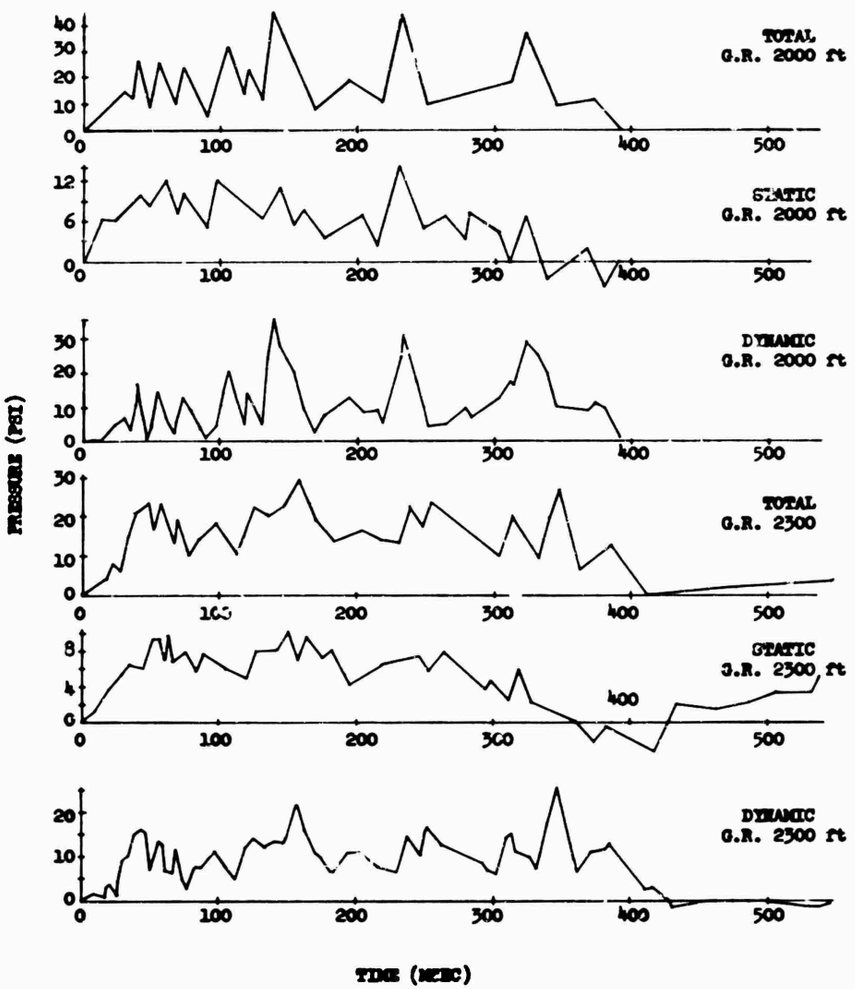

Fig. E.30 Pressure-Time Records from q-Gage for Shot 14, Desert Surface

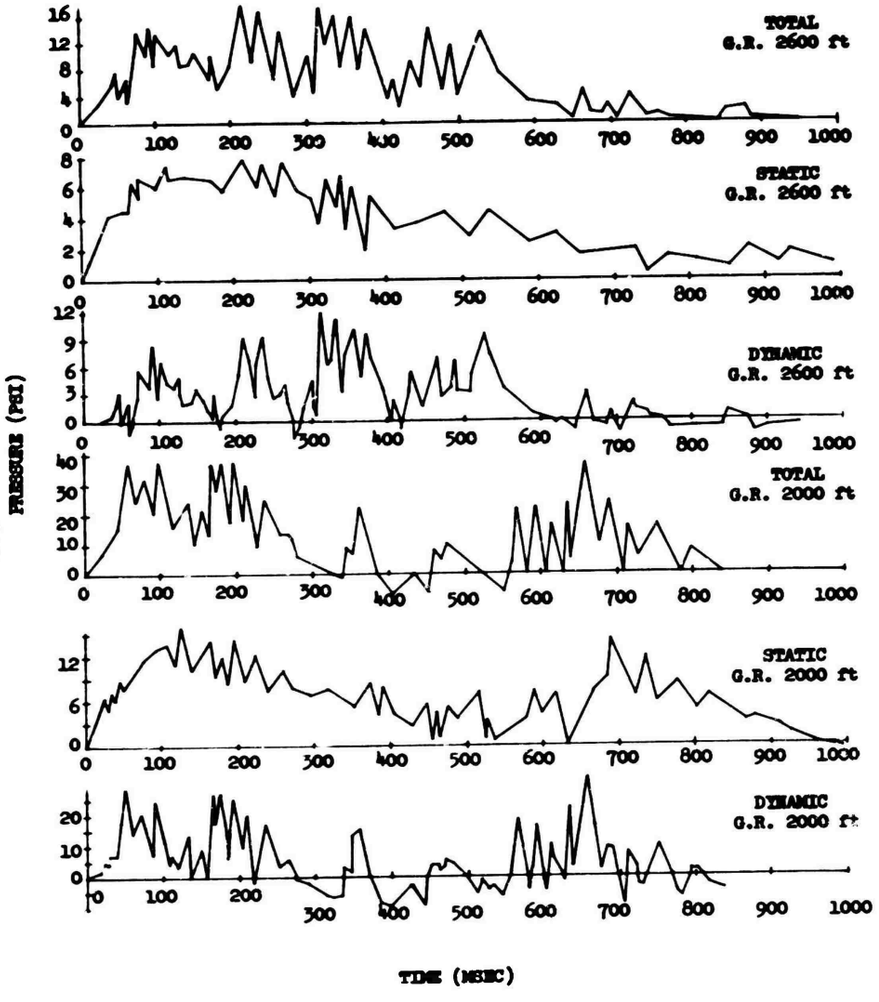

Fig. E.31 Pressure-Time Records from q-Gage for Shot 14, Desert Surface (GR 2600 ft) and Asphalt Surface (GR 2000 ft)

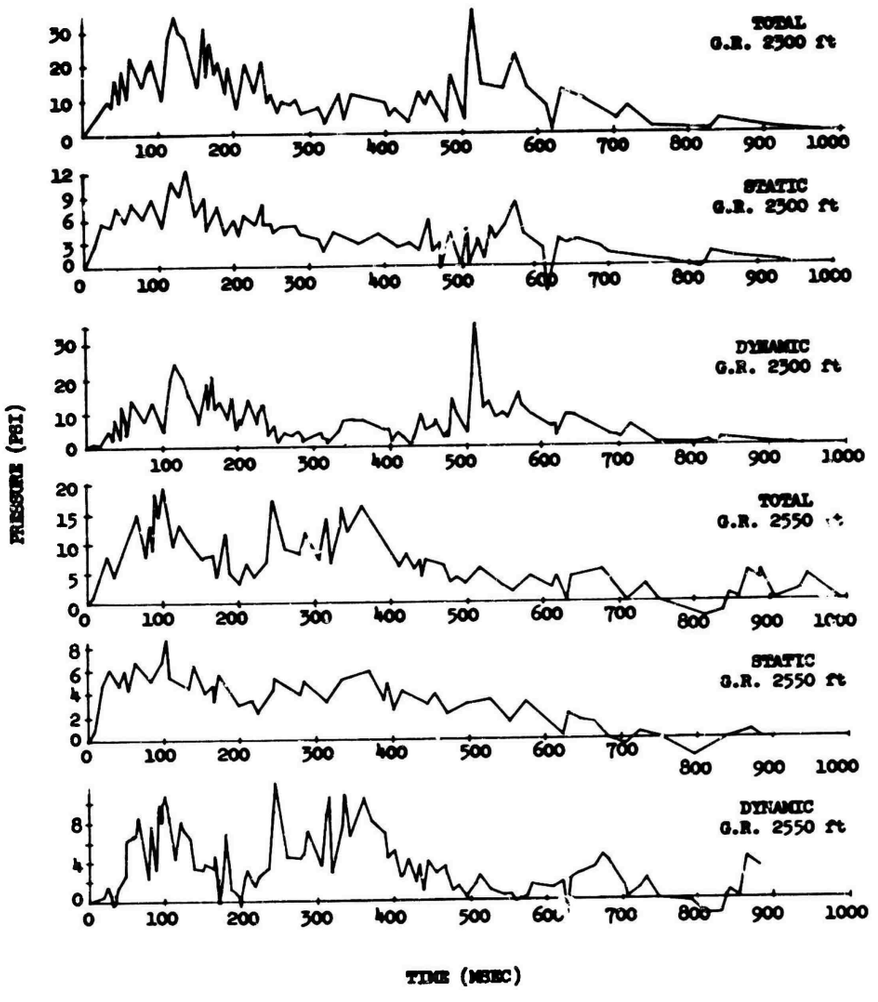

Fig. E.32 Pressure-Time Records from q-Gages for Shot 14, Asphalt Surface

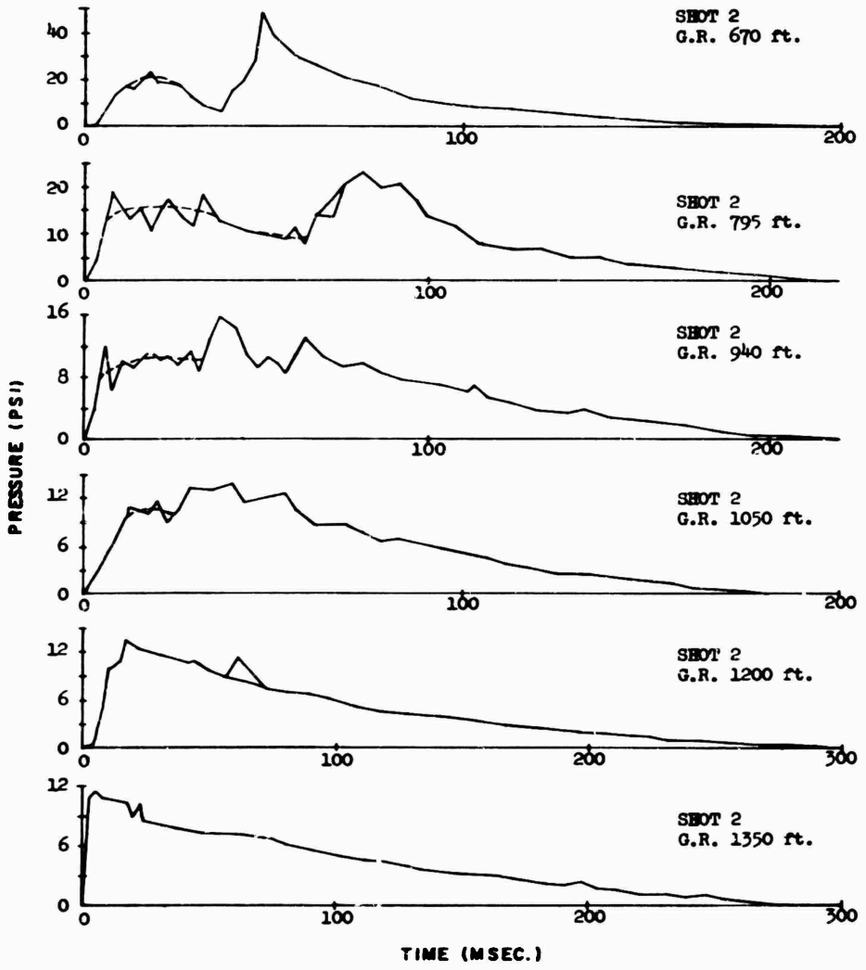

Fig. E.33 Pressure-Time Records from p_t-gage for Shot 2

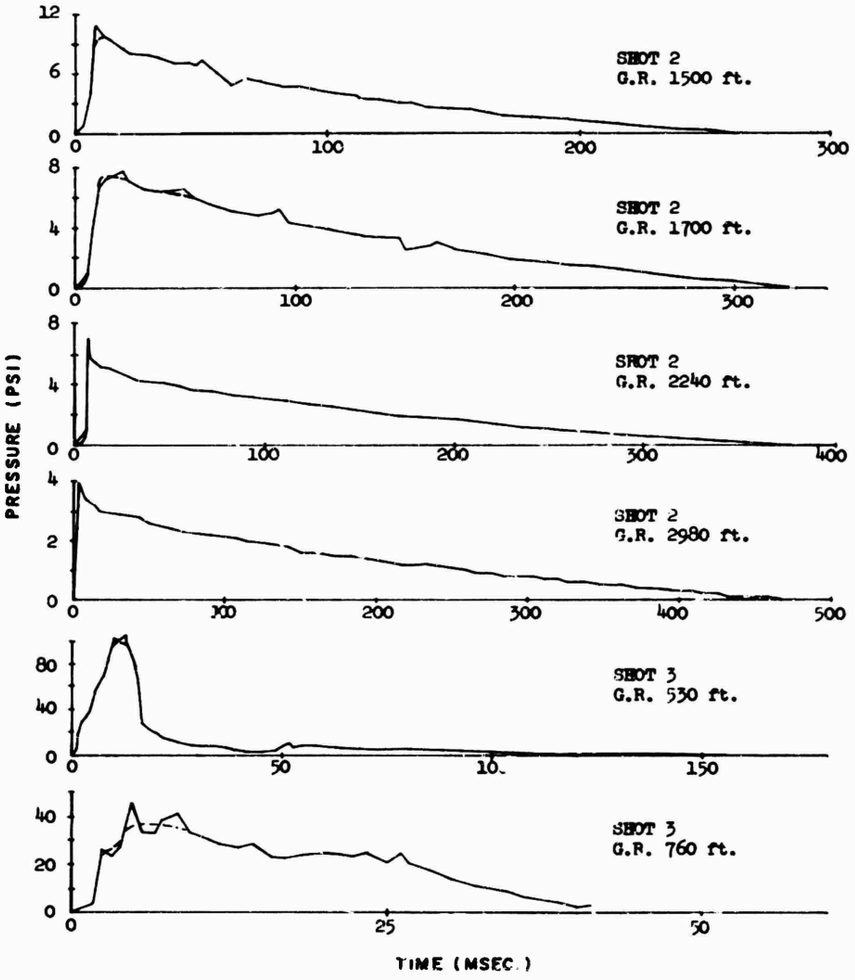

Fig. E.34 Pressure-Time Records from p_t-gage for Shot 2 and Shot 3

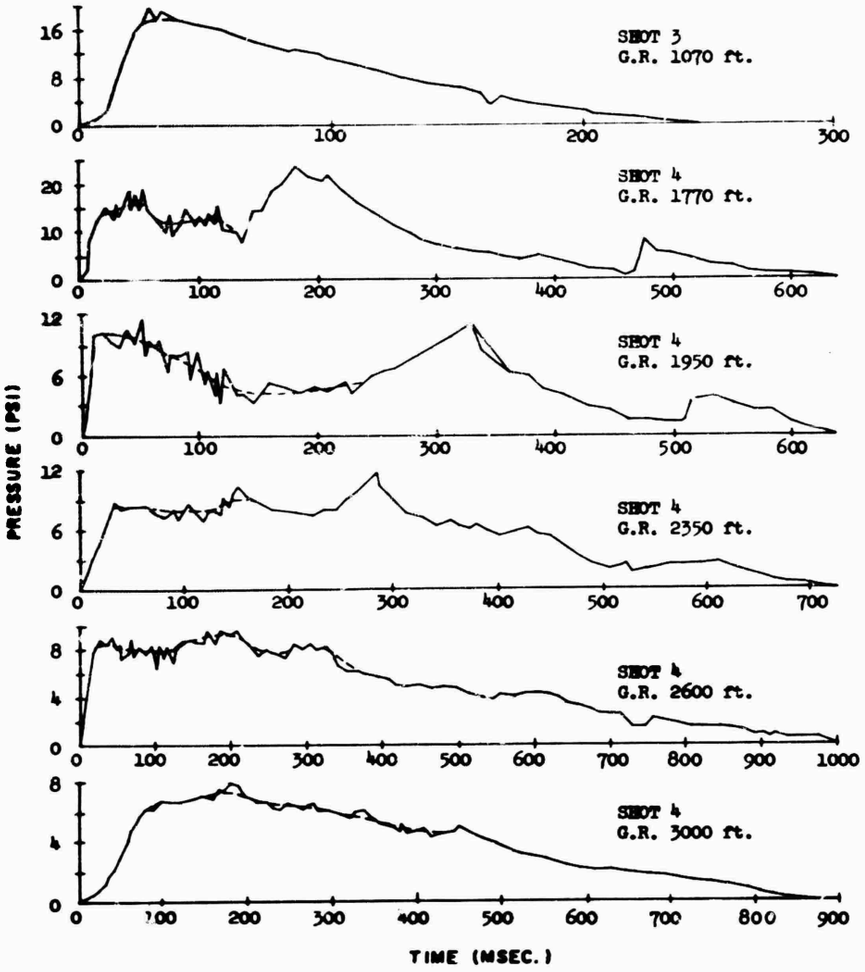

Fig. E.35 Pressure-Time Records from p_t-gage for Shot 3 and Shot 4

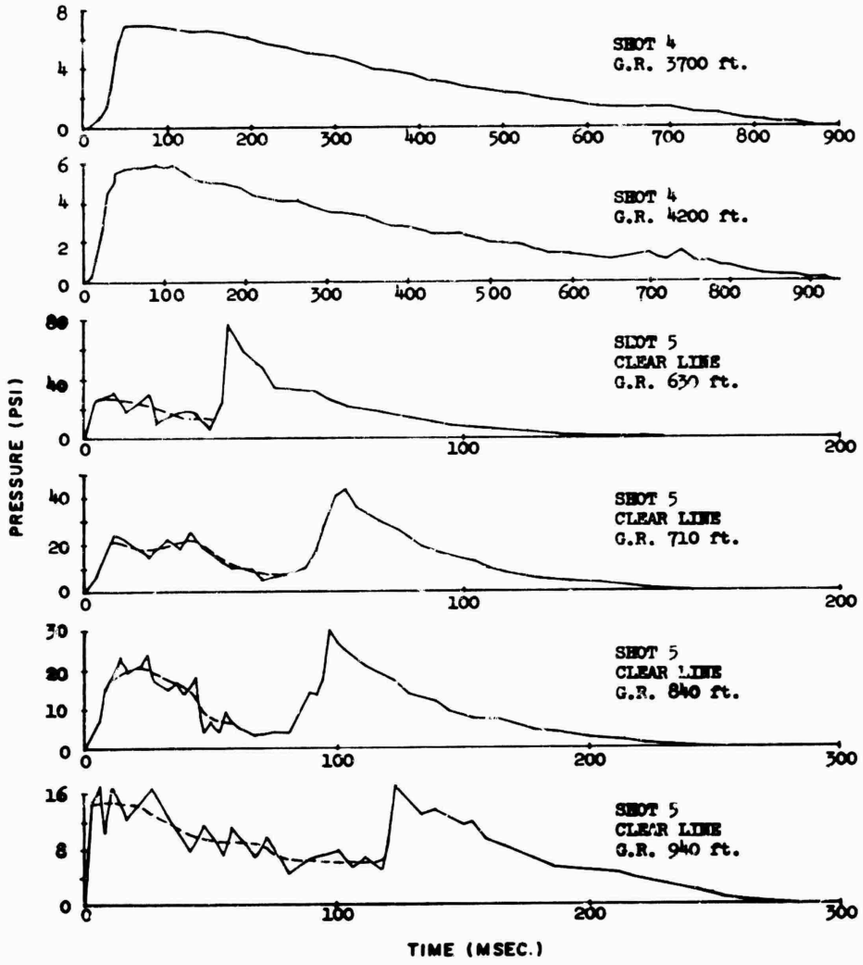

Fig. E.36 Pressure-Time Records from p_t-Gage for Shot 4 and Shot 5 (Clear Line)

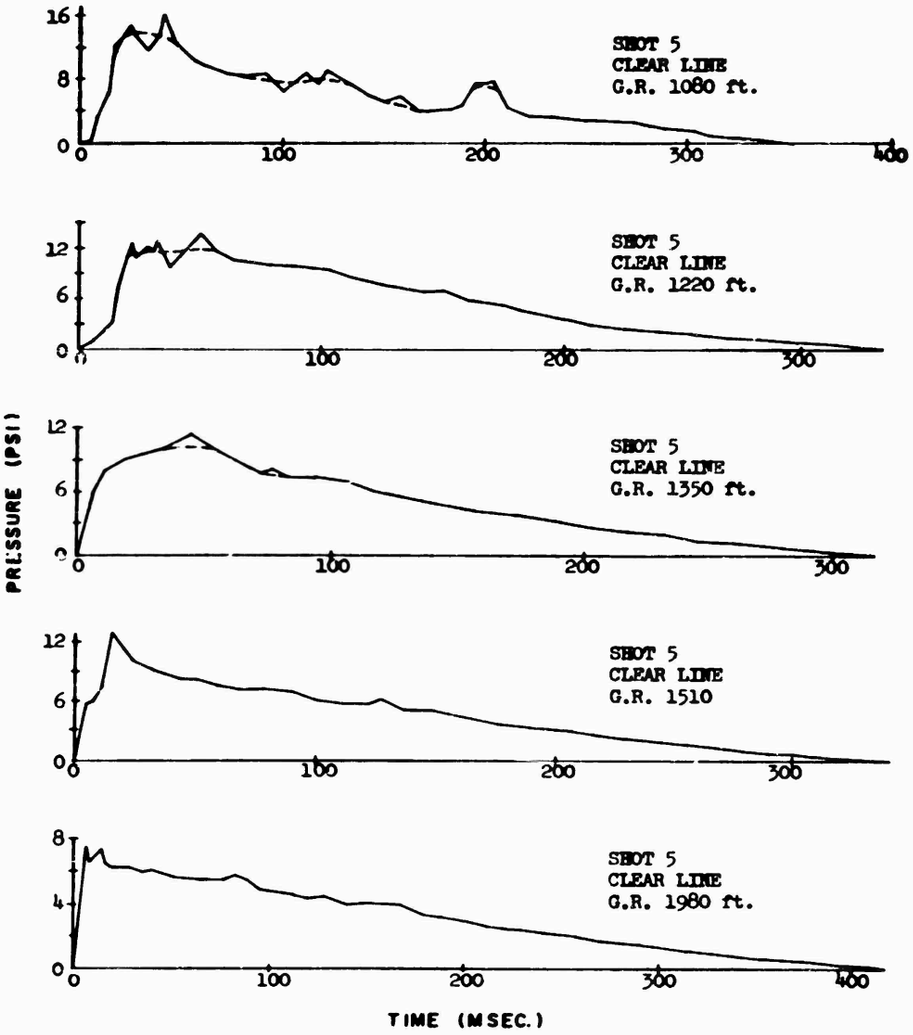

Fig. E.37 Pressure-Time Records from p_t-gage for Shot 5 (Clear Line)

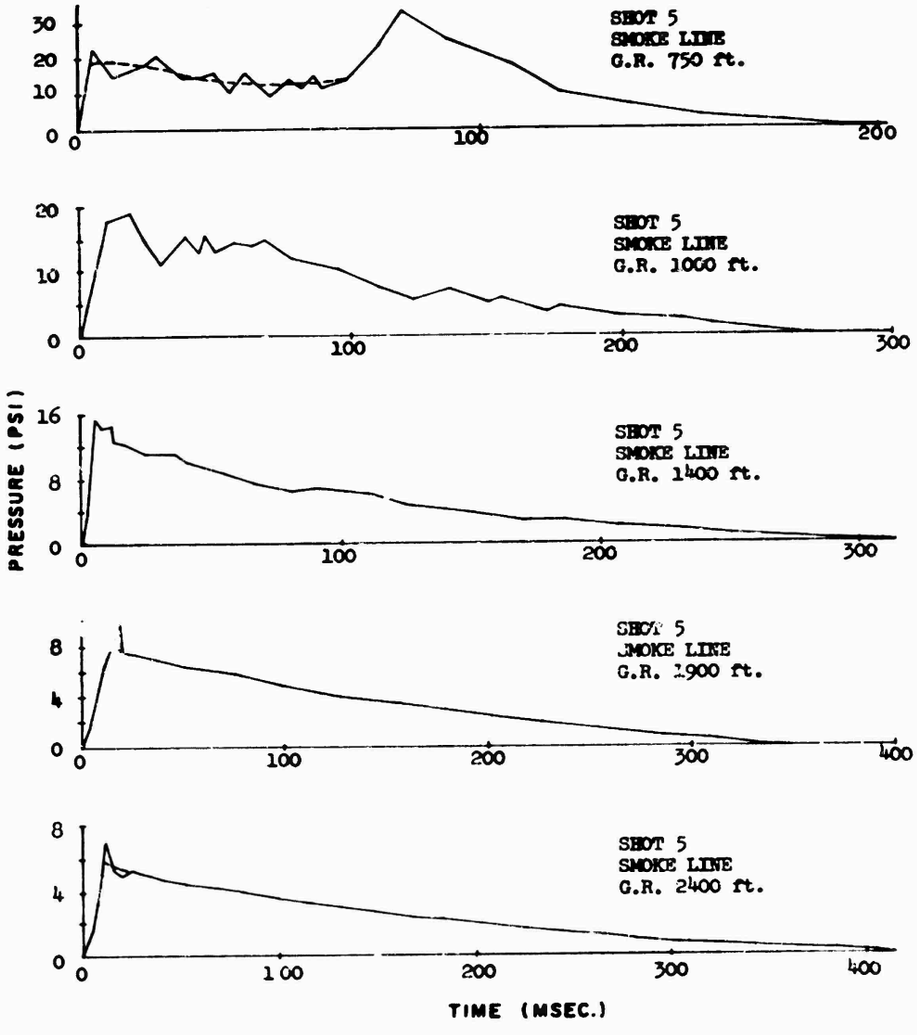

Fig. E.38 Pressure-Time Records from p_t-Gage for Shot 5 (Smoke Line)

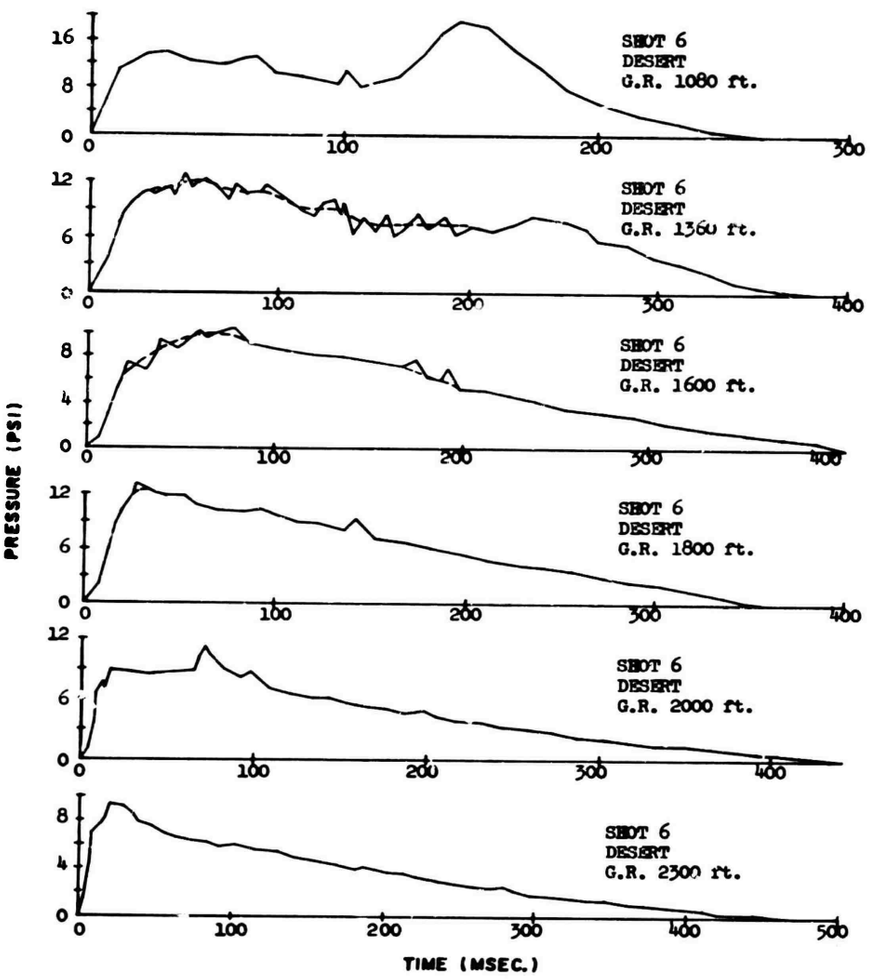

Fig. E.39 Pressure-Time Records from p_t-Gage for Shot 6 (Desert Line)

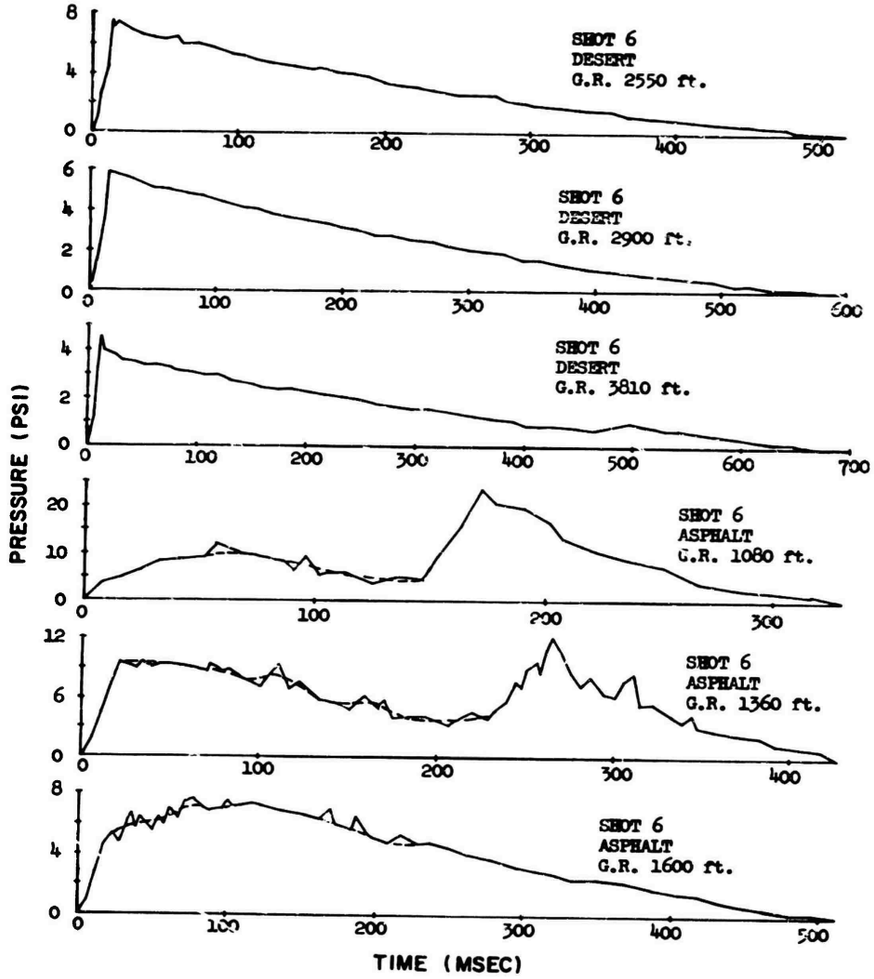

Fig. E.40 Pressure-Time Records from p_t-Gage for Shot 6 (Desert and Asphalt Line)

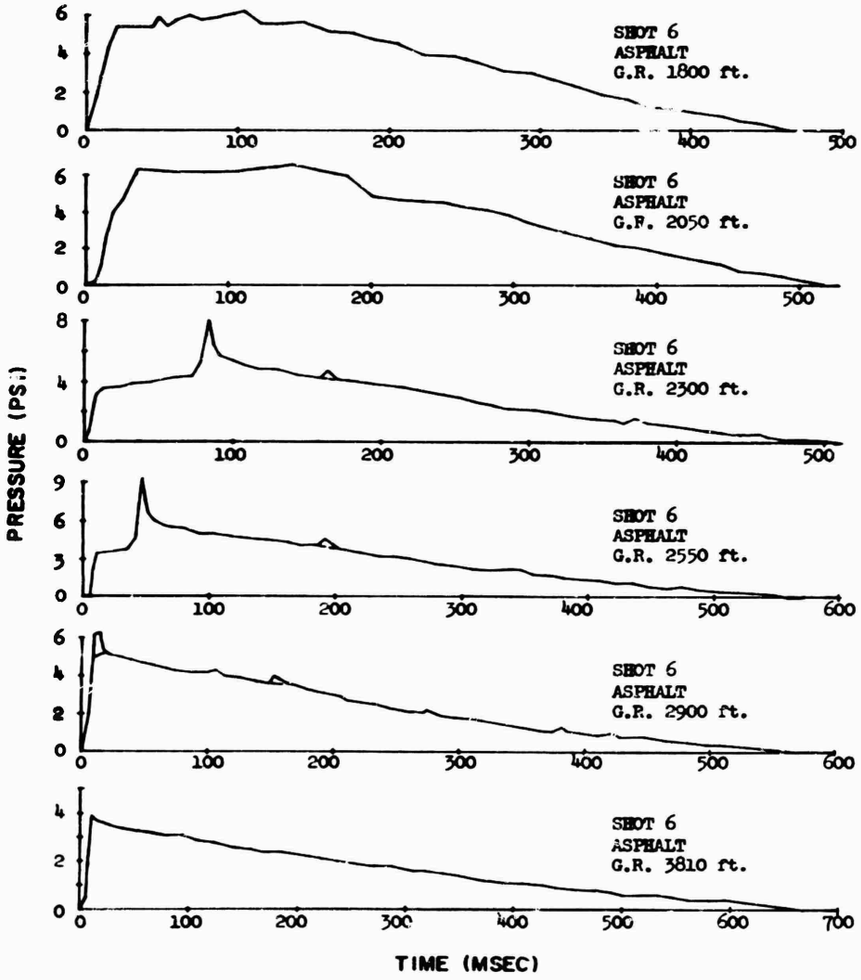

Fig. E.41 Pressure-Time Records from p_t-Gage for Shot 6 (Asphalt Line)

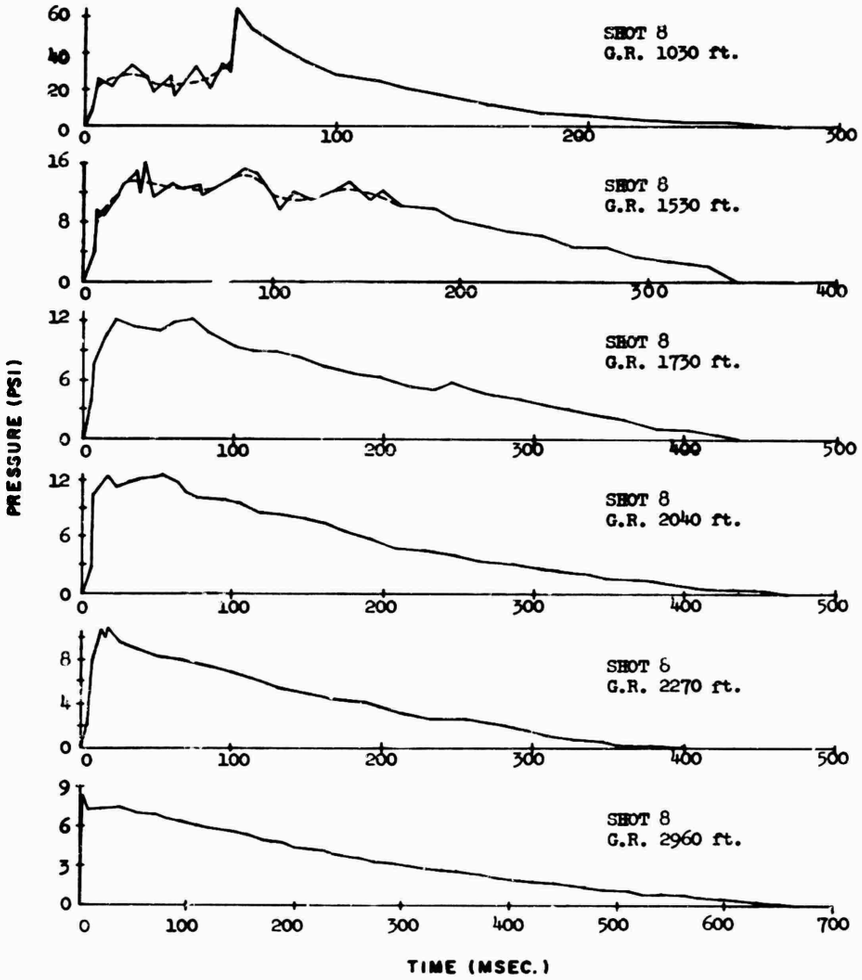

Fig. E.42 Pressure-Time Records from p_t-Gage for Shot 8

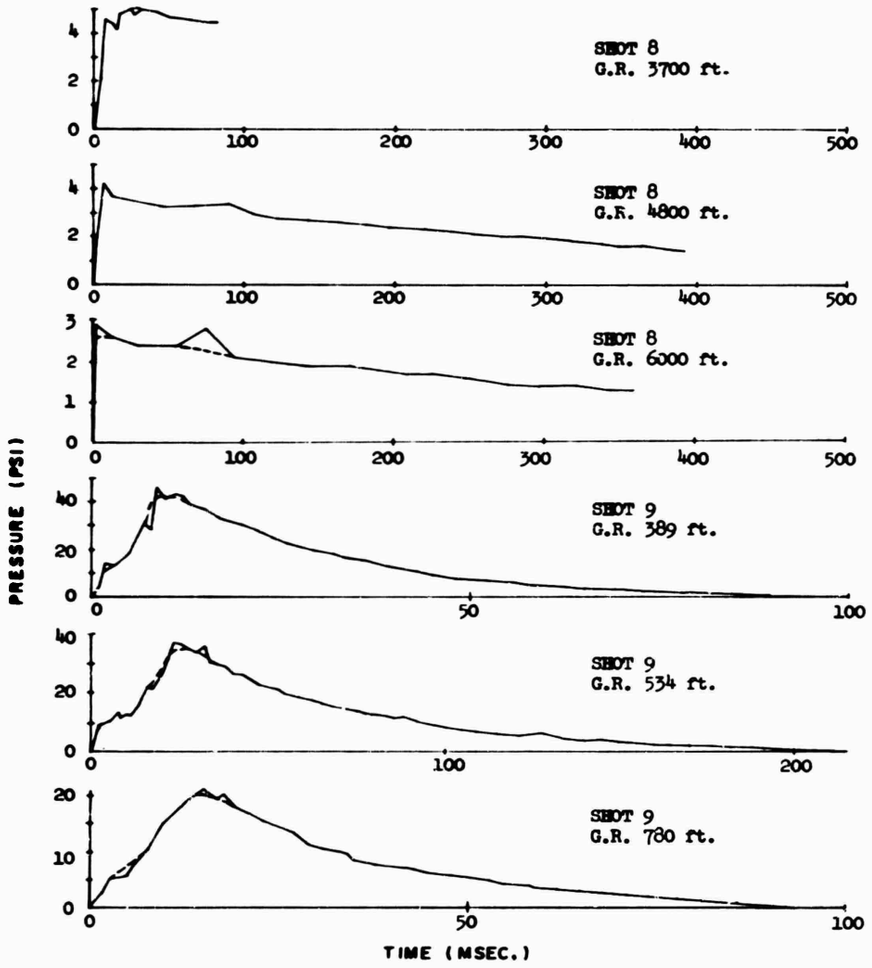

Fig. E.43 Pressure-Time Records from p_t-Gage for Shot 8 and Shot 9

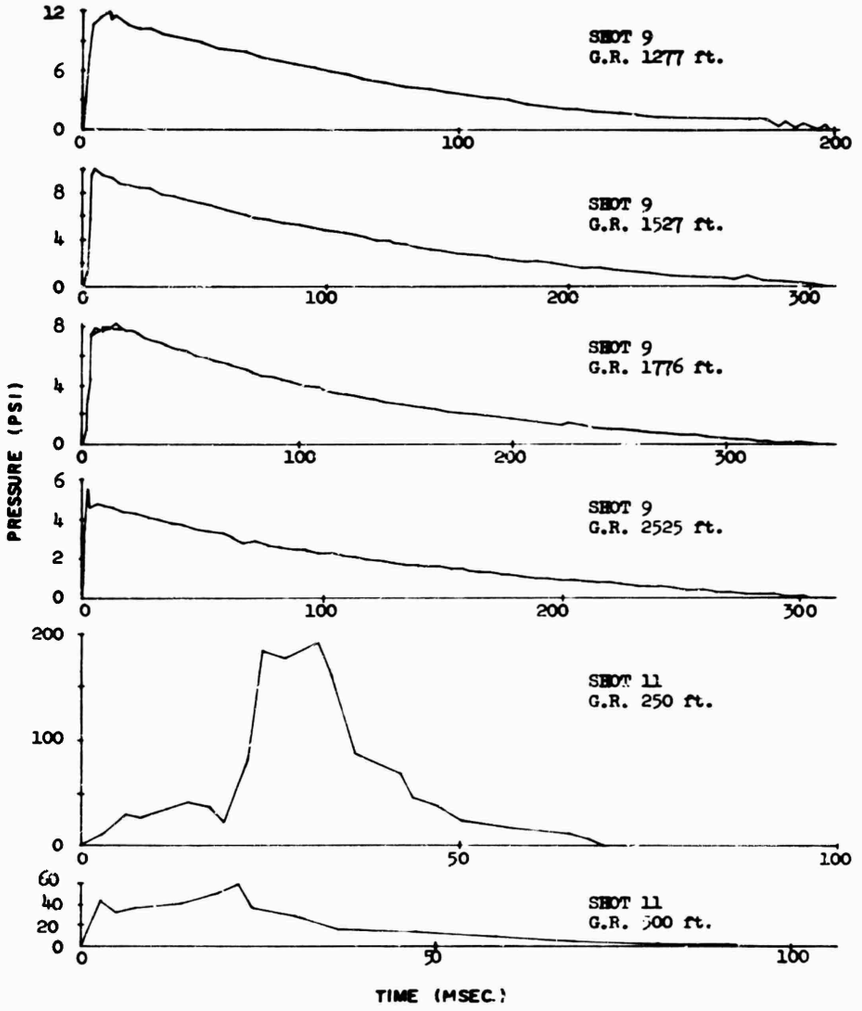

Fig. E.44 Pressure-Time Records from p_t-Gage for Shot 9 and Shot 11

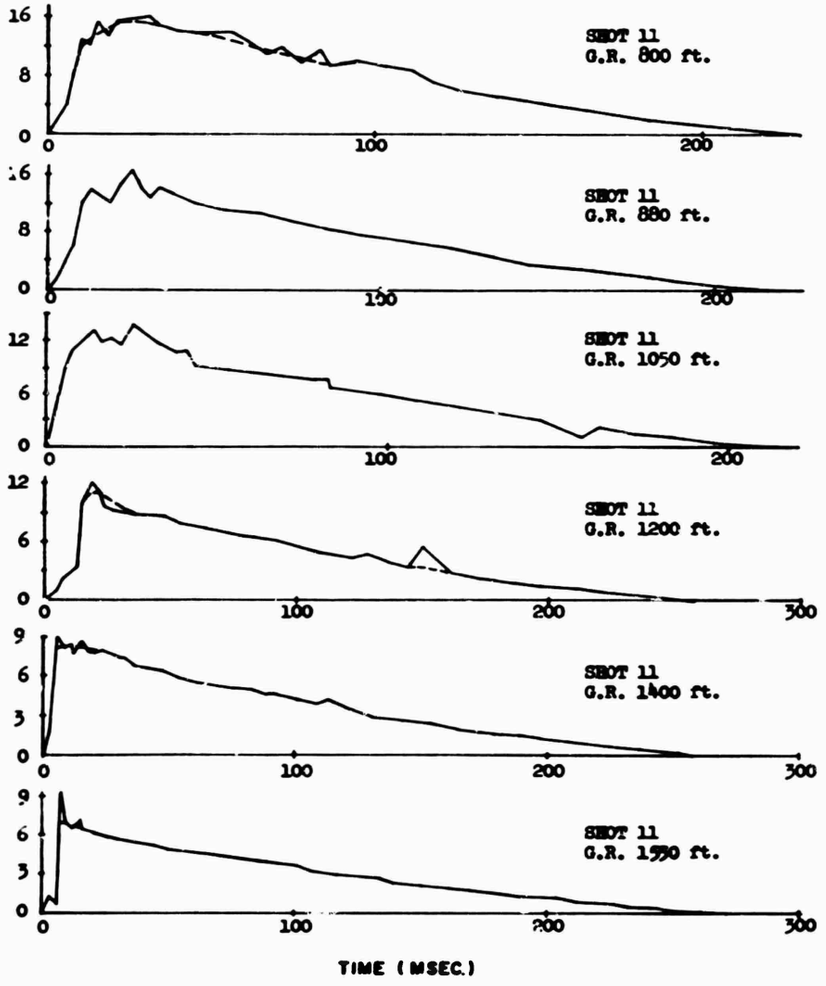

Fig. E.45 Pressure-Time Records from p_t-Gage for Shot 11

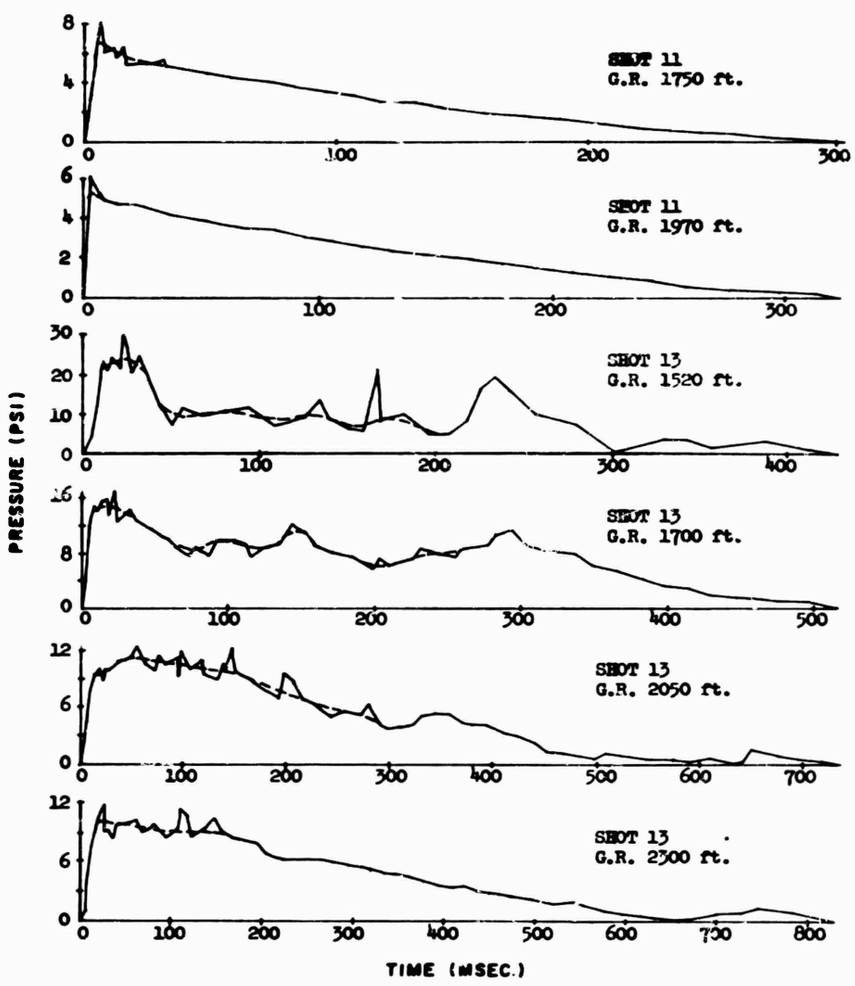

Fig. E.46 Pressure-Time Records from p_t-Gage for Shot 11 and Shot 13

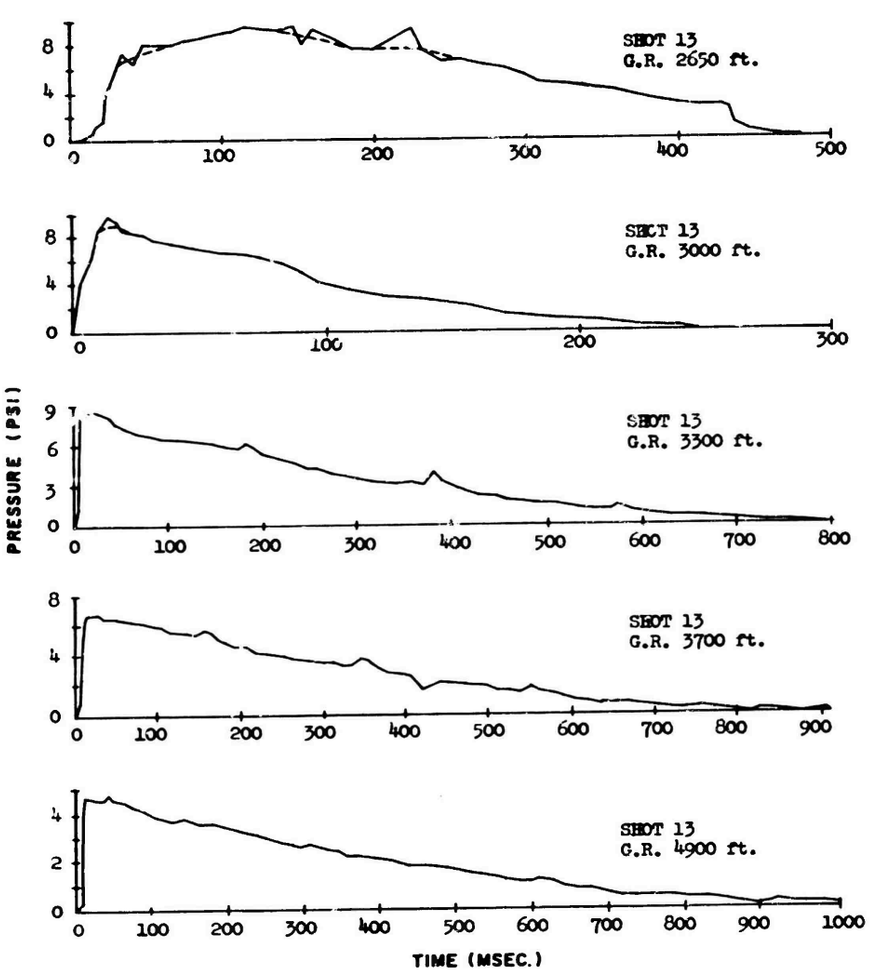

Fig. E.47 Pressure-Time Records from p_t-Gage for Shot 13

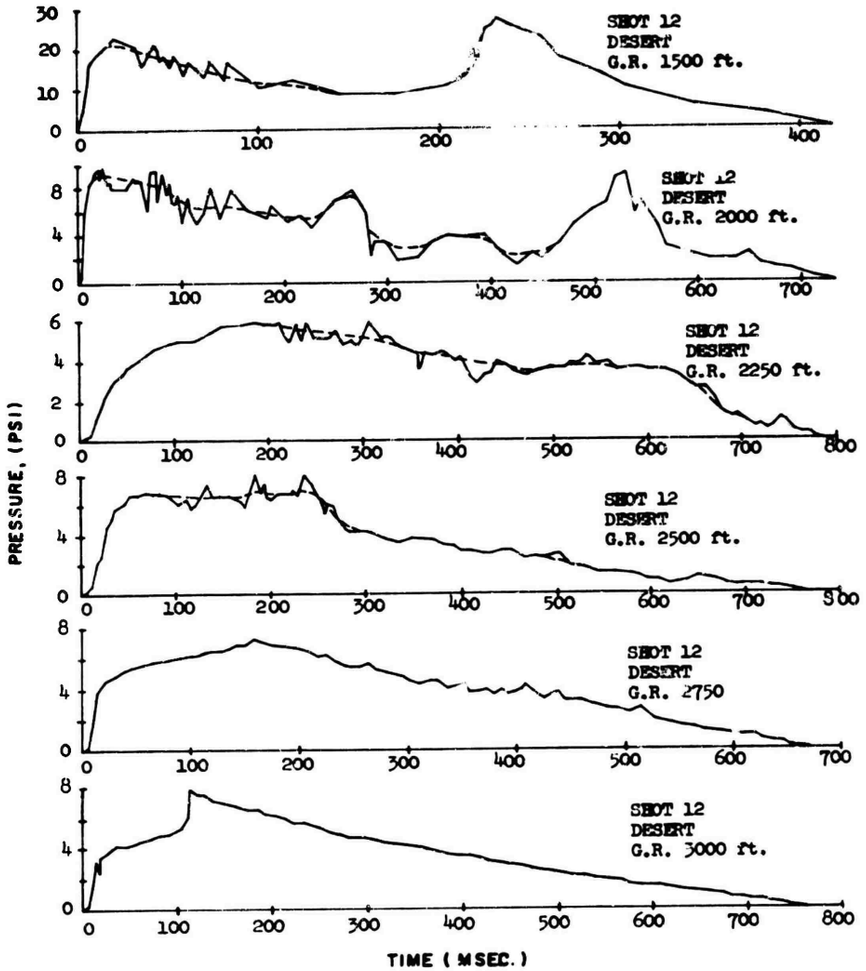

Fig. E.48 Pressure-Time Records from p_t-Gage for Shot 12 (Desert Line)

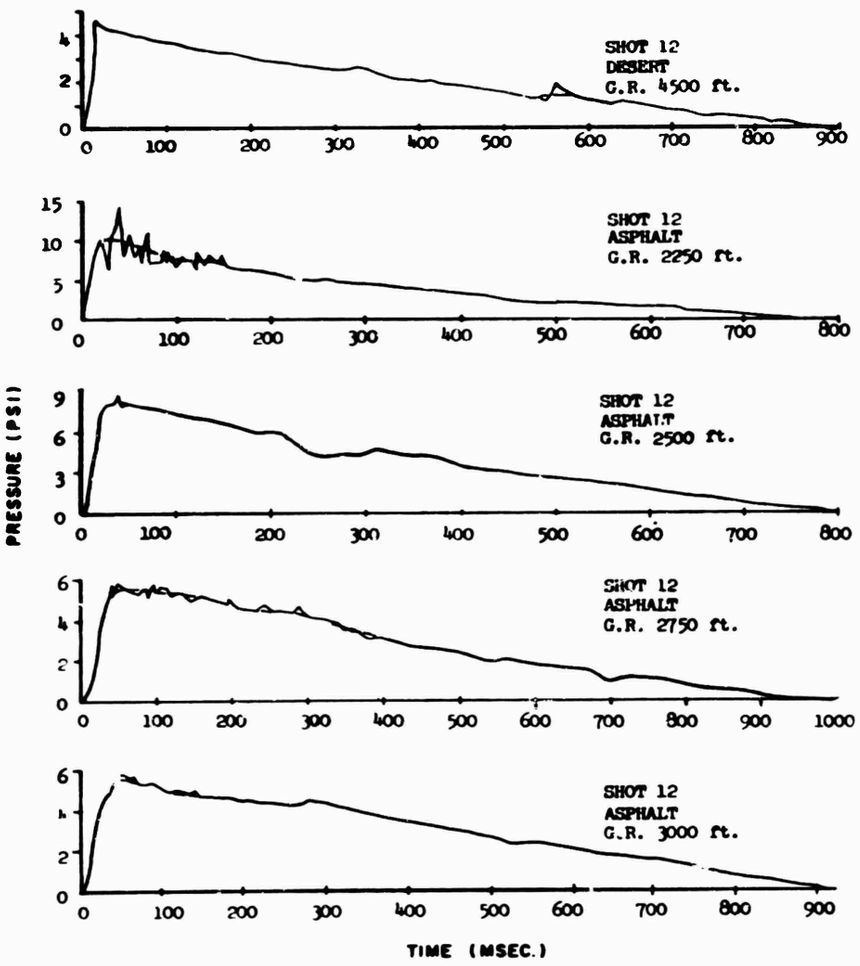

Fig. E.49 Pressure-Time Records from p_t-Gage for Shot 12, (Desert and Asphalt Line)

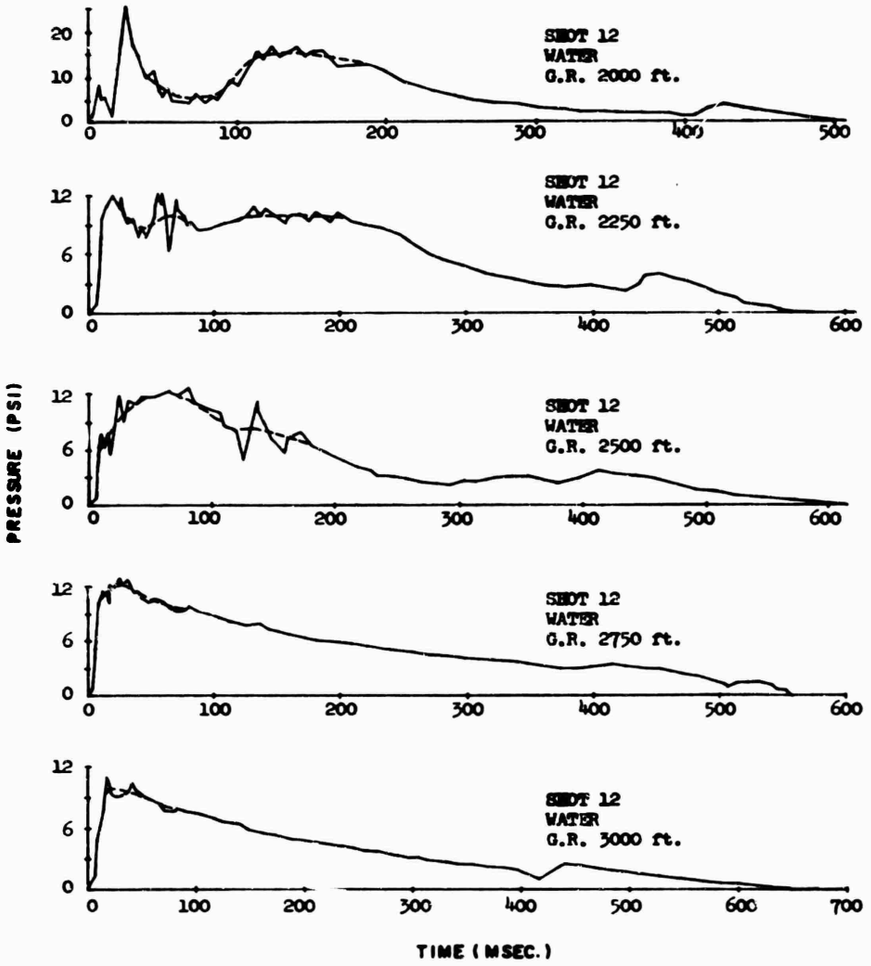

Fig. E.50 Pressure-Time Records from p_t-Gage for Shot 12 (Water Line)

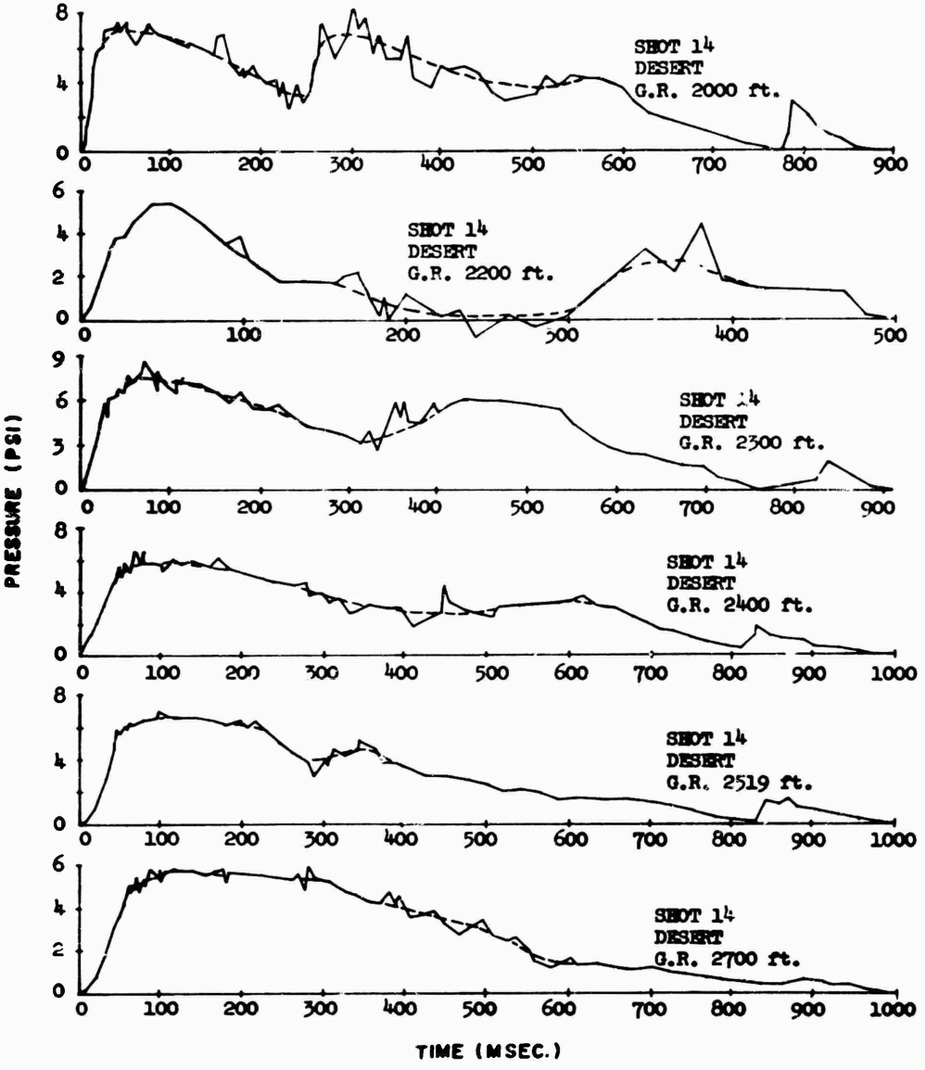

Fig. E.51 Pressure-Time Records from p_t-Gage for Shot 14 (Desert Line)

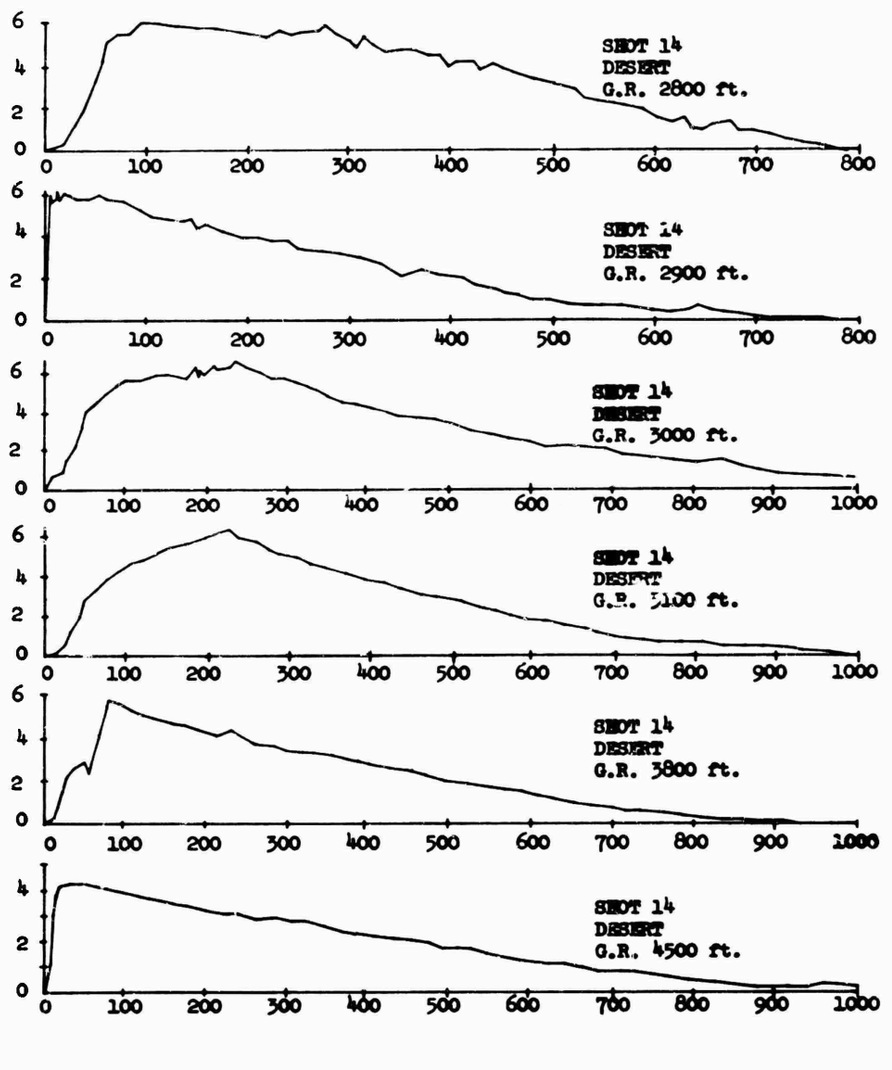

Fig. E.52 Pressure-Time Records from p_t-Gage for Shot 14 (Desert Line)

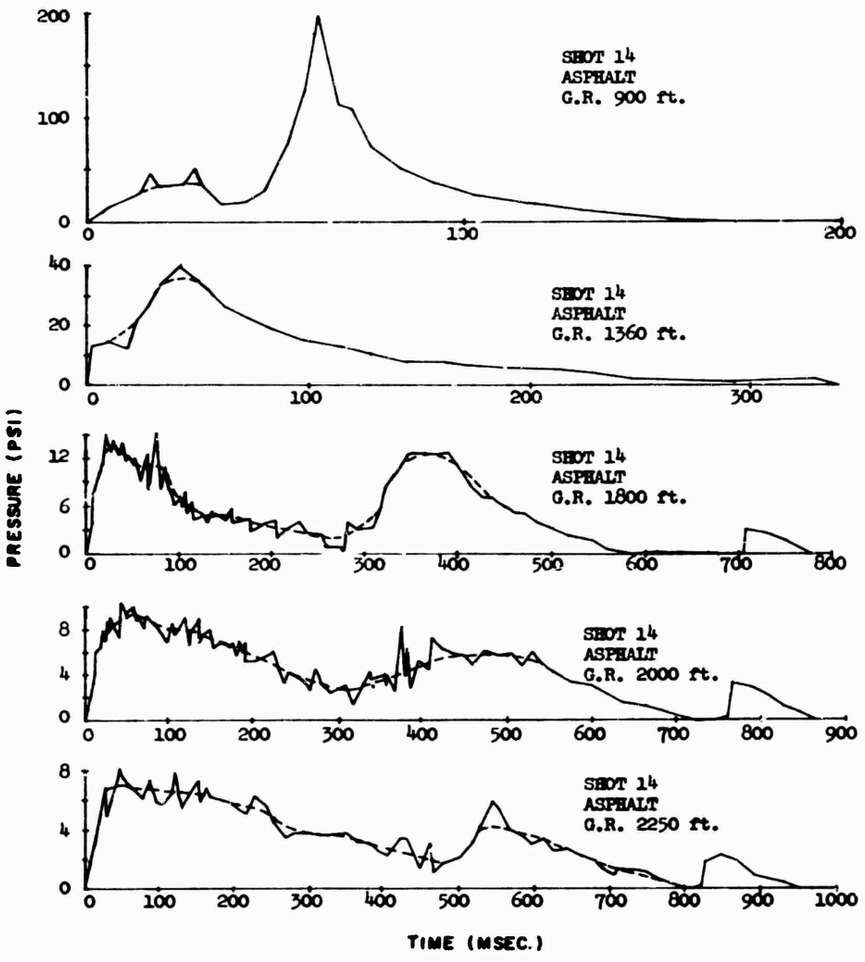

Fig. E.53 Pressure-Time Records from p_t-Gage for Shot 14 (Asphalt Line)

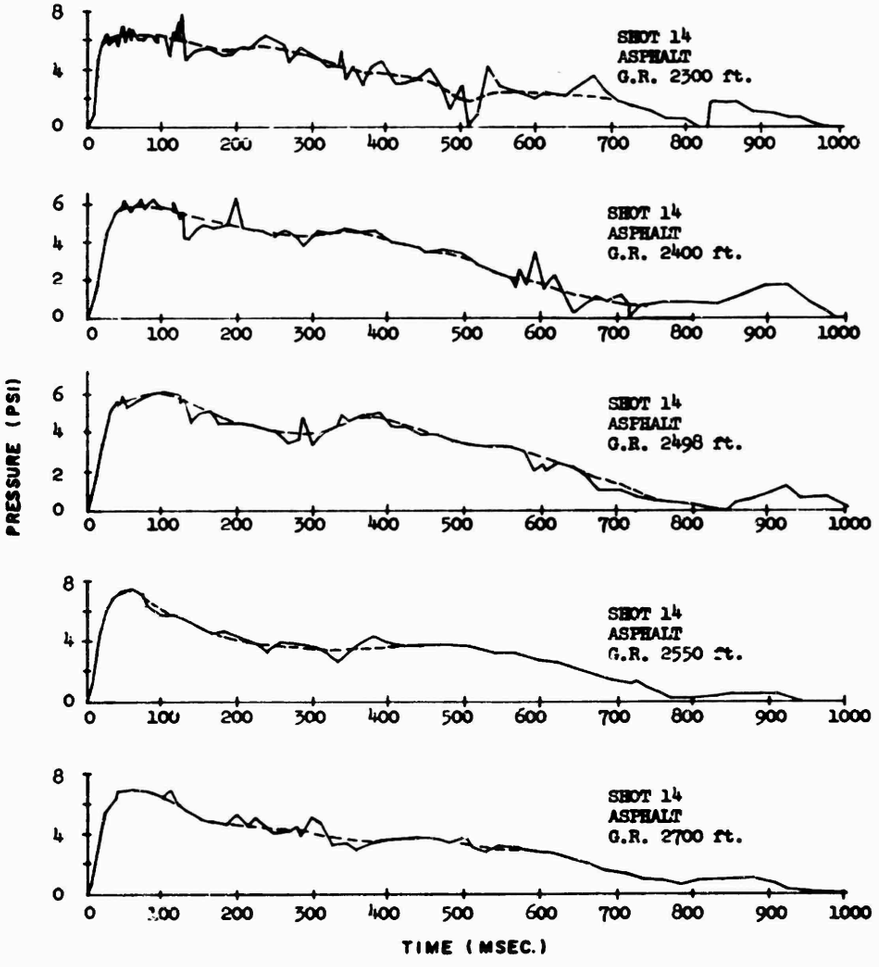

Fig. E.54 Pressure-Time Records from p_t-Gage for Shot 14 (Asphalt Line)

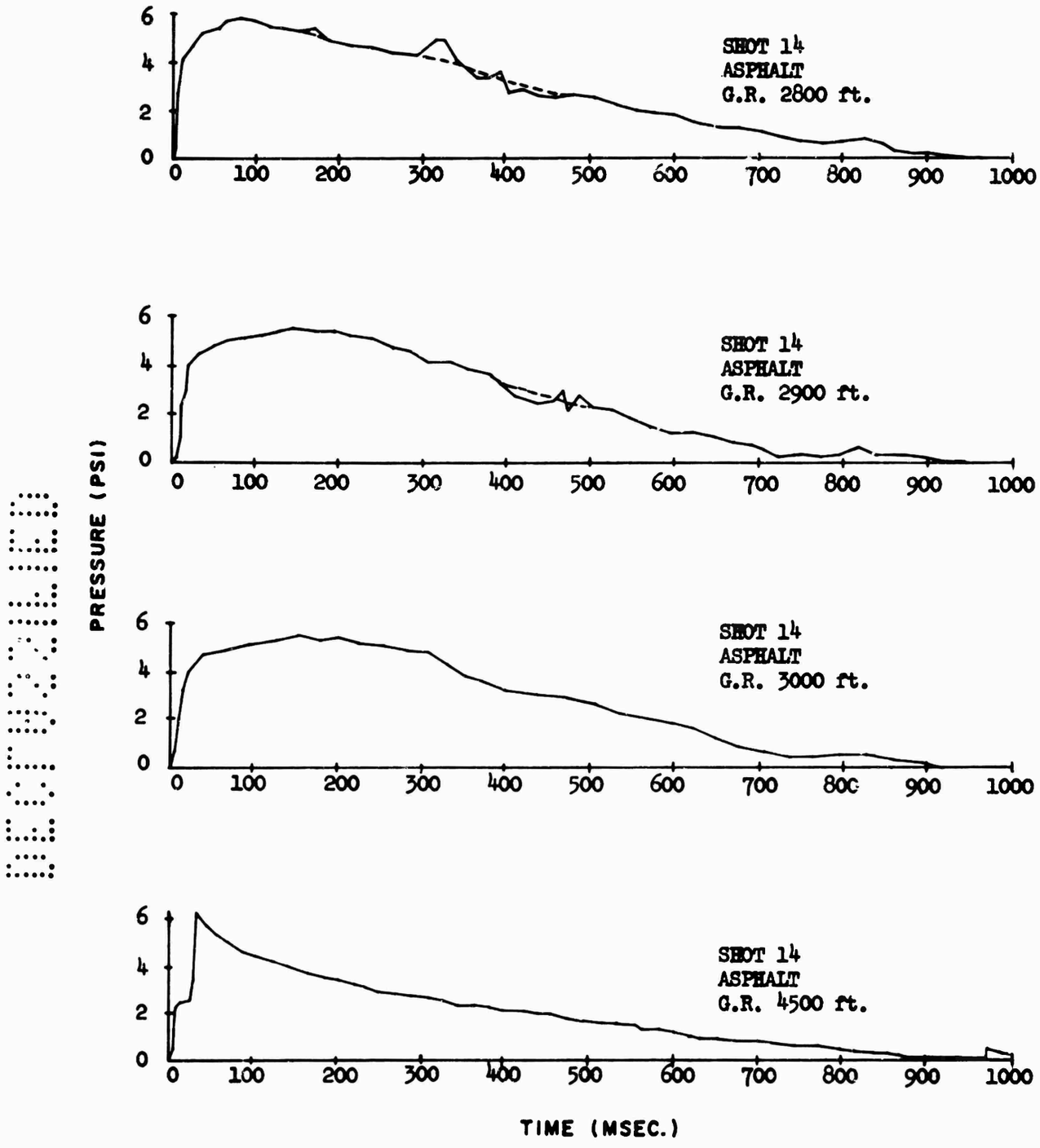

Fig. E.55 Pressure-Time Records from p_t-Gage for Shot 14 (Asphalt Line)

REFERENCES

1. J. J. Meszaros and C. N. Kingery, Ground Surface Air Pressure vs Distance from High Yield Detonations, Project 1.2b, Operation CASTLE ITR-905, May 1955.

2. Capabilities of Atomic Weapons, Prepared by Armed Forces Special Weapons Project, Revised Edition, 1 June 1955.

3. E. H. Engquist and J. J. Mahoney, Protection Afforded by Operational Smoke Screens Against Thermal Radiation, Project 8.3, Operation TEAPOT, WT-1144, August 1956.

4. F. B. Porzel, Theoretical Blast Curves (Draft Copy) J-17837 (Letter) May 25, 1953; Theoretical Blast Curves, Draft Copy, J-19704 (Letter) August 20, 1953.

5. F. H. Shelton, The Precursor-Its Formation, Prediction and Effects, Sandia Corporation, SC-2850 (TR), July 1953.

6. L.M. Swift and D. C. Sachs, Air Blast Overpressure and Dynamic Pressure Over Various Surfaces, Operation TEAPOT, ITR-1109, May 1955.

7. W. E. Morris, et al, Air Blast Measurements, Operation UPSHOT-KNOTHOLE, WT-710, August 1955.

8. L.M. Swift and D. C. Sachs, Air Pressure and Ground Shock Measurements, Operation UPSHOT-KNOTHOLE, WT-711, January 1955.

9. C. D. Broyles, Dynamic Pressure vs Time and Supporting Air Blast Measurements, Operation UPSHOT-KNOTHOLE, WT-714, February 1954.

10. H. W. Liepman and A. E. Puckett, Aerodynamicsof a Compressible Fluid John Wiley and Sons, New York 1947.

11. M. R. White and F. A. Gross, Jr., The Dynamic Pressure Behind a Shock Moving Parallel to a Heated Layer, P. V. Interim Memorandum No. 48, DI/USAF-ONI, 27 August 1955.

12. H. Margenau and G. M. Murphy, The Mathematics of Physics and Chemistry, D. Van Nostrand Company, 1943, pp 494-498.